CHAPTER 1. INTRODUCTION

1.1 Biomaterials

Biomaterials are materials intended to interface with biological systems to evaluate, treat, augment, or replace any tissue, organ, or function of the body (Williams, 1999). The first simple biomaterials were inert metals, such as gold, which were used by ancient civilisations in dentistry thus improving the local people's health and wellbeing (Anderson et al., 2004). Since 1929, when the production of stainless steel paved the way for the first surgically implanted artificial hip, biomaterials have become an integral part of the medical device industry and of healthcare in general. Initially these medical devices were only implanted into the patient as permanent prostheses; however, over time the technology in this area of medical science has advanced greatly. Currently biomaterials can support growing tissues and deliver drugs to target sites whilst, of course, remaining vital in the replacement of joints and valves which are no longer functioning correctly (Kohn, 2004).

Biomaterials are no longer solely used in permanent biological or biomedical implants. Biomaterials, specifically polymeric biomaterials, are essential as tissue scaffolds for the support of regenerating soft and hard tissues both internally and externally, as the external coatings of many pharmaceutical preparations, for implanted devices such as stents and catheters and as extracorporeal devices for contact lenses etc. (Kroschwitz, 1989). Each of these varied applications requires specific physical and chemical properties from the material. When polymers were first used for biomaterial applications, during the Second World War, these were off-the-shelf materials, including Poly(methyl methacrylate) and Poly(ethylene terephthalate), were initially developed for other applications and although these were successful in advancing modern medicine their long term compatibility within the patient was a concern (Nair and Laurencin, 2006). Since this time very few further polymers have been approved by the Food and Drug Administration (FDA) for medical implantation and thus there is a serious lack of diversity in this area of biomaterial science (KOHN, 2004). Currently, most polymers used in this area are based on glycolic, lactic or other linear α-hydroxy acids which has seriously limited diversity and applicability. Combinatorial chemistry has been recently suggested as a route towards broadening

biomaterial material discoveries and thus greater attention has been given to the use of high throughput techniques and accurate testing to discover new polymeric materials which can be used within the human body in the most efficient manner (Taylor et al., 2008).

1.2 Polymers

Naturally occurring polymers are an essential part of our everyday lives; from the DNA present in nearly every cell to the cellulose based fibres and materials which are used to make the shelter and clothing which are vital to life; polymers are indispensable.

Synthetic polymers are a more modern invention with the first, Bakelite, being synthesised in 1907 (Baekeland, 1909), and subsequently only becoming commercially viable after the discovery of the Ziegler-Natta catalyst in the 1950s. Since this time, large branches of polymer science have been focused on finding innovative uses for this novel set of compounds. Polymers are useful candidates for biomaterials as it is simplistic to alter their properties *via* variation of the monomers used in synthesis. The alteration of these building blocks does not only change the polymer backbone, but in addition can change the length of polymer chains, the degree of branching and cross-linking and their eventual physicochemical properties within the patient. Polymers have a vast array of properties including thermoplastics which can melt and be deformed upon the addition of heat, thermosetting polymers which are hard, brittle and are unaffected by temperature as they have been cured irreversibly all the way through to polymer surfactants which are able to disturb the surface tension of liquids. The ability of polymers to be altered via the use of differing monomer units or routes to synthesis has made them a critical area for research to determine new, innovative biomaterials for permanent prostheses, drug delivery and tissue scaffolds (Shoichet, 2010).

Simply, polymers are long chain molecules synthesised by the linking of repeated low molecular weight units called monomers via either addition or condensation polymerisation reactions (Clayden et al., 2012). Depending on the monomers used and the type of reaction employed several polymer architectures can result which determine the polymers own specific structural and biological function. In industrial preparations the three most common types of polymer are linear, branched and dendric (Odian, 2004). These possess

varying degrees of branching and cross-linking (Figure 1- 1) which leads to much of the variation observed between the classes (Billmeyer, 1984). All three of these polymer architectures are currently seen in biomaterials, however, linear and dendritic species are vastly more common. Branched polymers are an interesting "middle ground" between the simplicity of their linear analogues and the costly dendritic alternatives. Thus, branched polymers are the focus of this research.

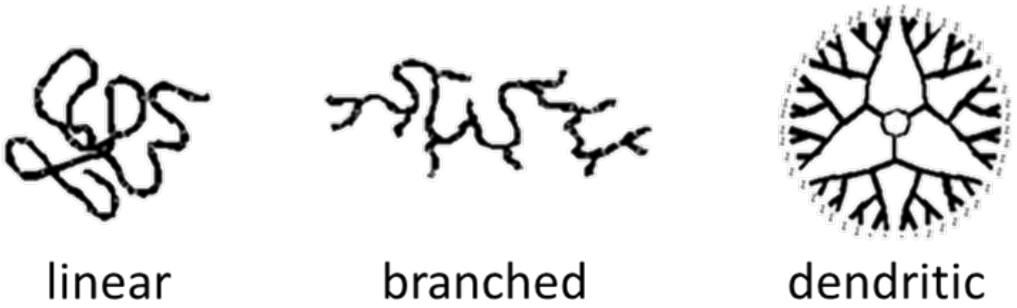

Figure 1- 1 Schematic of a small number of polymer structures described: linear, branched and dendric. With increased crosslinking and branching comes greater complexity, picture adapted from (Young and Lovell, 1991).

1.2.1 Synthesis

Polymer synthesis (polymerisation) is the process by which a number of small molecules, monomers, are joined together covalently into a macromolecular chain or network structure. Wallace Hume Carothers, leader of organic chemistry at DuPont who is credited with the invention of nylon, suggested that the majority of polymers could be categorised into one of two categories, condensation or addition. These terms have in time been replaced by step-growth (condensation) and chain (addition) polymerisation as these provide a more accurate and comprehensive description of the reaction taking place (Sperling, 2005). Polymerisation reactions now can be carried out with or without the presence of a catalyst. The monomers utilised during these differing polymerisation mechanisms are quite different with condensation polymerisation monomers tending to contain functional groups including -COOH, -COOR, $-NH_2$ or OH, whilst for addition polymerisations the monomers contain C=C double bonds or ring structures (Ghosh, 2001), (Figure 1- 2). Chain polymerisation monomers are added to the chain one at a time in contrast with step-growth polymerisation in which monomers can combine with one

another directly; this leads to a difference in reaction rates due to the number of active sites present at any time. Thus the monomers which react to form the polymer not only dictate the type of reaction and its rate but also the molar mass of the resultant material. Step growth polymers generally have a lower molecular mass, less than 30,000 g mol^{-1}, and a higher distribution of molecular weights; however chain polymerisation results in polymers with a higher molar mass, upwards of 50, 000 g mol^{-1}, along with a much narrower weight distribution (Painter and Coleman, 2008). During polymerisation a number of chemical groups may be lost from either monomer in order to form the repeating unit; this is a section of each monomer that is incorporated repeatedly into the polymer. The repeating unit of the polymer, designated by the monomers chosen, has an effect on the polymers behaviour during latter testing.

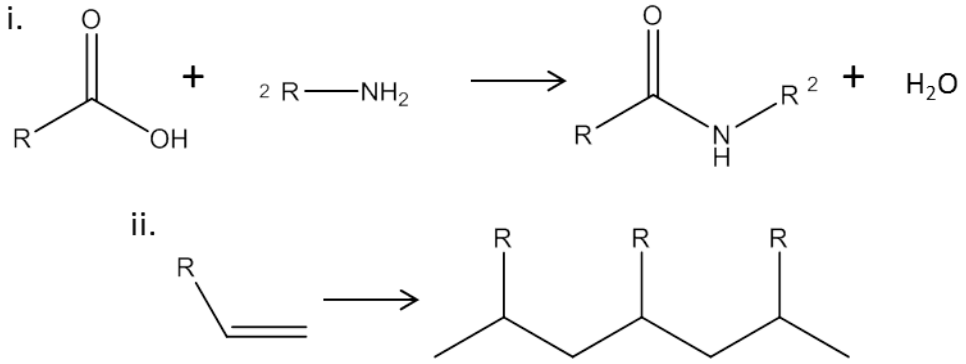

Figure 1- 2 Simple schematics of condensation, i, and addition, ii, polymerisation. Condensation polymers grow in a stepwise manner resulting in lower mass chains: addition polymers grow via a radical reaction resulting in more varied and higher mass products.

1.2.2 Linear Polymers

Linear polymers are the most conveniently and cheaply synthesised as they are in the simplest conformation and thus have been investigated most fully. These long chain macromolecules have no/limited cross-linking or branching between strands and so are held together by physical interactions, including van der Waals forces, which are weaker than covalent bonds and are in general easily overcome by the action of heat on the solid material. Due to their chemical uniformity (backbone moieties are consistent throughout the length of the polymer chain) and intermolecular properties, the long uniform polymer chains can pack closely together producing highly crystalline material which can be easily softened and melted (Painter and Coleman, 2008). Linear polymers can also form

amorphous structures which gives them a multitude of different properties. In addition, linear polymers can generally be dissolved in suitable solvents which further increases their ease of processing and therefore their usefulness on an industrial scale (Shi, 2004). The chain lengths present in any of these polymers are determined only by random events; therefore the final product is always a mixture containing varying chain lengths and therefore varying molecular weights (Asthana et al., 2006). This can be detrimental if specific molecular weights are required for an application. Most plastics used in medical applications at present are linear polymers ranging from simple polyethylene to more complex polyacetals and polycarbonates. The most important step forward in this area of research in recent years has been the invention of medical grade polymers which do not release any toxic or carcinogenic compounds into the patients' blood stream whilst in use or via their degradation pathways, for example PLA (Polylactic acid) (Rincon Lasprilla et al., 2011). PLA was approved in the 1970s by the Food and Drug Administration (FDA) for use in in direct contact with biological fluids, it has many advantages over other biomaterials in that it is biocompatible, easily processed, and comes from renewable sources but most importantly its degradation productions, H_2O and CO_2, are neither toxic nor carcinogenic (Rasal et al., 2010). A number of the polymeric materials used in medicine at present remain flawed as interactions with the blood stream can result in unsatisfactory outcomes. This is in part due to the potentially massive differences between the mechanical properties of plastics implanted and the blood vessel walls (Hasegawa and Azuma, 1979). Further to this complication, caused by the mechanical properties of the polymer insert, the implantation of currently utilised polymers can often cause inflammatory responses to be triggered and the coagulation of blood forming potentially fatal clots. Bioactivity is generally desired as it allows both cell adhesion and cell proliferation to take place promoting healing, however some materials are incompatible with biological fluids and are toxic to the patient, can cause clots to form or promote bacterial adhesion followed by biofilm growth. It is important to note however that for some biomaterial applications there are very specific qualities required; heart stents require minimal cell adhesion properties as increasing mass around the implant can occlude the valve and reduce function endangering the patient. These problems are not known to be specific to linear polymer devices, however the more complex dendric and branched polymers have not been used or tested to the same extent (Billmeyer, 1984). All polymers used for biomedical devices are required to be bioavailable, biocompatible and show minimal immunogenicity.

Linear polymers have been essential to the growth of biomaterials for medical devices as all the original polymers used had this structure. The focus has shifted, however, with more complex chemistries being examined to determine beneficial properties, novel mechanical behaviours and in some cases improved healing and cell growth (Hubbell, 1995).

1.2.3 Dendritic Polymers

Dendric, network, or hyperbranched polymers, in contrast to linear polymers, have a number of additional branched side chains due to reactions occurring at the initial polymerisation. These network polymers all possess highly branched structures, which are formed when monomers containing more than two functional groups are used to form the polymer in a step wise reaction. Although these polymers are both highly branched, dendrimers and hyperbranched polymers have greatly differing structures (Figure 1- 3) dendrimers are amorphous and exactly branched with regularly spaced branching units whilst hyperbranched polymers can be crystalline are not completely "perfect" (Hult et al., 1999).

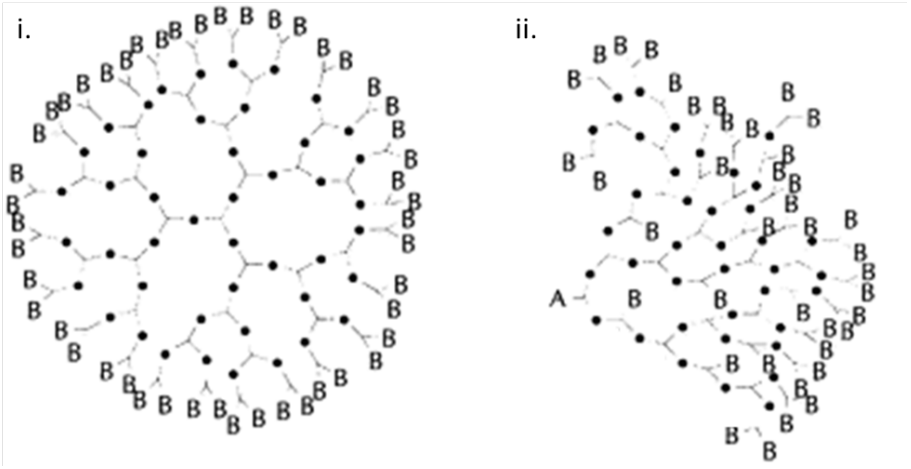

Figure 1- 3 Schematic showing the complex branched structure of a i. dendric polymer and a ii. hyperbranched polymer (Jang and Bae, 1999). Dendrimer is built up around a single core molecule with deprotection steps whilst hyperbranched polymers can be synthesised via one-pot techniques and do not necessarily contain a core molecule.

These more complex polymers can withstand much higher temperatures than their linear counterparts and thus have been used successfully in thermosetting plastics and resins.

This is due to the large number of covalent crosslinking bonds present within these polymers which can withstand a much greater degree of heat before the bonds are broken in comparison to the weak van der Walls forces allowing linear polymers to remain solid. Dendrimers are incredibly complex and expensive to synthesise, even on a lab scale, with multi-step protection and deprotection reactions required and gelation is a constant problem. After preliminary investigations, dendric polymers were deemed to be too complicated to synthesise on a large industrial scale, however, hyperbranched polymers, with the potential for single step reactions, have generated more interest in this field (Gaynor et al., 1996). The synthesis of hyperbranched polymers is considerably less complex than that of dendrimers as the repeated protection and deprotection steps can be negated due to the inclusion of some linear polymer units and the imperfect nature of the final product (Hult et al., 1999).

Recent studies have shown that large dendrimers are passed into the urine of the patient and excreted within two days whilst smaller dendrimers appeared to accumulate in the liver, spleen and kidneys with no urine excretion (Roovers, 1999). This observation prompted an interest in the area of drug delivery as these excretion pathways could be used to specifically target active drug compounds to the site of interest without loss (Hult et al., 1999). Dendrimers are being explored for a wide variety of drug delivery applications: these have included the traditional oral and transdermal routes along with more complex ocular and targeted drug delivery systems (Nanjwade et al., 2009). Dendrimers are also being used as novel carriers for cancer chemotherapies which have increased their notoriety (Majoros et al., 2006). Due to these unusual properties within the human body dendrimers have become of great interest in the scientific community of late. If their size and chemistries can be efficiently tweaked, these novel polymers could potentially be used for targeted therapies including chemotherapy which have the potential to massively reduce side effects and increase efficacy of treatment.

1.2.4. Branched Polymers

This group of polymers is the focus of this research but at present remains one of the least studied. Branched polymers consist of linear polymer chains with branched side units of significant length bound to the main chain at branching points. These individual chains are in general not cross-linked extensively and therefore exist as discrete units within the bulk

material. This gives branched polymers a physicochemistry that is between linear and dendritic counterparts, potentially giving the best of both worlds, i.e. ,branched polymers possess a number of characteristics that are similar to their linear or dendric counterparts; thus they are an attractive middle ground in the field of biomaterials design. This research focuses on the idea that this hybrid style species may hold some answers to the current questions regarding the manufacture and biocompatibility of polymers for medical applications. Branched polymers have the potential to be synthesised via a method comparable to that of linear polymers i.e. easily, quickly and using minimal solvents to generate a low cost, highly pure product whilst also expressing some of the most desired dendritic polymer behaviours such as the ability accumulate in specific organs for targeted treatment of disease. Until recently, similarly to dendrimers, branched polymer commercialisation has been hindered by difficulties in synthesising the polymers in an economical and efficient manner. The first major breakthrough in this area was the research carried out by Fréchet et al. which utilised self-condensing vinyl polymerisation (SCVP) to produce branched polymeric material (Frechet et al., 1995). This route, and the others that followed, was complex and contained many multi-step reactions in organic solvents using transition metal catalysts, similarly to dendrimer synthesis. This unsurprisingly lead to low product yields and several purification steps even on a lab scale ruling out further scale up. The Strathclyde methodology developed in 2006 showed that branched polymer methacrylates could be successfully synthesised in an aqueous environment employing only a single synthetic step (Baudry and Sherrington, 2006b). This new “one-pot” synthetic route has great applicability for industrial scale up due to the lowered costs and minimal environmental impact. This methodology is currently the optimum method of branched polymer synthesis as it boasts high conversion of simple and readily available monomer units in aqueous emulsion using an emulsifier, free radical initiator and a thiol to ensure the desired product is formed. This method is revolutionary as under bulk aqueous suspension these reactions undergo cross linking irrespective of the amount of chain transfer reagent and thiol added. Almost simultaneously with the Strathclyde route, the synthesis of branched polymers in the absence of solvent was published by Morbidelli *et al.* However, this method requires the use of high temperatures, over 300°C, making it less attractive to large scale production (Campbell et al., 2005).

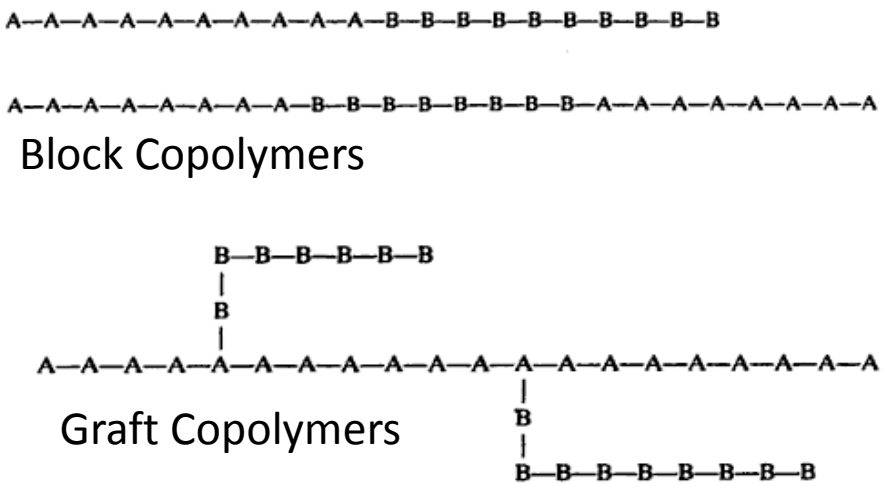

Figure 1- 4 Schematic of the monomer dispersion in block and graft copolymers, random copolymers have an arbitrary arrangement of the monomer units within the chain. For simplicity polymers containing only 2 monomers are described, A and B (Young and Lovell, 1991).

Branched polymers most often include more than one species of monomer in their skeletal structure and as such are known as copolymers (Young and Lovell, 1991). In general, these can form as either block or graft copolymers which include properties of each of the constituent homopolymers along with unique characteristics arising from the novel chemical linkages. Branched polymers require at least one of the monomers to have two or more functional groups present in a similar way to dendrimer synthesis. This allows the branching to occur and has a remarkable effect on both the structure of the product and its molecular mass. Even in the primary stages of these reactions, the polymer formed has a branched structure which leads to the molar mass increasing more rapidly than that for a linear polymer. If continuous branching is allowed to occur then ultimately a hyperbranched state is reached and a cross-linked structure results as previously described. These cross-linked branched polymers have a tendency to gel during their synthesis resulting in a semi-solid polymer with low solubility in both organic and aqueous media (Ambade and Kumar, 2000). Branched polymers can be synthesised using a multitude of methods, thiol-ene synthesis of branched polymers is shown schematically in Figure 1- 5, via a simple click chemistry reaction (Lee et al., 2004). "Click Chemistry" was first described in 2001 to describe chemical reactions which have the ability to generate products quickly and reliably by joining small units together. Minimal by-products are produced and the syntheses can be conducted in simple solvents (Kolb et al., 2001).

For the synthesis of acrylate polymers throughout this project a free radical polymerisation in the presence of a vinyl monomer to produce these polymer species, Figure 1- 6. This method suggests the use of a chain transfer agent in order to reduce cross-linking however, this has been removed from the synthesis as it shortens the polymeric chains and a solid material is required for these experiments. This process also requires the use of an organic solvent which renders it uneconomic for use on a large scale but as this route to synthesis is simple and easily reproducible on a small scale using parallel synthetic techniques, such as Radley's carousel, it is ideal for the experiments in this research (Isaure et al., 2003a). The current advances in the production of branched polymers have prompted a change in focus to determine suitable applications for these more unusual materials. Biomaterials is only one field in which these novel products could become valuable but, for this to become a viable option, extensive testing and characterisation must first be undertaken to ascertain their safety and applicability.

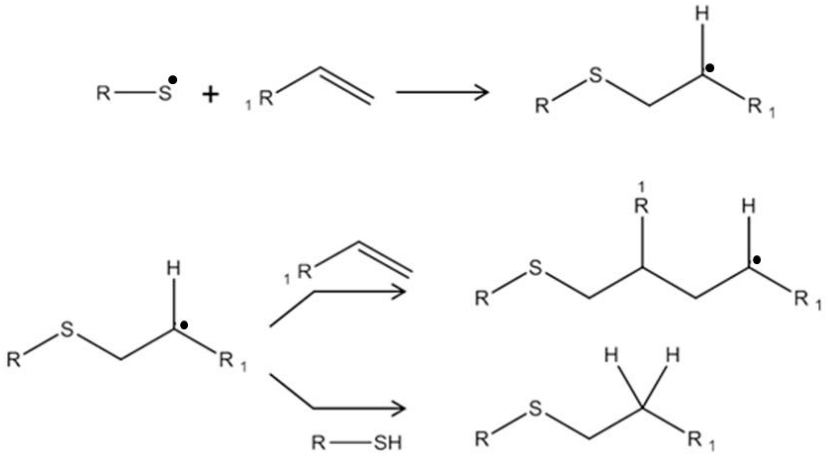

Figure 1- 5 Thiol-ene branched polymer synthesis via click chemistry reaction (Lee et al., 2004).

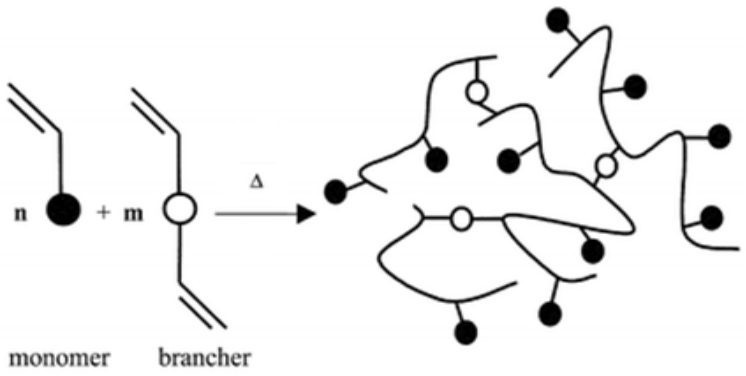

Figure 1- 6 Schematic representation of the concept of the acrylate synthesis used throughout this research. The synthesis is via a conventional free radical polymerisation of a vinyl monomer in the presence of a multi-

functional comonomer (brancher) in toluene (Isaure et al., 2003b). Circles represent carbon backbone and functional groups of monomer and brancher species chosen.

1.2.5 Hydrogels

One potential property of polymeric chains and self-assembled systems is the ability to increase the volume of water which can be taken up. These polymers are known as hydrogels and are natural or synthetic superabsorbent insoluble hydrophilic polymer networks which can contain over 99% water (Slaughter et al., 2009). Upon the integration of this large volume of water, the polymer swells and greatly increases in mass (Kim et al., 1992). Hydrogels tend to be highly flexible due to their high water content and thus have a very similar character to natural tissue making them ideal biomaterials (Peppas et al., 2000). Common synthetic polymers for biomaterial applications, more specifically tissue scaffolding, include, poly(ethyleneglycol) (PEG), poly(vinyl alcohol) (PVA), and poly(acrylates) such as poly(2-hydroxyethyl methacrylate) (PHEMA) (Lee and Mooney, 2001). Natural hydrogels have also been produced using chitosan, collagen and a number of others(Malafaya et al., 2007).

The unique physical properties of this group of polymers have been of great interest within drug delivery and tissue scaffolding fields. These polymers are generally extremely biocompatible due to their high water content and physiochemical similarity to the patients native extracellular matrix, compositionally and mechanically (Hoare and Kohane, 2008). These can additionally be impregnated with a variety of other materials to improve their function including human cells to promote tissue repair and differing drug molecules to fully utilise their sustained release capabilities. Hydrogels can be synthesised to include a highly porous structure that can be tuned to permit the loading of combinations of drug molecules to release at specific rates (Hoare and Kohane, 2008).

1.3 Polymers as Biomaterials

The most essential prerequisite for any material to be suitable as a biomaterial is that it must be biocompatible. Biocompatibility is defined as the ability of a material to perform with an appropriate host response in a specific application (Williams, 1999). It is vital to note that the properties of a material used as a scaffold to regenerate bone mass (strength,

inflexibility and promotion of bone cell growth) are vastly different to those required for an arterial heart stent (flexibility, mechanical strength and minimal cell growth to avoid blocking the artery) and thus the conditions for defining the eventual biocompatibility of a material depend on its application (Butany et al., 2005, Porter et al., 2000). A wide range of materials have been investigated as biomaterials, these include all classic groups of materials including metals, ceramics, glasses, and polymers (Nair and Laurencin, 2006). Polymers currently form the most versatile class of biomaterials that have been comprehensively investigated for medical applications. This is in part due to their intrinsic flexibility and in their ease of modification in order to match the physical and mechanical requirements of the countless tissues or organs of the body.

1.3.1 Uses

Polymeric biomaterial development has taken place over numerous years with the first being the application of natural polymers to medicine (Ikada, 2002). Synthetic polymers have been a more recent addition however, with their origins in the 1940s around the Second World War. The first polymer used within this field was poly(methyl methacrylate) (PMMA) as a biostable artificial cornea. After some success, a variety of known polymers were employed for medical applications including hip replacements (Castner and Ratner, 2002). More recently, the interest in materials science shifted to include the engineering of novel polymers with specific biocompatibilities and mechanical properties for a single application. Biomaterials require to not only be biocompatible but also they need to be able to be simply sterilised and possess the physical properties for their desired application as shown previously; finally, they must also be easily manufactured on an industrial scale. A schematic of all factors to be considered in the manufacture of novel biomaterials is shown in Figure 1- 7. This approach to design requires the combination of many specialities to generate the most applicable final product; thus this has led to an interdisciplinary approach to the invention of novel biomaterials.

It can be seen that the uses of polymeric biomaterials are far ranging including prosthetics, dental materials, medical implants, dressings, tissue engineering scaffolds and drug delivery systems, thus a vast range of materials are required to not only fulfil all criteria for all functions but all applications there within. For example, tissue engineering and drug delivery applications require the polymers used to be biodegradable. This allows the

patient to have a single operation to implant the device followed by polymer degradation, via a known safe pathway, to restore function. This is obviously vastly different to the requirements for a hip replacement polymer which must remain in its original conformation for up to 15 years. These immeasurably differing properties have caused some of the limitations of current biomaterials.

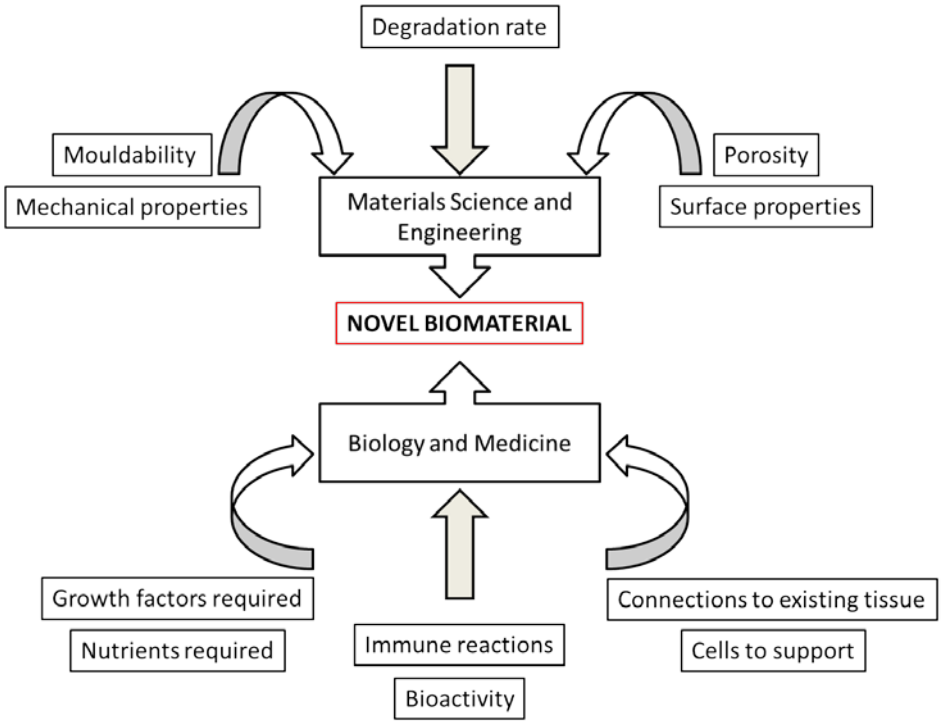

Figure 1- 7 Illustration showing the number of factors which must be considered when designing a novel biomaterial. This includes the integration of engineering, medical and biological properties. Altered from an illustration by Seal *et. al.* 2001 (Seal et al., 2001).

1.3.2 Limitations

As the number of materials specifically available as biomaterials increases, it becomes more important to ensure that all products are suitable for their desired application however, there are inevitably some limitations to these systems. Material manufacturers tend to operate extensive quality assurance programs including good laboratory practice (Seiler, 2012), good manufacturing practice (Nally, 2006) and finally good clinical practice (Kolman et al., 1998). The combination of these specifications helps to ensure that no "unsafe" material ever reaches the patient. However, man-made materials are never perfect and as such manufactured devices do have a failure rate. There are limitations to medical devices

which arise due to the compromises that must be made to get the product to market and complications that occur thereafter. Obviously biomaterials in general should not be toxic, mutagenic or carcinogenic, however, in some instances this can be necessary, i.e. biomaterials specifically designed for chemotherapy drug delivery (Rogero et al., 2003). Toxicology also encompasses any break down products entering the patient, thus any and all degradation pathways must be fully understood, these can be beneficial or detrimental to the product depending on their purpose (Nair and Laurencin, 2007). Biomaterials must also promote an appropriate host response which generally includes no blood clotting, resistance to biofilm colonisation and normal healing. Within the body there are unique processes which are invoked upon implantation of a material or device and the following healing. The inflammatory reaction sequence is triggered which leads to healing but due to the implant the "foreign body reaction" takes place, this is well documented and the reaction is dependent on the foreign body and its position within the patient (Babensee et al., 1998). Essential to the final “usefulness” of the biomaterial, in addition to patient safety and material efficacy, it must be suitable for production on an industrial scale. This includes the synthesis of the material along with its packaging, sterilisation, long term storage and quality control. Industrial synthesis, unlike much research, must be cost effective, facile, rapid and make use of the minimal volume of organic solvent (Riegel and Kent, 2003). Finally, more pertinently to this research, are the innovations into bioresistive implants. To date there has been the inclusion of antibiotic agents within the polymer matrix. This can aid healing and reduce biofilm infections however, the problem of antibiotic resistant bacteria is a growing one and this must be considered when contemplating the use of such materials (Campoccia et al., 2010). Further to this the growth of cells and bacteria must both be controlled on the implants surface. This can be done by the inclusion of signalling molecules within the polymer structure or by altering the surface characteristics (Mieszawska and Kaplan, 2010). Cell growth is imperative to the success of a permanent prosthesis however, for vascular grafts and catheters implanted into the venous system cell growth, and thus healing, requires to be controlled or it could effectively block the arteries and be detrimental to patient health (Furth et al., 2007). For any biomaterial to become significant within this field it must be safe, aid healing in the appropriate manner, possess the structural properties required for its use and be industrially applicable. To fulfil the majority of these criteria, solvent free or low solvent processes were used in the synthesis of the polymers and UV methodologies were employed where applicable to reduce time.

1.4 Biofouling

Biofouling is the impairment or degradation of a device as a result of the growth and activity of living organisms inhabiting its surface. These organisms can be plants, algae or animals but, bacterial biofouling is of particular interest. To improve efficiency of polymeric biomaterials the reduction of biofouling has been investigated. This can be done using the innate properties of the polymer or via impregnation of the plastic with antibacterial agents. The use of antibiotics within the polymer structure however, can exacerbate the problem of antibiotic resistant bacteria. To avoid this issue the reduction of biofilms using the polymers physical and chemical properties alone is beneficial. Biofilms are complex structures which can adhere to the solid, liquid or soft tissue surfaces of a material establishing chronic infections (Dougherty, 1988). These bacterial communities are extensive and after adhesion to a surface within the patient and secrete extracellular polymers and polysaccharides (Stewart and Costerton, 2001) generating the "slimy" appearance. Biomedical devices are particularly susceptible to biofilm colonisation both immediately after implantation and subsequently if the patient suffers from a secondary infection (Merritt and Chang, 1991). It is also pertinent to note that biofilms are predominantly dead bacterial cells which are used as a shield to protect the living bacterial infection at the centre of the biofilm mass, this makes them particularly resistant to antibiotic therapy as it is challenging to penetrate this dead layer to achieve the appropriate level of chemotherapeutic effect where required.

Biofilms are highly resistant to antibiotic chemotherapy and generally require implant excision followed by an aggressive course of intravenous antibiotics to be effectively eliminated (Costerton et al., 1999); even patients with an uncompromised immune system rarely fend off biofilm infections without treatment (Stewart and Costerton, 2001). As a result, biofouling remains the leading cause of medical implant failure (Gristina and Costerton, 1985). It is thought that the reason for this reduced susceptibility to antibacterial agents is due the polymer matrix surrounding the biofilm, this reduces the infusion of the of the antibiotics into the biofilm itself (Gordon et al., 1988) and slows down the diffusion on solutes within the film (Stewart, 1998); obviously this all depends on the antibacterial agent used and the biofilm being attacked (Suci et al., 1994) (Hoyle et al.,

1992). In all cases, this treatment process is costly and invasive to the patient. A schematic of the lifecycle of a biofilm is shown in Figure 1- 8.

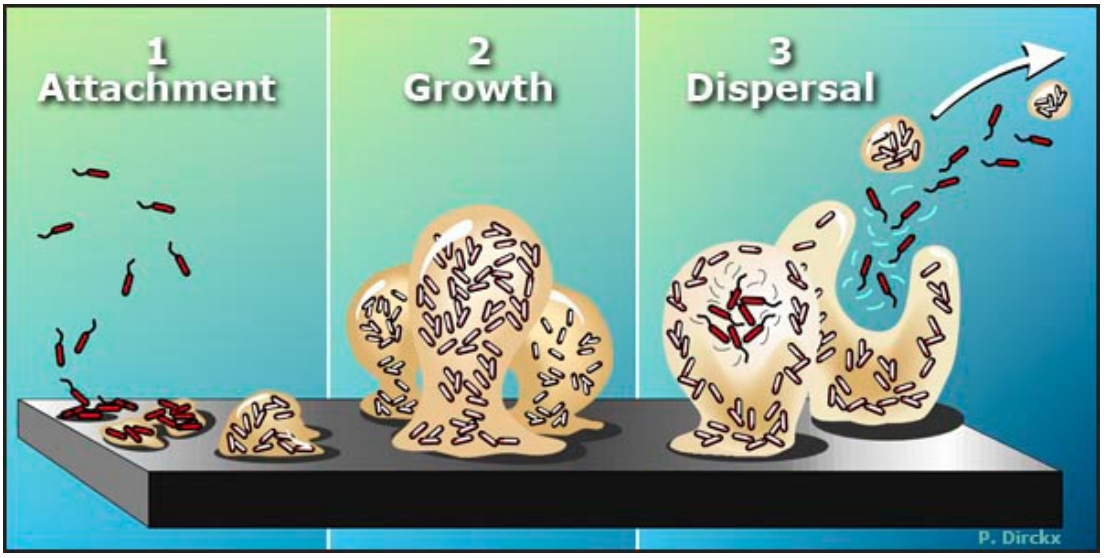

Figure 1- 8 Lifecycle of a biofilm. 1. attachment of a small number of bacteria to the implant surface, 2. growth of biofilm occurs by using the external bacteria as a sacrificial shield to protect living core, 3. dispersal of bacteria from original biofilm in order to colonise further. Due to this growth and development process, it is exceptionally difficult to remove a biofilm in comparison to free floating bacteria (Williams et al., 1997), (Padera, 2006)

The most prolific biofilm forming bacteria that have been identified include *Staphylococcus aureus*, *Pseudomonas aeruginosa* and *Staphylococcus epidermis* (Stewart and Costerton, 2001). *Staphylococcus aureus* and *Pseudomonas aeruginosa* have been used throughout this study to examine the biofouling properties of synthesised polymers for potential biomaterial use due to not only their biofouling nature but their interest in the media at present.

1.5 Summary and Research Aims

To research the possible use of branched polymers as biomaterials, this project will investigate a wide spectrum of novel branched polymers synthesised using established experimental procedures before, using traditional and alternative analysis to determine physical and chemical properties. The main focus of this project is to investigate the effect of branched polymer structures on the proliferation of biofilms upon their surface.

The key project objectives are as follows:

1. The synthesis of a library of novel branched polymer species, these include both acrylate and thiol-ene polymers synthesised using a wide range of starting materials (Figure 1- 9).
2. Analysis of products using a variety of analytical instrumentation to determine polymer structure, surface properties and crystalline behaviour. This includes Contact angle goniometry (CAG), IR, Raman, differential scanning calorimetry (DSC) and atomic force microscopy (AFM).
3. The investigation of thiol-ene polymer mechanical behaviour pre and post swelling in water to determine applicability as a potential hydrogel type biomaterial.
4. To determine the effect of polymer structure, mechanical properties and behaviour on biofilm proliferation using *Staphylococcus aureus* and *Pseudomonas aeruginosa.*

This research will allow the use of novel monomer species in branched polymer architectures to be investigated as possible innately bioresistive coatings for permanent biomaterial implants.

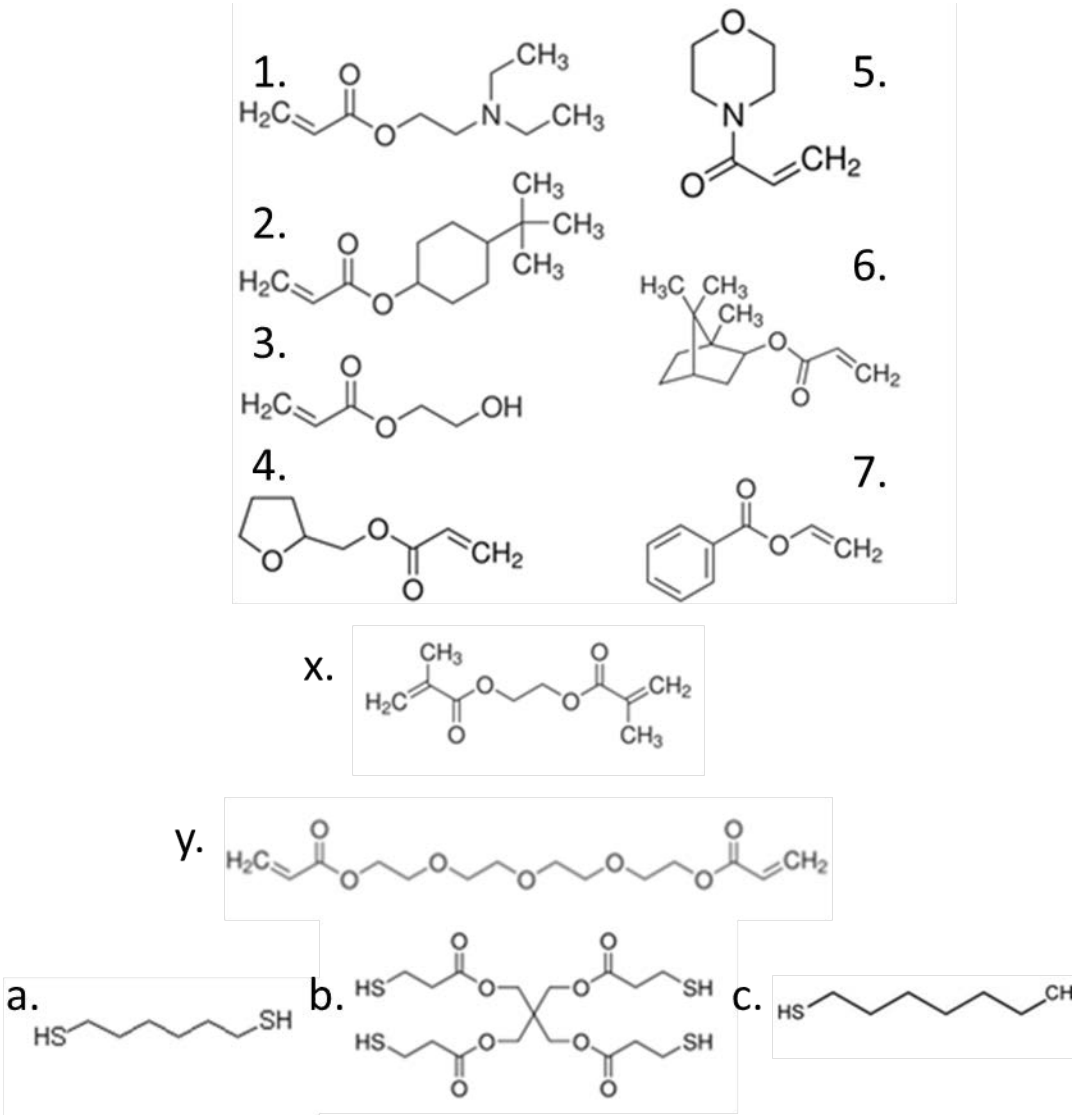

Figure 1- 9 All monomers, branchers and thiols used throughout this thesis. Numbering scheme used to identify polymers as IUPAC names would be complex and lengthy. Monomers: 1. 2(Dimethylamino) ethyl acrylate, 2. 4-tert-butylcyclo hexylacrylate, 3. 2-hydroxyethyl acrylate, 4. Tetrahydrofurfuryl acrylate, 5. 4-acryloylmorpholine, 6. Isobornyl acrylate and 7. Vinyl benzoate. Branchers: x. Ethylene glycol dimethacrylate and y. Tetra ethylene glycol diacrylate. Thiols: a. 1,6-hexanedithiol, b. Pentaerythritol tetrakis(3-mercaptopropionate) and c. 1-octanethiol.

CHAPTER 2. MATERIALS AND METHODS

2.1 Chemicals

A wide range of chemicals were used throughout this study including a range of acrylate monomers and thiols. Chemicals were purchased from SigmaAldrich and were reagent grade.

Monomer Species

2(Dimethylamino) ethyl acrylate

4-tert-butylcyclo hexylacrylate

2-hydroxyethyl acrylate

Tetrahydrofurfuryl acrylate

4-acryloylmorpholine

Isobornyl acrylate

Vinyl benzoate

Ethylene glycol dimethacrylate

Tetra ethylene glycol diacrylate

1,6-hexanedithiol

Pentaerythritol tetrakis(3-mercaptopropionate)

1-octanethiol

All monomer species were purchased from Sigma-Aldrich (St Louis, MO, USA).

Chemicals

1,1'-Azobis(cyclohexanecarbonitrile)

2,2 – dimethoxy 2-phenyl acetophenone

Tryptone

Yeast extract

Sodium chloride

Agar

Crystal Violet Stain

All chemicals were purchased from Sigma-Aldrich (St Louis, MO, USA).

Solvents

De-ionised water

Ethanol

Toluene

Hexane

Isopropanol

Dimethyl formamide

Ethylene glycol

Diiodomethane

Chloroform (deuterated)

Dimethylsulfoxide

All solvents were purchased from Fischer Scientific (Fair Lawn, NJ, USA) with the exception of deionised water which was produced in house.

Bacteria

Pseudomonas aeruginosa (PA01)

Staphylococcus aureus (clinical MRSA isolate from the Scottish MRSA reference laboratory – Stobhill hospital, Glasgow, UK)

Bacillus subtillis

GFP Pseudomonas aeruginosa

2.2 Polymer Synthesis

Branched acrylate and thiol-ene polymers were manufactured for this study due to their novel properties and facile synthesis. The "Strathclyde Route" (Baudry and Sherrington, 2006a) was nominated as an interesting methodology for branched acrylate synthesis due to its aqueous nature, however in order to ensure the synthesis was efficient and water removal from the system did not have to be undertaken, a more conventional organic method was eventually chosen.

2.2.1 Acrylate Synthesis

Acrylate polymers were synthesised in toluene using a modified method from Isaure et al, 2003 (Isaure et al., 2003b). This method was selected due to its simplicity although it was

carried out in organic solvent, which is not ideal. This reaction did however not suffer from oxygen inhibition and had minimal post synthesis work up requirements. For efficiency, low volume reactions were carried out in parallel using a Radley's carousel set up which allows rapid parallel-pot synthesis of polymers (Figure 2- 1). Dodecanethiol was stated in the method to have been used to inhibit gelation due to crosslinking of the branched polymer chains. However, for these experiments this reagent was removed in order to allow gelation of the synthesised polymers and generate a solid product which could be dissolved and coated onto other surfaces or alternatively tested in bulk.

2.2.1.1 Parallel Synthesis of Branched Polymers

Monomers and comonomers of interest were first identified and then used, in varying proportions, to produce a bank of polymers. Using a Radley's carousel (Carousel 12 Plus, Radleys Discovery Technologies, Essex), which allows 12 experiments to be run simultaneously, 18 novel branched polymers and 5 linear polymer controls were synthesised using the following procedure.

Figure 2- 1 Radley's Carousel used for multiple parallel synthesis of polymer samples (Technologies, 2013)

Monomers 2-(Dimethylamino) ethyl acrylate (monomer **1**), 4-tert-butylcyclohexylacrylate (monomer **2**) and 2-hydroxyethyl acrylate (monomer **3**) were used along with comonomers ethylene glycol dimethacrylate (brancher **x**) and tetra ethylene glycol diacrylate (brancher **y**) to create initial polymers, Figure 1- 9. The reactions were again carried out in 15ml of toluene using 1mol% 1, 1'-Azobis (cyclohexanecarbonitrile) as the thermal initiator.

Brancher species were added to the reaction in 20%, 30% and 50% ratios in order to produce solid polymers which were most appropriate for biomaterial applications. Reaction flasks were heated, using a Radley's carousel, to 80°C with stirring until the solid polymer crashed out of solution. These were then allowed to cool before polymers isolated from each reaction were dried in a vacuum oven (Medline OV-11) at 70cmHg and 45˚C overnight to ensure the removal of all residual toluene. The proportions of reagents used in all branched acrylate polymers synthesised are shown in Table 2- 1.

In order identify all polymers synthesised a labelling system was employed. Samples were named using their monomer number, brancher letter and the percentage of brancher used, **1**+**x** 20% is monomer and 20% brancher **x** (ethylene glycol dimethacrylate). This system has been employed throughout this thesis.

2.2.1.2 Synthesis of Linear Control Polymers

In order to compare the biomaterial properties of the novel branched species synthesised, linear analogues were also generated. These were prepared in the same manner as that used previously to generate the branched species however, with the obvious exception of a branching comonomer. 2.5g of monomer or brancher species was added to 7.5ml of toluene and 1mol% 1,1'-Azobis(cyclohexanecarbonitrile) was added. As with the branched polymers, these were heated to 80°C with stirring until a solid product formed and crashed out of solution. Finally linear polymers were dried overnight in a vacuum oven at 70 cmHg and 45˚C to ensure complete solvent removal.

Polymer Number	Reaction time (h)	MONOMER			COMONOMER		1,1'-Azobis(cyclohexanecarbonitrile) (g)
		1	2	3	x	y	
1+**x** 20%	5.25	100			20		0.0605
1+**x** 30%	5	100			30		0.0672
1+**x** 50%	5	100			50		0.0864
1+**y** 20%	6	100				20	0.0587
1+**y** 30%	3	100				30	0.0705
1+**y** 50%	3	100				50	0.0901
2+**x** 20%	5.25		100		20		0.0397
2+**x** 30%	5		100		30		0.0487
2+**x** 50%	5		100		50		0.0574
2+**y** 20%	5.5		100			20	0.0418
2+**y** 30%	5		100			30	0.0443
2+**y** 50%	5		100			50	0.0590
3+**x** 20%	2.5			100	20		0.0735
3+**x** 30%	3.5			100	30		0.0841
3+**x** 50%	2.5			100	50		0.1051
3+**y** 20%	3.5			100		20	0.0735
3+**y** 30%	2.5			100		30	0.0841
3+**y** 50%	3.5			100		50	0.1051

Table 2- 1 Relative proportions of monomers, comonomers and initiator for Radley's carousel experiments and time taken for solid polymer to precipitate of solution

2.2.2 Thiol-ene synthesis

Thiol-ene polymers were chosen as a contrasting polymer to the acrylate species investigated initially due to their ultraviolet (UV) synthesis methodology and their "click chemistry" behaviour. A library of polymers were again synthesised primarily using the monomers investigated in the acrylate work but this was increased due to the short reaction time and simplicity of work up. Thiol-ene polymer discs were synthesised using a UV methodology adapted from Rydholm *et. al.* ,2007 (Rydholm et al., 2007). To dimethylsulfoxide (DMSO) a monomer, brancher and thiol species were added in a ratio of 1:1:1 with 0.1% 2,2–dimethoxy 2-phenyl acetophenone (DMPA) photoinitiator, for a full list of reagents see Table 2- 2. The labelling scheme used was similar to that employed previously, polymers were named after their monomer and thiol species alone as the brancher, tEGDA, remained constant throughout i.e. polymer **1A** consists of a 1:1:1 ratio of monomer **1**, thiol **A** and brancher **y**.

Table 2- 2 Table showing the monomer, brancher and thiol species used in synthesis of thiol-ene branched polymers and their labels.

Monomer	2(Dimethylamino) ethyl acrylate	Monomer **1**
	4-tert-butylcyclo hexylacrylate	Monomer **2**
	2-hydroxyethyl acrylate	Monomer **3**
	Tetrahydrofurfuryl acrylate	Monomer **4**
	4-acryloylmorpholine	Monomer **5**
	Isobornyl acrylate	Monomer **6**
	Vinyl benzoate	Monomer **7**
Thiol	1,6-hexanedithiol	Thiol **A**
	Pentaerythritol tetrakis(3-mercaptopropionate)	Thiol **B**
	1-octanethiol	Thiol **C**
Brancher	Tetra ethylene glycol diacrylate (tEGDA)	Brancher **y**

To DMSO (which was used as a solvent to ensure thorough admixing of all reagents), solid initiator, monomer, brancher and thiol were added before being vigorously agitated for 30s. Aliquots of reaction mixture (0.5ml) were added into wells of a specially cut metal curing plate, see Figure 2- 3. Polymer mixtures were irradiated in UV oven (light source

DYMAX 5000 Flood, 320-390 nm wavelength) for 2min until solidification had entirely taken place.

Figure 2- 2 Metal curing plate for UV synthesis of thiol-ene polymers. Aluminium foil coated onto one side using vacuum grease as fixative before wells (2 cm diameter) filled with reaction mixture and curing taking place.

Post curing, discs are easily manually removed from reaction plate before being dried overnight at 60°C and 75 cmHg in vacuum oven to remove all remaining DMSO. Solvent is observed to bead on the surface of the discs after cooling to room temperature and this is used to easily observe if effective the drying has taken place. As previously noted, the initial thiol-ene polymers were synthesised using the same monomers as the acrylate synthesis, monomers **1**, **2** and **3**. This was done in order to determine any similarities or differences between the thiol-ene and acrylate polymer behaviour when biologically tested using *Pseudomonas aeruginosa* and *Staphylococcus aureus*. Further samples were synthesised to make use of the high throughput nature of this methodology. Although the monomers used throughout this thesis lead to novel products the thiols used were chosen as they are well documented in literature for this type of synthesis. More specifically thiol **A** is difunctional, thiol **B** is quarternary functional and thiol **C** is monofunctional; this should allow some interpretation the differences between thiol behaviour dependant on functionality. Thiol **B** chosen specifically as it is a component of commercial significance in this field. In addition to this, it is environmental friendly and does not emit the "unique" thiol odour (Fan et al., 2008).

2.2.3 Polymer coating of coverslips

In order to carry out some of the analysis on the polymers synthesised from the experiments detailed above they has to be first be coated in a thin layer onto a solid support, in this instance 13mm diameter circular coverslips. This was done using dip coating or spin coating and both of these methodologies were utilised within this study.

2.2.3.1 Dip coating

Dip coating was used with the acrylate polymers as it was seen to be the most suitable way to ensure uniformity across the samples. This was simply achieved by dissolving the solid polymer in a suitable solvent, placing the glass to be coated into this solution and leaving for a nominated period of time before being removed and allowed to dry in air. However, for acrylate polymers synthesised in this research, this process was complicated by their insolubility in most solvents. A small number of polymers were chosen to determine the best solvent for dissolution. Isopropanol, ethanol, toluene and dimethyl formamide (6ml) were added to the polymer (0.5g) in a glass vial, this was then capped, heated to 37˚C and agitated for 24hrs. From the initial experiments, it was concluded that the most effective solvent to dissolve the library of polymers was toluene. Multiple coverslips were then added to each of the polymer solutions, recapped to ensure no solvent evaporation from the surface, and held for 1h before being removed using forceps and allowed to dry horizontally on an absorbent surface for 12hrs at room temperature to remove all traces of toluene. Ambient drying was chosen over hot air drying as the effect of evaporation rate on film thickness is minimal unless the solution has a high viscosity (Yimsiri and Mackley, 2006).

2.2.3.2 Spin coating

The thiol-ene polymer thin films were prepared using a spin coating methodology onto 13mm diameter glass coverslips, as before. The spin coater used was a Laurell Ws-400B-6NPP/LITE/8K, which operates within a closed chamber which helps to create a nitrogen rich environment above the substrate and ensures user safety. The evaporation rate of the polymer solution thus was significantly higher than that of the dip coating in ambient air. A speed of 6400rpm and a spin time of 40 s were used throughout the experiments. Approximately 0.2g of ground thiol-ene disc were added to DMSO (2ml) in individual vials

and sonicated (VWR ultrasonic cleaner) for 30mins at 60°C to ensure dissolution. These polymers, similarly to the acrylate species, were difficult to dissolve and thus limited the solvents that could be used. 300µl of polymer solution were dropped onto the glass surface in 100µl aliquots. After each addition spin coater was allowed to run for 40s before repetition. This was to ensure the maximum coating onto the glass surface due to the limited dissolution. After coating the coverslips were dried overnight at 60°C to ensure all DMSO was removed from the surface.

2.3 Chemical Analysis

The characterisation of novel branched polymers must determine both their bulk properties and their surface chemistry if they are to be used effectively as biomaterials. For biological applications, the surface structure and chemistry is particularly important and must be fully understood as this is the region that first interacts with the host's proteins and cells. Bulk chemical structure and degradation pathways should in turn be determined to ensure that the implantation of such materials in the patient will not result in harmful side effects over the total time of use. This is particularly pertinent if these polymers are to be employed in the area of drug delivery which would require the slow release of a pharmaceutically active compound over time from the disintegrating polymer. An overview of each of the techniques which will be used to determine the polymer properties is given below along with specific testing parameters.

2.3.1 Contact Angle Goniometry and Surface Energy

A contact angle (CAG) is the measurement of the angle (θ_C) made at the interface between a vapour and liquid at a solid surface (Good and Koo, 1979). Geometrically it is the angle formed by a liquid at a three phase boundary where a liquid, solid and gas interact after balancing the adhesive forces between the liquid and solid and the cohesive forces within the liquid (Amirfazli and Neumann, 2004). This can also be seen as a measurement of wetting, the ability of a liquid to stay in contact with a solid surface, which is governed by the delicate force balance between adhesive and cohesive forces. To measure this unique angle, drop shape analysis can be used. This allows both the contact angle and surface energy of the interaction to be determined whilst only making two simple assumptions: the drop is symmetric about the vertical axis and the drop is not in motion (Woodward). The

instrumentation used consists of a video camera connected to a computer with image analysis software that allows accurate determination of θ_c, Figure 2- 4.

Figure 2- 3 Basic components of a contact angle goiniometer.

Throughout this research the sessile drop method was employed to determine the contact angle and surface tension of the liquid, solid interactions present in the system, see Figure 2- 5. This method uses a goniometer which allows the measurement of θ_c to be made visually. A small droplet of liquid (~5/6 µL) is deposited onto the horizontal surface being analysed using a very fine, vertically orientated syringe. After approximately 20 seconds, a high resolution camera captures an image of the droplet on the surface which can then be used to calculate the contact angle either manually or using the instruments data analysis software. This angle should remain constant irrespective of the size of the droplet; however, if possible, many drops should be analysed across the total surface area of the sample to ensure homogeneity (Sklodowska et al., 1999).

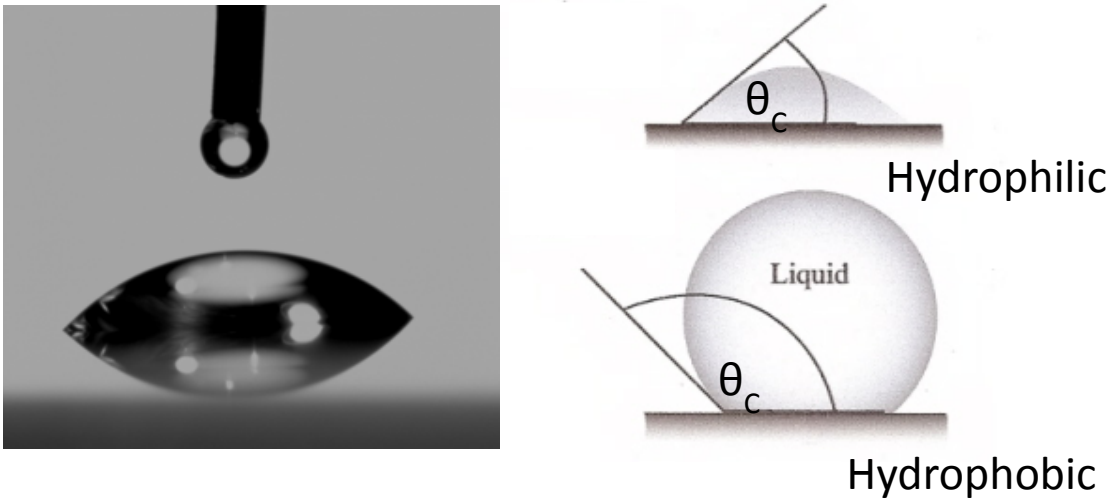

Figure 2- 4 Image capture of a sessile water droplet sitting on a solid surface and schematic of contact angles on two opposing surfaces, θc < 90°C hydrophilic (wetting) surface, θc > 90°C hydrophobic surface chemistry (Gajewski, 2005) image adapted from http://www.eku.edu/.

2.3.1.1 Surface Energy

Due to one of the important properties of these polymers synthesised being that they adhere to other substances, be it biological or synthetic material, the surface energies were determined. This will ensure that the materials synthesised have the potential to be combined with other, essential, matrices for final implantation into the patient as adhesion is basically the expression of the attractive forces which exist between atoms present within the system. Surface energy (SE) is measured using the interface tension at the interface of the probe liquids and the solid polymer surface and can be subdivided according to the interactions present in the system; these include acid/base, hydrogen bonding and polar interactions. SE is traditionally assumed to be quite simply the sum of the components considered; for example, the addition of the contributions from both the dispersive and polar interactions measured.

To determine SE the goniometer is again used with a series of well characterised wetting liquids. The values of θ_C gathered by this method are then further interpreted using Young's equation, Equation 2- 1, (Zisman, 1964b, Long et al., 2005).

$$\gamma_{LV}\cos\theta = \gamma_{SV} - \gamma_{SL}$$

Equation 2- 1 Young's equation for calculation of SE, where γ_{SV}, γ_{LV}, and γ_{SL} are the surface tensions of the solid-vapour, liquid-vapour and solid-liquid interfaces, respectively.

The three probe liquids used in this study were, filtered water (FW), diiodomethane (DM) and ethylene glycol (EG), and using the θ_C values collected in the same method as described above, SE can be calculated from the Young-Dupre equation and the Good-Girifalco-Fowkes rule, see Equation 2- 2 and Equation 2- 3. This method is known as the acid-base method.

$$\gamma_s = \gamma_s^{LW} + \gamma_s^{AB} = \gamma_s^{LW} + 2\left(\gamma_s^{+}\gamma_s^{-}\right)^{0.5}$$

Equation 2- 2 Young-Dupre equation used to SE.

$$\gamma_l\left(1+\cos\theta\right) = 2\left[\left(\gamma_s^{LW}\gamma_l^{LW}\right)^{0.5} + \left(\gamma_s^{+}\gamma_l^{-}\right)^{0.5} + \left(\gamma_s^{-}\gamma_l^{+}\right)^{0.5}\right]$$

Equation 2- 3 The macroscopic SE equation from the Good-Girifalco-Fowkes rule.

where in mJ m^{-2}, FW: $\gamma_l^{LW} = 21.8,\ \gamma_l^+ = \gamma_l^- = 25.5;$ DM: $\gamma_l^{LW} = 50.8,\ \gamma_l^+ = \gamma_l^- = 0;$ and EG: $\gamma_l^{LW} = 29,\ \gamma_l^+ = 1.92,\ \gamma_l^- = 47$ (Neumann and Good, 1979) (Janczuk et al., 1999) .

Goniometry allows macroscopic determination of the average surface properties of the polymer thus it cannot be used at a microscopic level. Further to this the surfaces used must be chemically and physically inert with respect to all probing liquids used (Gulec et al., 2006).

2.3.1.2 Measurement Parameters

Contact angle measurements were made using a Krüss DSA30B contact angle goniometer. Using this instrument ϑc and γ can be determined. To investigate the liquid-surface interactions at highest resolution contact angles (θc at 23 °C) of small drops (5µL) (×6 on each substrate) of ultrapure water (FW; Millipore, 18.2 MΩ cm; surface tension γ_L = 73.4 mN m^{-1} at 18.8 °C, lit. (Kaye and Laby, 1995)= 73.05 mN m^{-1} at 18.0 °C), DM (> 99 %; γ_L = 48.7 mN m^{-1} at 18.8 °C, lit. (Kaye and Laby, 1995)= 50.76 mN m^{-1} at 20 °C) and EG(> 99 %; γ_L = 47.7 mN m^{-1} at 18.8 °C, lit. (Kaye and Laby, 1995)= 48.40 mN m^{-1} at 20 °C) placed on horizontal substrates (×2) were measured using a goniometer (Krüss DSA30B, Hamburg, Germany). Advancing angles (ϑ_A) (± 0.1 °; with syringe needle removed to enable curve fitting of drop-shape image) were obtained for both 'left' and 'right' contact angles at 20 – 30 s after placement of the drop (Adamson and Gast, 1997). Surface energies of substrates (γ_s) were calculated from the contact angles and the interfacial energies of the three probe liquids from Equations 1 and 2 (Zisman, 1964a, Long et al., 2005) using a Visual Basic program (Lamprou, 2009).

2.3.2 Fourier-transform Infrared Spectrometry

Fourier Transform Infrared spectroscopy (FTIR) is a widely used analytical technique which can help to clarify the chemical composition of the sample including functional groups and their orientation by consideration of their constituent bonds. The major vibrations of organic groups occur in general between 400 cm^{-1} and 4000 cm^{-1} (Alpert et al., 1970). As with all vibrational spectroscopy, IR and Raman spectra are a result of the interaction between the vibrational motions of the molecule itself and electromagnetic radiation. All

molecules can absorb infrared radiation at specific resonant frequencies which causes them to vibrate with increased amplitude around their covalent bonds. Each specific vibration is related to a specific absorption of a certain IR wavelength and thus the bonds or groups present. However, for a vibrational mode to be "visible" by IR analysis it must also be associated with a permanent change in dipole moment resulting from either a symmetrical or asymmetrical stretching, scissoring, rocking, wagging or twisting movement, Figure 2- 6.

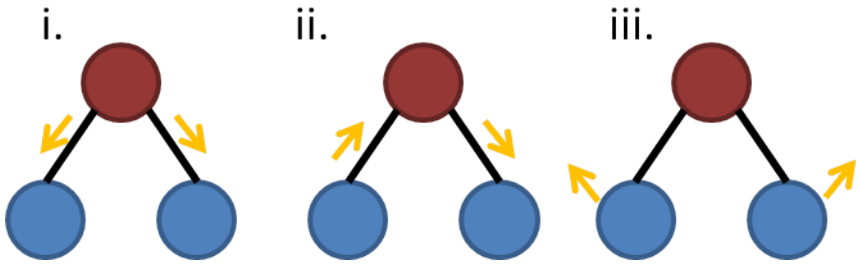

Figure 2- 5 Diagram of infrared dipole changes, i. symmetrical stretching, ii. asymmetrical stretching and iii. scissoring in a 3 atom molecule.

FTIR is the most common IR method and is a reference to the way in which data is collected and converted from an interference pattern into an interpretable spectrum. FTIR can identify chemical bonds present in a sample by producing a spectrum which is as unique as a fingerprint. In order to record an infrared spectra of a sample, a beam of IR radiation must first pass through the sample and be collected by a detector. The transmitted light can be analysed to determine how much energy was absorbed at each wavelength. FTIR examines all wavelengths simultaneously enabling the rapid collection of transmittance (%T) or absorbance (A) *versus* wavenumber (1/wavelength, cm^{-1}) sample spectra. Analysis of the spectra produced can aid in the identification of the molecule being analysed and its internal molecular structure however, this is technique is almost exclusively applicable to samples which only contain covalent bonds and is most effective if the sample is pure. Highly polluted samples produce complex spectra consisting of a mixture of molecular profiles which can be hard to distinguish. For polymer samples, IR spectra produced can provide information on the tacticity, chemistry, coil nature and the degree of polymerisation of the backbone however, if samples only differ slightly in molecular weight then the differences can be minimal (Koenig, 1999).

IR transmission measurements of solid polymer material were made using a Thermo Scientific Nicolet iS10 smart ITR, IR spectrometer with ATR capability. This eliminates any sample preparation and thus reduces analysis time. Spectra were recorded using in transmission mode. Spectra were taken post drying to ensure the polymer structure was accurately recorded. The results of this were used in to determine polymer structure, reaction efficiency and differences between the polymers synthesised using differing monomers and thiols. After initial analysis via inspection principal component analysis was carried out using SIMCA-P V11.0 to determine any patterns within the data which were not obvious.

2.3.3 Raman Analysis

Raman spectroscopy is a technique which allows the study of vibrational, rotational, and other low-frequency modes within a system (Gardiner et al., 1989). In contrast to IR analysis, Raman requires inelastic scattering -Raman scattering- of monochromatic light from a laser. The incident light interacts with molecular vibrations resulting in the energy of the laser photons being increased or decreased; this shift in energy gives information about the system. This technique is complementary to IR analysis as different information is collected. The polymer surface is illuminated with a laser beam and light from this illuminated spot is gathered by a lens before being sent through a monochromator. Elastic Rayleigh scattering is filtered out and the remaining collected light is dispersed onto a detector. Spontaneous Raman scattering is typically very weak, and thus the main drawback of Raman spectroscopy is the ability to separate the necessary, but weak, inelastically scattered light from the intense Rayleigh scattered light. Notch or edge filters are now used to reduce this problem. Raman scattering occurs when light interacts with molecule and causes an effect on the electron cloud and the bonds within it. Spontaneous Raman scattering occurs when a photon excites the molecule from its ground state to a virtual energy level. When the molecule then relaxes it returns to a different rotational or vibrational state emitting a photon. The energy difference between the original state and the final state leads to a shift in the emitted photon's frequency and thus inelastic scattering (Harris and Bertolucci, 1989). If after this process the final vibrational state of the molecule is higher, thus more energetic, than the initial state, then the photon produced will be shifted to a lower frequency, i.e. it possess lower energy than the incident photon. This shift is known as a Stokes shift. If the opposite is true and the final vibrational

state is less energetic then this is known as an Anti-Stokes shift. Raman scattering is inelastic as the energy transfer between the photons and the molecules is not equal. A graphical representation of this is shown in Figure 2- 7 for ease.

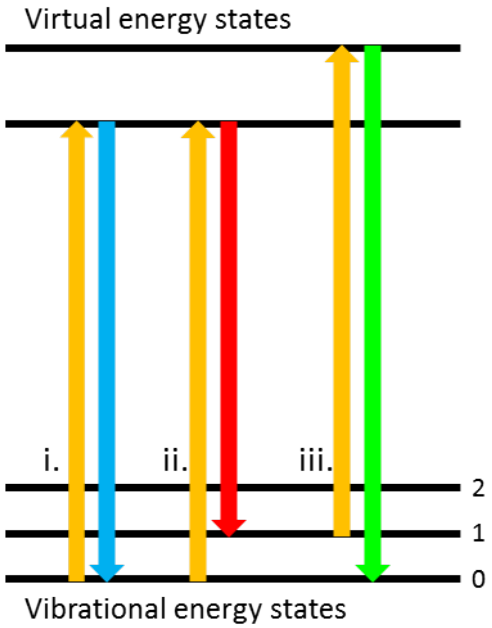

Figure 2- 6 Raman energy level diagram showing the states involved in the production of a Raman signal. i. Rayleigh scattering, ii. Stokes Raman Scattering and iii. Anti-stokes Raman Scattering. Rayleigh scattering is much more intense than Raman scattering (Ferraro et al., 2003).

Raman measurements were taken using a Thermo Scientific DXR Raman Microscope. These results were considered along with the IR data to determine structural and surface properties of the polymers synthesised. Raman and IR peaks identified using published tables (Socrates, 2004). As with the IR spectra, after initial inspection principal component analysis was again carried out using SIMCA-P V11.0 to determine any patterns within the data that are not obvious. After primary analysis, the spectra were re-run with any outliers removed in order to allow easier examination of the bulk of the data.

2.3.4 Atomic Force Microscopy

Atomic force microscopy (AFM) is able to produce a pseudo-three-dimensional image of the surface topography of a sample in liquid or gaseous environments over a range of temperatures (BLANCHARD, 1996, Morris et al., 1999, Jaschke et al., 1996). This allows analysis of biological materials in their native conditions. In addition to imaging, AFM is

capable of measuring nano-mechanical surface properties including adhesion, friction and roughness, thus can be used in the investigation of surface cleanliness, corrosion and indentation (Ricci and Braga, 2004, Miyagi et al., 2008).

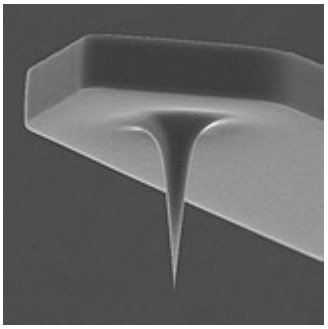

Figure 2- 7 Electron microscope image of an AFM cantilever and tip. Cantilever width ~40µm (www.team-nanotec.de).

AFM is a member of the scanning probe microscope family and uses a mounted rigid silicon nitride cantilever which has on the end a sharp tip (typically 2 µm long and <20 µm radius), see Figure 2- 8 (Smith, 1999). The AFM then analyses the contact forces between the surface of interest and this probe to determine the properties of the material including its mechanical characteristics (Meyer et al., 2004). This cantilever is brought very close to the sample and as the tip touches the surface the force created causes the cantilever to bend. This small movement is detected optically by the deflection of a laser beam which is reflected off the upper side of the cantilever; see Figure 2- 9. The tip of the cantilever is then scanned across the sample surface and the variations in topography are recorded and processed to form a 3D image of the surface structure (Bowen et al., 2001). The contact force between the cantilever tip and the surface is calculated using Hooke's law.

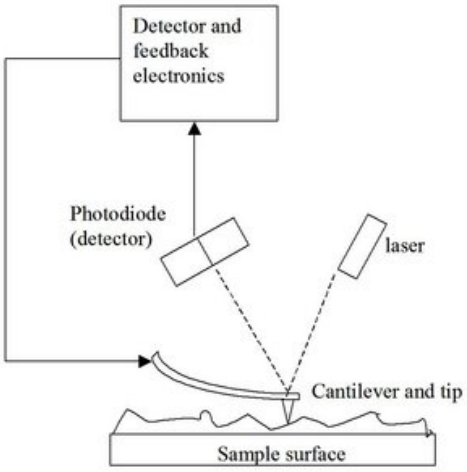

Figure 2- 8 Schematic depicting the main components of an atomic force microscope (www.emt.uni-linz.ac.at).

AFM can produce images from robust solid samples with atomic resolution relatively easily, however, the analysis of soft biological samples is more troublesome. This is because the forces created by the rastering of the AFM tip across the sample surface during imaging can damage the soft and mobile surface being studied rendering the results useless. To overcome this problem, tapping mode AFM was developed; this works using the same principle as conventional contact AFM however, during the analysis the cantilever tip is not kept in constant contact with the sample, but is instead tapped across the surface reducing the lateral forces exerted on the mobile elements present and thus reducing destruction (BLANCHARD, 1996, Sundararajan and Bhushan, 2002). AFM technology is not only a useful imaging technique but also can be used to determine forces of attraction and adhesion between biological materials and solid surfaces (Hugel and Seitz, 2001). The forces measured between the unaltered tip of the AFM probe and the surface can be attributed almost entirely to van der Waals interactions and these can be used to determine the force of adhesion between the tip and the surface. The use of an unmodified tip does not provide any biological information but it is relatively simple to chemically modify the AFM tip to make the interaction being measured highly specific to the system being analysed. The tip can be made highly hydrophilic or hydrophobic simply however, in order to achieve the most interesting results it must further be altered to have biological functionality (Jalili and Laxminarayana, 2004). AFM is fast becoming vital in the characterisation of the surface chemistries of many materials. For polymeric biomaterials in particular, the information gleaned from analysis using a biologically altered tip could be vital in determining the

interaction between the polymer and the bacterial or extracellular matrix proteins it will be in direct contact with within the course of its use.

AFM was used to investigate the surface properties of each of the acrylate polymers synthesised post coating onto glass coverslips. AFM can be used in two formats to give the maximum output of information, surface roughness measurements can give an accurate picture of the polymer surface rendering an image comparable to scanning electron microscopy (SEM) and surface adhesion can be determined, a measure of the adhesiveness of the polymer surface. All AFM measurements were measured using a Veeco MultiMode (TM) Scanning Probe Microscope (SPM) with NanoScope IIID Controller encompassing both tapping mode and contact Mode AFM. These measurements can be aquired in either air or liquid under different temperatures and humidity ranges.

2.3.4.1 Force Measurements

Force measurements were taken using the AFM described previously. Calibration of the system was undertaken using a hard silicon reference sample supplied by the manufacturer; this calibration is valid until the system is altered by moving the laser position etc..

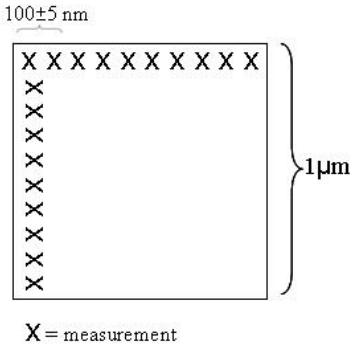

Figure 2- 9 AFM measurement grid, 10 x 10 square, 1 µm x 1 µm dimensions

Cantilevers used in this research were Bruker NP-10 (C) silicon nitride probes, length 120 µm, width 20 µm, frequency 56KHz and spring constant (k) 0.32N m^{-1}. The AFM was operated in contact mode to obtain all measurements. For each polymer sample, 100 measurements were taken with ramp size 800 nm in a 10 x 10 square area (Figure 2- 10). On each polymer surface, 3 areas were analysed, all 1000 nm apart, to determine sample homogeneity over the surface. Force curves were acquired for each measurement by

monitoring the deflection of the cantilever as it lifted away from the polymer surface, via the alteration in laser position, as a function of the tip-sample distance. For a full graphical explanation of the forces being measured, refer to Figure 2- 11.

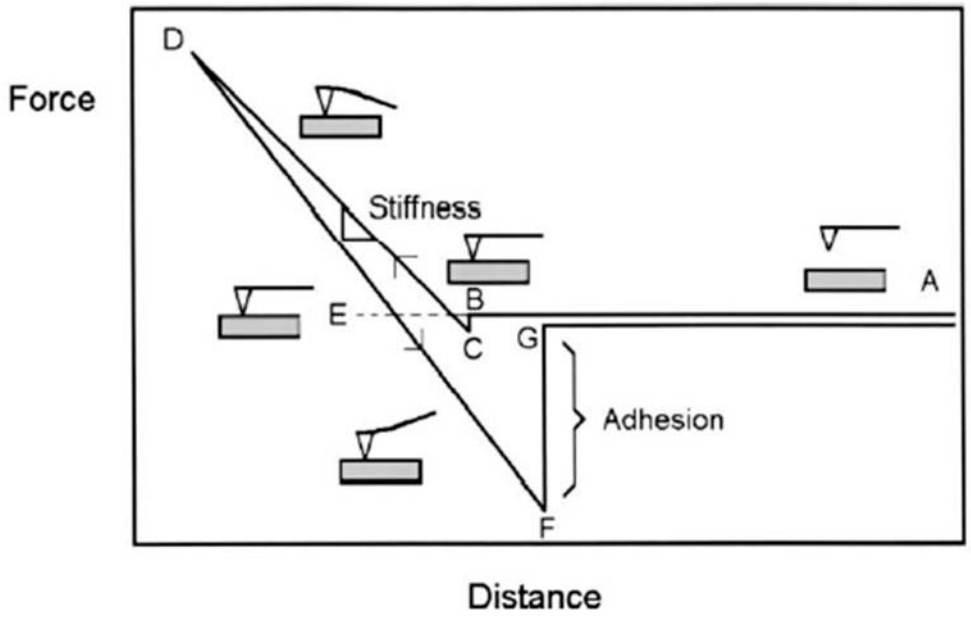

Figure 2- 10 AFM idealised force-distance curve. From A-B tip approaches polymer surface, B-C tip attracted to surface (van der Waals interactions), C-D tip forced into the surface, D-F tip withdrawn (at E no net forces between tip and sample), E-F tip is adhered to the sample surface and at point F it is suddenly released, F-G is where the adhesion information is gathered (Beech et al., 2002).

2.3.4.2 Surface Roughness

Measurements made by rastering the AFM tip over the surface of the polymer and the minor deviations in the laser beam, due to the vertical movement of the cantilever, were recorded and analysed using a computer program to give degree of roughness.

2.3.5 Differential Scanning Calorimetry

Differential scanning calorimetry (DSC) is the measurement of the alteration of the heat flow rate to the samples and to a reference sample while they are subjected to a controlled temperature program (Höhne et al., 2003). This is a thermal analysis technique which is based on the principle that accompanying the transformation of the physical state of a

compound is the absorption of heat. The instrumentation used consists of two separate pans: a sample pan (containing a small amount of the solid polymer sample) and a reference pan (treated in the same manner, but left empty). Both pans are placed on individual heaters, which are heated at the same rate. When a physical transition occurs, such as crystallisation or glass transition, thermal energy must be added to the sample pan to keep both pans at the same temperature (Merritt and Settle, 1981). The amount of energy used to keep both pans at the same temperature is recorded as a function of time and temperature, (δH/δT), and results in a trace which can be interpreted to determine physical changes in the sample, see Figure 2- 12.

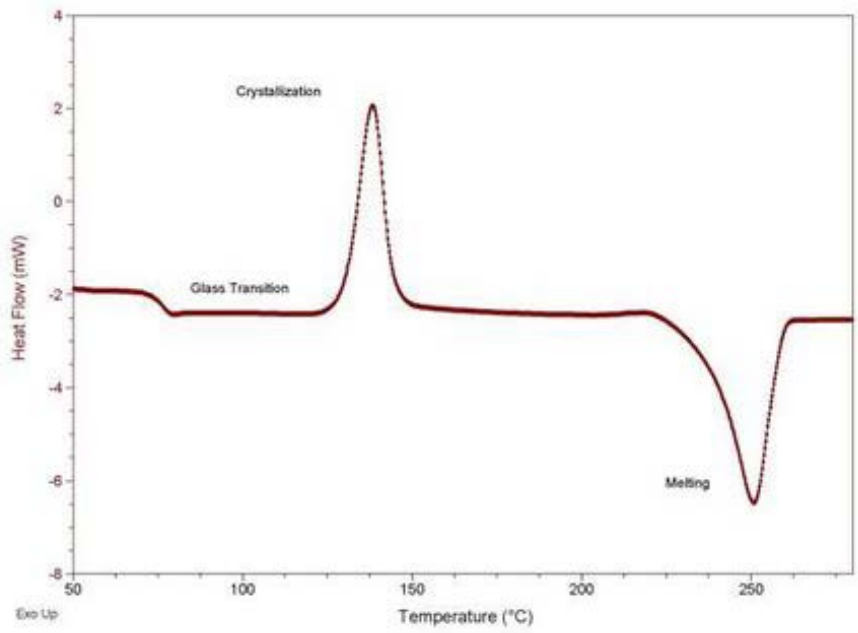

Figure 2- 11 Typical crystalline DSC trace labelled with the common changes in a crystalline polymer sample. These include glass transition temperature, shown by a decrease in the baseline, which is due to the sample undergoing a change in heat capacity where no formal phase change occurs. This is followed by crystallisation, resulting in the sharp peak and finally melting shown by a large negative peak. Some of these features observed on the trace can also be followed by use of a microscope (Laboratory, 2010).

The area under each of the peaks in the trace is directly proportional to the enthalpic change recorded and its direction around the y axis indicates whether the thermal event is endothermic or exothermic. DSC is used predominantly in polymer analysis to detect and quantify melting points and crystallisation behaviour. Polymer DSC is, in general, much more complex than its crystalline counterpart. In order to combat any solvent effects, polymer samples are, in general, heated twice to burn off any remaining solvent and

starting materials and clarify the points of interest. Samples were either analysed using a Jupiter Netzsch STA449C DSC system fitted with a Netzsch CC200 supply system and a Netzsch TASC 414/4 controller or a Mettler Toledo DSC822^e (TGA/SDTA851^e) DSC system. These were chosen for the differing polymer types depending on their temperature range.

2.3.5.1 DSC Sample Preparation

Sample preparation was kept constant despite DSC instrument employed and polymer type. DSC pans were weighed and punctured; a small hole was made in the lid using a pin. Between 2 and 5mg of polymer were added into the bottom of the pan, covering as much of the base as possible and not touching the lip. Pan was then reweighed including the sample to allow the sample mass to be calculated, this must be done to at least 4 decimal places. Finally the ends of the pan were crimped over the lid, ensuring a reasonable amount of force is applied to seal the edges but not destroy the base of the pan.

2.3.5.2 Temperature cycles

All samples run in this study were temperature cycled: this is common practice for polymer samples to ensure that all solvent is removed and an accurate portrayal of the transitions occurring is recorded. Branched acrylate samples were analysed according to the method stated in (Chisholm et al., 2009) by heating samples from 25°C to 200°C at 10°C min^{-1} before cooling to 30°C at 10°C min^{-1} and then reheating at 10°C min^{-1} to 350°C. Thiol-ene polymer samples were analysed using a method based on (Shin et al., 2008) samples were heated from 0°C to 200°C at 10°C min^{-1} before cooling to 0°C at 10°C min^{-1} and then reheating at 10°C min^{-1} to 200°C. All DSC data was processed using software linked to the instrumentation.

2.4 Principle Component Analysis

Principle component analysis (PCA) is a statistical analysis tool which can reduce the variability within a large dataset to a much smaller number of effective variables. Imagine a group of 100 people, from each person you take a number of measurements in an attempt to see which different measurements (variables) are related to one another. It is simple to plot weight versus height and observe an overall trend in these data; it is also possible to plot the weight, height and ethnicity of the subjects in a 3 dimensional manner which may

again cause a grouping of certain data points. However, if the aim is to compare all of the variables measured this would be unfeasible using this simple plotting approach. PCA uses complex mathematics to compare every value collected from every variable and plot them all in 'n-dimensional space'. Although this sounds complex it is based on the same basic principle as the simple 2D plotting approach. The dimension which accounts for the largest variation in the data will be selected as the first principle component (PC1), the next component will be an orthogonal axis which will account for the second most variation within the data (PC2) (Gendrin et al., 2008). This is shown in Figure 2- 13. Once these principle components have been generated the method creates two more important pieces of data: the scores and loadings plot. Scores plots are based on the samples present whilst loadings represent the variables under investigation. It is these which are used to show the grouping of the data and to deduce which variable has the greatest effect on the results. Figure 2- 14 shows the data from the last diagram but now displayed as if they were plotted from the PCA. These data is the value of the scores for the first two principle components of each sample in the data set. The data appears to be grouped into three separate sets. Finally an inspection of the loadings will show which variables have made the greatest contribution to this grouping, e.g., weight, height and exercise per week. PCA was used throughout this study in order to determine groupings within collected data.

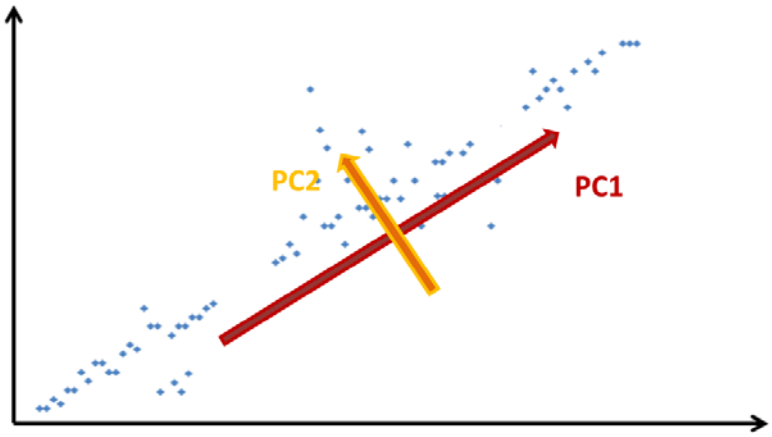

Figure 2- 12 Plot showing the data encapsulated by principle components 1 (PC1) and 2 (PC2). PC1 describes the majority of the variation in the data and the orthoganal PC2 describes the next most variation.

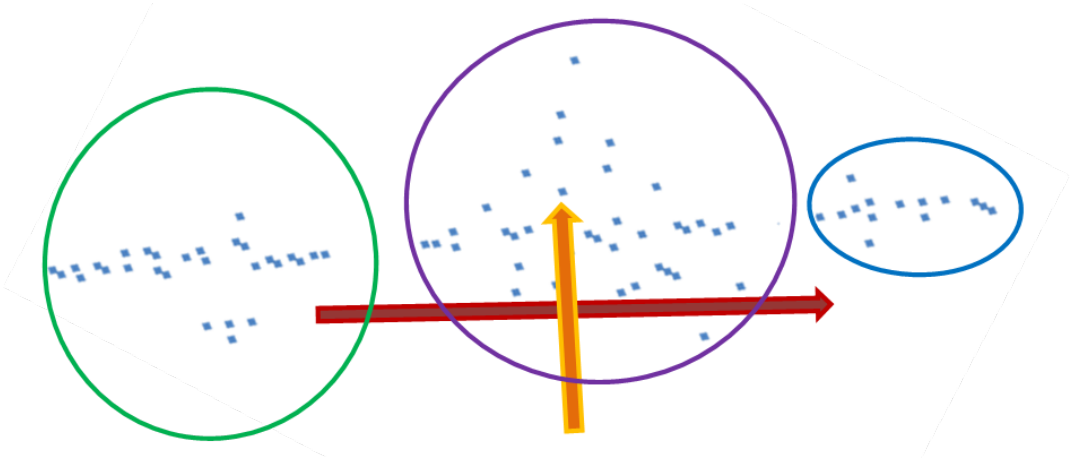

Figure 2- 13 Diagram to show the groupings within the sample data which are illustrated by the scores and loadings plots.

2.5 Bacterial Testing

Any novel polymer which is to be used as a biomaterial must be rigorously tested to ensure patient safety and applicability. Bacteria are robust organisms which can form difficult to eradicate biofilms and thus can be used in the first instance to gather information about the surface characteristics of a novel polymer. After these initial experiments, extracellular matrix proteins and cells can be used to determine the full polymer functionality within a patient. Whether the polymer promotes or deters bacterial biofilms, cellular or protein absorption and growth can then be used to suggest the most beneficial use for the polymer as a biomaterial, i.e., as a cell scaffold or anti-fouling prosthesis. To investigate the proliferation of biofilms on the surface of the synthesised polymers, known biofilm forming bacteria, *Pseudomonas aeruginosa*, *Staphylococcus aureus* and *Bacillus subtilis*, were cultured in 12 or 24 well plates in the presence of the polymers. A method, adapted from Pitts et. al. (Pitts et al., 2003), was used to determine quantitatively the level of bacterial growth supported by the surface.

2.5.1 Media Preparation

Luria Bertani (LB) media was prepared by the accurate addition of Tryptone (10 g), yeast extract (5g), sodium chloride (10g) and deionised water (1L) into a 2L flask before being autoclaved at 120˚C to ensure sterility (Sambrook and Russell, 2001). LB agar plates were also used extensively in this research and were prepared in the same manner but with the

addition of agar (20g) to the flask. These were again autoclaved to 120˚C before being poured (20-25ml) into 90mm diameter, 15mm deep sterile petri dishes for refrigeration and later use.

2.5.2 Preparation of Culture Plates

The 12 and 24 well plates were used in order to incubate the thiol-ene discs and polymer coated glass coverslips, respectively. These were both prepared in a similar manner, however, volumes were adjusted to ensure the surface of interest was covered.

2.5.2.1 24 Well Plate Preparation

Sterile LB media (1 ml) was added aseptically to each well of a labelled 24 well culture plate before the polymer coated coverslips were added using flamed forceps. Finally bacterial overnight culture (10 µL) was added to each well (1:100 dilution factor) before being warmed to 37˚C and left statically overnight to promote biofilm formation.

2.5.2.2 12 Well Plate preparation

Methodology similar to culturing of acrylate polymer samples however, due to larger polymer discs and therefore well plate volume, more media and stain were required to cover the surface and retain the reproducibility of each sample. In this instance sterile LB media (2ml) was added aseptically to each well of a labelled 12 well polystyrene culture plate before the polymer discs were added using flamed forceps. Bacterial overnight culture (20µL) was then added to each well (1:100 dilution factor) before being warmed to 37˚C and left statically overnight to promote biofilm formation.

2.5.3 Crystal Violet Staining of Bacterial Growth

In order to test the presence, and extent, of biofilms existing on a variety of surfaces a method must be used which can quickly screen a sample set and is repeatable. Until recently the methodology in place for this testing, viable cell plate counting, has been slow and very labour intensive. To combat this and make the process more high throughput a new methodology has been deduced using crystal violet staining to allow a quantitive measurement of biological material adherent to the biomaterial surface. This method will

primarily focus on the growth of prolific biofilm forming bacterial strains on novel polymer surfaces, including *Pseudomonas aeruginosa* and *Staphylococcus aureus*. The level of biofilm formation was measured through crystal violet staining according to the method of (Pitts et al., 2003). Briefly, following 24hr of incubation of bacterial strains with polymer and controls, media was removed from each well using a pipette before 0.5ml of 0.3% Crystal Violet (CV) solution was added to each well. After 5min incubation at room temperature the stain was removed from the well by pipette. The polymer coated coverslips were removed from the wells using forceps and washed in copious deionised water before being placed into a new, clean labelled well plate. This washing ensures that only adhered biofilm was measured and no free floating bacteria contaminated the results gathered. Aliquots (1ml) of ethanol were added to each well and left for 30mins to allow all stained bacteria to be taken into solution. Each solution was finally added into a disposable semi-micro cuvette and analysed using a Nanodrop UV-vis spectrometer at 580nm. Control samples were treated in exactly the same manner as all other polymer testing. The positive control used was cell culture polystyrene with 1:100 ratio bacteria stained with CV and removed with ethanol as previously. Negative control utilised the same set up but with not addition of bacteria.

2.5.4 Green Fluorescent Protein Bacterial Growth

In order to combat problems using stains, which can be unreliable and adhere to non-bacterial material altering the experimental outcome, green fluorescent bacteria (GFP) expressing bacteria can be used. GFP is a protein that exhibits a bright green fluorescence when exposed to light in the blue to ultraviolet range, Figure 2- 15 (Prendergast and Mann, 1978). It is composed of 238 amino acid residues and although many other marine organisms have other comparable green fluorescent proteins, GFP refers specifically to the protein first isolated from the *Aequorea forskilea* jellyfish (Tsien, 1998). The GFP gene has been introduced and expressed in many bacteria and thus is a useful tool for the imaging of bacterial colonies on surfaces of interest. Initial experiments were trialled with *Pseudomonas aeruginosa* PA14, expressing GFP constitutively to test thiol-ene disc biofilm proliferation.

Figure 2- 14 Expression of GFP in E. coli. Only the right hand side bacteria possess the GFP expression plasmid. Bacteria were imaged during irradiation long-wave UV source (Chalfie et al., 1994).

Bacteria were grown on the thiol-ene polymer discs in the same manner as previously and visualised using a using a Nikon SMZ1500 fluorescence microscope using a FITC filter (Excitation 494 nm; Emission 518 nm). Exposure times were 20 ms for phase-contrast and 100 ms for fluorescence imaging. Images were analysed using IPLab scientific imaging software version 3.7 (Scanalytics, Inc., Rockville, USA). Positive controls were cell culture polystyrene as previously but negative controls were thiol-ene discs with no added bacteria.

2.5.5 Plate Counting

In order to overcome problems of staining and innate polymer fluorescence a novel biofilm quantification methodology had to be developed. This was achieved by modification of the method stated in (**Cheung** et al., 2004).

2.5.5.1 Preliminary experiments

Staphylococcus aureus and *Pseudomonas aeruginosa* were grown on individual clean glass coverslips for 24hrs as previously before media was removed by pipette. Glass coverslips were removed from wells using flamed forceps and submerged in 10ml of LB media in a universal bottle. The bottle was vortexed to remove the adherent biofilm for 30, 60, 90, 120, 150, 180 and 240 seconds and after each time period 10µl of media was removed and dropped onto a LB agar plate. Plates were allowed to grow at 37°C overnight before individual colonies were counted and the optimum time for biofilm removal calculated. To ensure that all the biofilm was removed these plates were cultured and counted, after a

steady state was reached it was decided that this was the optimum time for agitation. These experiments were used to determine the reaction conditions for latter polymer coated coverslip experiments.

2.5.5.2 Polymer experiments

Using preliminary experiments as a guide thiol-ene polymer coated coverslips were cultured overnight as previously. Coverslips were removed using flamed forceps and added to 10ml of LB media. Each sample was vortexed for 30 s before 10µl aliquots were dropped onto LB agar plate in quadruplicate, see Figure 2- 16. For positive and negative controls cell culture polystyrene could not be used as previously as it could not be added into the bottles required for vortexing. To overcome this issue clean glass coverslips were used as both positive and negative controls for this experiment. After incubation at 37°C overnight individual colonies were counted to determine biofilm proliferation on different polymer surfaces. Biofilm quantity was finally calculated by use of dilution factors. Using basic geometry the surface area of each glass coverslip was calculated to be 1.33 cm^2, disc was only spin-coated on one side. As this method only takes into consideration the adherent bacteria the original dilution factor of the overnight culture is irrelevant. Therefore, the number of bacteria present in the 10 ml bottle is $10e^{-1}$. 1 1000^{th} of this was used in each spot, 10µl, so to determine the number of bacteria per disc the number of colonies is multiplied by 1000 and then by 10e-1, the number of bacteria in the bottle. Finally this was dived by the area of the disc to give the number of colonies per polymer sample.

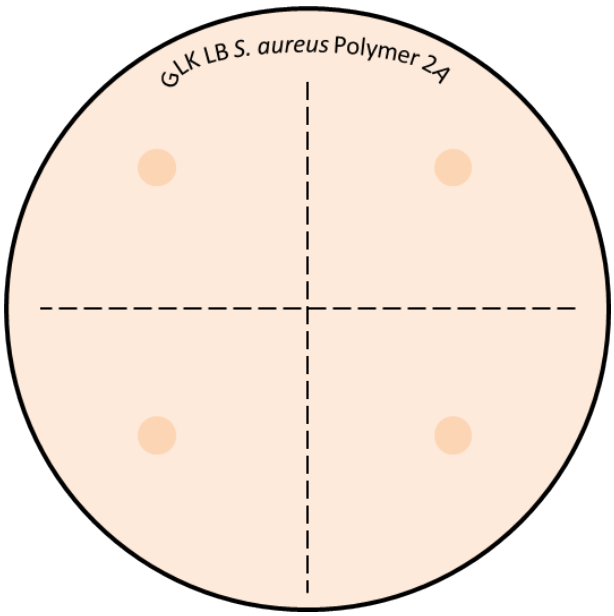

Figure 2- 15 Example of plate counting methodology. Each polymer cultured in triplicate and then plated in quadruplicate in order to give 12 replicates and statistical validity.

2.5.6 Hyperspectral Imaging for Biofilm determination

To determine biofilm proliferation on polymers, in a high throughput manner, without the use of staining or fluorescence hyperspectral imaging (HSI) was employed. HSI techniques have become useful in pharmaceutical research during the last decade due to their non-destructive nature and rapid data collection (Amigo, 2010). In this work HSI was used in order to visualise the relatively large microbial communities forming the biofilm adherent to the polymer surface. Using the work published by Polerecky et al. a methodology for the quantification of a bacterial biofilm was applied (Polerecky et al., 2009).

2.5.6.1 HSI

A hyperspectral image is one which contains a two dimensional spatial image and also contains a full set of spectral information at each pixel. This generates a cube of data which is erroneously called a hypercube (Ravn, 2009, Gowen et al., 2008). Imagine a deck of cards, each card has a picture, or representation, on its surface and as you move through the deck you can see a number of slight variations on that first image. In many respects this is analogous to a hyperspectral image; in a hyperspectral image you have a simple 2 dimensional display which may look much like something taken with an standard digital camera. However much like the deck of cards, a hyperspectral image has a number of

'layers' and each layer is the same image as the top layer but the intensities are different. These layers are showing the different wavelengths of information captured using this technique.

2.5.6.2 Hyperspectral Camera

While there are a number of different approaches to HSI they all involve the same basic instrumentation. The detector is the 'camera' as it would traditionally be considered; photons hit the detector which causes the electrons in the silicon to be stripped away which generates small electrical currents that are registered as counts. The detector is specific to both the type of HSI and the wavelength range being used; no one detector will work for all wavelengths and is a small box situated at the far end of the camera. The most important element of the camera is what is placed in front of the detector. Depending on how the system works this will be a very different piece of instrumentation. Some set ups use filters to restrict the wavelengths of light that hit the detector but for the work carried out in this study a spectrograph, which records the full wavelength spectrum, but only one thin line of pixels at a time, was used. The spectrograph is made up of three major components; the first is an objective lens which is used to focus the incoming photons in the same way as in a standard camera. The other two components are a series of thin slits and diffraction gratings, the thin slits are used to narrow down the broad beam of photons into a single narrow beam, with a height equal to a single pixel on the detector. This narrowed beam then passes through the diffraction grating which causes the single beam of photons (of all energies) to be split into a spectrum (in the same manner as a prism would split light in a visible camera) (Gendrin et al., 2008).

This spectrum will finally hit the detector such that every pixel has a full spectrum of information. An image of the camera set up used in these experiments is shown in Figure 2- 17. When using a spectrograph it is imperative to move either the camera or the sample, this is because the setup can only image a single narrow line on the target at one time so in order to achieve a full image of the specimen it must be built up from a number of these narrow lines. During the experiments carried out in this study, the sample was moved using a motorised stage which allows the user to determine not only the speed of movement but also the distance travelled.

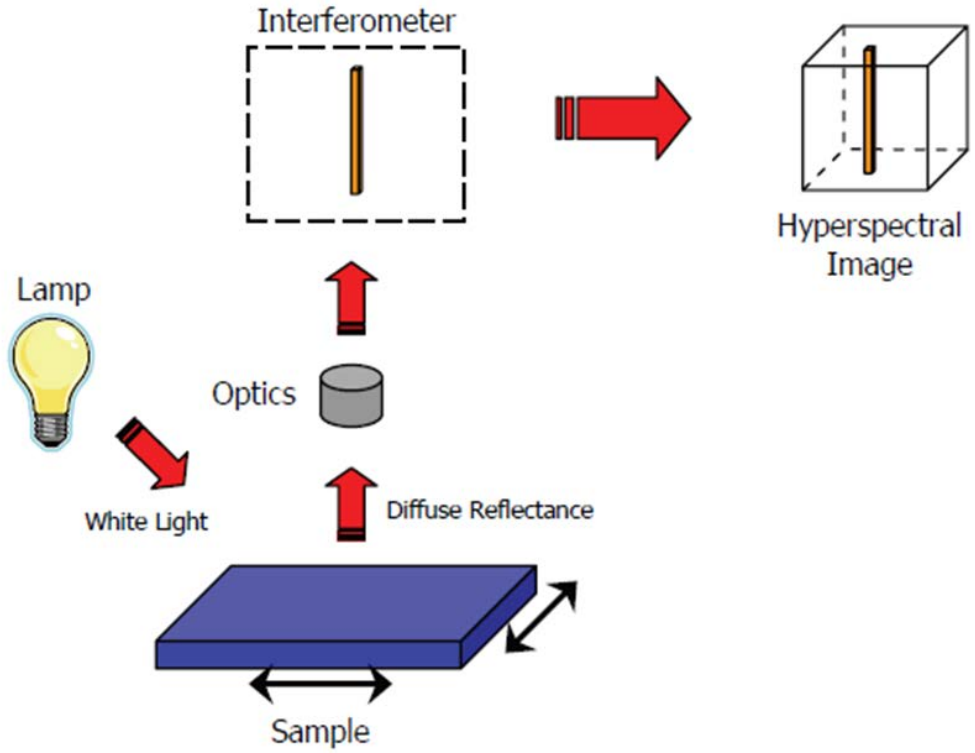

Figure 2- 16 Schematic of HSI camera used throughout this study. Essential components identified (Burger, 2006).

2.5.6.3. Imaging Parameters

Data was captured in the Hyperspectral Imaging centre, Strathclyde University. The system in situ consists of a spectrograph (Specim V10E, 400 - 1000 nm) attached to a detector (Hamamatsu ORCA 05G, 300 - 980 nm). In order to move the sample there is a MDrive 17 plus motor which powers the Zolix TSA2000-BF motorised stage. Imaging was performed using SpectraSENS software to create the hypercube. The images were captured using an exposure time of 100ms with 2x2 binning being used on the data. The motorised stage was controlled using code written for MATLAB with a total imaging distance of 125mm with the stage moving at a speed of 1.5 mms^{-1}.

2.6. Material Properties

In order to determine the behaviour, before and after swelling, of the polymers synthesised their material properties must be tested. Preliminary tests just use increasing mass as an indicator of the volume of water imbibed before more specific measurements were carried out.

2.6.1 Polymer Swelling

Polymer swelling is a well-established phenomenon, so much so it has given rise to the term hydrogel. Hydrogels are superabsorbent hydrophilic polymers which are made up of a network of polymer chains allowing them to have flexibility similar to natural tissue, due to their substantial water content (Peppas, 1986). During hydration water imbibes into the polymer matrix in a specific manner via the erosion front though the diffusion front and finally into the dry core, Figure 2- 18 (Colombo, 1993). As swelling progresses the described fronts move from the outside of the polymer matrix inwards and eventually the swelling and dissolution fronts synchronise. This is thought to allow constant drug release in situations where this is pertinent and the velocity of these fronts moving controls the polymer swelling behaviour (Colombo, 1993). Modelling of this swelling behaviour, and subsequent drug release, has been carried out in order to fully understand the role of the polymer matrix in drug dissolution (Harland et al., 1988).

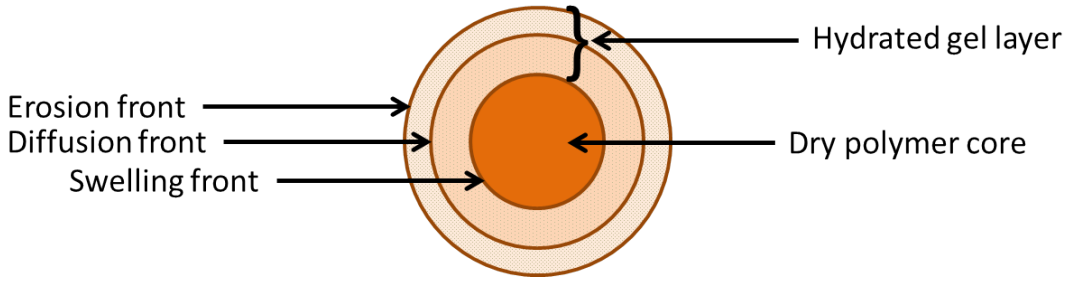

Figure 2- 17 Schematic of a hydrophilic hydrogel polymer matrix during hydration. Hydrated gel layer fronts illustrated (erosion, diffusion and swelling) and dry polymer core (Colombo, 1993).

The initial testing of polymers in this study was carried out in order to determine the volume of water imbibed over time and whether this swelling caused chain detangling and thus polymer breakdown (Brochard and Degennes, 1983). Method used simply recorded

the mass and dimensions of the polymers before and after water submersion over a period of days and recorded changes in physical form. After these initial swelling experiments further analysis of polymers post submersion in water was carried out using more sophisticated techniques.

2.6.1.1 Water Swelling

5 discs of polymers **1B** and **1C** which were to be initially investigated were synthesised using methodology previously stated. Polymers were dried and allowed to cool before being weighed and measured, height and diameter using callipers. All discs were submerged separately in 50ml of nano-pure water and placed in a 37°C environment with no agitation. 1 disc was removed from water every 24hours for 1 week. Upon removal the polymer discs were re-weighed and measurements were taken in same manner as before. Percentage changes in mass and dimensions were calculated.

2.6.1.2 PBS Swelling

Preparation of phosphate buffered saline (PBS) buffer was carried out using PBS tablets (P4417-50TAB, Sigma-Aldrich) and ultrapure water according to instructions given. The water swelling experiment was then repeated using 50ml of PBS buffer in exchange for ultrapure water.

2.6.2 Texture Analysis

Polymer swelling has been characterised using microscopy (Papadimitriou et al., 1993), proton NMR imaging (Rajabisiahboomi et al., 1994), confocal laser scanning microscopy (Adler et al., 1999) and light scattering techniques (Gao and Meury, 1996), amongst others, but these tend to be time consuming, difficult to perform and expensive so for this study texture analysis was used. Texture analysis (TA) been a versatile research and development tool widely used within in the food industry for some time and the application of this instrument in the pharmaceutical industry has significantly increased over recent years (Li and Gu, 2007). Texture analysis is a method of materials testing which makes use of a compression probe attached to a load cell, for instrument schematic see Figure 2- 19. Upon testing the analytical probe is lowered to the surface of the sample and then depressed to a

maximum force/distance depending on the desired information. This technique is capable of measuring the stress-strain profile for the material under investigation via this method.

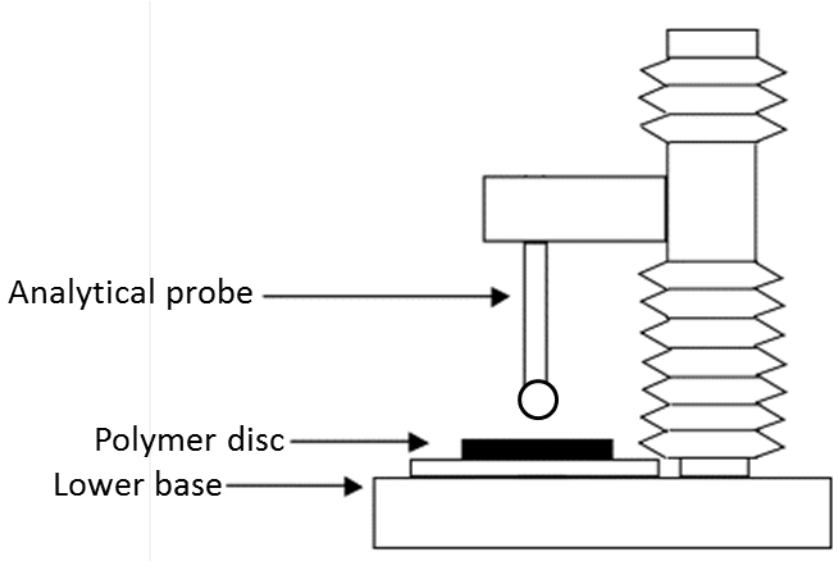

Figure 2- 18 Schematic of texture analyser set up, altered from image by (Repka et al., 2005)

In this study the texture analyser has been used in order to determine the differences between thiol-ene polymers pre and post swelling in water.

1.8.2.1 Texture Profile Analysis

In order to determine the mechanical properties of the polymeric systems in this study texture profile analysis (TPA) was employed (Jones et al., 1996) in an attempt to gain as much information about the polymer mechanical behaviour as possible. In this method, the analytical probe is depressed twice into the polymer with a defined recovery period between the end of the first and the beginning of the second compression. From the force-time curve generated, see Figure 2- 20 for example graph, many mechanical properties can be derived including hardness, compressibility, adhesiveness and cohesiveness (Jones et al., 1997). TA was used to determine the differences in mechanical properties between dry (synthesised thiol-ene polymers, no swelling) and wet (thiol-ene polymers post submersion in water for 24 hr) thiol-ene discs. TPA was used to allow the greatest volume of information to be gathered using this technique.

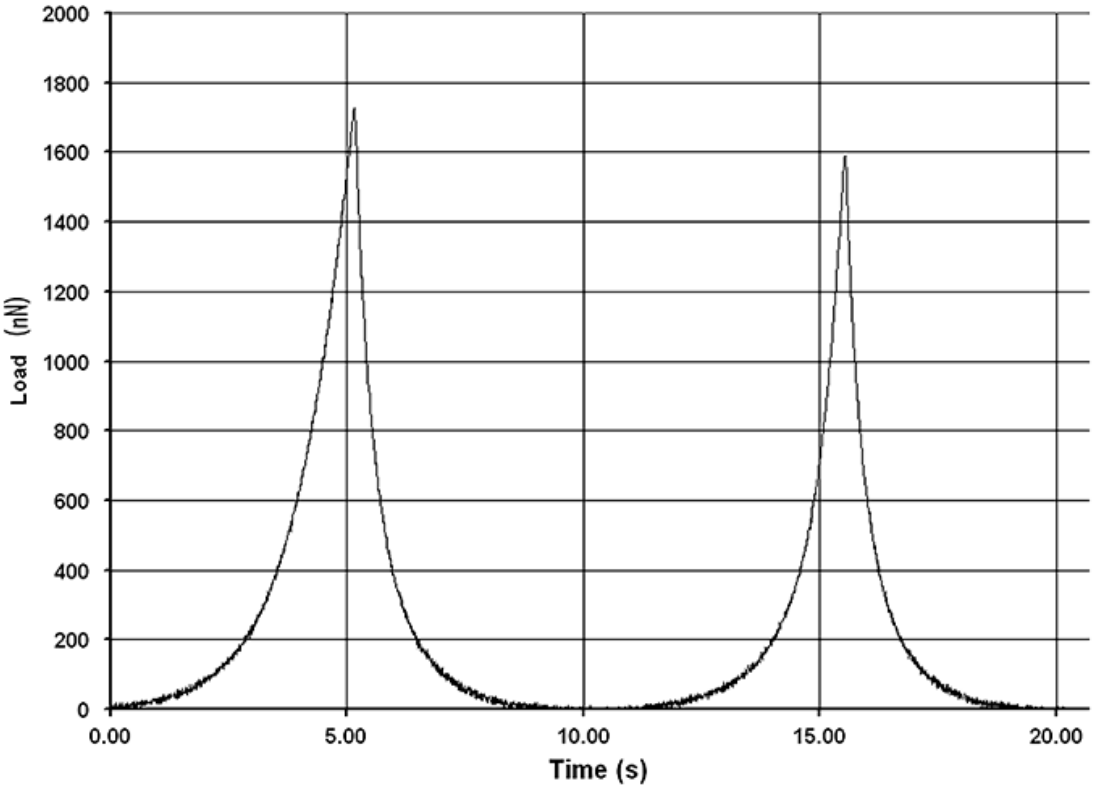

Figure 2- 19 A typical force-time curve from TPA measurement(Rosenthal, 2010).

2.6.2.1Methodology

Using a method adapted from that stated in (Mao et al., 2000) thiol-ene polymer discs were placed onto the metal base plate of a Stable Microsystems TAXT2 texture analyser and fixed in place using adhesive. Compressions were carried out using a round, 5mm diameter, stainless steel pin head probe, Figure 2- 21, in order to improve accuracy as smaller heads tend to have lower errors associated. For each polymer sample, performed in quadruplicate, compression speeds of 0.1 mms^{-1}, 1 mms^{-1} and 3mms^{-1} were tested. Compression depth was kept constant at 75% of the total depth of the polymer disc (1mm) and a 10s delay, in order to allow the sample to recover, was retained throughout testing. The probe was finally lifted from the sample surface at a constant 1mm/s. Samples were only tested once each to ensure that no change had occurred from previous compression. Thiol-ene polymer discs were swollen overnight at 37°C in 50ml of water and tested to determine any changes between the wet and dry polymer material.

Figure 2- 20 5mm stainless steel pin head probe used for texture analysis measurements (Technologies, 1998-2011).

2.6.3 Polymer Compression

This technique, commonly used in the analysis of cartilage of biomechanics, was used to determine the "stiffness" of the polymers before and after swelling. In simple terms this technique compresses the polymer between 2 plates and measures the forces associated with this change in material properties. Confined and unconfined compression testing was carried out using a Bose Electroforce 3200 material characterisation system which allows the differences between wet and dry polymers to be determined with a high degree of sensitivity. Young's modulus was calculated for both compression studies and compared to determine whether the polymer gained or lost rigidity upon swelling.

2.6.3.1 Confined compression

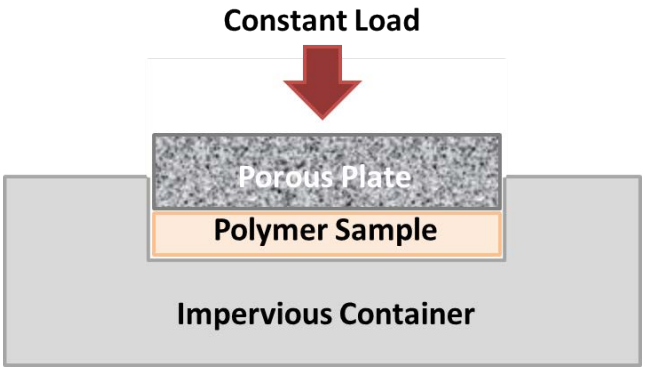

Figure 2- 21 Schematic of the apparatus used to perform a confined compression experiment on thiol-ene polymer samples. 5mm diameter polymer disc placed into the water filled well of an impervious container. A constant load is then applied via the porous plate. Any flow through the polymer will be vertical and can be measured (Mansour, 2008).

Confined compression was used in "creep" mode for this study. In this mode, a constant load is applied to a small disc of the swollen polymer through a porous plate, and the displacement of the polymer is measured as a function of time (Figure 2- 22). Confined compression allows the aggregate modulus and thus the permeability of the polymer samples to be determined along with the rigidity. Confined compression can only by carried out on water swollen samples thus all discs to be used were swollen as previously, in 50ml ultrapure water at 37°C for 24hr. For a confined compression study, the analysis rig is set up in a water bath, polymer thickness is first accurately measured before the polymer is compressed. This is done at 5% over 1min and then allowed to return to equilibrium over 40mins. The force of any water being forced out of the polymer matrix, or any water travelling through the porous medium into the polymer, is calculated. Using MATLAB for data analysis the stiffness of the polymer discs was calculated.

2.6.3.2 Unconfined Compression

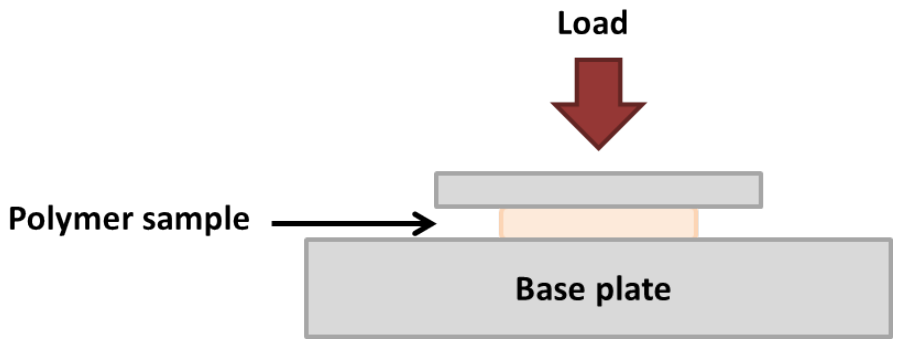

Figure 2- 22 Schematic of apparatus used to perform unconfined compression experiments on thiol-ene polymer discs. 5mm diameter polymer disc placed onto base plate with water based lubrication. Load is applied to displace the polymer and the force required to maintain this is measured.

In contrast to confined compression, this test is carried out on dry 5mm discs of polymer. Also known as relaxation mode, in this test, a constant displacement is applied and the force required to maintain this displacement is measured, set up shown in Figure 2- 23. Unconfined compression allows the calculation of Young's Modulus and the final stress upon the sample to be calculated. In order to further define the mechanical properties of the polymers being studied, compression testing, common for determination of cartilage properties, was employed. For this work, 5mm diameter polymer discs were punched from

original 20mm diameter discs, these were accurately cut in order to ensure all samples were identical for testing. For confined testing the polymer discs were swollen before the smaller samples were punched from them as cutting the disc may alter its swelling capabilities. Unconfined compression was carried out on dry polymer samples. 5mm discs were cut from original polymers before being lightly coated in a water based lubricant, to ensure disc doesn't stick to base plate. The thickness and the area of the sample were then accurately determined using the instrument before each sample was compressed to 5% of its total depth and this was retained for up to 40mins. Analysis of these samples was carried out by calculation of young's modulus, equations shown below, Equation 2-4.

$$final\ stress = \frac{applied\ force}{initial\ contact\ area}$$

$$Young's modulus = \frac{final\ stress}{strain}$$

Equation 2-4 Equations used to calculate Young's modulus from data collected during unconfined compression studies, applied force, initial contact area and strain data provided by instrument during analysis.

CHAPTER 3. ACRYLATE POLYMER SYNTHESIS AND TESTING

3.1 Introduction

Acrylate polymers are used extensively in biomaterials due to their ease of synthesis and the multitude of differing morphologies available on the addition of diverse monomers into the reaction mixture. Some of the most common acrylate polymers are poly (2-hydroxyethyl methacrylate) (pHEMA), poly(methyl methacrylate) (PMMA) and polymethacrylate (PMA). These have been used extensively for biological applications to date as they have varying properties; PMMA's hard morphology lends itself to applications such as bone cement (Callaghan et al., 2007) whilst pHEMA's hydrogel nature allows it to be used in soft contact lenses (Holly, 1975). Polymerisation of acrylates can be achieved using a variety of methods however, the most preferable allow the reaction to run to completion rapidly and at near ambient conditions (Peppas et al., 1985).

The majority of acrylate polymers which are currently being used for biomaterial applications at present are linear, or cross-linked linear, in nature. In this research project, the use and synthesis of branched acrylate species is being investigated to determine any novel biological responses due to their innovative morphology. The synthesis of branched polymers is readily achievable in both aqueous and organic media using monomers which were purchased from Sigma Aldrich. For this chapter of research well established methods were used to synthesise the polymers of interest using novel monomers before being tested by numerous analytical techniques to determine their chemical composition. Bacterial testing was carried out do determine the levels of biofilm proliferation upon differing polymer surfaces.

3.2 Methods

All synthesis and analysis methodologies are detailed in Chapter 2: Materials and Methods.

3.3 Results

Post successful synthesis of all branched polymers and their linear control analogues testing was carried out using a variety of analytical techniques. All results from these experiments are detailed below.

3.3.1 Polymer Synthesis

A library of 23 acrylate polymers generated via synthesis using differing proportions of the monomers and brancher species, refer to Figure 1- 9.

3.3.1.1 Branched Polymers

All branched polymers were successfully synthesised using the methods stated previously in chapter 2 and resulted in solid or gel type material which are plausible as biomaterials. Polymers resulting from monomer **1** were all translucent and yellow to light brown in colour with a strong odour which is potentially due to the amino groups present. These polymers were sticky in nature and tended to be more similar to pliable gels than those resulting from monomers **2** and **3**. Polymers synthesised from monomer **2** were also translucent, but in this instance, colourless and more solid in nature than monomer **1** polymers. In general, these polymers took longer to precipitate from toluene than monomer **1** or **3** polymers which could be due steric issues with the carbon ring in this monomer. Polymers from monomer **3** were opaque, white and much more solid than the product from any of the other monomers. The length of time taken to gain a solid product from these polymer types was also significantly less than the other suggesting a highly reactive monomer. All products of this synthesis were isolated from toluene before being dried for 12hr at 45°C and 70 cmHg to ensure the removal of all solvent. These were then stored in the fridge until testing was carried out.

3.3.1.2 Linear Polymers

In order to compare the branched polymers synthesised throughout this study to the linear polymers which are the predominant biomaterial at present, linear analogues of each monomer and brancher species were also synthesised. This was done via the same methodology as the branched species to limit variability and allow direct comparisons.

Linear monomer **1** was highly coloured, dark brown, and never achieved solidity. This polymer, or more accurately oligomer, was a semi-solid gel type substance and was highly sticky. This unusual morphology limited some testing. Linear polymers prepared from monomers **2** and **3** were similar to their branched counterparts in colour and opacity which was unsurprising. Both of these polymers were gel type solids which were malleable in nature. Linear brancher **x** and **y** polymers were the most facile to synthesise with the shortest reaction time, which was unsurprising as they are bi-functional in nature. These were again translucent, colourless solids with a more rigid structure than the monomer polymers.

Linear analogues were treated in the same manner as the branched polymer species and used to test the differences between linear and branched polymers.

3.3.2 Contact Angle Goniometry and Surface Energy

Contact angle measurements and surface energies were calculated in order to glean an understanding of the wettability of the polymers.

3.3.2.1 Contact Angle

Contact angle goniometry is a measure of the interaction between a solid surface and a liquid droplet. The lower the water contact angle the more wetting, or hydrophilic, the surface is and conversely the higher the water contact angle the more hydrophobic the surface. With the instrument used to carry out this analysis, angles below 10° are not able to be accurately measured as they are lower than the limit of angle detection. These results are noted as <10° in the table of results, Table 3- 1.

Table 3- 1 Advancing contact angles (□A) of the probe liquids (FW, EG and DIM) on glass surfaces (n = 6; 23 ˚C).

Surface	Mean advancing contact angles, ϑ_A / ˚		
	FW	DIM	EG
1+**x** 20%	81.8±11.5	37.6±3.1	45.8±6.2
1+**x** 30%	54.1±12.5	39.9±3.3	27.0±3.8
1+**x** 50%	<10°	15.1±1.0	16.6±0.7
1+**y** 20%	36.3±8.2	39.2±3.1	55.1±6.0
1+**y** 30%	80.7±5.6	37.7±2.5	75.4±2.1

1+**y** 50%	<10°	21.0±1.5	25.8±2.5
2+**x** 20%	79.6±9.4	45.3±5.3	68.0±1.6
2+**x** 30%	84.5±7	33.9±3.3	67.4±7.4
2+**x** 50%	52.7±1.8	51.8±3.1	35.5±1.2
2+**y** 20%	79.6±2.7	<10°	77.4±2.9
2+**y** 30%	43.5±10.4	<10°	<10°
2+**y** 50%	89.2±4.8	25.2±3.2	75.4±2.1
3+**x** 20%	82.7±0.7	45.8±2.2	30.4±4.6
3+**x** 30%	61.3±1.5	20.4±2.1	43.4±3.3
3+**x** 50%	96.5±3.1	20.4±2.9	66.0±8.0
3+**y** 20%	95.6±2.9	51.4±2.9	68.5±3.1
3+**y** 30%	83.1±1.9	21.6±3.3	59.1±6.5
3+**y** 50%	66.6±2.3	22.1±0.7	37.9±2.7
Linear **1**	24.5±9.2	32.5±3.4	57.4±2.9
Linear **2**	97.6±0.4	54.1±2.1	75.5±1.6
Linear **3**	64.6±9.2	36.0±2.6	62.9±3.1
Linear **x**	22.1±0.0	44.1±3	47.1±3.3
Linear **y**	40.8±6.2	34.2±1.9	27.4±3.3

3.3.2.2 Surface Energy

Using the average FW contact angles in conjunction with the average angles collected from the EG and DIM testing surface energies have been calculated; no standard deviations have been noted as these are calculated from a number of average and as such there is some variation in the data. These are shown in Table 3- 2.

Table 3- 2 Surface energies (γS) as calculated from the advancing contact angle values (n = 6; 23 °C).

Surface	γ_s^+ / mJ m^{-2}	γ_s^- / mJ m^{-2}	γ_s^{LW} / mJ m^{-2}	γ_s / mJ m^{-2}
1+**x** 20%	3.1	0.3	40.8	42.8
1+**x** 30%	24.4	0.5	39.7	46.3
1+**x** 50%	65.9	0.1	49.1	53.7
1+**y** 20%	69.1	1.3	40.0	59.1
1+**y** 30%	15.1	2.0	40.8	51.8

1+**y** 50%	70.4	0.2	47.5	55.1
2+**x** 20%	12.8	0.5	36.9	41.7
2+**x** 30%	7.2	0.7	42.5	46.9
2+**x** 50%	24.6	0.7	33.3	41.4
2+**y** 20%	16.7	4.5	50.0	67.3
2+**y** 30%	31.9	0.1	50.0	52.9
2+**y** 50%	6.2	2.1	46.1	53.3
3+**x** 20%	0.9	2.5	36.6	39.6
3+**x** 30%	21.1	0.1	47.7	50.5
3+**x** 50%	0.6	0.6	47.7	48.9
3+**y** 20%	1.3	0.0	33.5	33.5
3+**y** 30%	5.2	0.3	47.3	49.9
3+**y** 50%	12.8	0.0	47.1	48.2
Linear **1**	87.6	2.8	43.2	74.3
Linear **2**	1.9	0.1	32.0	32.9
Linear **3**	29.1	1.1	41.6	53.0
Linear **x**	80.3	0.5	37.5	50.7
Linear **y**	41.7	0.0	42.4	44.8

3.3.3 Fourier-transform Infrared Spectrometry

IR transmission spectra were obtained for all acrylate polymers post isolation and drying. Spectra were examined to determine significant differences between the monomers used and the proportion of brancher added to the reaction.

3.3.3.1 Monomer 1 polymers

Polymer spectra from samples containing monomer **1** and brancher at 20 or 30% exhibited similar features. The 50% brancher species were seen to differ from the lower proportion polymers with a possible broad OH peak. The linear polymer of monomer **1** and the monomer, as purchased from Sigma Aldrich, were also compared to the polymers to

determine any differences. The IR spectra collected for the polymers using each brancher are shown below, Figure 3- 2 and Figure 3- 3.

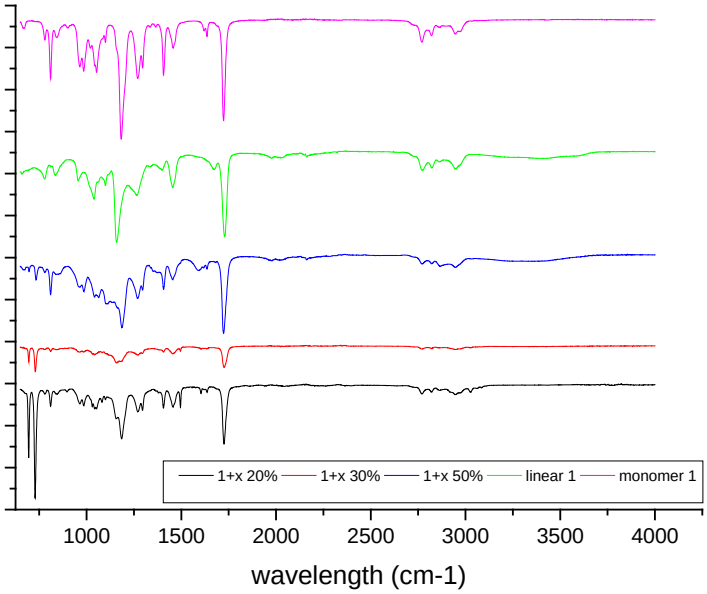

Figure 3- 1 IR transmission spectra collected from polymers synthesised from monomer 1 and brancher x, linear polymer and monomer 1 added for comparison.

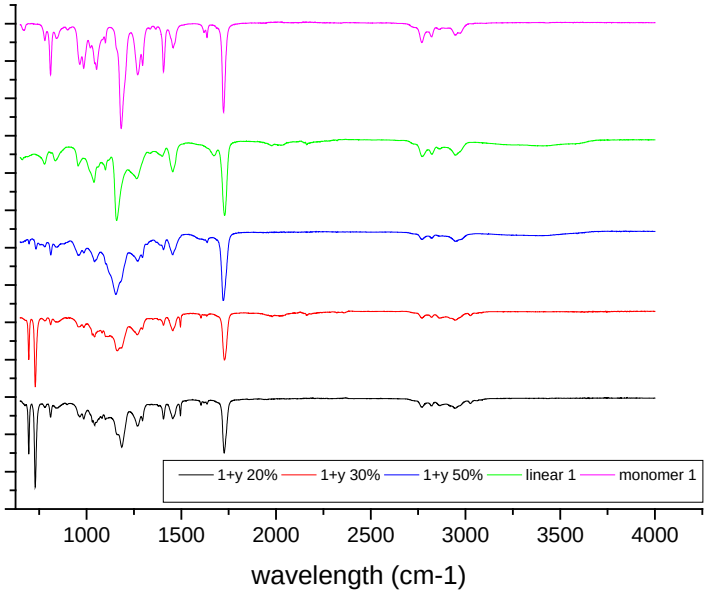

Figure 3- 2 IR transmission spectra collected from polymers synthesised from monomer 1 and brancher y, linear polymer and monomer 1 added for comparison.

3.3.3.2 Monomer 2 polymers

All polymers within this set have very similar IR spectra with intensities and shifts comparable. Again there are strong peaks observable in the regions noted above and an absence of any C=C stretching. Comparison of linear control polymer and monomer was carried out as before, in this instance the only alteration was the addition of the alkene stretch in the monomer. As above all IR transmission spectra are shown below in Figure 3-4 and Figure 3- 5.

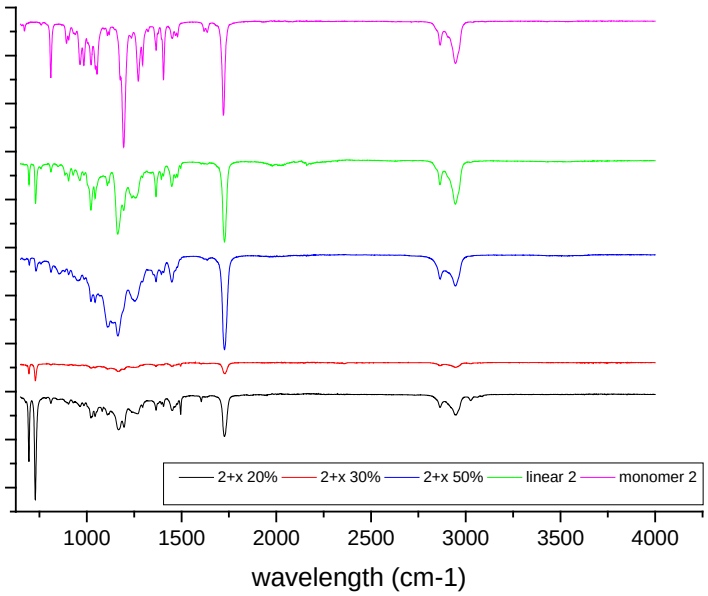

Figure 3- 3 IR transmission spectra collected from polymers synthesised from monomer 2 and brancher x.

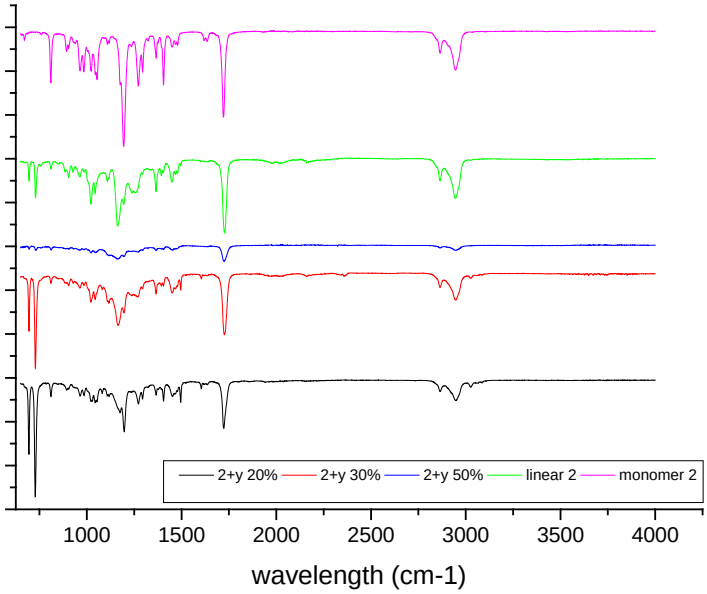

Figure 3- 4 IR transmission spectra collected from polymers synthesised from monomer 2 and brancher y.

3.3.3.3 Monomer 3 polymers

Monomer **3** polymers show similar features to those seen in monomer **1** and **2** polymers with the addition of an OH peak in every spectrum, from 3300 to 3600cm^{-1}. For monomer **3** there were no polymers synthesised using brancher **x** as brancher **y** was deemed to be more bioresistive from preliminary bacterial data and thus brancher **x** species were tested no further. Spectra illustrating the differences in the linear and branched polymers using brancher y are shown in Figure 3- 6.

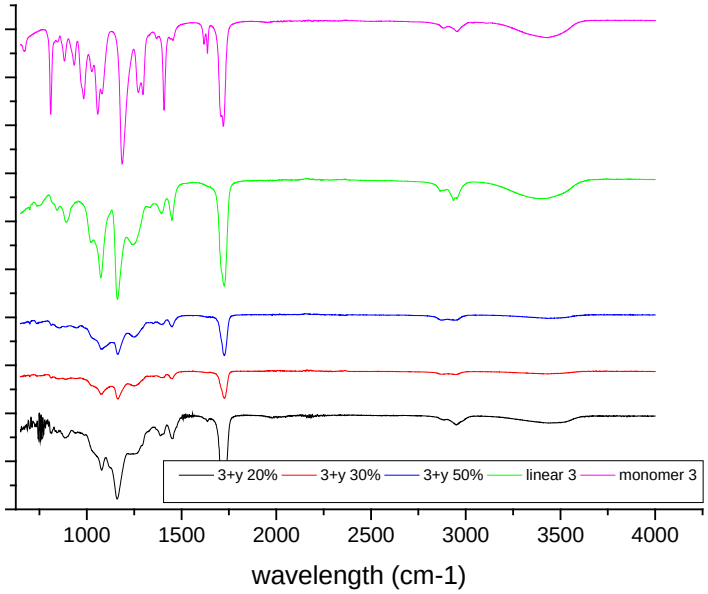

Figure 3- 5 IR transmission spectra collected from polymers synthesised from monomer 3 and brancher y.

3.3.4 Raman Analysis

For further structural information, Raman analysis of the polymers was carried out using a Thermo Scientific DXR Raman Microscope. Comparison of the resultant plots was carried out and analysis is shown below.

3.3.4.1. Monomer 1 Polymers

Comparisons of the polymers synthesised using monomer **1** are shown in Figure 3- 7 and Figure 3- 8, below. For this set of polymers, the linear control appears to be significantly different to the other polymers; this is due to the signal being shifted up approximately 50. This observation is further qualified after inspection of the principal component analysis (PCA) results from the RAMAN experiments, Figure 3- 23, Linear **1** is an outlier and thus is significantly different to the rest of the data set.

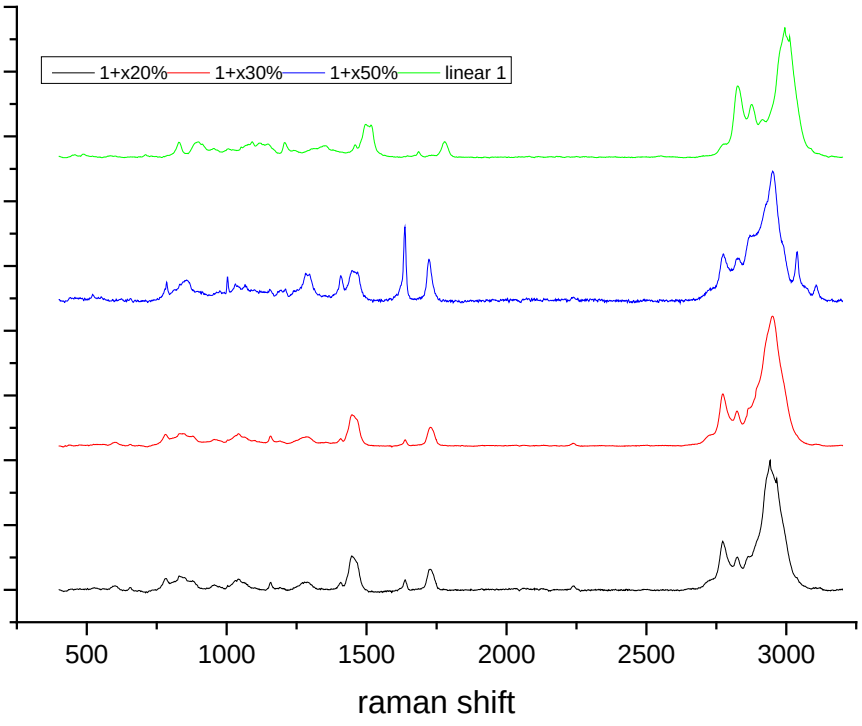

Figure 3- 6 RAMAN spectra for polymers synthesised using monomer 1 and brancher x.

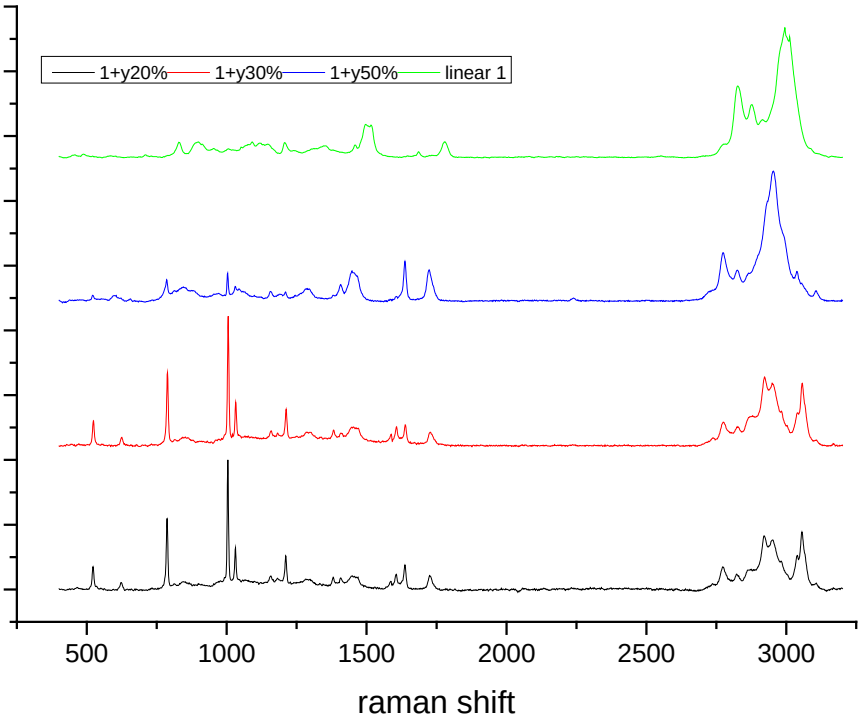

Figure 3- 7 RAMAN spectra for polymers synthesised using monomer 1 and brancher y.

3.3.4.2 Monomer 2 Polymers

All spectra collected for monomer **2** polymers are very similar upon inspecition. The number of peaks generated, and those that match all others within the dataset, is higher in this data set than for all others investigated. The baseline observed is also significantly less noisy than that collected the other polymer libraries.

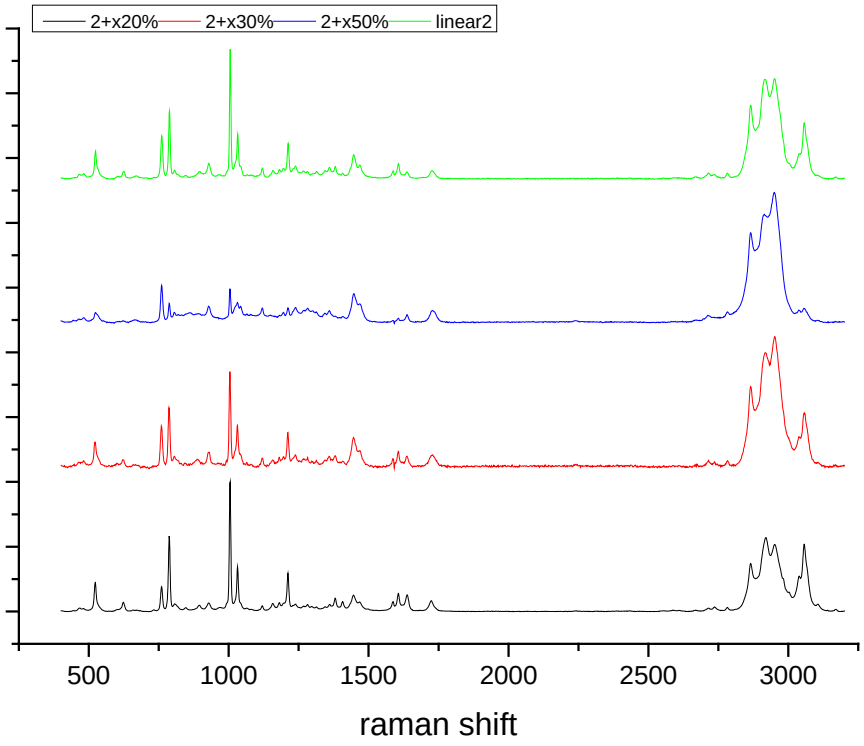

Figure 3- 8 RAMAN spectra for polymers synthesised using monomer 2 and brancher x.

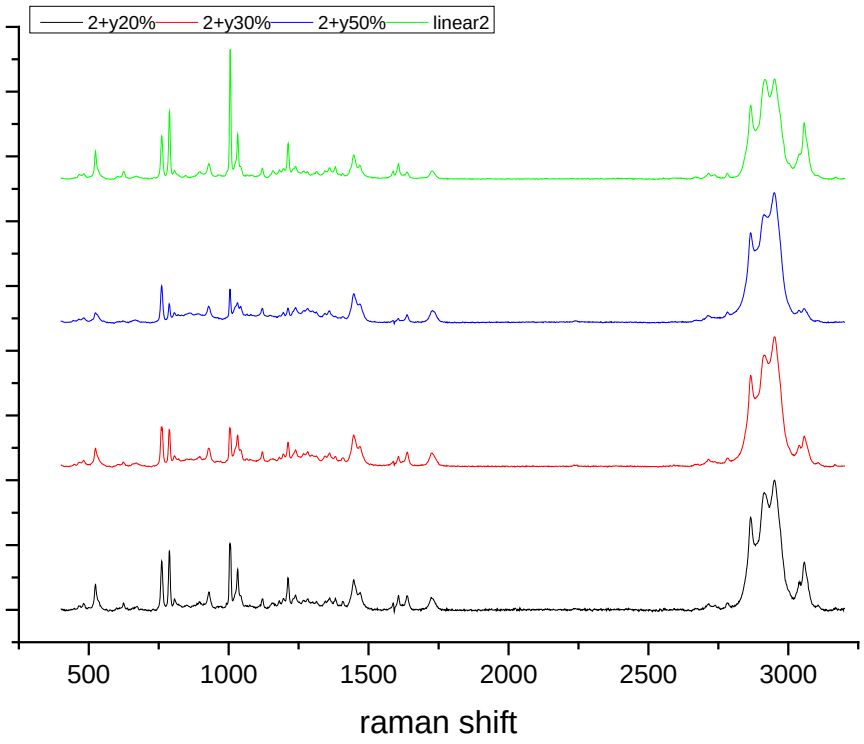

Figure 3- 9 RAMAN spectra for polymers synthesised using monomer 2 and brancher y.

3.3.4.3 Monomer 3 Polymers

The polymers synthesised using this monomer fluoresce which makes the collection of a Raman spectra considerably more complex. In order to minimise this, the collection time is altered and the laser chosen specifically to minimise the problem. However, even with these measures in place, all monomer **3** polymers Raman spectra were noisy and affected by fluorescence. One obvious "peak" which is visible in a number of spectra produced is a blip at around 1600cm^{-1}, this cannot be attributed to any signal from the polymer as it is too sharp and negative so is likely to be a fault with the detector.

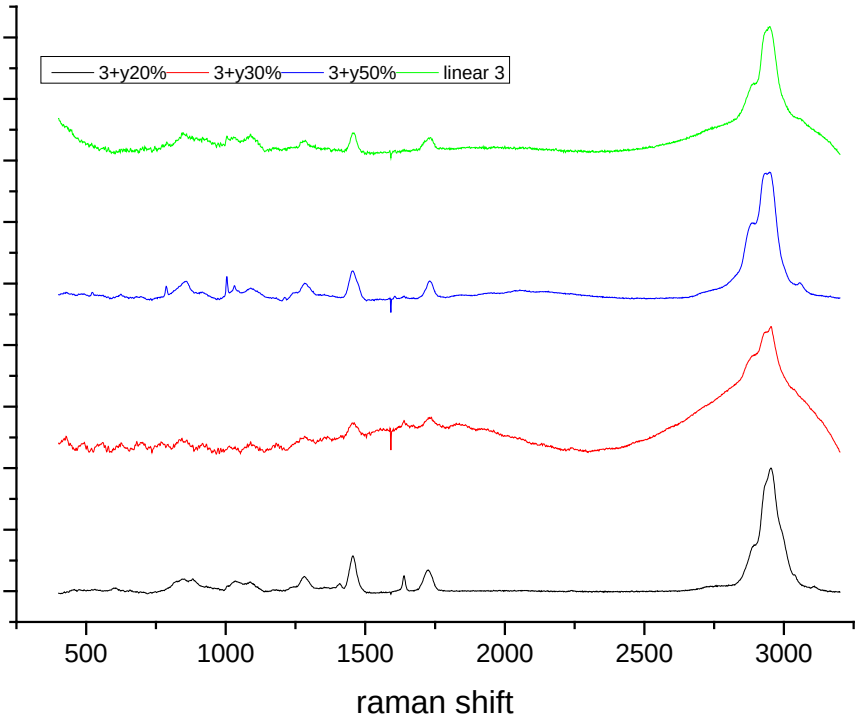

Figure 3- 10 RAMAN spectra for polymers synthesised using monomer 3 and brancher y.

3.3.5 Atomic Force Microscopy

AFM was used to determine the roughness of the polymer surface coating the glass coverslips along with the force of adhesion present between the polymer coating and the cantilever. Solid polymer material generated from the reaction could not be analysed independently as the surface is required to be flat for AFM to be carried out. To allow for accurate analysis polymers were dip coated onto a number of glass coverslips and AFM experiments were carried out using the method detailed in chapter 2.

3.3.5.1 Surface Roughness

As shown in Table 3- 3, samples **1**+**x**50% (49.2nm) and **1**+**y**20% (20.6nm) have very high surface roughness in comparison to the average values observed in other samples, less than 10nm. The surface roughness could not be measured for the linear polymer of monomer 1 as it was too adhesive; this meant that the cantilever tip could not move over the surface to generate a result. This can also result in the breaking of the AFM cantilever.

Table 3- 3 AFM surface roughness measurements.

Sample Name	Surface roughness (R_a) /nm
linear 1	- (too adhesive)
linear 2	1.31
linear 3	8.72
linear x	3.06
linear y	1.72
1+**x** 20%	1.38
1+**x**30%	2.06
1+**x**50%	49.2
1+**y**20%	20.6
1+**y**30%	6.98
1+**y**50%	0.46
2+**x**20%	1.31
2+**x**30%	3.9
2+**x**50%	5.23
2+**y**20%	0.46
2+**y**30%	0.46
2+**y**50%	2.57
3+**x**20%	12.4
3+**x**30%	3.83
3+**x**50%	4.27
3+**y**20%	1.34
3+**y**30%	1.26
3+**y**50%	0.94

3.3.5.2 Force of Adhesion

From the results are shown in Table 3- 4 it can be seen that the force of adhesion for samples linear **1**, **1**+**x**50%, **1**+**y**50% and **2**+**y**50% could not be determined due to the surface being too sticky. Sample **2**+**y** 20% also could not be measured, but in this instance it was due to the surface being too soft. The linear polymers measured had, in general, much

lower forces of adhesion in comparison to their branched counterparts with the exception of **1**+**y**20% which had an unusually low value. This peculiarly low force of adhesion corresponds to the exceptionally high surface roughness measured by the same technique.

Table 3- 4 Force of adhesion measured using AFM.

Sample Name	Force of Adhesion (F_{ad})/ nN
linear 1	- (too adhesive)
linear 2	22.6 ± 4.5
linear 3	77.5 ± 25.0
linear x	18.5 ± 4.8
linear y	26.1 ± 1.9
1+**x** 20%	130.27 ± 5.11
1+**x**30%	141.23 ± 9.75
1+**x**50%	- (too adhesive)
1+**y**20%	28.00 ± 0.59
1+**y**30%	98.3 ± 1.9
1+**y**50%	- (too adhesive)
2+**x**20%	129.81 ± 18.35
2+**x**30%	101.97 ± 39.52
2+**x**50%	111.9 ± 6.8
2+**y**20%	- (too soft)
2+**y**30%	95.60 ± 1.94
2+**y**50%	- (too adhesive)
3+**x**20%	89.1 ± 2.6
3+**x**30%	85.8 ± 11.1
3+**x**50%	81.5 ± 15.8
3+**y**20%	121.0 ± 5.4
3+**y**30%	115.0 ± 2.2
3+**y**50%	84.2 ± 32.4

3.3.6 Differential Scanning Calorimetry

For the analysis of the acrylate polymers produced dynamic temperature changes were utilised to allow for solvent removal, there were detailed in section 2.3.5.2. Not all acrylate

polymer samples were viable for testing using DSC and thus a number were analysed using TGA (Thermogravimetric analysis), a similar technique which gives some of the information of the DSC, see Figure 3- 12 for an exemplary TGA plot. The applicability of polymer samples for DSC testing was dependent on the TGA weight loss; a large loss in mass can suggest solvent trapped within the polymer matrix and thus damage to the DSC instrument. Due to this TGA was determined to be the only experiment that could be carried out safely. When DSC analysis could be carried out, plots similar to that shown in Figure 3- 13 were produced. Whether DSC or TGA were utilised, the temperature ramps were kept constant to allow for the largest number of comparisons to be made. All plots are detailed in appendix 1.

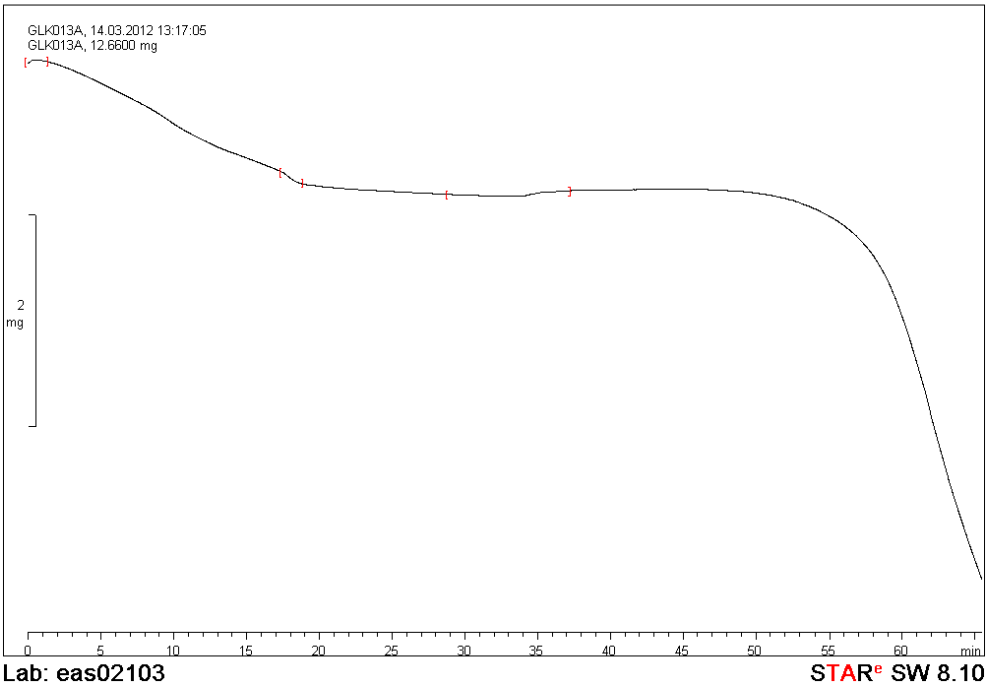

Figure 3- 11 TGA plot of polymer 1+x20% as an example of the traces generated using this technique.

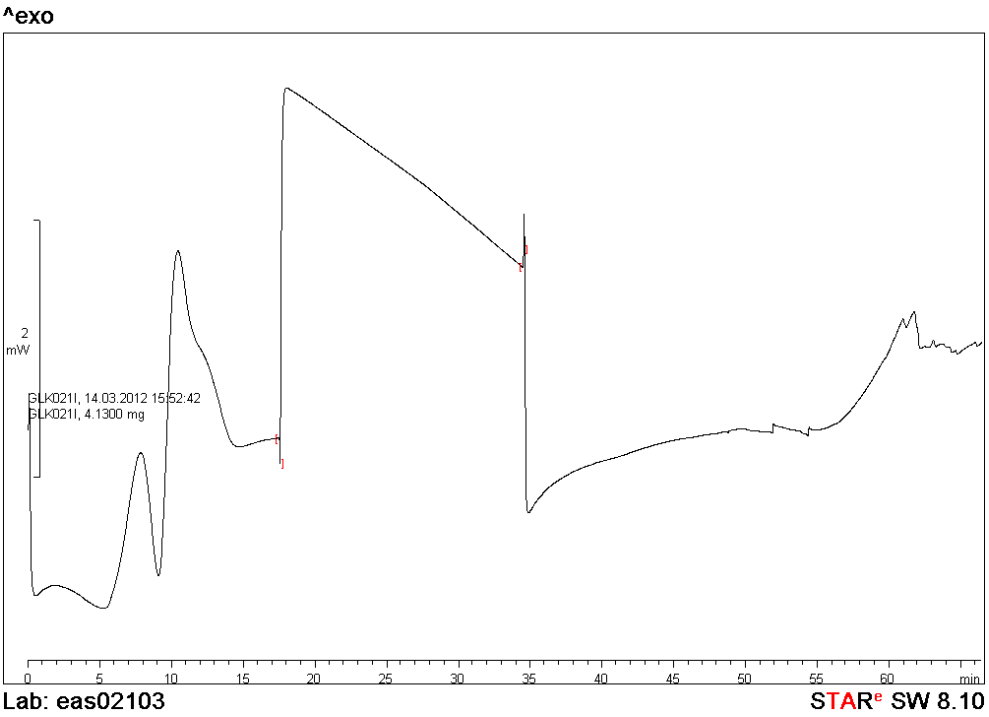

Figure 3- 12 DSC trace polymer 1+y50% as an example of the traces generated from acrylate polymers using this technique.

3.3.6.1 Monomer 1 Polymers

Neither DSC nor TGA analysis of the linear polymers of monomer **1** could be attaine;, this was due to its liquid nature which could not be analysed using the equipment available. Thus there can be no comparison to the linear polymer in this instance. In addition, with the exception of polymer **1**+**y**50%, all monomer **1** species were only analysed using TGA due to their solvent content, this could contribute laterally to the bacterial responses noted. The temperature cycle used for each acrylate polymer studied, whether it was via DSC or TGA, was 25°C to 200°C at 10°C min^{-1} before cooling to 30°C at 10°C min^{-1} and then reheating at 10°C min^{-1} to 350°C.

From the TGA analysis carried out, it can be seen that there is a relatively large loss in mass which is consistent with the samples being "wet". It can also be observed that there are areas where there are small increases or decreases in mass; these are marked using red markers. These can be distinctive of changes in the polymer including melting and crystallisation.

3.3.6.2 Monomer 2 Polymers

Similarly the linear polymer of monomer **2** could not be analysed using TGA or DSC due to its proportion of imbibed solvent. All branched polymers resulting from synthesis using monomer **2**, however, could be successfully analysed using DSC and the methodology previously described. DSC analysis outputs a greater volume of information about the sample being studied than can be gleaned from TGA analysis. For all polymers, a large stepwise increase in mass could be observed when the temperature gradient changed from heating to cooling and in the majority of cases, most of the significant changes in the material mass can be observed during the first heating cycle.

3.3.6.3 Monomer 3 Polymers

Monomer **3** polymers were tested using the same methodology and in this instance, all branched polymers and the linear polymer could be analysed using DSC. This is beneficial as it allows comparisons between the linear and branched polymers synthesised. As previously, there appears to be a large jump in mass when the cooling cycle starts and the majority of obvious changes in the polymer occurred within the first heating cycle. As with all other polymers studied, reasons behind the similarities and differences between synthesised materials are developed in the discussion.

3.3.7 Bacterial Testing – Crystal Violet Staining

Bacterial proliferation on polymer coated glass slides was analysed using growth methodology detailed previously and UV-visible spectrometry, see section 2.5. Samples were run in triplicate to ensure that results were both reproducible and significant. Three bacterial strains were used for acrylate testing, *Pseudomonas aeruginosa, Staphylococcus aureus* and *Bacillus subtilis*, the results of which are detailed below.

3.3.7.1 Pseudomonas aeruginosa

After 24hr incubation, bacteria were stained using CV stain and analysed using UV-vis spectroscopy: results of this analysis are shown below, Table 3- 5. Standard deviations were calculated and data was presented as a bar graph to show alterations due to polymer type (Figure 3- 14 and Figure 3- 15). All samples prepared and tested on the same day using one overnight culture to ensure a fair comparison can be drawn.

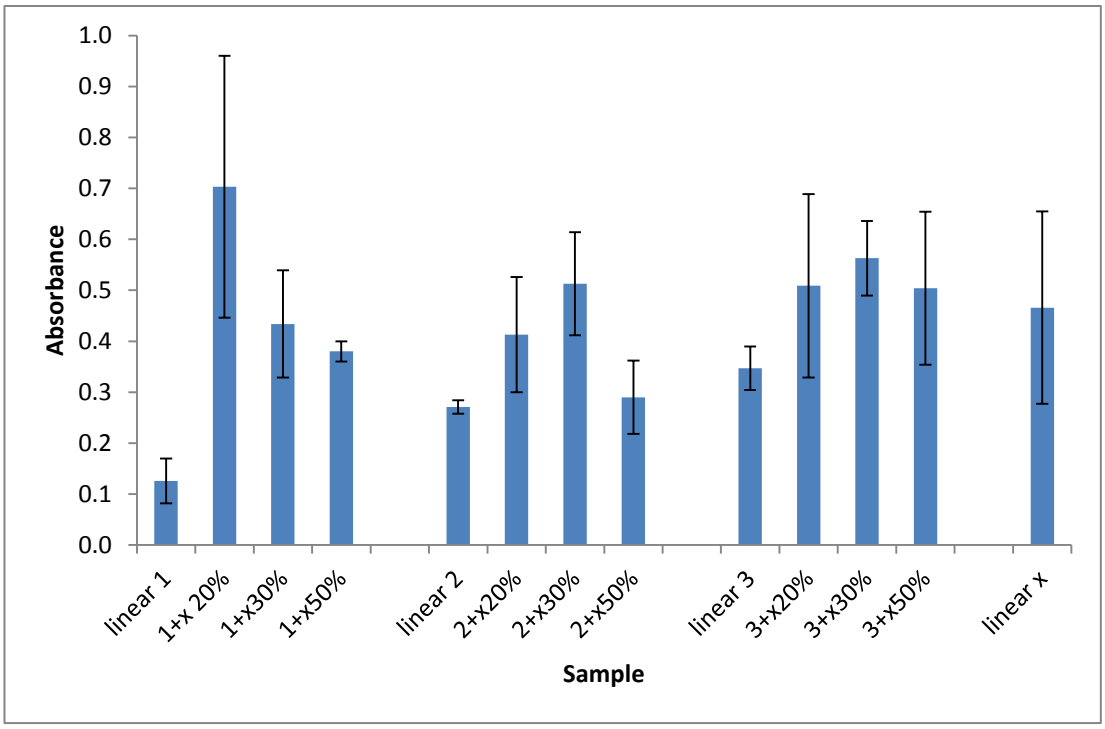

Figure 3- 13 *Pseudomonas aeruginosa* biofilm proliferation on polymer coated glass slides over 24hrs, including standard deviations. Brancher x species.

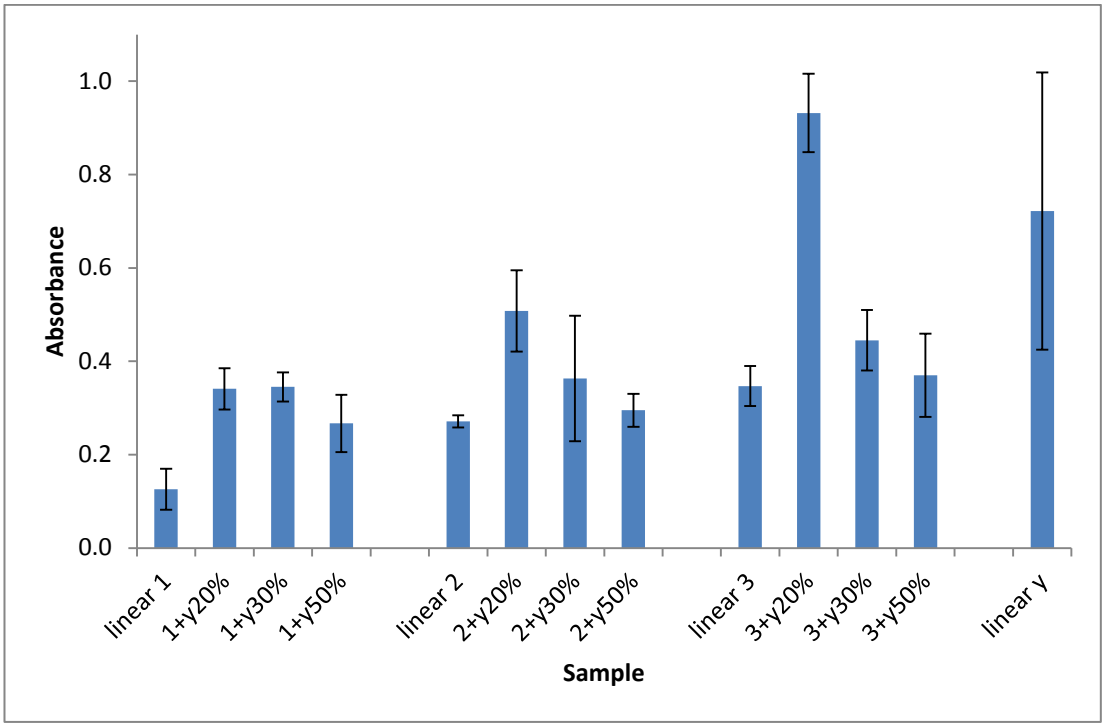

Figure 3- 14 *Pseudomonas aeruginosa* biofilm proliferation on polymer coated glass slides over 24hrs, including standard deviations. Brancher y species.

Table 3- 5 Crystal violet absorbance at 580nm for *Pseudomonas aeruginosa* bacteria after 24hrs incubation. Data corrected using the negative control (glass coverslip, no bacteria) after 24hr incubation with standard deviations.

Sample	Mean Absorbance (au)	Standard Deviation	% Standard Deviation
linear **1**	0.126	0.04	35
linear **2**	0.271	0.01	5
linear **3**	0.347	0.04	12
linear **x**	0.466	0.19	41
linear **y**	0.722	0.30	41
1+**x** 20%	0.703	0.26	37
1+**x**30%	0.434	0.11	24
1+**x**50%	0.380	0.02	5
1+**y**20%	0.341	0.04	13
1+**y**30%	0.345	0.03	9
1+**y**50%	0.267	0.06	23
2+**x**20%	0.413	0.11	27
2+**x**30%	0.513	0.10	20
2+**x**50%	0.290	0.07	25
2+**y**20%	0.508	0.09	17
2+**y**30%	0.363	0.13	37
2+**y**50%	0.295	0.04	12
3+**x**20%	0.509	0.18	35
3+**x**30%	0.563	0.07	13
3+**x**50%	0.504	0.15	30
3+**y**20%	0.932	0.08	9
3+**y**30%	0.445	0.07	15
3+**y**50%	0.370	0.09	24

3.3.7.2 Staphylococcus aureus

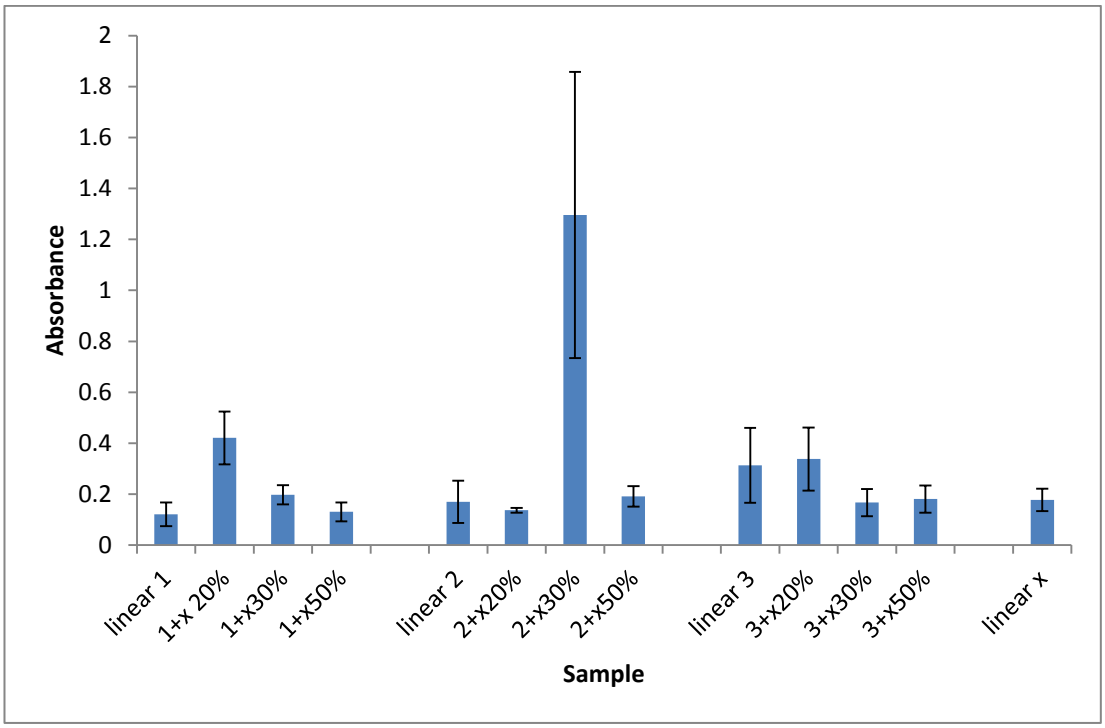

Figure 3- 15 *Staphylococcus aureus* biofilm proliferation on polymer coated glass slides over 24hrs, including standard deviations. Brancher x species.

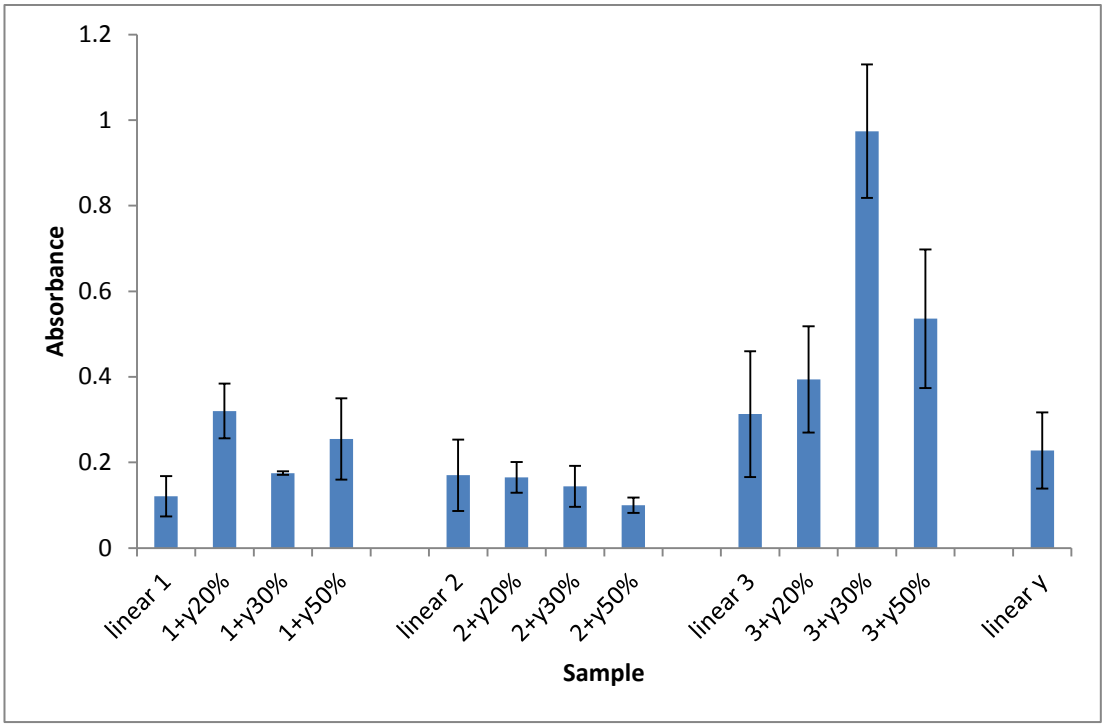

Figure 3- 16 *Staphylococcus aureus* biofilm proliferation on polymer coated glass slides over 24hrs, including standard deviations. Brancher y species.

Experiments were repeated using *Staphylococcus aureus* in order to determine differences between bacteria types. Experiments were carried out in the same manner with positive and negative controls shown in Table 3- 6. Details of the results of these experiments are tabulated in Table 3- 6 and further clarified to show trends (Figure 3- 16 and Figure 3- 17).

Table 3- 6 Crystal violet absorbance at 580nm for *Staphylococcus aureus* bacteria after 24hrs incubation. Data corrected using the negative control (glass coverslip, no bacteria) after 24hr incubation with standard deviations.

Sample	Mean Absorbance (au)	Standard Deviation	% Standard Deviation
linear **1**	0.121	0.047	39
linear **2**	0.17	0.083	49
linear **3**	0.313	0.147	47
linear **x**	0.178	0.044	25
linear **y**	0.228	0.089	39
1+**x** 20%	0.421	0.104	25
1+**x**30%	0.198	0.038	19
1+**x**50%	0.131	0.037	28
1+**y**20%	0.32	0.064	20
1+**y**30%	0.175	0.004	2
1+**y**50%	0.255	0.095	37
2+**x**20%	0.137	0.010	7
2+**x**30%	1.296	0.562	43
2+**x**50%	0.191	0.040	21
2+**y**20%	0.165	0.036	22
2+**y**30%	0.144	0.048	33
2+**y**50%	0.1	0.018	18
3+**x**20%	0.338	0.124	37
3+**x**30%	0.167	0.053	32
3+**x**50%	0.181	0.053	29
3+**y**20%	0.394	0.124	31
3+**y**30%	0.974	0.156	16
3+**y**50%	0.536	0.162	30

3.3.7.3 Bacillus subtilis

The final bacteria these polymers were tested with was *Bacillus subtilis*. Following from the original data collected using the other bacterial strains only polymers synthesised using brancher y were tested due to the synthesis of brancher **x** species being halted due to initial bacterial results. The results, as previously, are shown in Table 3- 5 and Figure 3- 18.

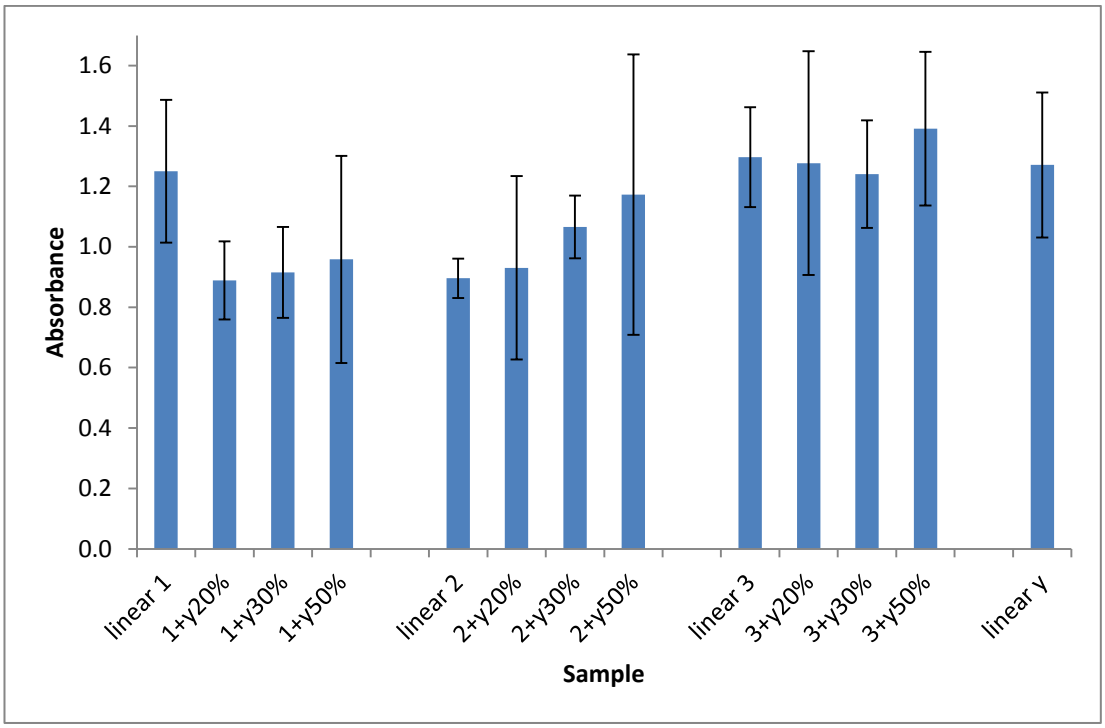

Figure 3- 17 *Bacillus subtilis* biofilm proliferation on polymer coated glass slides over 24hrs, including standard deviations. Brancher y species.

Table 3- 7 Crystal violet absorbance at 580nm for Bacillus subtilis bacteria after 24hrs incubation. Data corrected using the negative control (glass coverslip, no bacteria) after 24hr incubation with standard deviations.

Sample	Mean Absorbance (au)	Standard Deviation	% Standard Deviation
linear **1**	1.25	0.24	19
linear **2**	0.90	0.07	7
linear **4**	1.30	0.17	13
linear **y**	1.27	0.24	19

1+**y** 20%	0.89	0.13	15
1+**y** 30%	0.92	0.15	16
1+**y** 50%	0.96	0.34	36
2+**y** 20%	0.93	0.30	33
2+**y** 30%	1.07	0.10	10
2+**y** 50%	1.17	0.46	40
3+**y** 20%	1.28	0.37	29
3+**y** 30%	1.24	0.18	14
3+**y** 50%	1.39	0.25	18

3.3.7.4 Controls

In order to allow comparison of results collected using all bacteria, the data must be corrected using negative controls and compared to their positive controls which in this instance were polystyrene well plate cultures. These details are shown in Table 3- 6 below. The negative controls are not noted as they have been previously used to correct the data in tables Table 3- 5, Table 3- 6 and Table 3- 7.

Table 3- 8 Positive controls for comparison. All tested on cell culture grade polystyrene, a common biomaterial. Negative controls used to correct data.

Bacteria	Mean. Absorbance (au)	St. Deviation	Percentage St. Deviation (%)
P. Aeruginosa	2.47	0.33	13
S. Aureus	2.52	0.11	4
B. Subtilis	0.78	0.07	9

3.4 Discussion

3.4.1 Polymer Synthesis

All polymers were successfully synthesised and the result was a solid or gel material which could be applicable for use as a biomaterial due to the desire for flexibility in some applications, including heart valves (Martin and Williams, 2003). The polymers synthesised using monomer **1** were translucent and yellow to light brown in colour with a strong odour, it is thought that this is due to the amino groups present on the monomer which do not appear to be removed upon polymerisation. This group of polymers also possessed a

different morphology to the remainder of the polymer library; a semi-solid pliable gel consistency which at times felt tacky to the touch.

All monomer **2** polymers were translucent and colourless with a much more solid and friable nature than those synthesised from monomer **1**. This group of polymers took, in general, longer to form solid material than those from the other monomers. This could be a result of steric hindrance due to the cyclohexane present in the monomer; this issue has been previously noted in radical polymerisations (Matyjaszewski and Davis, 2003). It would also suggest that within the polymer structure there is less close packing of the polymer units. It must also be noted that the method employed for the synthesis of polymeric material can also cause variations in the chain packing (Boyle, 1994). This may explain differences to previous polymers synthesised using this monomer but not within the set as all material generated in the same manner.

In contrast to the other monomers, the polymers generated using monomer **3** were opaque, white and had a more solid structure than the others in the library. Synthesis times for these polymers were also significantly less than the others suggesting a highly reactive monomer which can easily form long polymer chains. The opacity of the final product suggests a more crystalline or porous polymer structure (Heaton, 1994). This is because there is a greater proportion of light scattering due to the numerous boundaries between the crystalline and amorphous regions within the polymer (Sencadas et al., 2006). The crystallinity of this set of polymers will be clarified by the use of DSC (section 3.4.6).

3.4.2 Contact Angle Goniometry and Surface Energy

Two polymers were too wetting to allow measurement of their water contact angle, **1**+**x** 50% and **1**+**y** 50%. This would tend to suggest that highly branched polymers synthesised using monomer **1** were very hydrophilic irrespective of the brancher used. Polymers synthesised using monomer **1** and brancher **x** also showed a trend in that, when the proportion of brancher within the polymer increased the water contact angle fell, however this was unique to this polymer set. As ethylene glycol dimethacrylate (brancher **x**) is a hydrophilic entity, this would imply that in this instance there is a surface preference for the brancher molecule over monomer **1**. The linear polymers synthesised using the monomers alone had vastly differing contact angles with linear polymer **1** measuring a very low 24.5 ± 9.2°. Linear polymer **2** in contrast had a high contact angle of 97.6 ± 0.4° which also had a very low standard deviation for these experiments. Finally, linear **3** had a contact angle which fell in the mid-range at 64.6 ± 9.2°. The linear polymers of the

brancher species had relatively low contact angles and brancher x had the lowest measured angle and standard deviation of the set at 22.1 ± 0.0°. This would potentially suggest that all polymers synthesised using monomer **x** would have a lowered contact angle when compared to those containing polymer **y**, however this was not always the case, with the highest branched polymer contact angle of 96.5 ± 3.1° being generated by polymer **3**+**x**50%. This would suggest that the orientation of some functional groups may be shielded in certain polymers to alter the contact angle. In general the standard deviation of the contact angles measured was high; this could be due to the polymer film on the coverslips being uneven and altering the surface morphologies. This could potentially be eliminated using solid polymer to carry out these experiments however, the surface being characterised must be completely flat and thus, this is rather complex in a thermally synthesised polymer. From the surface energy information calculated using the contact angles from test liquids further information on the surface nature of the branched polymers synthesised can be gleaned. In contrast to the wide spread of data in the water contact angle the measured surface energies of all tested polymers were between 30 and 60 mJm^{-2}. The only exception to this was the linear polymer of monomer **1**, 74.3 mJ m^{-2}, this polymer was different to the other polymers produced as it was never truly a solid and tended toward, at room temperature, a viscous liquid. This may explain its peculiar behavior in these experiments. The polymers synthesised using monomer **1** and either brancher did solidify suggesting that the oligomeric behavior of this material was unusual. All other linear polymers behaved as the branched polymeric material.

3.4.3 Fourier-Transform Infrared Spectrometry

All spectra collected shown in section 3.3.3 above.

3.4.3.1 Monomer 1

Polymer spectra resulting from the use of monomer **1** and brancher at 20, 30 or 50% exhibited similar features: symmetric and asymmetric CH_2 and CH_3 stretching at 2940 and 2860cm^{-1} along with substituted alkene C-H stretching at 2810 and 2770 cm^{-1}. This is all expected if the polymerisation has occurred. In polymer **1**+**y** 30%, there are three unique peaks at 1950, 2000 and 2160 cm^{-1}. These are suspected to be due to C=C from starting materials, which would further suggest that in this instance, polymerisation, was not completed within the reaction time. There is no C=C signal (1630-1680cm^{-1} and 1900-

2000cm^{-1}) in any of the other polymer species which would suggest that the reaction has gone to completion, leaving no starting material unreacted. This however could be unrealistic and the C=O peak is masking the signal generated by the C=C; this will be clarified using the Raman data collected. Polymer **1**+**y** 50% also has an unusual peak between 3070 to 3670cm^{-1}; this broad signal is most likely due to an OH reside. In all spectra there is a strong single peak at 1720 cm^{-1} relating to the C=O stretch of an ester pendant chain. Finally within the fingerprint region there were a large number of peaks which were represented in all spectra: 694, 728, 775 cm^{-1}, 810 and 840 cm^{-1}, 970 and 980 cm^{-1} and 1400, 1450 and 1490 cm^{-1}. These are all due to CH, CH_2 and CH_3 bending or deformations.

The linear polymer synthesised from the monomer alone was compared to the monomer bought directly from Sigma Aldrich. There were a number of differences between these traces, the monomer spectra was sharper and more intense than the linear which included a similar OH stretch to that seen in the 50% brancher spectra. There was a strong alkene asymmetric stretch from 1970 to 1980 cm^{-1} present in the monomer spectra, as expected, along with a 5 cm^{-1} increase in wavenumber in all peaks in the fingerprint region in comparison to the linear polymer.

3.4.3.2 Monomer 2

All polymers: 20, 30 and 50% brancher species, show very similar IR spectra with intensities and shifts comparable between them all. Similarly to the monomer **1** species, these polymers all possessed peaks at 2860 and 2940 cm^{-1} which represent CH, CH_2 and CH_3 stretching. In addition, polymers containing 50% brancher also had a single peak at 3020 indicative of a =CH or =CH_2 peak suggesting again that polymerisation may not have occurred fully in these high brancher species. Again, all polymers had an intense stretch at 1720 cm^{-1} representing the ester C=O residue. Similarly to monomer 1, these polymers had a number of peaks which were retained throughout the fingerprint region, these include: 690, 730 and 750 cm^{-1}, 810 and 900cm^{-1}, 960 and 980 cm^{-1} and 1160, 1360, 1450 and 1600 cm^{-1}. These represent the CH character of the polymer backbone by via a number of vibrational modes including αCH2 bending, CH, CH_2 and CH_3 deformation.

Comparison of linear control polymer and monomer was carried out as before; in this instance the only variation between the spectra collected was the addition of the alkene stretch in the monomer.

3.4.3.3 Monomer 3

Monomer 3 polymers show similar features to those seen in monomer **1** and **2** polymers with the addition of an OH peak, as expected, in every spectrum, from 3290 to 3850 cm^{-1}. These polymers have lower intensity spectra than those previously discussed. Peaks were observed at 2940 and 2860 cm^{-1} in these spectra corresponding to those in all other polymers. The strong C=O stretch was also clearly visible in these spectra in the same position. Additionally, there was a single weak signal at 1630 cm^{-1} which can be attributed to a C=C. As previously, the fingerprint peaks which overlapped were noted: 690, 730, 800 and 940 cm^{-1}, 1070 and 1160 cm^{-1}, 1250 cm^{-1} and 1540 cm^{-1}. The comparison of the linear and monomer spectra was carried out as previously. The fingerprint region in these spectra were different to one another and the OH peak was significantly higher in the linear spectrum than in the purchased monomer suggest that that these polymers could have been affected by external influences including O_2 in the atmosphere.

3.4.3.4 Statistical Analysis

To determine any differences or similarities between the spectra that were not obvious on inspection, principal component analysis (PCA) was carried out on the data collected. This generated a graphical plot of statistical similarity, Figure 3- 19. This PCA, principal component 1, shows which polymers are most similar to each other; the ones in the centre (and especially the few that overlap) are very similar in their spectra, while the more outlying data is very dissimilar to other results. For further clarification, the loadings plot for this analysis is shown, Figure 3- 20. These loadings show the effects of the variable within the dataset, in this case the wavelength, therefore it is expected that the peaks and shapes observed within the loadings correspond to the peaks which are causing the variation within the spectra. The most notable signals in PC1 are the broad OH signal (5500 to 6750 cm^{-1}) the CH_2, CH_3 region (4800 to 5500 cm^{-1}) and finally C=O signal around (2400 to 3000 cm^{-1}).

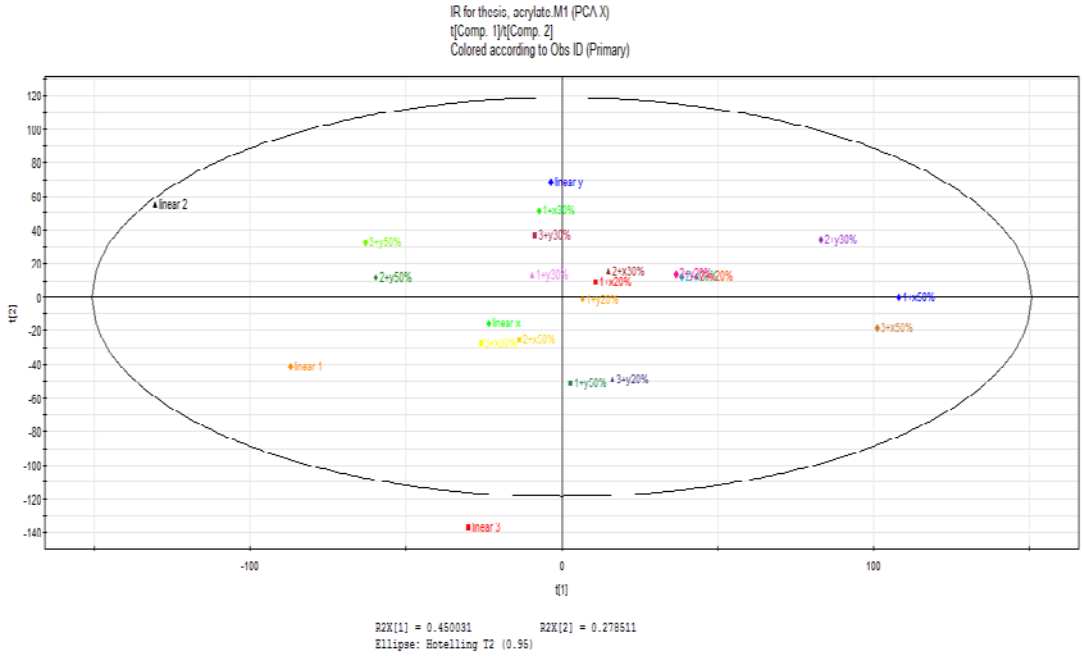

Figure 3- 18 Principal component analysis (principal component 1) of IR data collected on acrylate polymers. Data points which are grouped together suggest greater similarity and any values which fall outside the oval are outliers from the rest of the data, in this instance linear polymer 3, $p<0.05$.

From these results it can be concluded that linear polymers **1** and **3** have unique characteristics which are not observed in any of the other samples. Polymers synthesised using brancher **y** tend to have results which are further from the centre of the data, especially when the proportion of brancher is increased. The majority of polymers made using monomers **1** and **2** are quite closely related suggesting similarity.

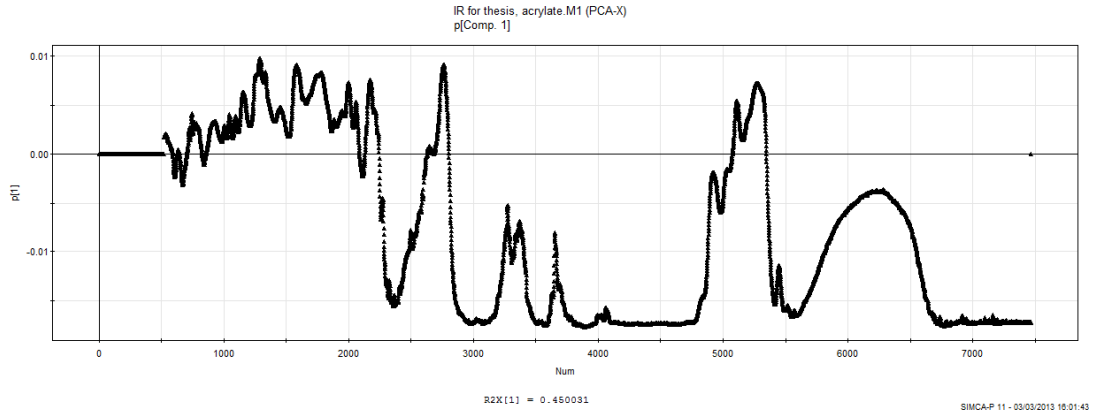

Figure 3- 19 Loadings plot for IR analysis, principal component 1.

After inspection of the first principal component, principal component 3 was investigated to determine whether further separation could be achieved, see Figure 3- 22. This is the same

data which has simply been further analysed using PCA. It was shown that all polymers synthesised using monomer 3 lie above the x axis, data enclosed in box within plot. This suggests that principal component 3 describes the monomer 3 polymers more than all others within the data set. The loading plot for this component is also shown to allow further clarification of the areas which are causing the separation of the data, Figure 3- 21. All other loadings plots are shown in the appendix for completion.

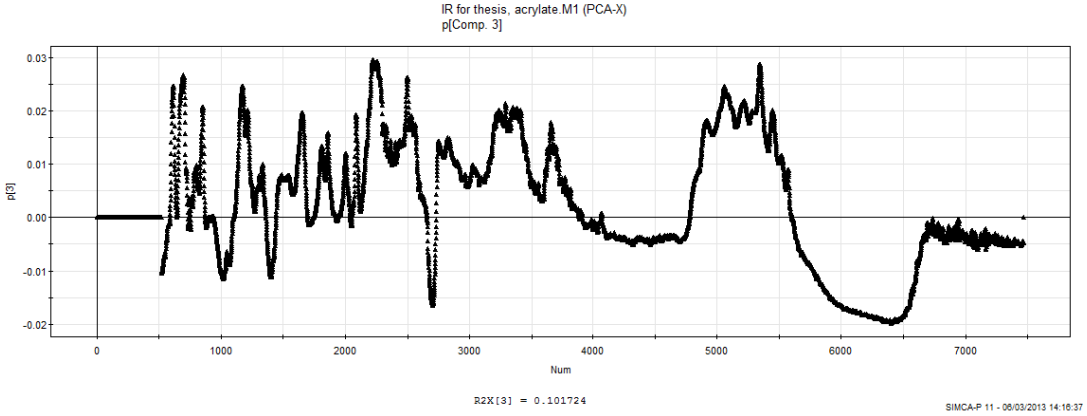

Figure 3- 20 Loadings plot for IR analysis, principal component 3.

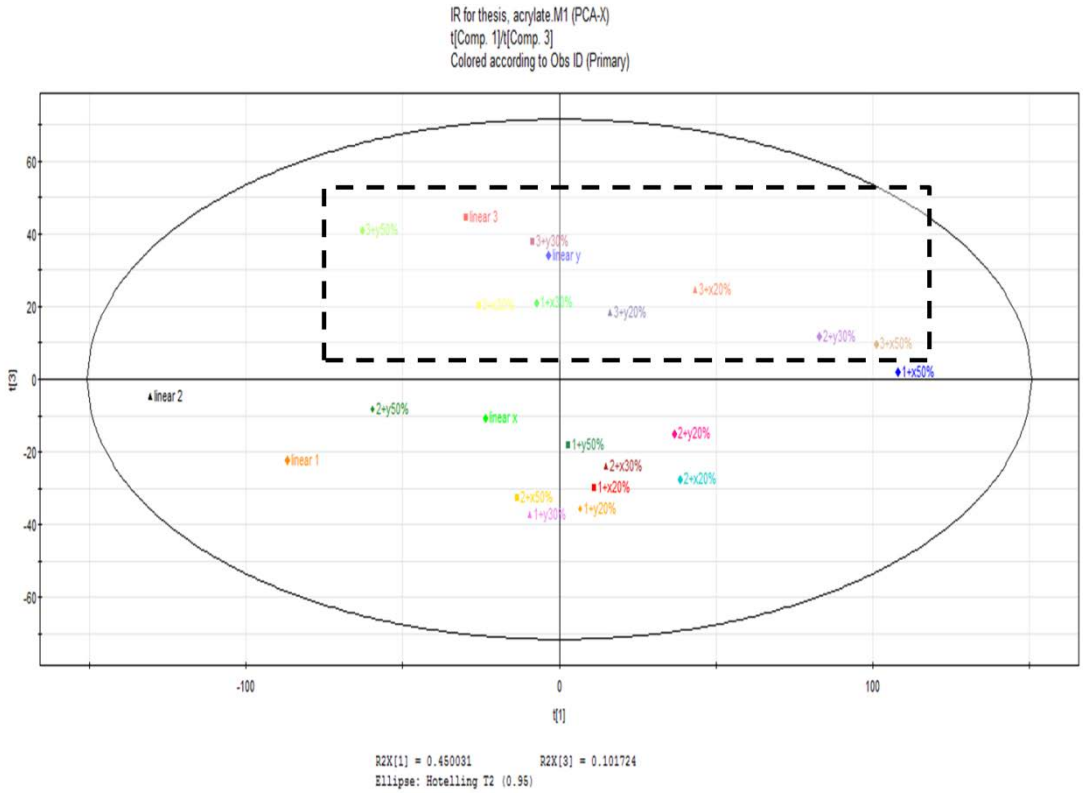

Figure 3- 21 Graph showing outcome from principal component 3, all polymers synthesised using monomer 3 are positive, lie above the x axis. Principal component 3 describes monomer 3 polymers and separates them from other data.

3.4.4 Raman Analysis

Raman graphs collected during this analysis shown in section 3.3.4 above.

3.4.4.1 Monomer 1

The Raman from monomer **1** polymers have a great majority of peaks which are consistent throughout the spectra. The peak at 2940 cm^{-1}, shoulder at 2850 cm^{-1} and the peaks at 2830 and 2770 cm^{-1} are in every spectra. These represent CH vibrations. There is a peak at 3052 cm^{-1} which is only shown in polymer **1**+**y** 20% and 30%, this is indicative of =C-H species which could be indicative of incomplete polymerisation. In polymer **1**+**x** 20% and 30% there is also a very weak signal observed at 2240 cm^{-1} which is again representative of C=C character and suggests that some starting material remains in the final polymer. In the lower region of the spectra, the peaks are more closely packed and thus more difficult to interpret however, there remain a number of peaks which are present in every spectra

recorded. These are situated at 1720 cm^{-1}, a C=O signal similar to that observed in the FTIR analysis, 1635 cm^{-1} which is a C=C double bond stretch, and 1400 and 1450 cm^{-1}, CH_2/CH_3 asymmetric stretching. Peaks at 1210 and 1150 cm^{-1} are much weaker than the others noted but are important as they represent C-C chain vibrations and C-O-C vibrations respectively. The signals at 780 and 650 cm^{-1} are due to the deformation of CH bonds.

As noted previously the linear polymer synthesised using monomer **1** was not a solid and thus had an unusual morphology when compared to the remainder of the library; this may be the reason for the shift in all peaks within this spectra of around 50 cm^{-1}. This significantly affects the PCA analysis but may simply be due to a topography issue (Robinson et al., 2009).

3.4.4.2 Monomer 2

Spectra collected for monomer **2** polymers were almost identical throughout. Peaks were noted at 3050, 3040 cm^{-1} and 2950, 2920, 2860 and 2775 cm^{-1} which are representative of =CH and -CH character. The signal at 2240 cm^{-1} shows C=C character again which suggests that the polymerisation reaction in this set of polymers may not have run to completion. There is again a signal at 1720 cm^{-1} (C=O) and 1630 cm^{-1} (H_2O) which have been observed in the previous polymers. The CH3 and CH2 character of the polymer is represented by the peaks at 1450, 1400 and 1380 cm^{-1} whilst the C-C backbone of the polymer chain is shown by the signal at 1210 cm^{-1}. In this instance, in contrast to the spectra from monomers **1** and **3**, the asymmetric (1030, 1000 cm^{-1}) and symmetric (930 cm^{-1}) C-O-C vibrations can both been observed. Finally there are a number of peaks between 500 and 800 cm^{-1} which show the deformation of the CH bonds within the polymer structure. The linear polymer of monomer 2 was also analysed in the same manner, this shows a remarkable similarity to the branched polymers within this set. There is however a lower intensity for the linear polymer.

3.4.4.3 Monomer 3

The spectra collected from the polymers synthesised using monomer 3 were all hindered by fluorescence. Every effort was taken in the analysis of these samples to reduce the impact of this effect using altered collection parameters however; there is still an obvious difference between these spectra and those taken of the remainder of the library. It is

possible to still gain some information about the polymer structure from these poor quality plots, as previously there are peaks at 2950 and 2880 cm^{-1} which show the CH character of the species. Again there are C=O (1730 cm^{-1}) and H_2O (1630 cm^{-1}). The majority of peaks below this are masked by fluorescence but the signal at 1450 cm^{-1} (CH2/CH3) and 1280 cm^{-1} (C-C chain vibrations) remain along with a small number of peaks showing the deformation of CH bonds. The plot from linear polymer 3 is less hindered by fluorescence than the polymer samples and as such has a number of additional peaks which can be deconvoluted. Similarly to the monomer 2 spectra the intensity is lowered throughout.

3.4.4.4 Statistical Analysis

Statistical analysis of the Raman output was carried out in order to determine if there are any differences which, although not apparent on first inspection, are significant between the polymers synthesised. The results of this statistical analysis are shown below, Figure 3-23 and Figure 3- 24.

In the primary PCA analysis of this Raman data, Figure 3- 23, there are three exceptionally strong outliers. These strong shifts make it vastly more complex to analyse any clustering within the core data. Thus these points were removed from the dataset and the area within the box was analysed further in order to analyse the data more effectively. The remainder of the data points are clustered in the centre of the plot showing similarity. Upon removal of the outliers and re-analysis there is little separation of the remaining polymers, to combat this the central area is simply magnified to give an accurate portrayal of the information, Figure 3- 24. In Figure 3- 24, the majority of the data is now clustered in the top left corner of the plot. The polymers synthesised using brancher x at 20% and linear brancher x move the right of the chart which would suggest some difference between them and the majority of the polymers. This would also suggest that the 20% polymers are more similar to the brancher than the monomers or the polymers with a higher percentage of the brancher present, which is surprising. To allow the data from these scores plots to be accurately analysed the loadings data is shown, Figure 3- 25, the highly positive, or negative, areas observed correlate to the areas within the raman data which have caused the majority of the variation in principal component 1.

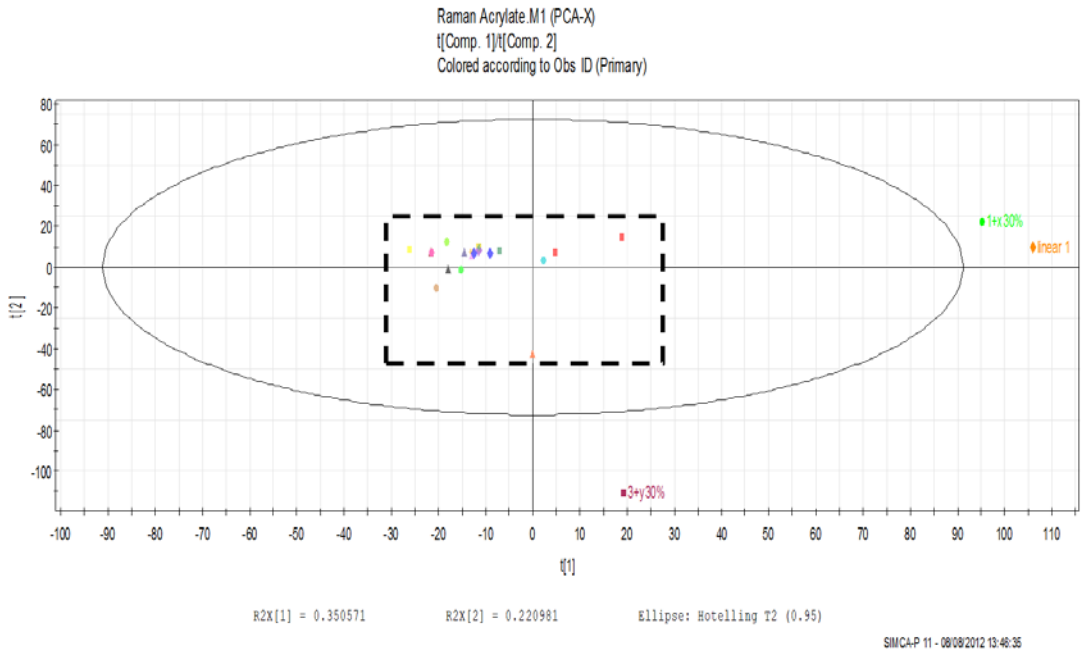

Figure 3- 22 Principal component analysis plot of RAMAN data collected from acrylate polymers. Any values which fall outside the oval, 95% confidence interval, are outliers from the rest of the data, in this case Linear 1 and polymer 4+y 30%.

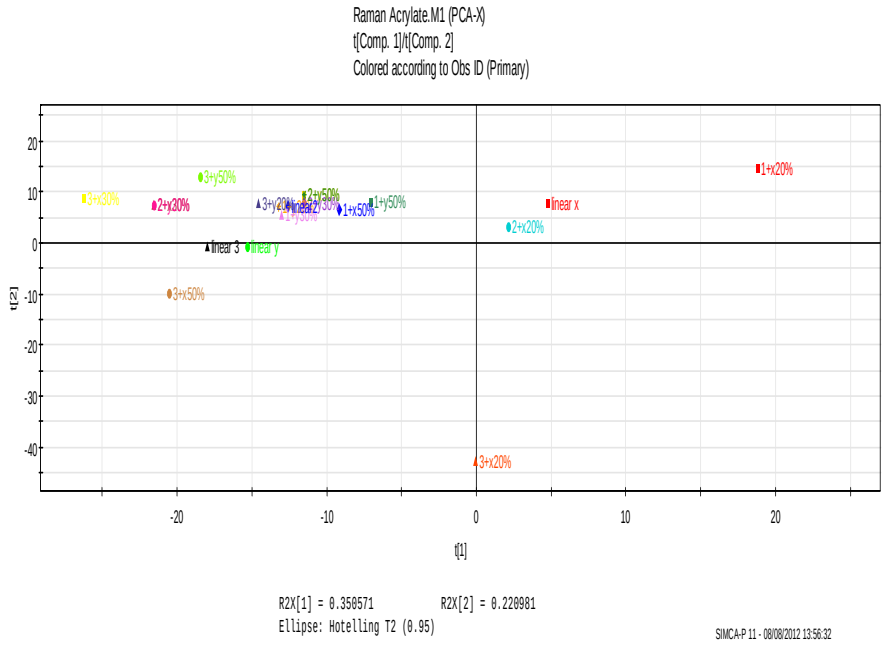

Figure 3- 23 Principal component analysis plot from Raman data as shown above with the outliers removed and central data reanalysed.

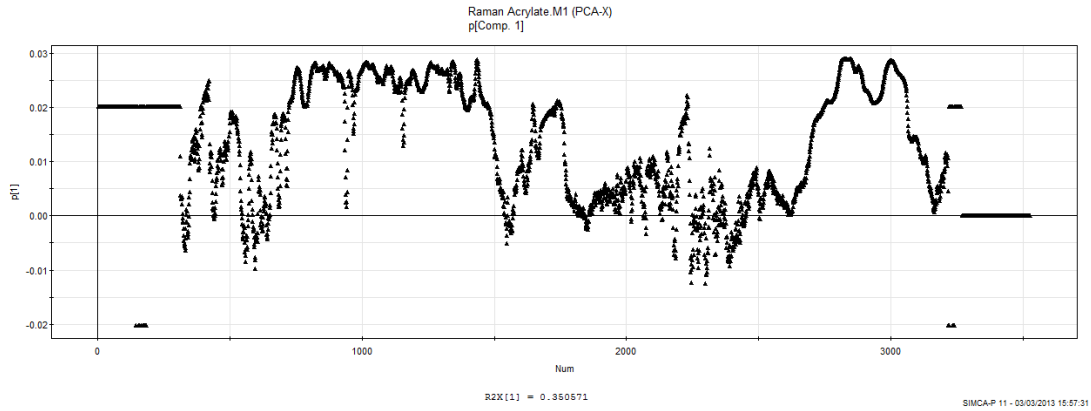

Figure 3- 24 Loadings plot principal component 1, Raman analysis.

3.4.5 Atomic Force Microscopy

Surface roughness and force of adhesion were determined using AFM. These two measurements can give an indication of the morphology of the polymer coating upon the glass slides. Surface roughness' are ascertained by rastering the AFM cantilever tip over the polymer surface and measuring the rise and fall over the surface topography. Linear polymer **1** was too sticky to allow measurement of the surface roughness, due to the gel type nature of the polymer the dipping of glass slides result in a tacky coating which stops the rastering of the AFM tip over the surface and can be detrimental to the instrumentation. From the results of this analysis polymers **1**+**x**50% and **1**+**y**20% have exceptionally high surface roughness values (49.2 and 20.6nm respectively). All other polymers tested had surface roughness' lower than 10nm with **2**+**y**20% and 30% measuring at 0.46nm. This would suggest that both these polymers coat evenly onto the glass surface with comparable topographies.

The force of adhesion between the cantilever tip and the polymer surface was also calculated for each sample. These forces give a measure of how "sticky" the polymer surface is in relation to all others within the set. The force of adhesion for polymer **2**+**y**20% could not be gauged as the polymer surface was too soft. This means that the cantilever tip was pushing into the surface rather than adhering to it. This result coupled with the exceptionally high surface roughness measured previously would suggest that this polymer was unique amongst this library. There were also a number of polymers which could not be measured as they were too sticky. This means that upon touching of the polymer surface the tip adheres too strongly and measurements are inaccurate. The other polymers of interest from these results are the linear species and **1**+**y**20%. These, in general, had a very

low adhesion of less than 30nN in comparison to the others recorded which were between 100 and 140nN. These lower values for the linear species in comparison to their branched counterparts may alter the biological properties of the polymer as the adherence of the bacteria to the surface could be hindered, or promoted, in comparison to the others being tested. The standard deviations for several polymers were considerably greater than the others within the set suggesting again that the coating onto the surface may not have been even. This would further suggest that there was a significant variation between the test sites upon each slide. This could affect biological activity as there is a greater surface area for the bacteria to adhere to; it has been shown that bacteria adhere in greater numbers to surfaces with numerous topographical features, whether these be greater or larger than the bacteria themselves (Mitik-Dineva et al., 2008). To combat these potential coating problems spin coating was employed in latter experiments to reduce pooling etc.

3.4.6 Differential Scanning Calorimetry

DSC or TGA was carried out on all applicable samples and plots shown in appendix 1. Polymer DSC is not as simple to interpret as that of small molecules or crystalline materials but there are specific shifts which should be visible within the spectra and can give a multitude of information about the polymer. These are the glass transition temperature (Tg), crystallisation temperature (Tc) and finally the melting temperature (Tm), a schematic of how these appear within a DSC trace is shown in Figure 3- 26 below. Glass transition is a small upward shift which then remains steady, crystallisation results in a loss of heat and thus a small dip in the trace whilst melting requires energy and thus is observed as a large peak in the DSC plot. TGA in comparison results in a plot which resembles that in Figure 3-27 which has a lot less available information than the DSC trace previously discussed. For this reason DSC is always the preferred technique but cannot always be safely utilised with volatile or “wet” samples.

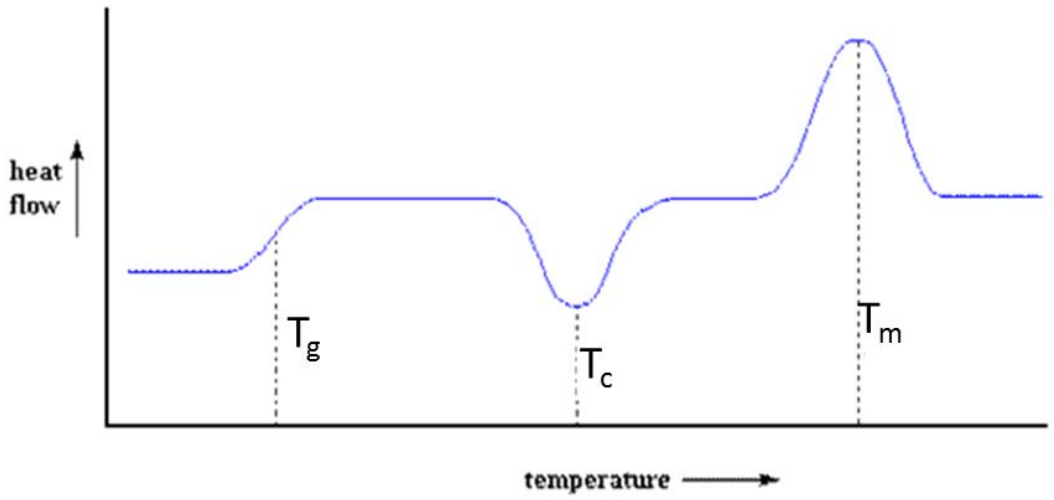

Figure 3- 25 Schematic of a polymer DSC trace showing the characteristic shifts resulting from the three most common polymer transitions, glass transition (Tg), crystallisation (Tc) and melting (Tm).

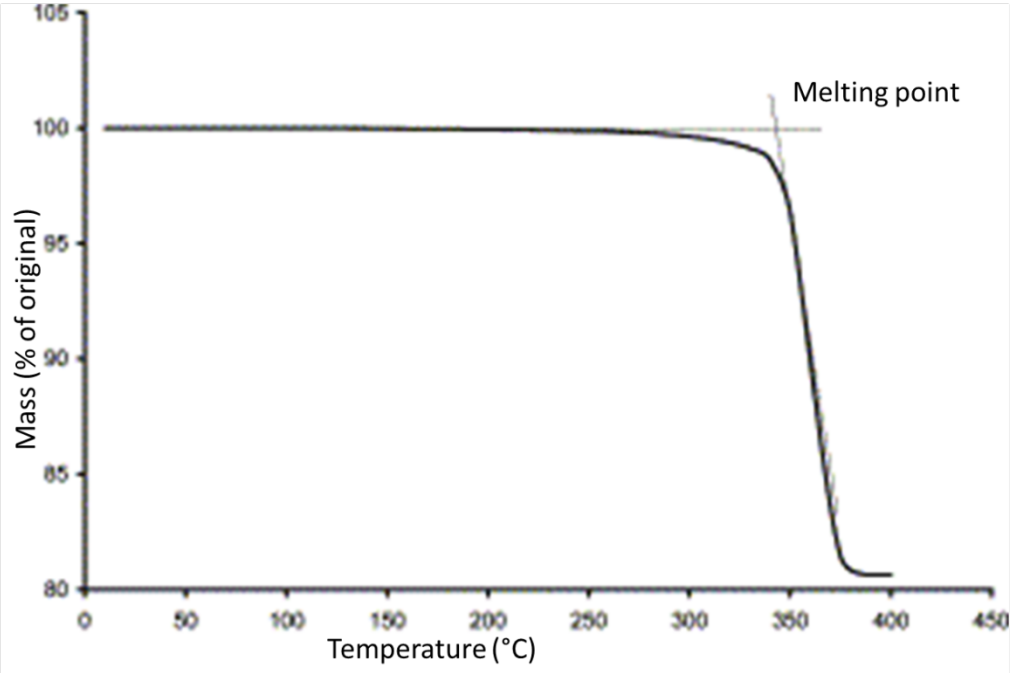

Figure 3- 26 Typical TGA plot showing the change in mass of a sample over time with increasing temperature. The sharp fall in mass represents the melting of the sample (Goodrum, 2002).

3.4.6.1 Monomer 1

Monomer **1** plots have a lot less information in general as the majority are TGA plots not DSC traces, however information regarding the melting points of the polymers can be gleaned from these experiments. Upon inspection of the TGA traces resulting from the investigation of polymers **1**+**x**20%, **1**+**x**30% and **1**+**x**50%, it can be seen that polymers containing 20 and 50% brancher have a large initial drop in mass, upon first heating cycle, of 2-3mg whilst the polymer containing 30% brancher drops less than 0.5mg. This is most probably due to the 20% and 50% samples being solvent or water wet prior to investigation. It can also be seen at the beginning of the 2nd heating cycle (34.5mins) in every sample a stepwise increase in the mass which could be an indication of the samples T_g which was masked in the first heating by solvent loss, this occurs at 30°C. Melting points for polymers synthesised using monomer **1** are all around 200°C and can be seen in the second heating cycle. As the linear polymer of monomer **1** was liquid it can be assumed that its melting point is lower than room temperature and thus the structure is significantly different to that of the branched polymers synthesised during this study.

Polymers **1**+**y**20% and **1**+**y**30% were again analysed using TGA whilst **1**+**y**50% was investigated using DSC. In these instances the initial drop in mass (during the first heating cycle) was much lower, less than 0.5mg in each case. Melting points for the 20% and 30% polymers were raised to around 220°C and the apparent Tg was absent at 30°C: this however could be an artefact produced upon the change in heating cycle in these samples. Sample **1**+**y**50% has 3 sharp peaks present in the first heating cycle at 45°C, 105°C and 130°C which could be representative of some melting behaviour but could also be the result of the loss of imbibed solvent. The small sharp changes observed at 52 and 55mins respectively are most likely due to a shape change within the polymer causing an uneven mass within the pan. It is obvious from this plot that the changes observed within the first heating cycle are not repeated within the second heating cycle and thus they may be irreversible or due to wet samples.

3.4.6.2 Monomer 2

Polymer **2**+**x**20% appears to have a Tg at 25°C followed by a melting point at 10mins (125°C) with a shoulder at 155°C and a small dip, which would normally suggest Tc however this is in the wrong order, at 170°C. This all occurs within the first heating cycle and there are no peaks or dips within the 2nd heating cycle however at 300°C there is a sharp drop off

which resembles the melting point in TGA however; is a sign of polymer degradation (Td) where the molecules vibrate so fiercely that they break their bonds and the polymer degrades, this can be exothermic or endothermic but in this case (and the case of other polymers within this set) is exothermic. Polymer **2**+**x**30% has a Tg at 50°C and a melting point of 145°C, both slightly raised from the 20% species which could be due to an increase in the rigidity of the main chain, more/bulkier side chains being present and increased crosslinking which are all possibilities of increased brancher. Again there is a dip at 175°C which resembles a Tc. At 300°C there is a sharp downward peak which could be explained by the bursting of the pan lid before the Td for this sample at 320°C, again raised from the 20% species. Finally the **2**+**x**50% polymer has a single peak at 130°C, Tm, and a shoulder at 155°C. During the second heating cycle a pan distortion can be observed at 170°C before Td occurring at 230°C then 300°C, this would suggest there are 2 distinct regions within this polymer which degraded at different temperatures however there are not 2 Tg, Tc or Tm signals observed.

Polymers synthesised using brancher **y** were also analysed; **2**+**y**20% has a Tg at 25°C, similarly to **2**+**x**20%, and a Tm at 145°C. There are 2 pan distortions observed during the 2nd heating cycle at 40 and 62mins before Td occurs at 60mins. **2**+**y**30% has a Tg at 30°C, higher than the 20% species as previously seen in the brancher **x** polymers, however possesses a Tm at 135°C which is contrary to previous experiments. Td is 320°C as observed numerous times previously. Polymer **2**+**y**50% melts at 115°C and degrades at 300°C (60mins). There is little other information able to be gleaned from this plot as there are no observable peaks or troughs within the spectra.

3.4.6.3 Monomer 3

Polymers synthesised using monomer **3** were also investigated using DSC and in this instance the linear polymer of monomer **3** was also able to be tested allowing comparisons to be made between the samples. The plot resulting from **3**+**x**20% showed a possible Tg at 35°C followed at 105°C by a very sharp high peak representing Tm with a shoulder at 155°C, there were no areas of note within the 2nd heating cycle possibly suggesting that the polymer was changed by initial heating. Polymer **3**+**x**30% had what appeared to be 2 glass transition temperatures at 35°C and 115°C, this is unusual and would suggest 2 distinct entities within the polymer. A clear melting point at 145°C was observed followed again by a small dip from the baseline which would suggest a crystallisation of the material at 165°C,

again there were no deviations in the second heating cycle. Polymer **3**+**x**50% again appeared to have 2 Tg values of 30°C and 85°C, this is similar to **3**+**x**30% if slightly unusual. There were a great number of peaks and troughs observed within this polymer's first heating cycle, Tm at 125°C, 145°C and 185°C whilst Tc was implied at 135°C and 165°C perhaps adding to the idea that there are distinct areas within polymers synthesised from these starting materials. Within the 2nd heating cycle it could be seen that there was some pan distortion at 48mins into the test and the polymer degraded at 290°C similarly to others which have been previously discussed.

Polymers synthesised from monomer **3** and brancher y had fewer signals observed in their DSC analysis; **3**+**y**20% had a Tg at 85°C which is significantly higher than any observed from monomer 1 or 2 polymers, and a Tm at 125°C with a smaller peak at 145°C potentially due to a second melting within the polymer. **3**+**y**30% had a much lower observed Tg at 45°C which is more in line with previous materials and a Tm at 115°C. These signals were followed by a potential crystallisation of the material at 135°C and a second melting at 145°C. Within the second heating cycle only pan distortions could be picked out at 41 and 54mins respectively. Polymer **3**+**y**50% again had a higher than expected glass transition temperature of 115°C followed by melting at 145°C, this polymer also degraded at around 300°C which is surprising as it would have been anticipated that the polymers with higher brancher content would be more resistant to heat and thus no degradation would occur. The linear polymer of monomer **3** had a much clearer and more distinct trace than those gathered from its branched counterparts, in this plot it is clear to see a glass transition at 55°C followed by a crystallisation of the material at 125°C and finally polymer melting at 145°C. However, at 300°C there is a shallow dip in the baseline which may be due to polymer degradation but is unlike the artefacts observed within other spectra. From all these observations it can be seen that the polymers synthesised, in general, had a glass transition below 40°C and melting occurred between 100°C and 150°C. The crystallisation of these polymers is more complex with the majority showing dips from the baseline only after melting, which is out of line with the expected results. Only the linear polymer of monomer **3** showed a clean, easy to interpret, DSC spectra which is most likely due to the lack of interference from the branched side chains.

3.4.7 Bacterial Testing –CV Staining

CV staining was used to determine the biological growth upon the polymer coated glass slides. Three strains of bacteria were used to determine the differences, if any, between their growth on the polymer surfaces.

3.4.7.1 Pseudomonas aeruginosa

The first of the bacteria used for testing was *Pseudomonas aeruginosa*. This is an aerobic gram-negative, rod-shaped bacterium which possesses unipolar motility and is a known biofilm producing strain (Ryan et al., 2010).

In all instances, the linear polymers of the monomers had a lower biofilm proliferation than the branched polymer species for this bacterial strain. The linear polymer synthesised from brancher **x** had a similar bacterial count than the monomer species and thus could explain the higher bacterial count on the polymers synthesised using both species. For linear polymer **1** the lower bacterial proliferation could be due to the polymer not solidifying upon synthesis however, for the other two linear polymers, this behaviour is less easily explained. It could however, be suggested that from this data linear polymers have a lower affinity for biofilms than their branched counterparts. For the branched polymers synthesised using monomer **1** and brancher **x**, as the percentage of brancher increases the biofilm proportion decreases; this is interesting, as there is no evidence of remaining starting material, acrylates are relatively toxic to bacteria (Blaschke et al., 2010), in any of the **1**+**x** polymer species from IR and in the Raman results these suggestion would be that the **1**+**x** 20 and 30% species would have less proliferation. For the polymers synthesised using monomers 2 and 3 with brancher **x**, the 30% species had the highest bacterial proliferation. Using the IR data polymer **2**+**x**50% potentially has unreacted material present which could drop its bacterial adhesion but this is not true of its 20% counterpart. From the Raman it would be easy to deduce that all polymers had a percentage of unreacted monomer or brancher present and thus a lower extent of biofilm would be present in every case: this is simply not the experimental outcome.

For the polymers synthesised using brancher y there are more obvious trends; in every instance as the brancher increases the biofilm decreases. The linear polymers synthesised from the monomers still have a lower absorbance than the branched species however the linear brancher has a higher presence of bacteria than the majority of the branched species. This is a more surprising result, as it would be thought that the addition of a greater

proportion of the highly biofilm promoting brancher would increase the bacterial growth but it is contrary to the experimental results. Thus it appears that via some symbiotic effect the addition of the brancher species to the linear lowers the bacterial affinity in a stepwise manner. For all samples there is a significant standard deviation in the data, this is due to bacteria being living organisms which are more complex to control than chemical synthesis or analysis. In an attempt to combat these problems each sample was run in quadruplicate and any outliers removed from the dataset.

3.4.7.2 Staphylococcus aureus

This bacterium is a gram-positive coccus which is facultatively anaerobic and appears as clusters which resemble grapes when viewed under a microscope (Ryan et al., 2010). This bacterium is also known to form biofilms and is of particular interest at present due to the rise of MRSA (Methicillin-resistant *Staphylococcus aureus*) within a hospital environment.

The results from this bacterium are shown in section 3.3.7.2, Figure 3- 16 showing the polymers synthesised using brancher **x**. It is obvious on first inspection that polymer **2**+**x**30% has the highest proportion of biofilm by a large margin, absorbance of 1.296 when all others are lower than 0.4, and this data point also has a high standard deviation. As with the **1**+**x** polymers previously there is a pattern within this data set; as the brancher increases the biofilm decreases. In this instance the brancher **x** polymer sample has a similar proliferation to the branched polymer species, with exception of **2**+**x**30%. The polymers resulting from synthesis using monomers **2** and **3** show no obvious pattern.

Polymers synthesised using brancher **y** are plotted separately for ease of inspection. In this case, all polymers resulting from monomer **3** have higher bacterial biofilm adhesion than those from either monomer **1** or **2** with **3**+**y**30% being noticeably higher than the others within the dataset. Polymers synthesised using monomer **2** are also lower than the others tested with this bacterium and all branched samples have a lower biological activity than their linear polymer control. Additionally brancher **y** has a higher absorbance than all monomer **2** polymers which would suggest that again the reaction between the monomer and brancher is causing a bioresistive surface. All testing carried out using *Staphylococcus aureus* had a lower absorbance than that of the *Pseudomonas aeruginosa* samples, this is due to the biofilm produced from this strain being less prolific than that of the previous investigation. This fact is utilised later in order to limit testing time.

3.4.7.3 Bacillus subtilis

The final bacterium used in this study to determine biological activity is the gram-positive, rod-shaped *Bacillus subtilis* (Madigan et al., 2010). This bacterium again forms biofilms and is able to survive in harsh conditions. As this was the concluding bacteria used to test the polymers the data collected from the earlier experiments using *Staphylococcus aureus* and *Pseudomonas aeruginosa* were taken into consideration and only polymers using brancher y were tested as there were more, and better defined, trends within the data. The results from this final test were inconclusive: all polymers had a very similar growth, with absorbances between 0.9 and 1.4, and when the standard deviation within the data was considered the polymers all had nominally the same activity for this bacterium. Due to this Bacillus subtilis was not used to test any further polymers synthesised.

3.5 Conclusions

From the data collected using a number of analytical techniques, it can be concluded that acrylate polymers can be synthesised in a facile manner using parallel synthesis techniques with minimal solvent. These polymers should require no work up and can be dried simply, overnight, in a vacuum oven. The fact there was solvent remaining within the polymer matrix suggest that the reactions should have been allowed to run longer, to completion, and the drying should have been more thorough. The resultant material is, in general, fully polymerised and easily manipulated as it can be dip or spin coated onto glass slides to allow for further testing.

Bacterial testing concluded that for a number of samples the biological proliferation upon their surface can be altered via changing the proportion of brancher species present in the original reaction mixture. This is most notable in polymers synthesised using brancher y and tested using Pseudomonas *aeruginosa.* From these results it was decided that the subsequent thiol-ene polymers would be synthesised using the same monomers chosen for this work in order to allow comparisons. Brancher y was also carried forward as it produced more interesting results from the biological testing. Finally *Bacillus subtilis* was dropped from the biological testing as it did not produce any significant data upon the polymers synthesised.

CHAPTER 4. THIOL-ENE POLYMER SYNTHESIS AND TESTING

4.1 Introduction

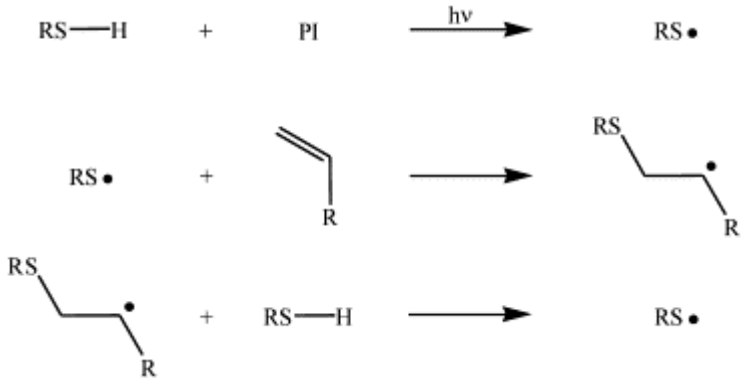

Figure 4- 1 Thiol-ene reaction mechanism using monofunctional thiol and alkene molecules (Cramer et al., 2003).

Thiol-ene polymers were reported as early as 1905 when it was observed that thiol and alkene species could react together spontaneously (Posner, 1905). This process was further developed over the years until the middle of the last century when the photo polymerisation of the thiol-ene species was first applicable on an industrial scale (Hoyle et al., 2004). However, due to the unpleasant odour and yellow colouring of the polymers produced along with the simultaneous boom in acrylate synthesis this route to polymer synthesis was to a large extent deserted (Lundberg, 2010). There have been many attempts to return this vital chemistry to an industrial market including Jacobine and colleagues in the early 1990s (Jacobine et al., 1992) but to a large extent these were unsuccessful. Thiol-ene chemistry has however been boosted in recent years with the clarification of the efficient click chemistry process taking place. Thiol-ene polymers are generated via a free-radical step growth reaction mechanism which proceeds by means of a two-step propagation process, Figure 4- 1 (Hoyle et al., 2004). This has prompted a renewed interest in possible applications of these unusual polymer species (Hoyle and Bowman, 2010); (Lowe, 2010); (Kade et al., 2010). A linear polymer is formed upon the reaction of a difunctional alkene with a difunctional thiol, whereas a crosslinked polymer

system is formed when the thiol or the alkene reagent has a functionality greater than two (Roper et al., 2004). In these experiments a range of thiols and acrylate monomers along with a difunctional acrylate brancher were chosen to give a variety of polymer outputs.

Thiol-ene reactions proceed most efficiently via a photo polymerisation route as this is rapid and less hindered by oxygen inhibition (Fu et al., 2008). This facile synthesis leads to high product yields with a tolerance for functional groups on both the thiol and alkene monomer units. Reaction solvents and purification steps are greatly unnecessary in these reactions making them an attractive prospect for large scale industrial synthesis once more (Iha et al., 2009). To date a number of thiol-ene based polymers have been examined for use as biomaterials, these include polysaccharides (Mergy et al., 2012) and Poly(ethylene glycol) (PEG) hydrogels (Aimetti et al., 2009). Work has also been carried out to determine the applicability of encapsulations of human mesenchymal stem cells (hMSCs) in thiol-ene synthesised (PEG)-based hydrogels to induce the process of cartilage formation, chondrogenesis (Salinas et al., 2007, Salinas and Anseth, 2008). Using thiol-ene click chemistry a library of branched acrylate polymers will be synthesised before being tested using numerous analytical techniques to determine their structure, crystallinity and surface properties. Bacterial testing using known prolific biofilm forming bacteria will then be carried out to determine the levels of bacterial proliferation upon the surface of the materials in comparison to control materials.

4.2 Methods

For reference, methods used to synthesise and analyse the polymers used within this chapter are detailed previously in Chapter 2: Materials and Methods.

4.3 Results

Synthesis of the majority of the branched thiol-ene polymers was successful; testing was carried out using a variety of analytical techniques to determine material and biological properties. All results from these experiments are detailed below.

4.3.1 Polymer Synthesis

All components used to synthesise these polymers are shown in Figure 1- 9. All polymers were successfully synthesised using UV methodology other than polymer **1A**. Polymer morphology, reaction time and colour however, varied wildly across the range of material synthesised.

The largest differences could be observed between the polymers synthesised using monomer 1,2-(dimethylamino)ethyl acrylate, and the rest of the polymer library. All were yellow-brown in colour, similar to the material generated during the previous acrylate work but alteration of thiol generated significantly different solid forms. The polymer made with thiol A did not entirely solidify on curing but, instead became a sticky semisold gel which did not hold its shape on removal from the synthesis plate. This is in direct contrast with the polymer made using thiol **B**, the highly substituted thiol used appeared to cause the polymerisation reaction to take place without the requirement for additional UV light, i.e. solidification is spontaneous upon addition of thiol **B** to reaction mixture. Polymers resulting from this self-polymerising reaction were solid and friable without the malleability observed in the other species synthesised from monomer **1**. Due to this interesting observation, polymers synthesised using thiol **B** were studied when cured in UV oven, similarly to all other polymers, and without any additional curing; polymers **1BC** (**1B** cured) and **1BN** (**1B** non-cured). The final polymer in this group, **1C**, had properties which were a hybrid of the other 2, malleable but solid and more similar to all other polymers made throughout the study.

The tendency of all polymers in this study was to the malleable, solid morphology without any “sticky-ness” or friability. All polymers were colourless to dark yellow depending on the monomer used and the odour from each was, although lessened from the pure thiol, strong and consistent with the thiol species used to generate the discs. As previously mentioned thiol B had a lessened odour in comparison to conventional thiols and thus these polymers were relatively odour free. After drying all polymers shrank slightly from around **2C**m to 1.8cm in diameter and all apparent beading of DMSO on the surface was entirely eliminated. It was observed that some polymers started to curl up slightly at the edges; this was difficult to see with the naked eye but became apparent under observation for contact angle measurements. Numerous analytical techniques were carried out at this juncture to determine whether the specific characteristics of monomers and thiols used in synthesis had been carried through to the final product and ensure that complete reaction had taken

place. Contact angle measurements taken in the first instance to gather information on the behaviour of water on these polymer surfaces.

4.3.2 Contact Angle Goniometry and Surface Energy

Contact angle measurements couldn't be taken for solid polymer discs as they had a slightly curved nature upon close inspection which rendered CAG un-useable. In order to combat this difficulty, individual polymers were coated onto glass coverslips as previously and analysed in the manner described above.

4.3.2.1 Contact Angle Goniometry

Contact angle measurements were taken using the instrument detailed previously and standard deviations calculated. All data from the three liquids investigated are noted in Table 4- 2.

Table 4- 1 Advancing contact angles (γA) of the probe liquids (FW, EG and DIM) on glass surfaces (n = 6; 23 °C).

Polymer	Mean advancing contact angles, ϑ_A / °		
	FW	DIM	EG
1BC	<10°	28.6±0.7	21.3±1.1
1BN	44.0±2.6	29.2±2.2	37.3±1.8
1C	48.6±3.2	41.1±3.3	72.0±3.0
2A	46.5±1.4	32.7±3.5	30.6±0.6
2B	78.5±1.8	44.8±2.7	65.7±2.1
2C	55.9±2.9	48.4±1.1	37.5±3.3
3A	45.7±1.0	32.2±2.2	27.3±1.6
3B	42.7±1.8	36.2±2.5	62.0±3.1
3C	44.3±2.1	43.4±1.1	40.6±0.6
4A	<10°	<10°	11.2±1.4
4B	45.2±1.7	36.6±0.3	31.3±1.5
4C	39.7±2.9	26.9±1.1	30.2±2.0
5A	32.1±4.0	27.1±1.0	25.7±0.5
5B	56.2±2.5	43.8±2.7	48.6±2.8
5C	31.8±2.5	39.1±2.4	28.6±2.0

6A	38.3±3.6	41.5±0.5	39.9±1.7
6B	75.5±1.3	36.2±2.2	47.6±1.8
6C	47.7±3.2	56.2±2.7	69.8±0.6
7A	31.3±1.4	31.8±1.7	35.1±2.6
7B	62.0±3.3	45.7±1.2	63.5±2.2
7C	67.1±1.6	34.4±3.0	32.6±1.9

4.3.2.2 Surface Energy

Using the contact angles from all three liquids surface energies of the polymer coatings were calculated. These are shown in Table 4- 3.

Table 4- 2 Surface energies (γS) as calculated from the advancing contact angle values (n = 6; 23 °C)

Surface	γ_s^+ / mJ m^{-2}	γ_s^- / mJ m^{-2}	γ_s^{LW} / mJ m^{-2}	γ_s / mJ m^{-2}
1Bc	-	-	-	-
1Bn	42.14	0.073	44.55	48.05
1C	66.84	3.91	39.05	71.40
2A	35.35	0.025	43.07	44.94
2B	12.83	0.32	37.12	41.19
2C	27.02	0.32	35.17	41.09
3A	34.94	0.062	43.29	46.23
3B	65.67	2.41	41.47	66.61
3C	45.01	0.00	37.86	38.27
4A	-	-	-	-
4B	37.75	0.041	41.28	43.78
4C	43.97	0.012	45.45	46.91
5A	51.44	0.007	45.38	46.61
5B	32.51	0.024	37.65	39.43
5C	54.31	0.013	40.06	41.73
6A	53.06	0.033	38.85	41.50
6B	8.00	0.054	41.47	42.78
6C	67.98	1.72	30.77	52.42

7A	58.17	0.13	43.46	48.88
7B	34.53	0.77	36.64	46.97
7C	11.11	0.44	42.31	46.76

4.3.3 Fourier-transform Infrared Spectrometry

Both polymers **1B** and **1C** have a large, broad peak at around 3550cm^{-1} which may be due to inclusion of water into the matrix, this is not present in monomer, brancher or thiol species. The polymers also show the removal of the C=C (1680-1640 cm^{-1}) and S-H (2550-2600 cm^{-1}) residues which would suggest a complete polymerisation has occurred. The only peak which is retained from the monomer and brancher is the C=O (1710-1740 cm^{-1}) similarly to the acrylate species previously synthesised. Both polymers have some similar peaks but their intensities vary wildly (see Figure 4- 5).

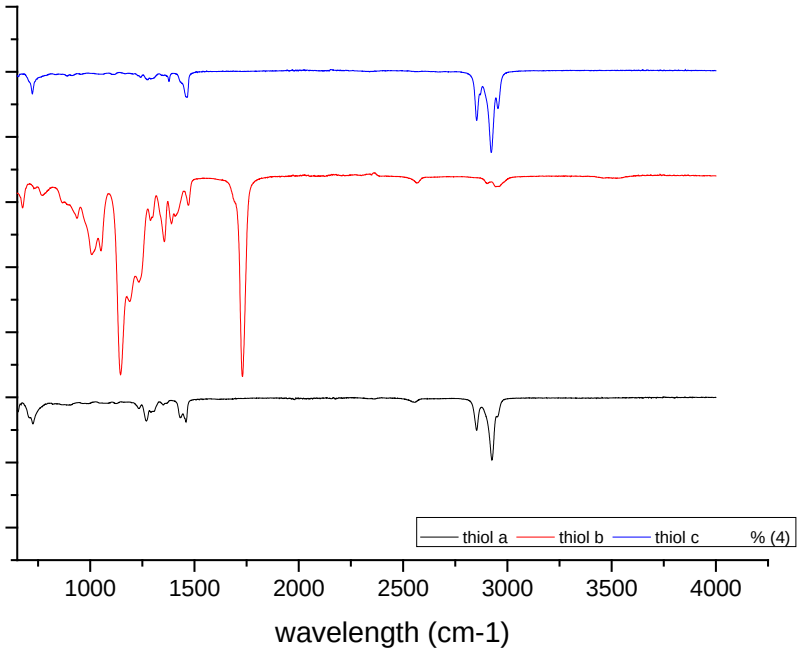

Figure 4- 2 FTIR spectra collected from the thiol starting materials used to synthesise thiol-ene polymers.

4.3.3.1 Monomer 1 Thiol-ene Polymers

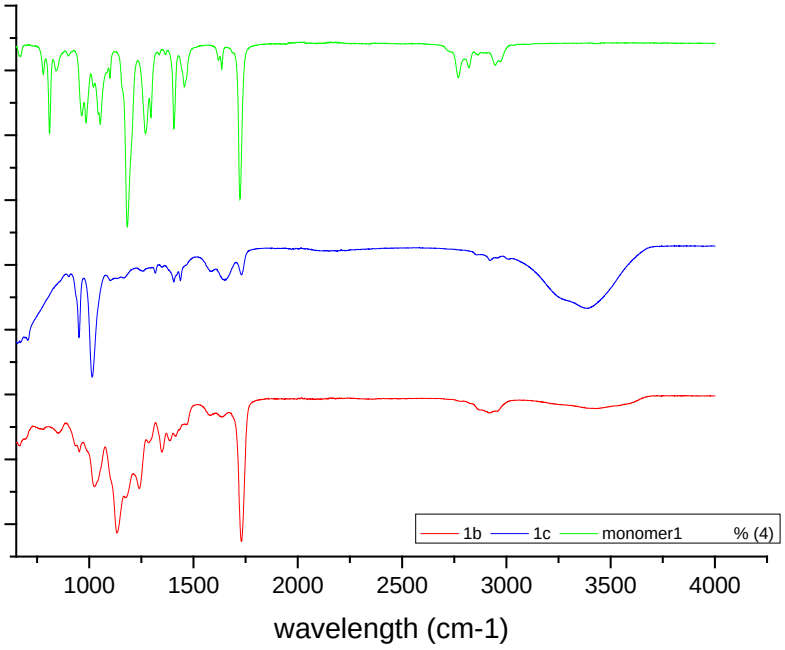

Figure 4- 3 FTIR results from polymers synthesised using monomer 1.

4.3.3.2 Monomer 2 Thiol-ene Polymers

Polymers **2B** and **2C** again have similar IR spectra, Figure 4- 6, even though their thiol component is vastly different. Polymer **2A** has no OH or C=O peak which are significant in the other 2 polymer spectra. As before, the SH and C=C groups appear to be absent from the polymer spectra indicating a thorough reaction has taken place.

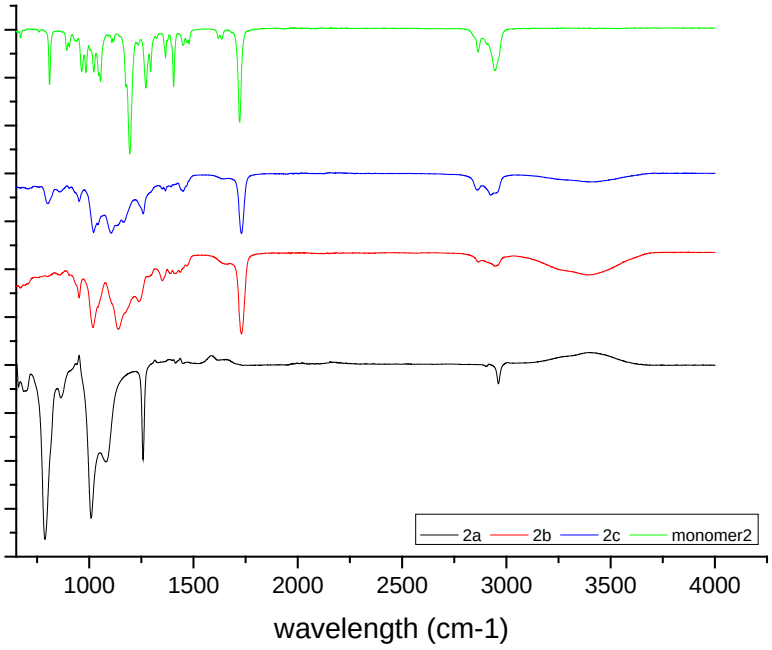

Figure 4- 4 FTIR results from polymers synthesised using monomer 2.

4.3.3.3 Monomer 3 Thiol-ene Polymers

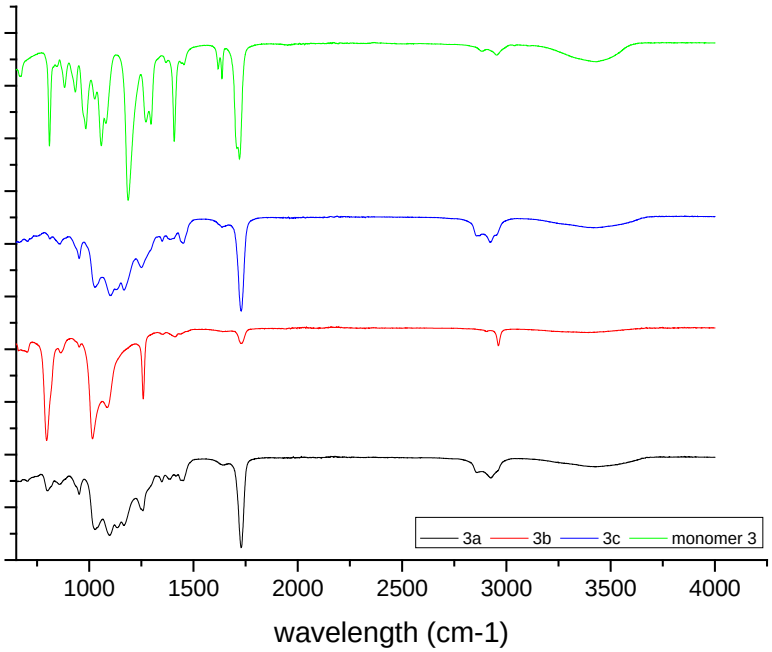

Figure 4- 5 FTIR results from polymers synthesised using monomer 3.

Polymers resulting from monomer **3** possess more similarities than those formed using the other monomers, Figure 4- 7. In this instance polymer **3A** and **3C** have almost identical spectra in both peak position and intensity. These polymers have the same features as polymers inspected previously with strong OH and C=O peaks. **3B** has lower intensities on the whole than the other 2 but has 3 high intensity peaks at 794, 1002, 1096 and 1258cm^{-1}. These may be indications of an S-OR ester, an O-C (doublet) and C-O stretching within this polymer. As previously all polymers show the CH_2, CH_3 and CH stretches between 2850 and 3000cm^{-1}.

4.3.3.4 Monomer 4 Thiol-ene Polymers

Polymer **4A**, **4B** and **4C** have very similar spectra from 1350-3500cm^{-1}, Figure 4- 8. All possess OH, CH_2/CH_3/CH and C=O residues in the same place at very similar intensities. Within the fingerprint region however there are some significant differences, **4A** has similarly intense peaks as observed in polymer **3B**. Polymers **4B** and **4C** have much closer fingerprint regions with some shifting with respect to one another at points. The intensities observed however are comparable. Please refer to for spectra for these polymers.

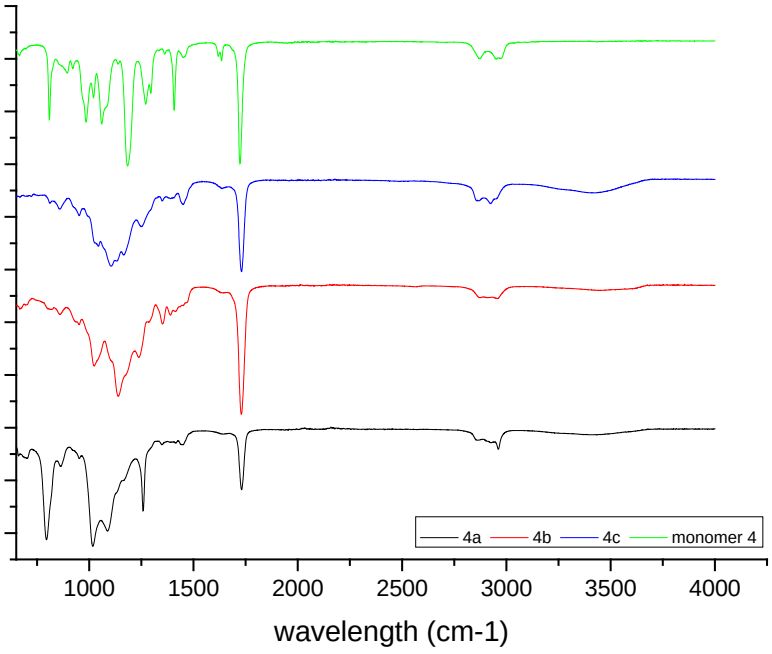

Figure 4- 6 FTIR results from polymers synthesised using monomer 4.

4.3.3.5 Monomer 5 Thiol-ene Polymers

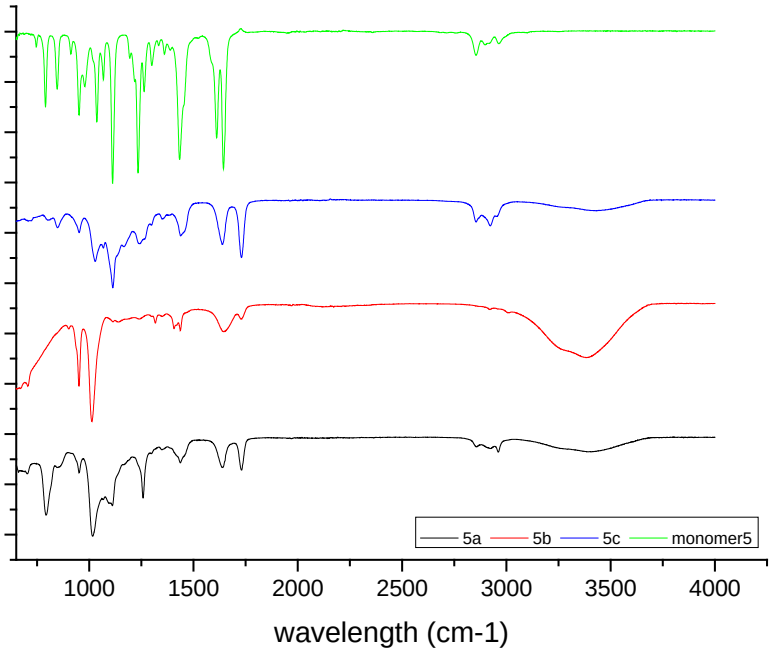

Figure 4- 7 FTIR results from polymers synthesised using monomer 5.

Polymers **5A**, **5B** and **5C** are very similar when inspected using IR spectroscopy, see Figure 4- 9. There is some peak broadening observed in the lower regions of the **5B** spectra but other than this there are few differences which would be indicative of vastly differing structures.

4.3.3.6 Monomer 6 Thiol-ene Polymers

Polymers from monomer **6** are again all very similar, with almost identical spectra, Figure 4-10. The intensities of the peaks in the fingerprint region do differ but the peak positioning and shape are unchanged.

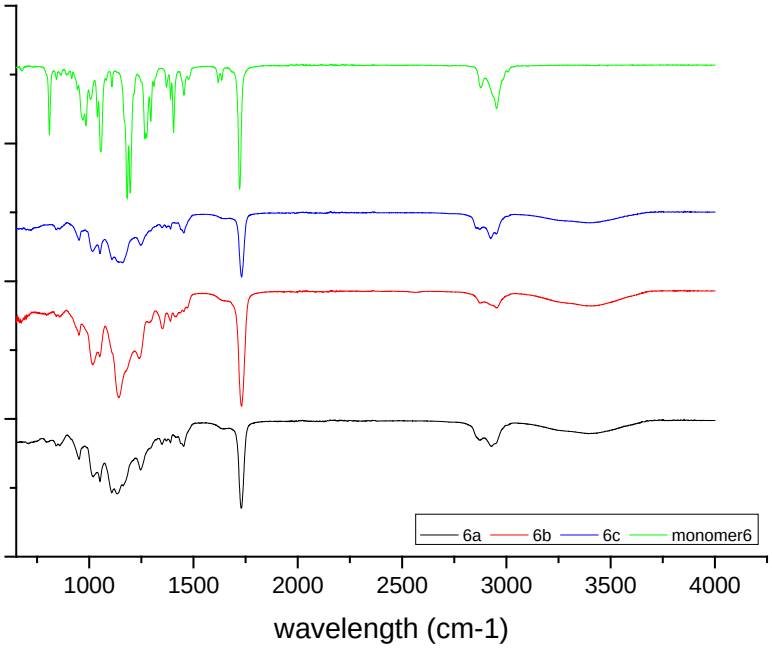

Figure 4- 8 FTIR results from polymers synthesised using monomer 6.

4.3.3.7 Monomer 7 Thiol-ene Polymers

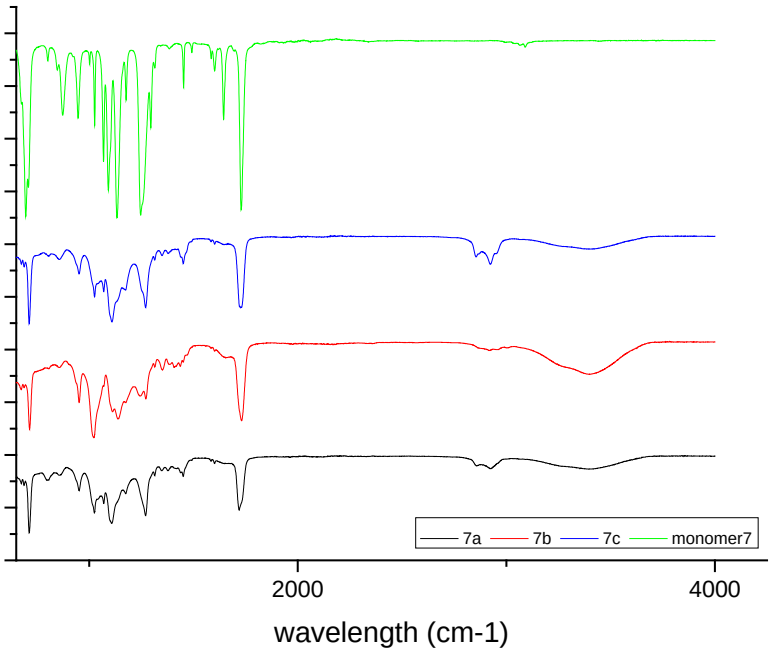

Figure 4- 9 FTIR results from polymers synthesised using monomer 7.

Similarly to polymers synthesised using monomer **3**, polymers **7A** and **7C** are alike whilst **7B** is distinguishably different, Figure 4- 11. There is a much larger OH peak observed in **7B** along with a broader and less distinct $CH_3/CH_2/CH$ region. The fingerprint regions of these polymers are similar with little changes in intensity.

4.3.4 Raman

Spectra were collected for all thiol-ene polymers synthesised using the methodology detailed in chapter 2. These spectra are shown below, Figure 4- 12 to Figure 4- 18. These spectra are very similar with the majority of peaks matching up irrespective of the thiol used for synthesis. Additionally to this there were a number of peaks present in all spectra, irrespective of the monomer and thiol species used in synthesis, these include 2970 and 2820cm^{-1} (C-H), 2470cm^{-1} (S-H), 1630cm^{-1} (C=O), 1500cm^{-1} (C=C), 1345cm^{-1} (CH_3), 1200cm^{-1} (C=S), 900cm^{-1} (C-O-C) and 750cm^{-1} (C-S). This would suggest that there is potentially some unreacted starting material (S-H and C=C) is present in the final product. However, these results do suggest that the reaction has successfully taken place, in the bulk of the material, due to the presence of C-O-C bonds. As these plots are so similar it seems illogical to analyse them separately but instead PCA of the data was carried out in order to group the resultant plots. The results of this analysis are interrogated in the discussion chapter to follow.

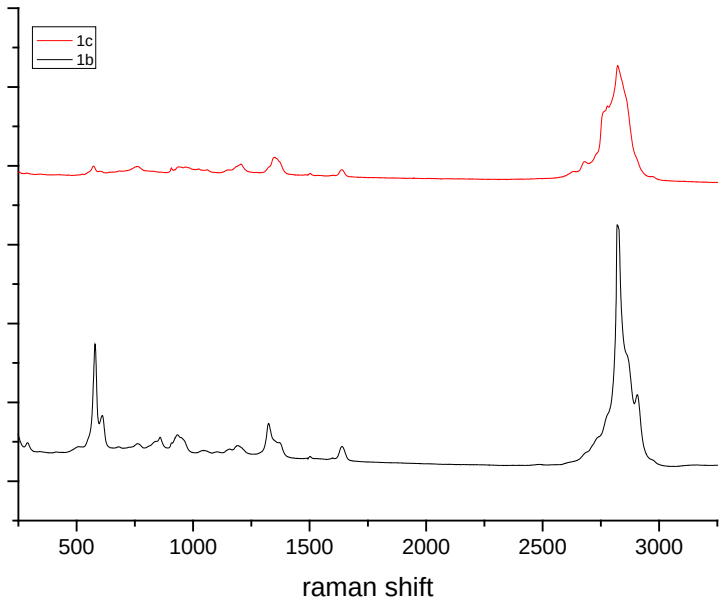

Figure 4- 10 Monomer 1 thiol-ene polymers Raman.

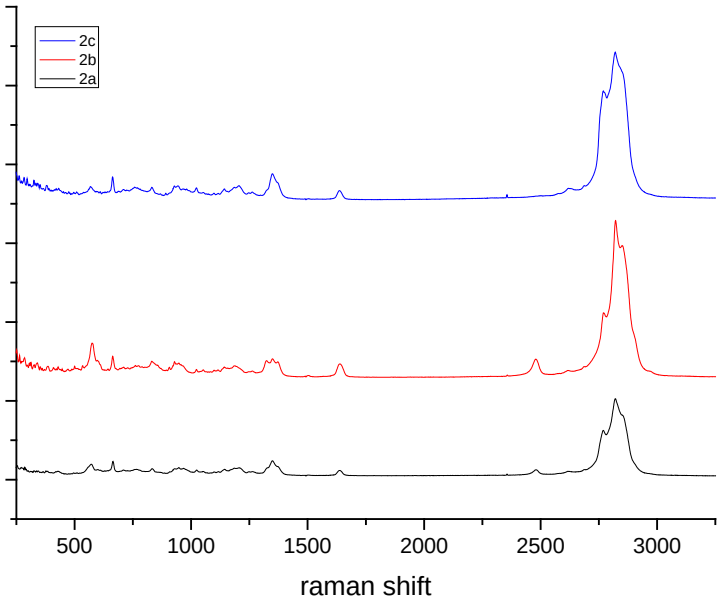

Figure 4- 11 Monomer 2 thiol-ene polymers Raman.

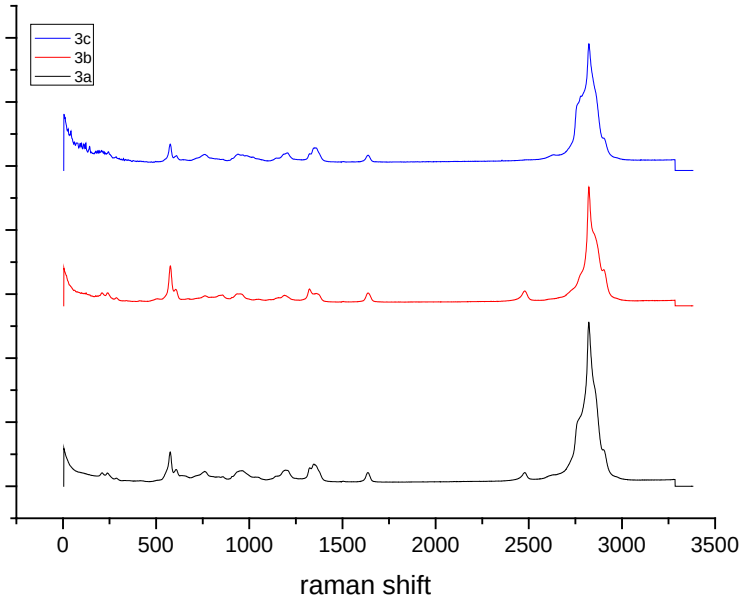

Figure 4- 12 Monomer 3 thiol-ene polymers Raman.

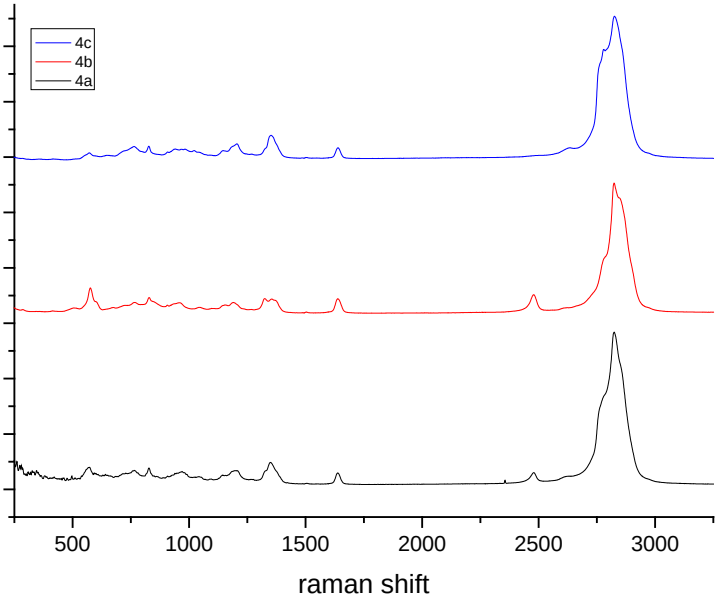

Figure 4- 13 Monomer 4 thiol-ene polymers Raman.

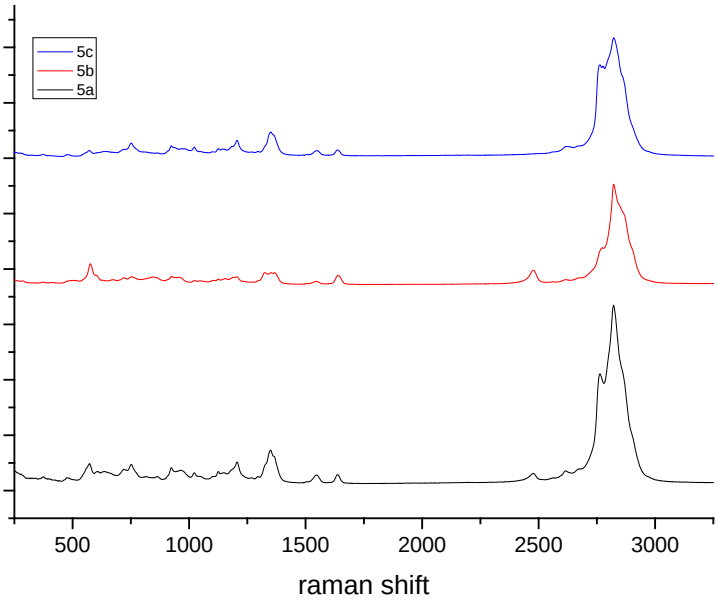

Figure 4- 14 Monomer 5 thiol-ene polymers Raman.

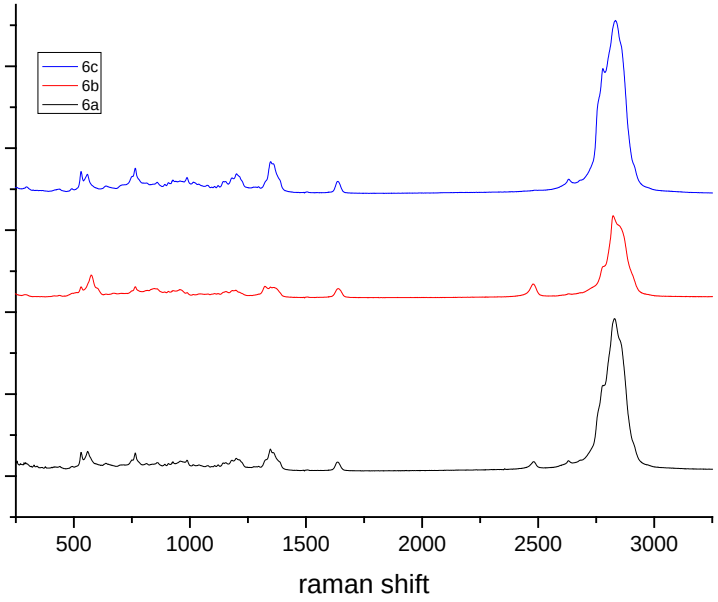

Figure 4- 15 Monomer 6 thiol-ene polymers Raman.

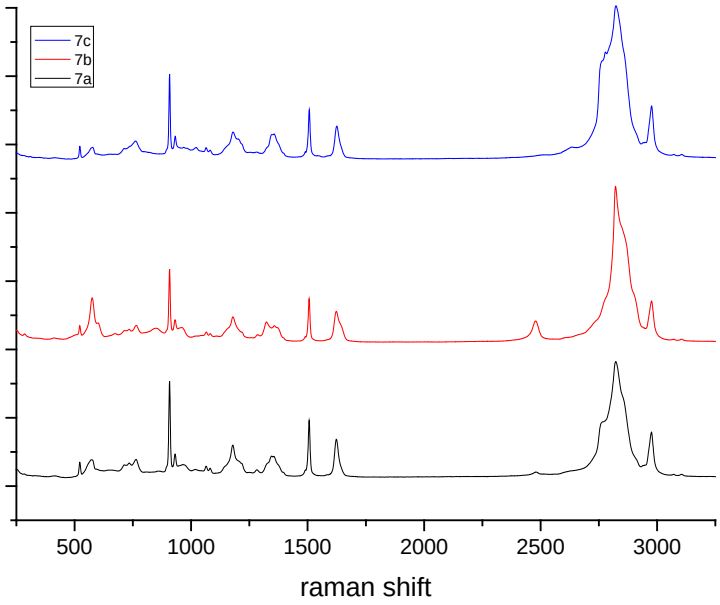

Figure 4- 16 Monomer 7 thiol-ene polymers Raman.

4.3.5 Differential Scanning Calorimetry

In contrast to the acrylate samples analysed previously, all thiol-ene samples were analysed using DSC. This was due to the mass loss, from solvent evaporation, being low enough that they were deemed safe to be used in this instrument. From this analysis graphs of mass

changes in relation to temperature were collected and analysed via inspection to determine the melting point and glass transition temperature of each polymer sample. Polymer DSC is much more complex than small molecule DSC and thus; the changes described are more difficult to define accurately and they look significantly different to the exemplar graph shown in Figure 2- 12. In general it was found that, when compared to other more conventional linear or cross-linked polymers, including acrylate species, thiol-ene polymers appear to have a highly uniform dense structure resembling a network and thus an inherently narrow glass transition temperature range (Roper et al., 2004, Lub et al., 1999). All thiol-ene polymer DSC are detailed in Appendix 2.

4.3.6 Bacterial Testing – CV Staining

Bacterial testing was carried out to determine the proliferation of biofilms on the surface of the thiol-ene polymers. Testing primarily was carried out using thiol-ene discs before polymer coated glass slides were utilised to combat staining and fluorescence issues. Details of all biofilm testing are noted below.

4.3.6.1. Thiol-ene Discs

Thiol-ene polymer discs tested using *Pseudomonas aeruginosa* and *Staphylococcus aureus* as previously and bacteria stained using crystal violet to allow quantification. However, in a number of samples the stain appears to adhere to the polymer disc along with the biological material causing erroneous results. In a number of instances the negative control sample, polymer disc in media with no added bacteria, had a higher UV absorbance than the corresponding samples. This could be due to the bacteria existing predominantly in pores present on the polymer surface preventing stain leaching into the surrounding material as happens in the control samples. As previously, positive control samples were untreated polystyrene wells stained to the correct volume (0.5ml of stain same total volume as polymer disc) after addition of bacteria. Negative controls were thiol-ene coated slides without the addition of the bacteria; these were used to correct data before comparison. In addition to the novel problem of the dye staining the thiol-ene discs it was noted that polymer discs **1BC**, **1BN** and **1C** were swelling, unidirectionally, in media overnight at 37°C. This led to further investigation of thiol-ene polymer properties.

4.3.6.2 Polymer Coated Cover Slips

Crystal violet staining was repeated using polymer coated glass slides and the results of this are shown in Figure 4- 19 and Figure 4- 20. From Figure 4- 19 it can be seen that all *Pseudomonas aeruginosa* samples gave positive results after correction using the negative controls. Sample **2C** and **7B** had the lowest biofilm proliferation but all polymers were lower that the positive polystyrene control.

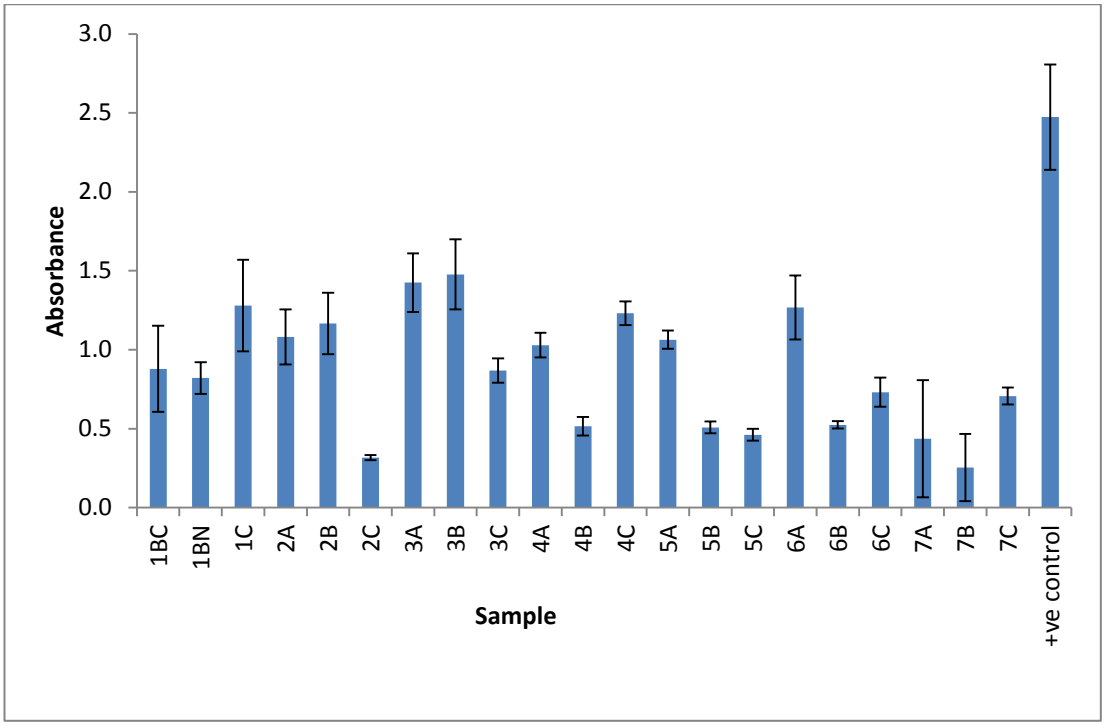

Figure 4- 17 Bar chart showing the *Pseudomonas aeruginosa* biofilm proliferation on thiol-ene polymer coated glass slides over 24hrs, including standard deviations.

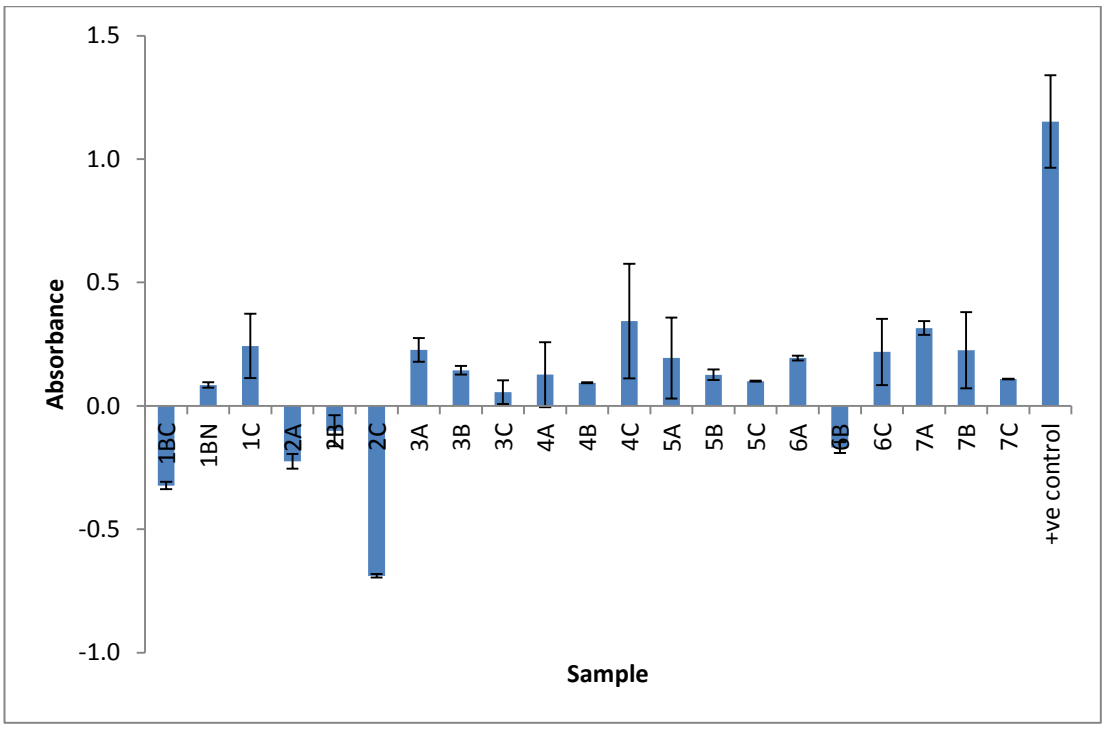

Figure 4- 18 Bar chart showing the *Staphylococcus aureus* biofilm proliferation on thiol-ene polymer coated glass slides over 24hrs, including standard deviations.

The results of the *Staphylococcus aureus* biofilm testing are shown in Figure 4- 20. In a number of cases the correction using negative control samples has given a "negative absorbance" this is obviously not possible but would suggest that similarly to the thiol-ene discs some polymers absorbed more stain than the bacterial samples, suggesting some kind of shielding from dyeing. Notably all polymers synthesised from monomer 2 have had this more unusual outcome. Again all polymer samples had a lower biofilm proliferation than the polystyrene positive controls.

4.3.7 Bacterial Testing – GFP Bacteria

In order to overcome the problems of staining bacteria and to investigate the unusual swelling of the thiol-ene discs on biofilm growth GFP *Pseudomonas aeruginosa* were grown on thiol-ene discs in the same manner as previously. Using a Nikon SMZ1500 fluorescence microscope using a FITC filter (Excitation 494 nm; Emission 518 nm) polymer samples with bacteria were visualised and images captured. However, it was discovered that all thiol-ene polymer discs generated were fluorescent at this wavelength. This is not an unusual phenomenon but it did render the GFP experiments useless and a further methodology had

to be used to determine accurate biofilm proliferation. An example of the images captured is given in Figure 4- 21.

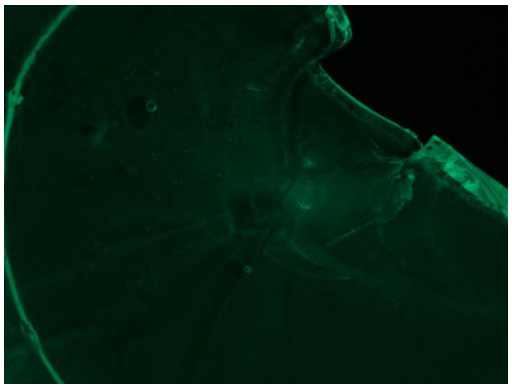

Figure 4- 19 Brightfield image of thiol-ene negative control disc (polymer 1BN) showing fluorescence at excitation wavelength.

4.3.8 Bacterial Testing- Bacterial Plate Counting

In order to determine bacterial growth without the use of stains or fluorescence bacterial plate counting was employed, method as previously noted, section 2.5.5..

4.3.8.1 Preliminary Experiments

The preliminary experiments were carried out in order to determine the optimum time to agitate each sample for. The results of these experiments for both bacterial strains are shown in Table 4- 4.

Table 4- 3 Preliminary experiment results for P. aeruginosa and S. aureus plate counting experiment.

Pseudomonas aeruginosa			***Staphylococcus aureus***		
Time (s)	**No. of colonies on plate**	**No. of colonies in biofilm**	**Time (s)**	**No. of colonies on plate**	**No. of colonies in biofilm**
0	0	0	0	0	0
30	4	30075	30	15	112782
60	4	30075	60	5	37594
90	3	22556	90	4	30075

120	2	15038	120	6	45113
150	3	22556	150	4	30075
180	2	15038	180	10	75188
240	2	15038	240	2	15038

It was decided from these results that 30s was sufficient time to dislodge the biofilm which was adherent to the polymer coated glass surface. This was due to the numbers of observed colonies not increasing in number with prolonged agitation from this point.

4.3.8.2 Polymer Testing

All further experiments therefore were vortexed for 30s before being spotted onto petri dishes and incubated overnight. There was a significant difference noted between the numbers of colonies visible after 24hrs on each different bacterial strain with *Staphylococcus aureus* having the greater number. Data from the testing is detailed in Table 4- 5 and plots of this data are shown in Figure 4- 22 and Figure 4- 23.

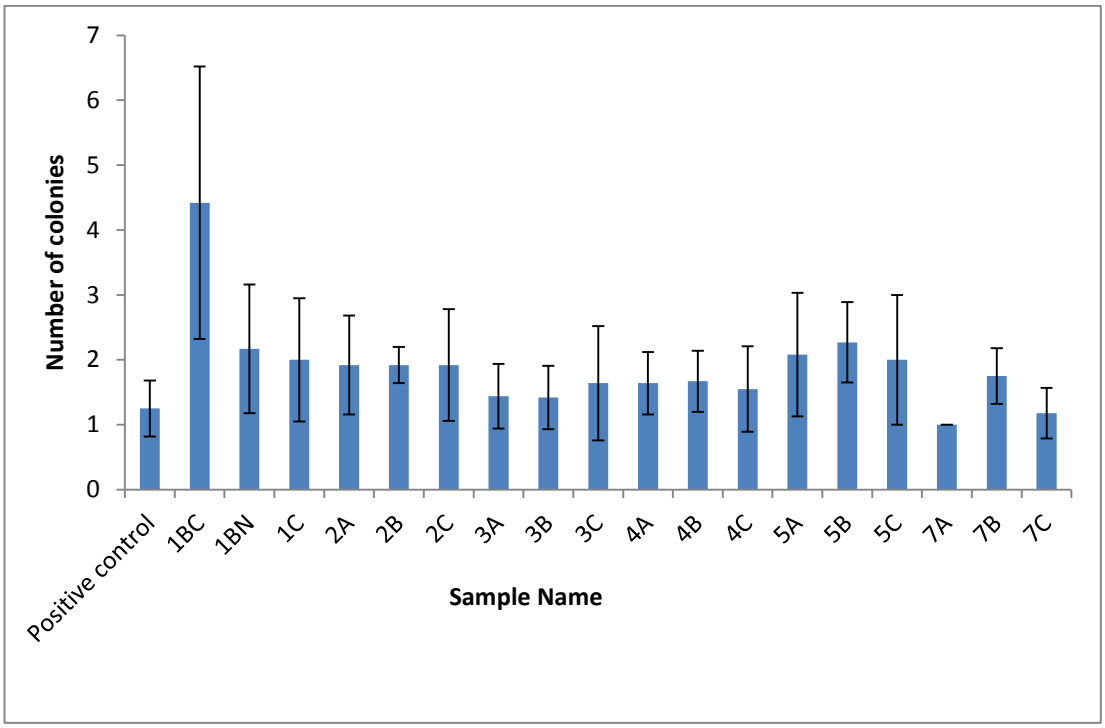

Figure 4- 20 *Pseudomonas aeruginosa* colonies present on polymer coated glass coverslip after 24hrs (mean), errors shown are standard deviations.

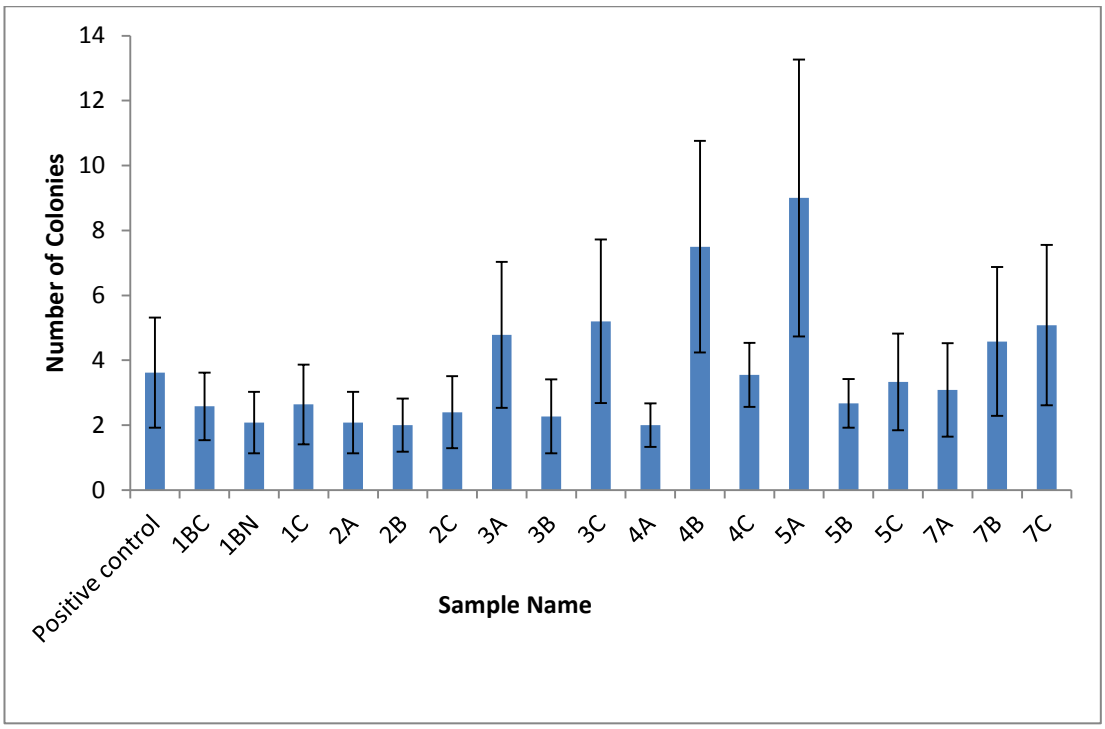

Figure 4- 21 *Staphylococcus aureus* colonies present on polymer coated glass coverslip after 24hrs errors shown are standard deviations.

	Pseudomonas aeruginosa			*Staphylococcus aureus*		
Sample name	Average number of colonies	Standard Deviation colonies	Number of bacteria on disc	Average number of colonies	Standard Deviation colonies	Number of bacteria on disc
Positive control	1.25	0.43	9398	3.62	1.70	27183
1BC	4.42	2.10	33208	2.58	1.04	19424
1BN	2.17	0.99	16291	2.08	0.95	15664
1C	2.00	0.95	15038	2.64	1.23	19822
2A	1.92	0.76	14411	2.08	0.95	15664
2B	1.92	0.28	14411	2.00	0.82	15038
2C	1.92	0.86	14411	2.40	1.11	18045
3A	1.44	0.50	10860	4.78	2.25	35923
3B	1.42	0.49	10652	2.27	1.14	17088
3C	1.64	0.88	12303	5.20	2.52	39098
4A	1.64	0.48	12303	2.00	0.67	15038
4B	1.67	0.47	12531	7.50	3.26	56391
4C	1.55	0.66	11620	3.55	0.99	26658
5A	2.08	0.95	15664	9.00	4.27	67669
5B	2.27	0.62	17088	2.67	0.75	20050
5C	2.00	1.00	15038	3.33	1.49	25063
7A	1.00	0.00	7519	3.09	1.44	23240
7B	1.75	0.43	13158	4.58	2.29	34461
7C	1.18	0.39	8886	5.08	2.47	38221

Table 4- 4 Number of colonies and therefore adherent bacteria on discs with standard deviations.

4.3.9 Bacterial Testing - HSI for Biofilm Quantification

To further investigate the adhesion of bacteria to the polymer surface a novel technique, hyperspecteral imaging, was employed. This method is preferential to staining as it is non-destructive and thus if no valid results can be gleaned, staining can still be carried out as a secondary experiment. For use in this this experiment polymers, as for all other bacterial visualisation studies, were cultured with bacteria for 12hrs at 37°C in appropriate well plates. Media was removed by pipette and bacteria covered discs were held within the well plates throughout testing. Using a method based on the work published by Polerecky et al. quantification of a bacterial biofilm was carried out (Polerecky et al., 2009). Images of every polymer disc were taken using the hyperspecteral setup detailed in Chapter 2 before being analysed using principal component analysis. The results from two representative images are detailed within this chapter, Figure 4- 24 and Figure 4- 27.

The first image investigated contains a bacteria coated polymer disc along with a polystyrene positive and a negative control sample and finally an empty well. This makes it an ideal image for showing the ability of HIS, if any, to distinguish between a polymer disc, and bacterial control samples. This analysis was carried out in two distinct ways, first a simple analysis of the collected spectra was run in order to assess any obvious variations between the samples before PCA of the whole image was completed in an attempt to distinguish distinct regions between polymers with and without bacteria and between differing polymer species. The raw image of this data, with no processing, is shown in Figure 4- 24.

Primarily spectral plots were analysed to determine any similarities within the samples, the spectrum were taken from a 10x10 pixel region at the centre of each of the wells. There is variation between the plots shown in Figure 4- 25 which appears to be a scaling due to light intensity. The signal derived from the top of the well plate is more intense than that at the base, this is simply due to shadowing as the camera takes the hyperspectral image however, it is shown in the resultant plots, as a difference within the samples. As such mean centring of the data was carried out to allow for more comprehensive comparisons. This technique is a simple subtraction of the mean of the spectrum from each point within it, ($X_{centred} = X_{\lambda} - \overline{X}$), which results in the spectrum being centred around the 0 point and resolves any issues caused by scaling. These corrected plots are shown in Figure 4- 26 and it can be observed that the majority of the data is actually identical.

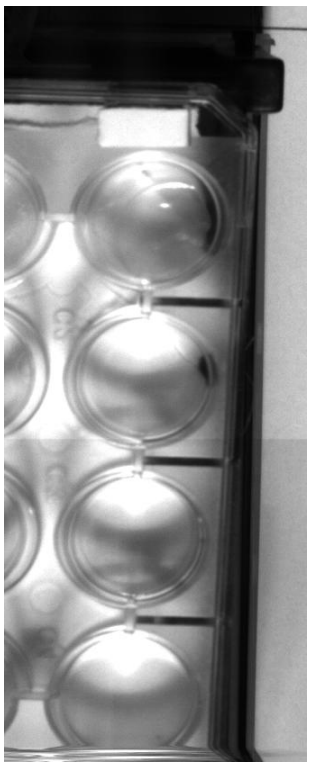

Figure 4- 22 Raw image of polymer disc coated in bacteria (well 1, top), positive bacterial polystyrene control (well 2, second), negative polystyrene control (well 3, third) and finally an empty well (well 4, bottom).

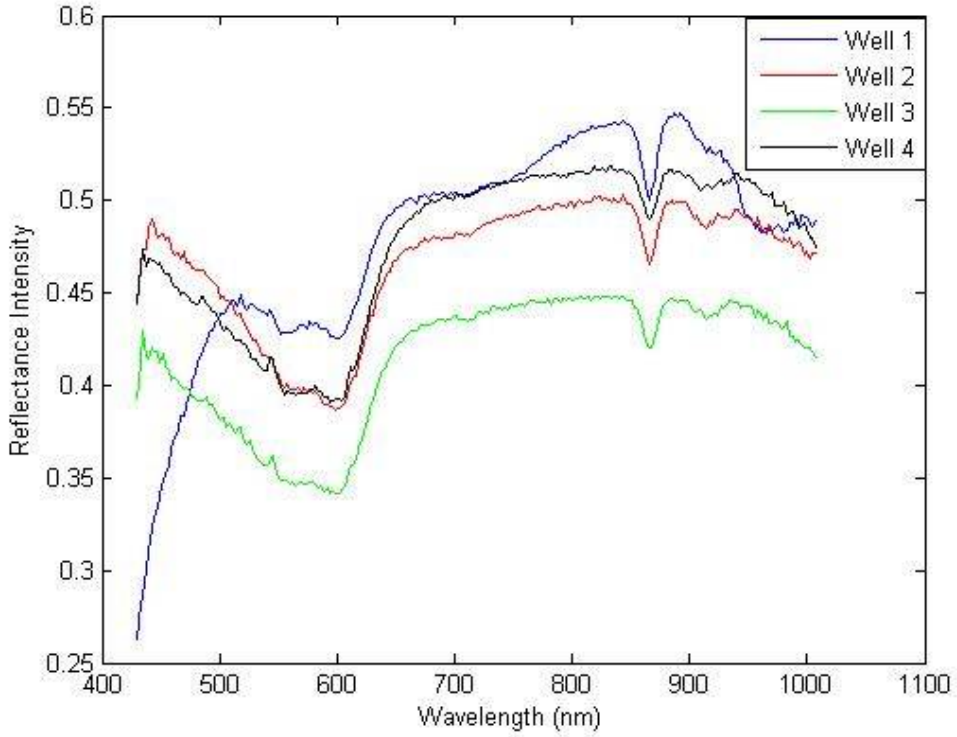

Figure 4- 23 Data collected from hyperspectral image shown in Figure 4- 24, all data looks very different however this is largely due to a scaling effect caused by intensity differences due to shadowing.

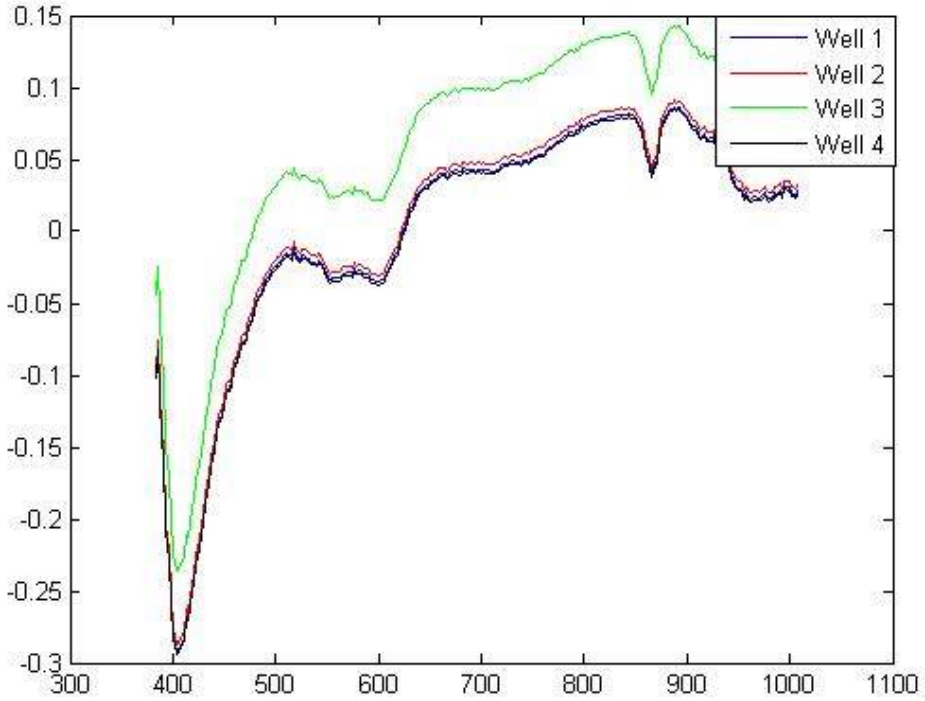

Figure 4- 24 Mean centred data collected from raw image, Figure 4- 24 above, it can now be easily observed that the majority of the data collected is identical and well 3 appears to still be scaled by intensity.

From this data little about the differences between the polymer samples and controls, or the differences between the positive and negative controls, could be easily gleaned. Thus principal component analysis (PCA) was carried out on the data collected in order to further differentiate between the samples. The PCA results in scores images shown in Appendix 3 and discussed further in section 4.4.9 below. The second raw image, Figure 4- 27, analysed consisted of 4 polymer samples, **5A**, **5B**, **5C** and **6A**. This image was chosen at random from the data in order to determine whether this technique can be used to determine the differences between polymers and also between differing levels of biofilm adhesion. As previously the spectra pulled from this image were mean centred, Figure 4- 28, before being analysed using PCA as previously. The four scores plots are shown in Appendix 3 and are investigated further in the discussion section below.

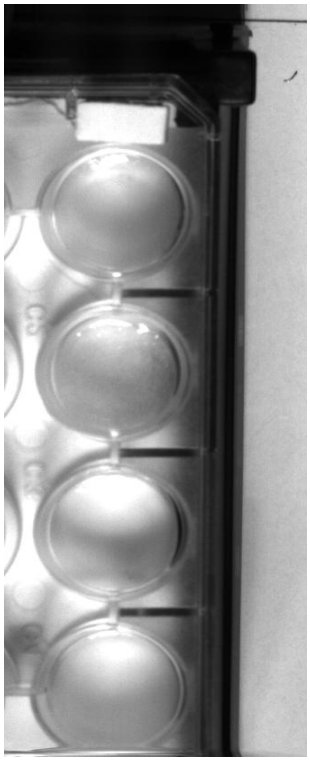

Figure 4- 25 Raw image of polymer discs coated in bacteria; 5A (well 1, top), 5B (well 2, second), 5C (well 3, third) and finally 6A (well 4, bottom).

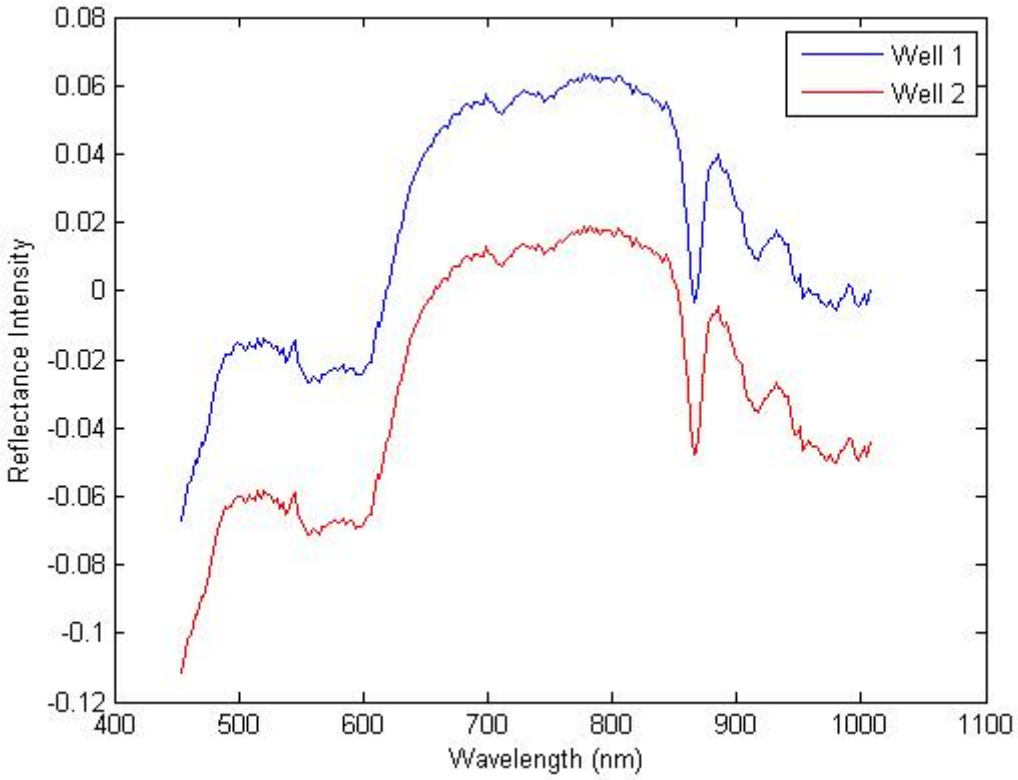

Figure 4- 26 Mean centred data collected from raw image, Figure 4- 27 above, only wells 1 and 2 were investigated in this preliminary work. Again it can be seen that the spectra are similar and only scaled by intensity.

4.4 Discussion

4.4.1 Polymer Synthesis

In general the polymer synthesis was successful, other than **1A**. All polymers were generated via the methodology stated in chapter 2. The vast majority of polymers prepared were facile to generate, components were added to the initiator in the order; solvent (DMSO), monomer, brancher and then finally thiol before being admixed for 30s via vigorous shaking. These mixtures remained in a liquid form until post curing using UV light. However, polymer **1B** synthesised using monomer **1** and thiol **B** spontaneously solidified post addition of the thiol component. This made synthesis more complex as the separation into 0.5ml aliquots in wells had to be performed prior to solidification. For **1B** polymers therefore it was unnecessary to cure them in the same manner as the other polymers within the library but, in order to investigate the properties of this interesting species

further a proportion of **1B** polymers were cured whilst the remainder was left to solidify naturally on the bench before being dried in the same way as all other polymers. This led to there being 2 polymer **1B**s, polymer **1BN** (non-cured) and polymer **1BC** (cured). All polymers synthesised were flexible solid discs which were translucent and colourless to light brown. The colour of the polymers appears to be dependent on the monomer used to synthesise them as, similarly to the acrylates prepared in the previous chapter, monomer **1** polymers were darker in colour than the others prepared. Interestingly polymer **1BN** was lighter in colour than **1BC** suggesting a difference between these two species caused by the curing process. All polymers synthesised possessed an odour related to the thiol they were prepared with however, the potency of this was seriously reduced from that of the monomer alone. Polymers were facile to remove from wells and post drying could be stored at room temperature until testing. Following synthesis and drying all polymers were taken forward for testing via a number of analytical and biological methods. Whilst this testing was taking place it was noted that the polymers resulting from monomer **1** imbibed water to varying extends. This suggested that these polymers were hydrogels and this property was further investigated in Chapter 5.

4.4.2 Contact Angle Goniometry and Surface Energy

Contact angle measurements were carried out in the manner described in Chapter 2 with results noted previously. It can be seen that, similarly to some of the acrylate polymers, polymers **1B**C and **4C** had a contact angle of less than 10° which is below the limit of detection for this instrument. This makes the generation of the surface energy for that specific polymer to be unable to be calculated.

Other than these two polymers with very low water contact angles all other contact angles measured in this data set lay between 30° and 80°; this indicates that all polymers within this set are wetting and thus are hydrophilic but to differing extents. In general polymers synthesised using thiols **A** and **C** are more wetting than those prepared using thiol **B**. This would suggest that thiols **A** and **C** are very hydrophilic and vastly different to thiol **B** which can be easily observed after inspection of the chemical structures, Figure 1- 9.

Thiols **A** and **C** are similar molecules with a single C-C chain backbone possessing terminal thiol groups in comparison to thiol **B** which is a highly complex branched compound with multiple terminal thiol groups. From these observations it is therefore unsurprising that

the highest water contact angle measured is that of polymer **6B** (75.5±1.3°) whilst the lowest angles measured are those of **5A** and **7A** (32.1±4.0°and 31.3±1.4°) suggesting that these are some of the most hydrophilic samples which could potentially support the largest proportion of bacterial life in the following experiments. Polymer **4A** is also interesting as the contact angle for DIM could also not be collected and the EG value is very low at 11°, this would suggest that this is the most hydrophilic thiol-ene polymer within the set.

From the surface energy data collected and calculated all values appear to be relatively similar, there are however some interesting results, γ_s^+ for polymer **2B**, **6B** and **7C** are lower than those for all other polymers. Polymer **6B** was previously indicated as it had a high contact angle but polymers **2B** and **7C** were not of note. Polymer **1C** had very high γ_s^- value mirrored in part in an elevated EG contact angle in comparison to all others within the set and thus would appear to be very different to the majority of the polymers generated, in contrast polymer **3C** had the lowest value in this set suggesting that the change is not related to the thiol molecule but instead is related to the monomer used for synthesis.

From all these results it can be seen that polymers **1BC** and **4C** differ from the others within the set however, all other polymers synthesised are similar. It would be expected that the differences between polymers **1BC** and **1BN** would become more apparent through testing as from these results they appear to be dissimilar whilst pertaining from the same reaction mixture.

4.4.3 Fourier-Transform Infrared Spectrometry

Spectra were collected from the monomer and thiol reagents (as purchased from Sigma Aldrich) along with the synthesised thiol-ene polymers. These were compared to determine similarities between the polymers themselves and their starting materials. All spectra collected shown in section 4.3.3 above. The region between 900 and 1200cm^{-1} has been successfully analysed to determine the tacticity of polymers (Sevegney et al., 2006) however, to date this has not been used on those synthesised using thiol-ene click chemistry.

4.4.3.1. Monomer 1 Thiol-ene Polymers

From the monomer **1** spectra collected it can be seen that polymer spectra and the thiol traces have a large broad peak most likely due to OH residues between 3350 and 3400cm^{-1}

however, this is not present in the monomer. The monomer **1** spectra contains an aldehyde CH signal at 2760 and 2815 cm^{-1} which is expected and this is not present in the polymer or thiol traces which only show CH, CH_2 and CH_3 stretching the region from 2890 to 2960 cm^{-1}. All three thiol IR spectra shows a small peak at 2550 cm^{-1} which is due to the thiol SH, this is not present in any polymer studied giving an indication that the reaction has run to completion. All spectra possess a high intensity sharp peak at 1720 cm^{-1} which is due to the presence of an ester pendant C=O group, this entity is retained throughout the polymerisation process and would suggest that the reaction is proceeding in the manner which has been theorised at the beginning of this study. A number of similar peaks were shown in the monomers, thiols and polymers fingerprint regions, these include 1045, 1180, 1270, 1405 and 1435 cm^{-1}, these signals are indicative of the bending and deformation of the CH, CH_2 and CH_3 moieties which make up the C-C backbone of the materials being studied. Polymers **1B** appears to have reacted to completion with no indication of residual C=C character in the 1630-1680 cm^{-1} and 1900-2000 cm^{-1} areas of the IR spectra however, polymer **1C** does possess a residue at 1635 cm^{-1}. These observations will be further confirmed by the interrogation of the Raman spectra collected in this work.

4.4.3.2 Monomer 2 Thiol-ene Polymers

As with the polymers in the previous section there is a large OH peak present in these spectra at 3360-3400 cm^{-1}, this was again not present in the monomer spectra. CH, CH_2 and CH_3 stretching can be observed between 2850 and 2970 cm^{-1} however, in comparison to monomer **1** there is no aldehyde CH character which can be identified. As with the monomer **1** polymers, all monomer **2** polymers have a strong signal at 1720 cm^{-1} due to the C=O of the ester. The fingerprint regions of these spectra again have a number of identical peaks at 950, 1015, 1105, 1235, 1350 and 1435 cm^{-1}; these peaks are all present in monomer **2** but are largely different to those seen in the thiol spectra collected. The monomer **2** spectra also has identifying peaks at 1630 cm^{-1} which are due to the presence of the C=C which reacts to form the polymer, these peaks are not present in any of the polymers studied.

4.4.3.3 Monomer 3 Thiol-ene Polymers

As the thiol spectra are largely different to that of the polymers, with the SH peak present in all instances at 2550 cm^{-1} they will no longer be compared to each polymer synthesised however, the plots of the spectra are shown in Figure 4- 4 for completeness. As previously all polymers have a large broad OH peak present at 3420 cm^{-1} however, in this instance the peak is also present in the monomer **3** spectra at 3412 cm^{-1}. CH, CH2 and CH3 stretching are again observed in every case between 2850 and 2950 cm^{-1} and the C=O signal is again present at 1727 cm^{-1}. The fingerprint regions of these polymer spectra again have a large number of peaks which are present in every instance; 795, 850, 950, 1025, 1090, 1250, 1350 and 1445 cm^{-1}. Polymer **3B** however has a far fewer peaks in this region of the spectra than polymers **3A** and **3C** which additionally have a signal at 1635 cm^{-1} which is indicative of a C=C stretch suggesting that there is monomer present in the final polymer. This would suggest that, in contrast to the polymers synthesised using monomer **1** and **2**, that an incomplete reaction has taken place in these cases. It is unsurprising that if any thiol-ene reaction was to remain incomplete it would be that of the polymers synthesised using thiols **A** and **C**, this is due to their much simpler structure with less SH moieties available to react with the monomer and brancher species present.

4.4.3.4 Monomer 4 Thiol-ene Polymers

Monomer **4** polymers have the same features present that can be observed in those previously described, OH (not present in monomer) at 3380-2450 cm^{-1}, CH stretching at 2850-2850 cm^{-1} and C=O at 1727 cm^{-1}. As previously, the majority of peaks in the fingerprint region are identifiable in the monomer and all polymer spectra and similarly to the polymers synthesised using monomer **3**, all polymers appear to have some residual C=C character at 1635 cm^{-1}.

4.4.3.5 Monomer 5 Thiol-ene Polymers

The monomer **5** spectra is unusual as it has a very small signal indicating the C=O of the saturated aldehyde and again shows no OH peak at around 3500 cm^{-1}. The polymers resulting from this monomer however are typical for this study. The broad OH stretch is present at approximately 3375 cm^{-1}, $CH/CH_2/CH_3$ stretches 2850-2950 cm^{-1} and the strong, sharp C=O signal at 1730 cm^{-1}. The fingerprint regions again show the character of the

carbon backbone bending and deforming and have, in this case, a large C=C signal at 1635 cm^{-1}.

4.4.3.6 Monomer 6 Thiol-ene Polymers

The spectra collected from the IR analysis of monomer **6** has a vast number of peaks present, a number of which are again recorded in the polymers synthesised using this monomer. As previously the monomer does not contain the OH peak present within the polymers suggesting that the material purchased from Sigma Aldrich has no water contamination and has been stored efficiently. The polymers synthesised have the OH peak present at 3370 cm^{-1} and the CH stretching of the backbone at 2850-2950 cm^{-1} along with the C=O of the pendant ester group present at 1720 cm^{-1}. As previously, the fingerprint regions are distinct but have a number of peaks repeated in every spectra, these can be identified from the spectra shown in the results section previously however it is interesting to note that the C=C signal at 1635 cm^{-1}, whilst still present in these materials, is now a shoulder rather than a distinct peak. This may suggest that although there is unreacted material within the polymer it is to a lesser extent.

4.4.3.7 Monomer 7 Thiol-ene Polymers

Finally monomer **7** polymers were analysed in the same manner with predominantly the same findings as the polymers synthesised using monomers **1**-**6**. Again the C=C signal is a shoulder in this case suggesting a lesser proportion of this unreacted monomer in the final polymer disc.

All plots are shown in the results chapter previously and in order to further identify any significant changes between the polymers, monomers and thiols PCA was carried out on the data to generate scores and loadings plots. These are shown and discussed below with all additional data held in appendix 2.

4.4.3.8 Statistical Analysis

Principal component analysis was carried out on thiol-ene IR data in the same manner as the acrylate polymers. In the plot of principal component 1 generated, Figure 4- 30, it can be seen that polymer **2A** and **5B** are outliers (they lie out with the oval representing the 95% confidence interval). The separation of these polymers however was not complete, in

general it can be observed that polymers synthesised using thiol B are on the left of the plot and polymers containing thiols **A** and **C** are on the right. In order to glean more information the higher principal components were investigated. Loadings plots for the principal components shown in Figure 4- 31 and Figure 4- 33, are included to clarify the areas of the spectra which are causing the separation: for PC1 it can be seen that the fingerprint region (750 to 1750) and the CH_2/CH_3 stretching have the strongest signals within the loadings and therefore are responsible for the differentiation. In Figure 4- 32, principal component 3 of this data, it can be seen that all polymers synthesised using thiol **C** are positive and thus lie above the x axis. The bottom left quadrant of the plot is also monopolised by thiol B polymers suggesting that this component also describes them to some extent. From the loadings plot it appears that an OH type signal above 5500 has had a great influence on the scores and thus the separation of the polymers synthesised using the differing thiols.

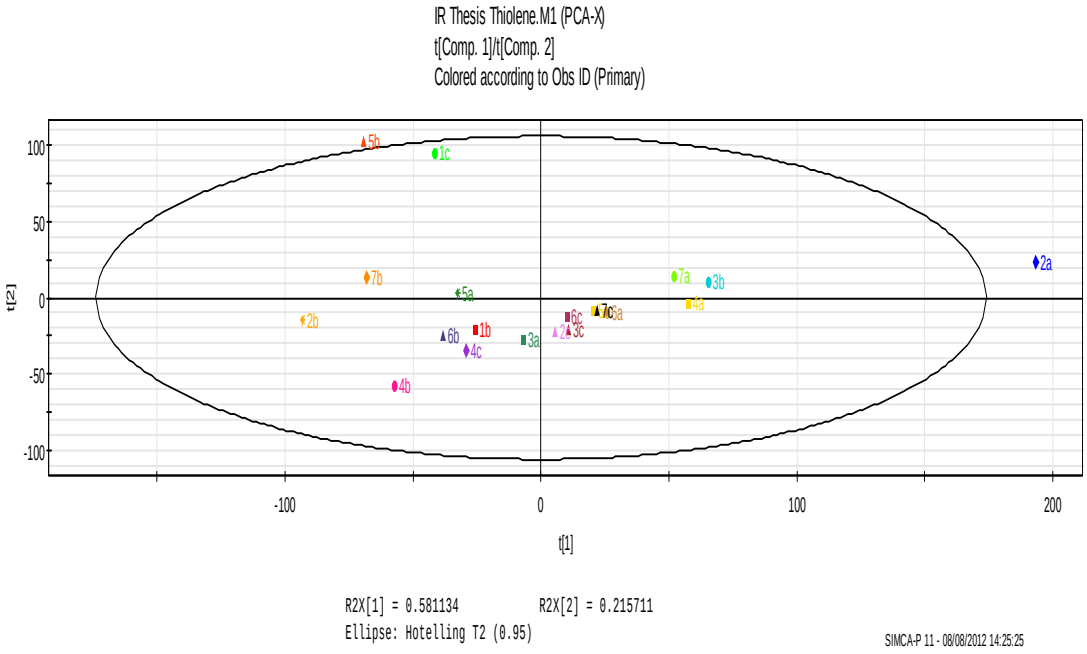

Figure 4- 27 PCA of IR data collected from thiol-ene polymers. Outliers are polymer 2A and 5B.

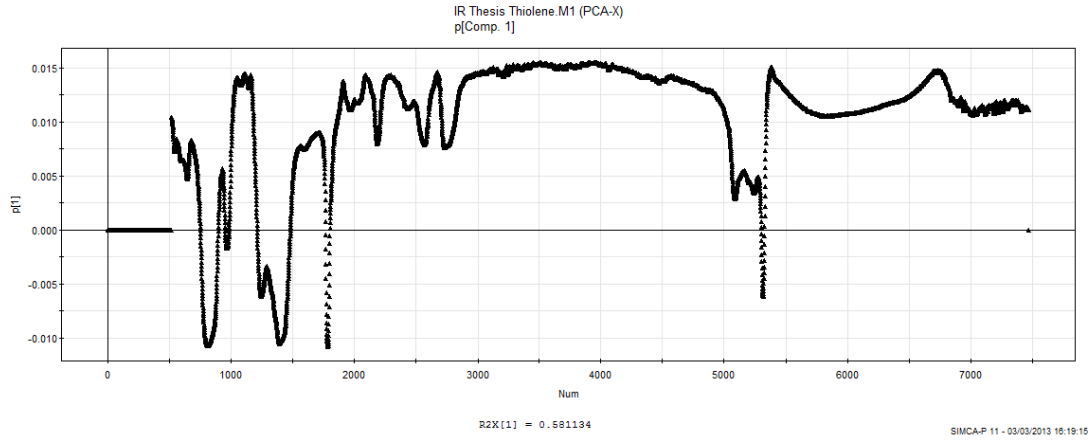

Figure 4- 28 Loadings plot for principal component 1, IR thiol-ene analysis.

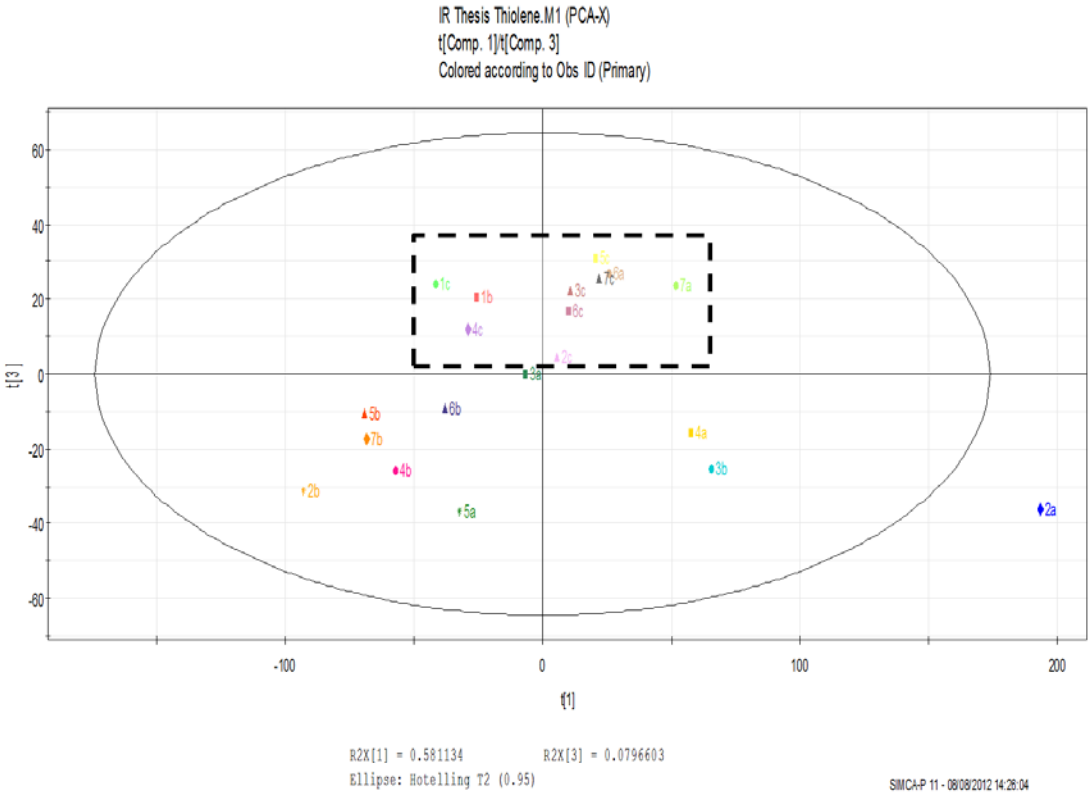

Figure 4- 29 Principal component 3 showing separation of all polymers synthesised using thiol C (1-octanethiol).

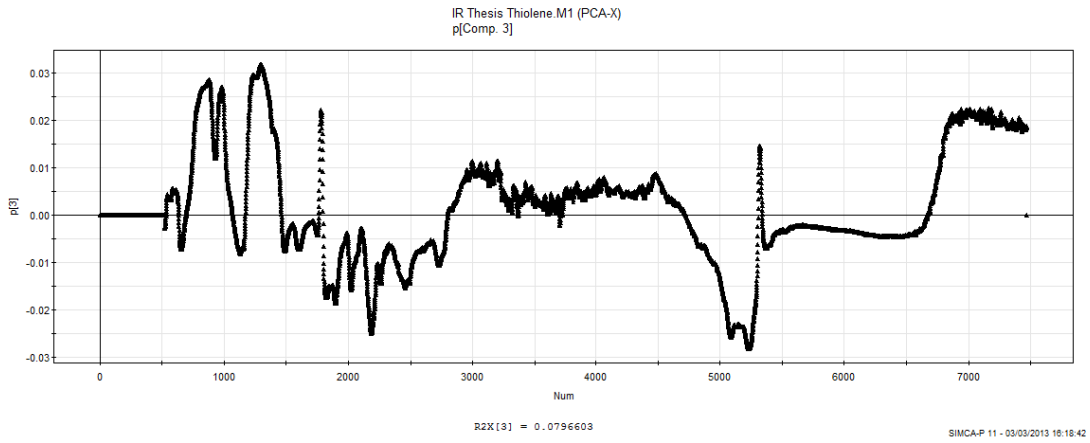

Figure 4- 30 Loadings plot for principal component 3, IR thiol-ene analysis.

4.4.4 Raman

In order to glean further information from this Raman data, principal component analysis of the Raman data collected from the thiol-ene polymers was carried out as previously. In Figure 4- 34 below it can be seen that the glass control is an outlier and thus the spectra collected relate to the polymers themselves, due to their thin nature it was suspected that the data could potentially relate to the glass mounting underneath and not the polymers themselves. It can also be seen that polymers **1B** and **1C** are close together on the left side of the plot separate from the majority of the data suggesting that they are different to the bulk of the polymers. Polymers **4A** and **C**, **5A** and C and **7A** and C are also on the left of the plot indicating some similarities between these and a significant difference to the thiol **B** polymers of the same species. Following this initial analysis further principal components were investigated, PC4 was of interest and thus is shown in Figure 4- 36. In Figure 4- 36 below it can be seen that all polymers synthesised using thiol **B** are grouped above the x axis, with exception of polymer **2B**. Polymer **1B** is also shifted in relation to all the other polymers to the edge of the 95% confidence interval. Polymers **4A** and **C**, **5A** and **C** and **7A** and **C** are again grouped in the lower left quadrant suggesting further similarity. Finally PC5 was inspected and the results are shown in the final plot.

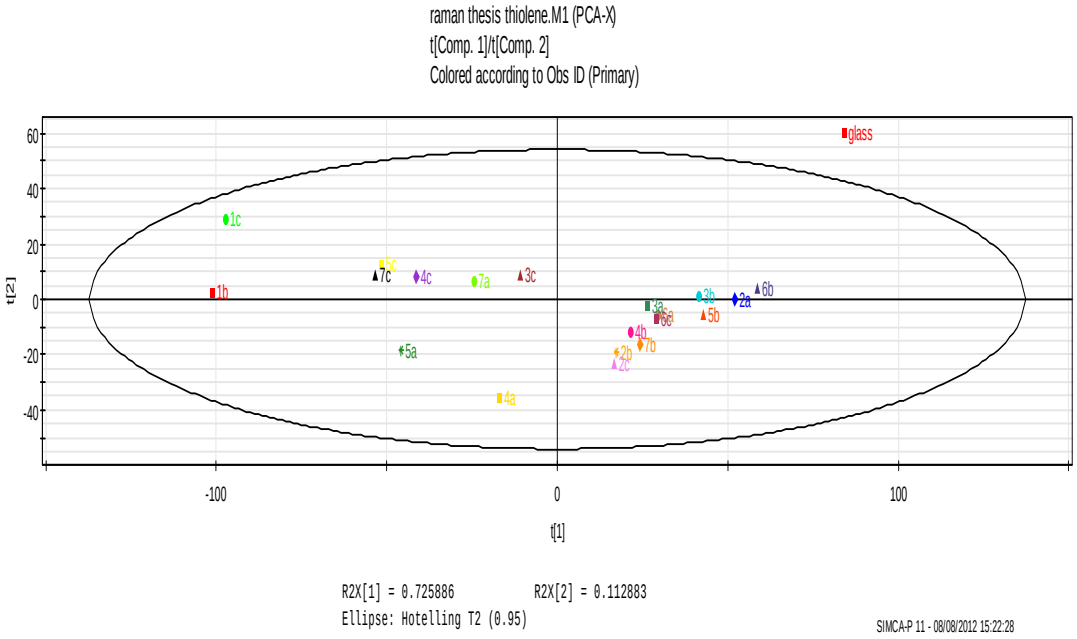

Figure 4- 31 PCA analysis of Raman data collected from thiol-ene polymers and glass control.

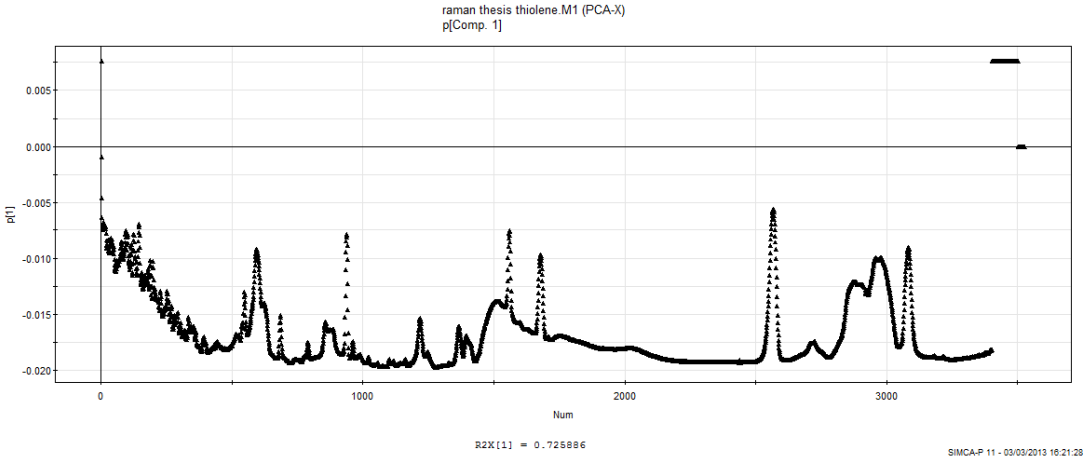

Figure 4- 32 Loadings plot for principal component 1, raman analysis.

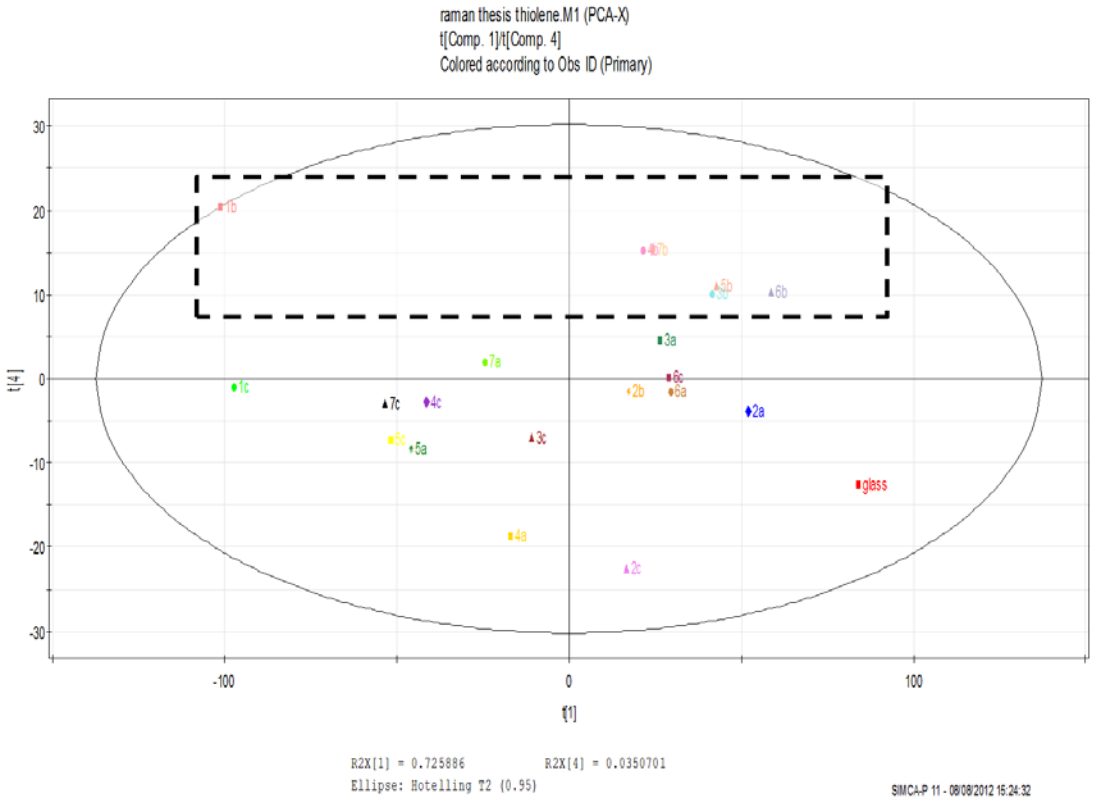

Figure 4- 33 Plot of PC4 of Raman data collected from thiol-ene polymers and glass control. Box showing the polymers synthesised using thiol B, with exception of 2B, grouped above the x axis.

The results of PC5 are shown in Figure 4- 39. The box within in this graph shows the separation of all polymers synthesised using monomer **7** from the rest of the data. This suggests that PC5 represents the variation in monomer **7** polymers most effectively. In this figure it can also be observed that polymers **1B** and **1C** are again closely linked and polymers **4A**, **4C**, **5A** and **5C** are again in the lower left in close proximity.

It is important to note that the glass control sample is separate from the polymer data in all instances, whether it is an outlier or not. This allows the assumption that the polymer Raman data is representative of the samples and is not simply reflected glass.

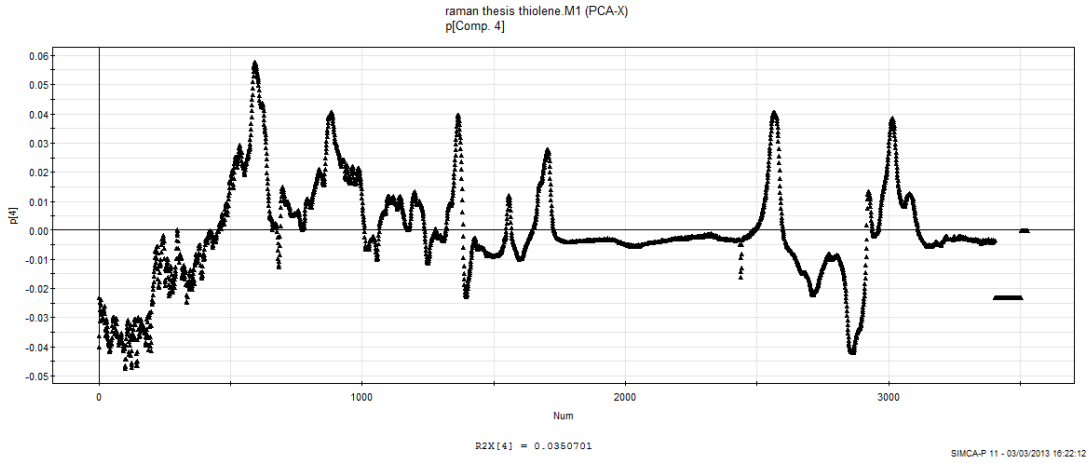

Figure 4- 34 Loadings plot for principal component 4, raman analysis.

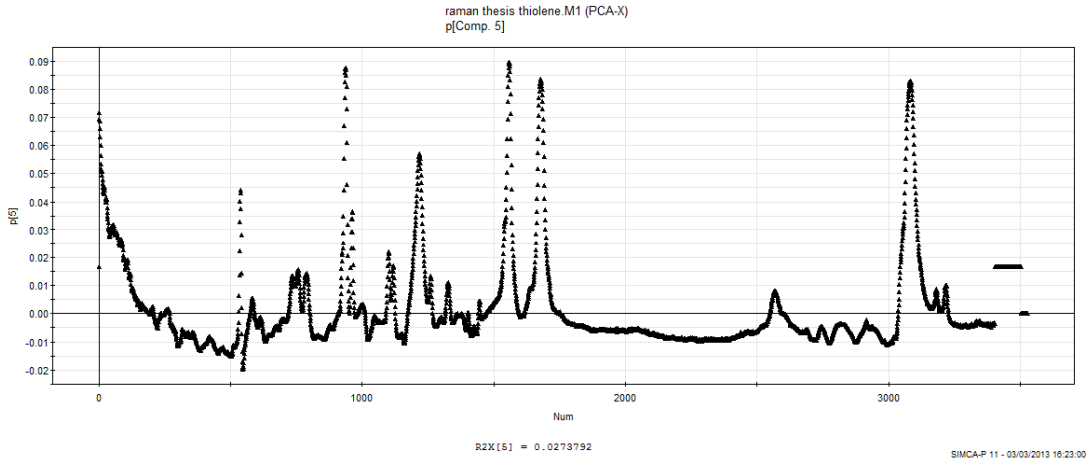

Figure 4- 35 Loadings plot for principal component 5, raman analysis.

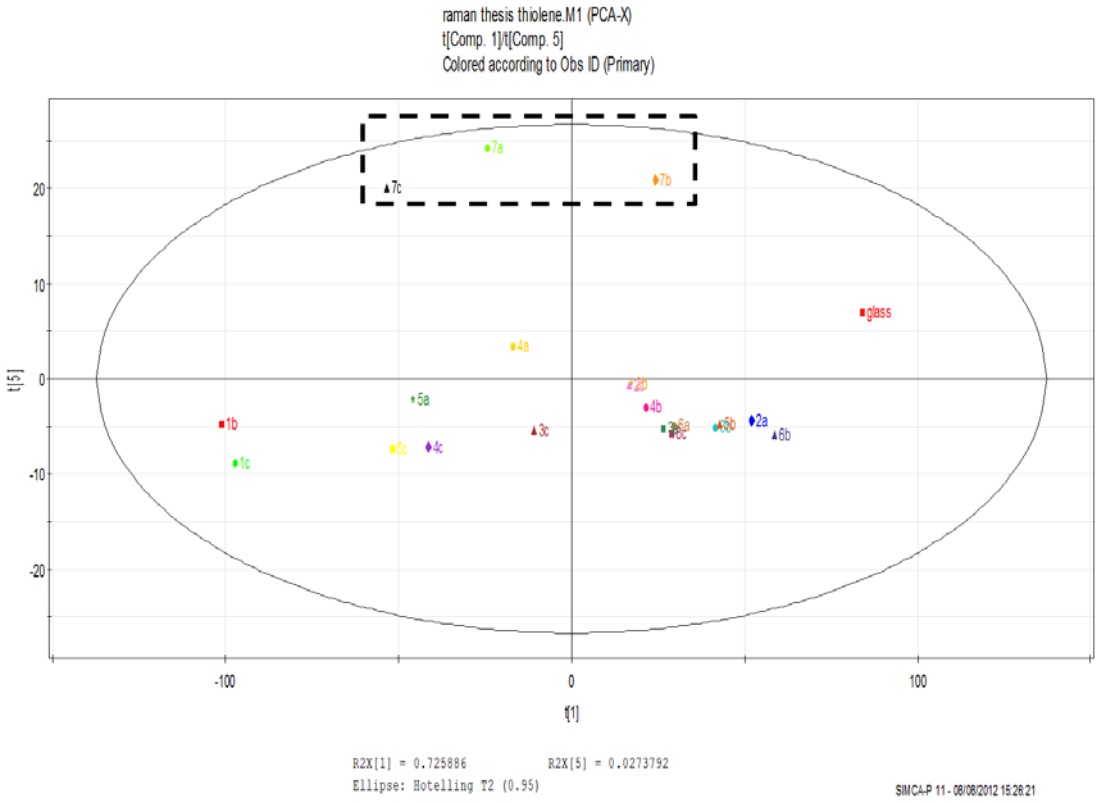

Figure 4- 36 Plot of PC5 of Raman data collected from thiol-ene polymers and glass control. Box showing all polymers synthesised using monomer 7.

As with all other principal component analysis the loadings plots are shown to allow for further clarification of the areas of the original spectra which are causing the majority of variation within each principal component.

4.4.5 Differential Scanning Calorimetry

A single DSC and TGA combination experiment was carried out on all thiol-ene samples and plots shown in appendix 2. As noted in Chapter 3, polymer DSC complex and as such is not facile to interpret however, specific shifts which should be visible within the spectra and can give a multitude of information about the polymer. Specifically the glass transition temperature (Tg), crystallisation temperature (Tc) and finally the melting temperature (Tm) are of note, see Figure 3- 26. The DSC plots resulting from these analyses are complex as the TGA, DSC and temperature gradients are overlaid; temperature is shown in red, DSC in black/burgundy and finally TGA in blue/red.

4.4.5.1. Monomer 1 Thiol-ene Polymers

Polymer **1B**C TGA shows a large weight loss at 115°C which is indicative of the polymer melting; see Figure3-22 for reference. All polymer DSC data unless otherwise stated is collected from the first heating cycle. All polymers synthesised using monomer **1** have a large sharp peak at the beginning of the trace which may be an artefact of the DSC itself or could be indicative of polymer melting. In polymer **1B**C there is a small dip in the baseline at 5°C followed by a stepwise upward change in baseline at 25°C and finally polymer melting at 45°C. Polymer **1BN** has a melting point in the TGA for 40°C which is significantly lower than that of **1BC** and would apparently show that the curing process made the polymer less susceptible to heat. In the DSC trace there is a sharp peak at around 0°C which would be unlikely to be melting as at room temperature the polymer is a solid, after this there is a dip in the baseline (Tc) at 10°C and finally a Tg at 30°C. These are all low temperatures however this is in keeping with the literature on these polymers. Finally polymer **1C**, the softest generated throughout this work, appears to melt twice from the TGA trace at 40°C and 155°C, this is unusual but may indicate the polymer possessing 2 distinct regions. The DSC again shows a peak at 0°C which would appear to be an artefact of the testing method and a Tg at 20°C, lower than that of the other two polymers within this set. All polymers synthesised using monomer **1** had low glass transition temperatures, however the melting temperatures are less obvious with no clear peak other than at very low temperatures when the polymers are solid, this could indicate that melting occurs at a higher temperature than the testing reached, i.e. over 200°C.

4.4.5.2 Monomer 2 Thiol-ene Polymers

Monomer 2 polymers were tested and analysed in the same manner. Polymer **2A** had a melting point in the TGA of 170°C which is significantly higher than for any of the monomer **1** polymers. In the DSC there appeared to be 2 glass transition temperatures at 130 and 135°C again suggesting that there are 2 different regions within the polymer analysed. There was also a small dip in the baseline at 110°C which is indicative of polymer crystallisation. There was no melting observed for this polymer suggesting that it may occur above the highest temperature reached in this study. In the TGA for polymer **2B** there does not appear to be a melting point suggesting it is elevated above 200°C however, in the DSC there is a peak at 95°C which could represent Tm, this is unexpected as this should be observed in both traces. Finally polymer **2C** had an observable melting point in

the TGA at 130°C and a potential mirroring of this in the more sensitive DSC as a small bump in the baseline at 165°C. In the DSC there is again a peak at 10°C which cannot be attributed to melting and a crystallisation temperature of 5°C followed by a glass transition temperature of 20°C, these results are in the wrong order according to Figure 3- 26 but could still be of note. All polymers synthesised using monomer **2** have a higher melting point than those of monomer **1**, this seems logical as monomer **1** polymers are significantly more flexible than all others generated and have the unusual property of imbibing a large volume of water suggesting chains which are more easily forced apart.

4.4.5.3 Monomer 3 Thiol-ene Polymers

From monomer **3** polymers onwards the temperature scale observed in the results plots changes from degrees Celsius to Kelvin, this was due to an instrument refurbishment between these test points. All values however still displayed in °C so it is more facile to compare results. Polymer **3A** had an observable decay at 57°C which appears to be polymer melting. From the DSC a small depression in the baseline at approximately 0°C could be due to polymer crystallisation followed by a peak at 10°C which cannot be melting but may be indicative of some other change within the polymer structure. There is also a small peak at 175°C which may be due to polymer melting or alternatively could be due to pan deformation at high temperatures. Polymer **3B** again has no obvious decay suggesting that melting occurs above the top temperature in this experiment. The DSC shows a Tc peak at 45°C followed by a Tg at 105°C and finally peaks which may be indicative of Tm at 115°C and 190°C. Polymer **3C** decays in the TGA at 140°C and melts in the DSC at the elevated temperature of 165°C. There is a secondary peak in the DSC at around 15°C is not polymer melting but is a strong signal which, as previously mentioned, may be due to the testing method or alternative is indicative of some other change within the polymer. At 35°C there appears to be a signal indicating crystallisation of the polymer which is similar to that seen in **3B**. All polymers synthesised using monomer **3** had melting points closer to 200°C than polymers from monomers **1** and **2**, this would suggest more crosslinking and thus less susceptibility to heating. In polymers **2B** and **3B** there was no melting observed in the TGA and upon inspection of the structure of thiol B this is expected due to the greater possible degree of crosslinking which can be achieved.

4.4.5.4 Monomer 4 Thiol-ene Polymers

Polymer **4A** shows no melting in the TGA which is unexpected as this has been a phenomenon of the thiol **B** polymers until this point, there is however Tg signal within the DSC observed at 50°C and a peak at 105°C which could be due to some melting behaviour within the polymer. Polymer **4B** melts in the TGA at 95°C which is in keeping with the potential melting point of polymer **4A**. In the DSC there is a dip in the baseline at 15°C which is an indicator of polymer crystallisation followed by a Tg signal at 35°C. There is again a large sharp peak early in the DSC at 40°C which could be a signal of solvent being driven off at low temperatures. Polymer **4C** melts at 165°C according to the TGA plot and at 80°C upon inspection of DSC chart. The DSC also shows the Tc for this polymer is at 40°C and the Tg is at 60°C. For these polymers it can be seen that the Tg values for polymer **4A** and **4C** are higher than that for **4B** suggesting again that polymers synthesised using thiol **B** are intrinsically different to that of thiols **A** and **C**.

4.4.5.5 Monomer 5 Thiol-ene Polymers

The TGA and DSC traces resulting from polymer **5A** are unusual, there appears to be a lot of noise in the system however, information can still be gleaned from this plot. The TGA results in a melting point of 125°C which is not mirrored in the DSC as this only shows a glass transition temperature of 30°C and no melting or crystallisation signals can be seen. This may be due to the test being noisy but, all other polymers synthesised using monomer **5** had very little information in their DSC traces. Polymer **5B** shows no melting within the TGA similarly to previous polymers synthesised using thiol **B**. There is however a signal which would indicate Tg at 55°C and a peak potentially indicating melting at 95°C, this is unusual however as it would be likely that a melting point of approximately 100°C would be observed in both the TGA and the DSC. Finally polymer **5C** shows more signals within the trace than the other two polymers synthesised using this monomer within the TGA there is an observed melting point at 120°C. Within the DSC there is a Tc signal at 15°C followed by a Tg signal at 30°C, there are also two small bumps in the baseline which may be pan deformations or shifting material within the system at 100°C and 165°C however this may also due to melting behaviour within the polymer.

4.4.5.6 Monomer 6 Thiol-ene Polymers

There is no melting observed in the TGA traces for any of the polymers synthesised using monomer **6**. This would suggest that the melting for these polymers occurs beyond 200°C and thus was not measured within this experiment. However, information about the polymer can be collected from the DSC traces. Polymer **6A** shows a Tg at 30°C and the same sharp intense peak early in the trace which is potentially an artefact of the testing or solvent being driven out of the system. Polymer **6B** in contract has a crystallisation temperature of 20°C followed by a Tg at 55°C and finally a Tm of 100°C. **6C** has a Tg at around 30°C followed by a melting point of 120°C and finally a small depression in the baseline at 155°C which is most likely to be due to a distortion in the pan at the elevated temperatures. Polymers **A** and **C** are again similar with lower Tg temperatures than **6B**, in contrast to previous polymers within the library, in this set polymer **6B** is the only one which appears to show a melting point which would indicate that it is lower than that of polymers **6A** and **6C** which seems counterintuitive when all other information is taken into account. This will hopefully be further clarified by experiments on physical form of the polymers synthesised in Chapter 5.

4.4.5.7 Monomer 7 Thiol-ene Polymers

The TGA for polymer **7A** shows a melting point of 155°C. The DSC for this polymer however only shows a Tg at 100°C and the same early peak observed in all spectra at 45°C, this would be a very low melting point and does not correlate with the TGA data collected simultaneously. Polymer **7B** has a TGA melting point at 110°C and from the DSC it can be seen that there is a Tc at 10°C followed by a Tg at 30°C. Yet again in this sample there is a small deviation in the baseline at 160°C which is most likely attributable to a pan deformation due to expulsion of gas, poor sealing or the movement of the sample within the pan. The TGA for **7C** shows no obvious melting point similarly to a number of other polymers tested. The DSC shows a potential Tm peak at 95°C and two Tg signals at 65°C and 145°C. There is a small blip in the baseline at 180°C which again appears to be some pan deformation. From all the DSC and TGA data collected it can be seen that there appears to be a difference between polymers synthesised using thiol **B** and those generated using thiol **A** and **C**. This result mirrors the data collected in the CAG and surface energy work which indicated that the polymers from thiol B had a more cross-linked structure

which is reinforced by inspection of the structure of thiol **B**. FTIR and Raman data backs up this finding.

4.4.6 Bacterial Testing - Crystal Violet Staining

Crystal violet staining was used initially on thiol-ene discs to determine the effect on biological growth during any swelling behaviour whist incubated overnight. This was achieved in a similar manner to the acrylate polymer testing previously with two strains of bacteria being used to determine the differences, if any, between growth rates on the polymer surfaces of interest. After problems with dye imbibing into the discs became apparent it was decided to coat the polymers of interest onto coverslips to allow more accurate determination of bacterial growth.

4.4.6.1. Thiol-ene Discs

Thiol-ene polymer discs were tested using *Pseudomonas aeruginosa* and *Staphylococcus aureus* as previously and bacteria stained using crystal violet to allow quantification via UV spectroscopy. However, it was noted that the stain was adhering to the polymer discs and not preferentially to the bacteria present which resulted in UV absorbances which could not be related to bacterial growth. In a number of instances it was also noted that the negative controls run simultaneously in order to correct the data and thus not containing any bacteria, had a higher UV absorbance than any sample which contained bacteria. This would suggest that the stain was doing the opposite to what was intended and preferentially adhering to the polymer and not the bacteria whilst the bacteria themselves were acting as a kind of shield in the samples which contained them. It was considered that the bacteria were filling pores on the surface of the discs and thus not coming in direct contact with the stain and as such these would protect the discs from dye in comparison to the negative control discs. An alternative theory also considered was that the polysaccharides and other extracellular substances were forming a barrier layer around the disc shielding it from staining. In order to determine which of these was most appropriate a number of experiments using microscopes were carried out. It was rapidly concluded that there were no visible pores upon the polymer surface and as such the extracellular matrix theory was adopted. In order to combat this issue, further testing of thiol-ene

polymers susceptibility to biofilm growth was carried out on spin coated glass coverslips rather than on solid polymer discs.

4.4.6.2 Polymer Coated Cover Slips

Crystal violet staining was repeated using polymer coated glass slides and the results of this were shown in Figure 4- 19 and Figure 4- 20 above. Standard deviations in the data were, as previously, high and this is due, in part, to bacteria being living organisms which can differ wildly from one another. The positive control used in this experiment was the polystyrene well plate and in all instances this had the highest bacterial proliferation. This shows that all thiol-ene polymers synthesised were more bioresistive than the polystyrene control to both *Pseudomonas aeruginosa* and *Staphylococcus aureus*. An average of the negative control samples run in these experiments were used to correct the data prior to plotting. From the data it can be seen that polymer **2C** has the lowest bacterial growth coupled with the lowest error, this would suggest that **2C** is highly bioresistive. It can also be seen that polymers synthesised using thiol **A** appear to have more adherent bacteria than those synthesised using **B** or **C**. Polymers **1BN** and **1BC** appear to have very similar bacterial adhesion and thus it could be deduced that the differences in physical form due to curing do not have an effect on *Pseudomonas aeruginosa* growth. The results of the *Staphylococcus aureus* biofilm testing were shown previously in Figure 4- 20 . For this bacterial strain the correction using negative control samples has, on a number of occasions, given a "negative absorbance" which is obviously impossible but may suggest that some similarity to the thiol-ene discs previously tested. Similarly to the *Pseudomonas aeruginosa* samples tested previously all *Staphylococcus aureus* absorbances from testing were lower than that of the positive control. There are also some samples of note within this set; all polymers synthesised using monomer **2** had a negative result and thus it could be deduced that this monomer polymerises to a material which is highly bioresistive. In this experiment the results of the **1BC** and **1BN** testing appear to be vastly different but, as negative absorbances are not possible this result should be zeroed and thus they are, in fact, very similar as they were in the previous experiment. *Staphylococcus aureus* absorbances in all cases are significantly lower than that of *Pseudomonas aeruginosa* samples as this bacterium is less prolific. Although polymer coated glass coverslips gave interesting information on the bioresistive properties of the polymers this data could not be used to determine the effect, if any, the swelling of the polymers had on the biofilm

formation. Additionally as the *Staphylococcus aureus* samples resulted, in some cases, in negative values this data cannot be used conclusively. In order to glean further information to clarify both these points of note bacterial testing was repeated using primarily GFP bacteria on polymer discs and then, finally, using cell counting.

4.4.7 Bacterial Testing - GFP Bacteria

In an attempt to overcome the problems of staining bacteria and to investigate the effect of swelling on biofilm growth GFP *Pseudomonas aeruginosa* were grown on thiol-ene discs in the same manner as previously. However, it was quickly noted that all thiol-ene polymer discs synthesised in this library were fluorescent at the same wavelength as the bacterium being investigated. Although this is not an unusual phenomenon it did render the GFP experiments on these polymers useless as the signal from the bacteria could not be de-convoluted from the bulk polymer. It therefore was necessary to find yet another method to clarify the growth of the bacteria upon the polymer surface; bacterial plate counting was deemed an effective, if time consuming, way of deducing accurately the number of bacterial colonies adherent to each polymer coated glass coverslip.

4.4.8 Bacterial Testing - Bacterial Plate Counting

Plate counting was used to determine accurately the number of bacterial colonies adherent on the polymer coated glass coverslip surface. This was achieved by allowing bacteria to grow on coverslips as previously before being removed from media, agitated in 10ml fresh media for 30s before being pipetted accurately into the 4 quadrants of a plate, method fully explained in chapter 2. After a further 24hr incubation the number of colonies were counted and then multiplied to determine the number of bacteria present. This data was plotted with its standard deviations to allow observation of differences between the polymer samples.

For the *Pseudomonas aeruginosa* samples the highest proliferation was observed in polymer **1BC** however, this was accompanied by the highest error in the measurement which brought this unusually elevated result into line with all other samples in the testing. The lowest level of bacterial proliferation and indeed the lowest standard error was observed in sample **7A**. The positive controls in this experiment required to be glass coverslips as the base of a well plate could not be removed and vortexed with the other

samples. This may explain why for these experiments the polymer samples all had a higher level of bacterial growth than the positive control. In general all poylmers tested in this manner using *Pseudomonas aeruginosa* had very similar bioresitive properties.

In contrast to the *Pseudomonas aeruginosa* samples the *Staphylococcus aureus* results from these experiments were much more varied although the standard deviations calculated again bring all samples back within range of the others. The number of colonies observed in this experiment was much greater than that of the *Pseudomonas aeruginosa* samples. Also is contrast to the *Pseudomonas aeruginosa* experiment not all the samples in this set had a higher proliferation than the positive control although some samples; **3A**, **3C**, **4B** and **5A** do have much higher bacterial growth. The results from this experiment would appear to indicate that the proliferation of bacteria on a polymer coated glass surface is higher than that of clean glass, a not entirely unexpected result, however there is little difference between the individual polymers over this time frame. In comparison to other studies carried out on these polymers it can also be determined that the polymer all have a lower proliferation than a commonly used polymer substrate, polystyrene. In order to gain one last piece of information regarding the growth of bacteria on the polymer discs specifically a novel technique, hyperspecteral imaging (HSI), was employed to non-destructively test one further batch of polymers cultured overnight with these bacterium.

4.4.9 Bacterial Testing - HSI for Biofilm Quantification

Following from the initial inspection of the spectra produced using the hyperspectral imaging technique it can be concluded that the majority of the data collected is identical. This result prompted the use of PCA to further analyse the data collected and glean more information. From the scores images, in appendix 3, a wealth of information about the similarities between the samples can be determined. Scores plots are generated a specific order from the most different area of the image to the least different thus, the lower the scores number the more significant the change within the image. Scores plot 1, Figure appendix 2- 24 , in this instance shows that the edges of the well plate are the most different to everything else within the image; this is expected as the polystyrene in this area is thicker than elsewhere in the plate and thus will have a stronger signal. Scores plot 2, Figure appendix 2- 25, shows the next significant area of difference within the image is that of the white calibration tile used to ensure that all images are corrected. This is obviously very different to the signal from anything else within the image as it is bright white and

made of different material. Scores plot 3, Figure appendix 2- 26, shows that well 1, containing the polymer is different to any of the other wells. This means that hyperspectral imaging can differentiate between the thiol-ene polymers synthesised and the polystyrene well plate used for testing, this is interesting as it means that very different polymers can be differentiated using HSI. Scores plot 4, Figure appendix 2- 27, may show that wells 1 and 2 are similar as are wells 3 and 4, this is however much less obvious than the difference observed in scores 3. This difference would suggest that HSI is also capable of determining the difference between polymer coated in a biofilm and that which is not. This could be very beneficial in the determination of biofilms in a non-destructive manner. Finally scores 5 and 6 are very similar and little information can be garnered from them, Figure appendix 2- 28 and Figure appendix 2- 29.

From this further investigation of the HSI results it can be seen that polymers can be differentiated using this technique and there is also some indication that surfaces which are coated in a biofilm are spectrally different to those which are not. In order to further clarify whether bacteria can be positively identified the positive and negative control wells were isolated and tested using PCA, see Figure 4- 40. From this grey scale scores plot it can be said that the polystyrene coated in a biofilm layer is different to that of the negative control sample and this can be observed by HSI, thus showing that HSI can in fact determine the difference between the same polymer surface coated in bacteria and that which is not. All loadings plots from this analysis are shown in the appendix for completeness.

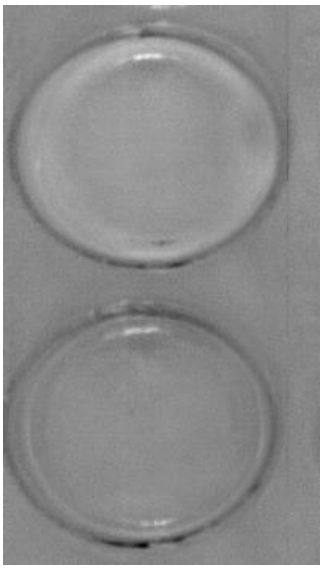

Figure 4- 37 Postive and negative bacterial controls in polystyrene well plate.

The real test of this method of analysis however is using the second image which has a number of differing polymers coated in varying levels of bacteria and whether these can be separated from one another. Simply put there little differentiation that can be seen in any of the scores plots. This could be due to a number of reasons, primarily that the thiol-ene polymers are all visually and chemically very similar, even with the use of different monomers and thiols. As visible HSI is being used in this instance, and the polymers synthesised are all of a similar colour, the small variances between the synthesised polymers which could be easily detected using a NIR HSI camera are missed rendering the analysis much more complex with little positive results. This effect is worsened as the polymer discs must be retained in their well plates during testing to limit contamination, as the samples are at the base of a relatively deep well shadowing them further and masking more of the potential differences between them. Finally the magnification of the HSI system available for use at the Strathclyde HSI Centre is not optimum for this type of work, the data collected has pixels which are approximately 300µm in size, this is between 60 and 300 times the size of a single *Pseudomonas aeruginosa* bacterium (*Pseudomonas aeruginosa* 1-5µm in length) and thus each pixel covers a huge area suggesting some averaging between the polymer and bacteria signals is observed. This is a much larger pixel size than that used in the reference paper for this technique (Polerecky et al., 2009). HSI has some potential in this area as shown in previous papers and in the early stages of this research however, a visible HSI setup is not ideal and the pixel size must be greatly reduced before accurate information can be collected using this technique. Nevertheless even if these hardware issues could be rectified there remain a number of other methodologies to collect information on the bacterial proliferation upon a surface which are more facile and require a significantly less intensive statistical work up.

4.5 Conclusions

From this body of work it can be concluded that thiol-ene polymers can be simply synthesised using UV light and minimal solvent. Similarly to the materials prepared in the previous section, all these polymers require is an overnight drying in a vacuum oven. The resultant polymers are malleable gel-like solid discs with differing properties which can be attributed to the monomer and thiol starting materials adopted. The most interesting synthesis however was that of polymer **1B** which polymerised rapidly upon the addition of the highly functional thiol molecule; this allowed the comparison of the cured sample

(irradiated in the same manner as all other polymers) and the non-cured polymer to be made. Several analytical techniques were used to clarify the level of polymerisation and the surface properties of these novel polymers.

Bacterial testing was carried out using *Pseudomonas aeruginosa* and *Staphylococcus aureus* bacteria as previously and in every instance it was concluded that the thiol-ene polymers synthesised lessened biological proliferation in comparison to a control however, there were obvious patterns observed which would suggesting the most beneficial reagent mixture. During the biological testing of these materials it was noted that the polymers synthesised using monomer 1 underwent swelling in biological media over 24hrs at 37°C. In order to further investigate this, synthesis of these polymers was repeated and the swelling capabilities of the polymers were tested further using a number of methodologies. These results are noted in the following work.

CHAPTER 5. THIOL-ENE SWELLING BEHAVIOUR AND MATERIAL PROPERTIES

5.1 Introduction

Polymer swelling in water is a well-established phenomenon which has led to the evolution of hydrogels, three dimensional networks of polymer chains into which water can infiltrate and fill the space between the macromolecules (Van Tomme et al., 2008). Polymers which are commercially used at present are in general acrylate based, including poly(ethylene oxide), poly(vinyl alcohol), poly(vinylpyrrolidone) and poly(hydroxyethyl methacrylate) (Bajpai et al., 2008). Hydrogels have seen success in several areas of research including agriculture however; drug delivery has been where they have seen the greatest applicability. At present these polymers are used as contact lenses (Ostrovidova et al., 2003), wound dressings (Vinogradov et al., 2002) and drug-delivery systems (Razzak et al., 2001) with particular interest being paid to in situ self gelling polymers.

Hydrogels tend to be highly biocompatible as the high percentage of water imbibed into the matrix ensures the physical properties of the implant match the native tissues as closely as possible. Chemical structure and the surface architecture of the polymers are also pertinent in the healing process however, on comparison of two biomaterials with the same chemical composition but differing physical attributes differences can be clearly seen especially in calcification of the inserts after implantation (Kopecek, 2009). Thiol-ene polymer swelling is less well understood in comparison to the polymer structure, and therefore swelling behaviour, is less well understood. Thiol-ene polymers have the capability for in situ polymerisation so they are of interest in drug delivery and tissue engineering although the mechanisms require clarification (Rydholm et al., 2005). Thiol-ene polymer swelling has been investigated as a result of unusual swelling behaviour observed during biological testing. In particular polymers synthesised using 2-(Dimethylamino)ethyl acrylate (monomer 1). Polymer discs displayed the ability to swell enormously in a horizontal plane whilst remaining virtually unchanged vertically, see Figure 5- 1. Further mechanical and material properties have been inspected via a series of unusual techniques in order to better understand the reasons for swelling behaviour.

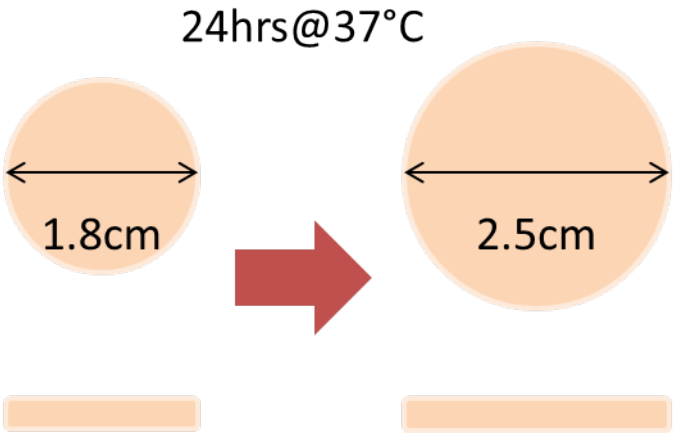

Figure 5- 1 Schematic of swelling behaviour of thiol-ene polymers synthesised using monomer 1 after 24 hours in 50ml of water at 37°C. Increase in size only observed in the horizontal plane.

5.2 Methods

All methods used to synthesise and analyse the polymers generated are detailed in materials and methods section 2.6.

5.3 Results

Synthesis of all polymers to be used in this study was successful; material properties were determined using conventional static swelling, texture analysis and compression testing before the molecular weight of the polymers was investigated. All results from these experiments are detailed below.

5.3.1 Polymer Synthesis

All polymers synthesised in same manner as stated in chapter 2 using a UV curing methodology. All polymers previously synthesised were remade in replicate to allow series of experiments to be carried out in several environments. The polymers of greatest interest, due to previously observed characteristics, contain monomer **1**, 2(dimethylamino)ethyl acrylate, brancher y, tEGDA, and one of thiol **B** or **C** in a 1:1:1 ratio, Figure 1- 9. Synthesis in every instance requires the use of solvent, DMSO, and photo initiator, DMPA, to generate solid polymer discs in this manner. The results of polymer synthesis for these experiments were identical to those observed in Chapter 4. Polymers were translucent and colourless to pale yellow/brown in colour with a solid and pliable

nature. These polymers were stored at room temperature prior to testing and showed no alteration to their physical form over time.

5.3.2 Swelling Behaviour

The first experiment carried out to understand the swelling behaviour of polymers **1BN**, **1BC** and **1C** was a simple gravimetric analysis with any changes in disc dimensions noted. This simple and inexpensive experiment can give data which is indicative of how the water is imbibed into the polymer and to what extent. It also indicates whether polymers continue to take up water until they are physically broken or whether there is a finite volume which can be absorbed. Experiments were initially carried out in water before PBS buffer was used to more accurately represent body fluids in both pH and salt content.

5.3.2.1 Swelling in Ultrapure H_2O

Preliminary work to determine swelling behaviour was carried out using a simple experiment which documents the changes in mass and dimension of the polymer discs being studied before and after submersion in water at 37°C for specific periods of time. The results of this study are shown in Table 5- 1. From these measurements it is obvious that after submersion in water there is a gain in both mass and an increase in the size of the polymer disc. This would suggest that water is imbibing into the polymer via some mechanism and altering its size and mass. There is a large increase in both mass and diameter in the majority of cases; however the height of the discs tends to remain largely the same.

Table 5- 1 Initial swelling experiment to determine gain in mass and change in dimensions over time submerged in ultrapure filtered water at 37°C.

Polymer 1B							
Time (hrs)	**Number**	**mass (g)**	**height (cm)**	**diameter (cm)**	**change in mass (%)**	**change in height (%)**	**change in diameter (%)**
0 (dry)	1	0.4183	0.12	1.94			
	2	0.4688	0.14	1.90			
	3	0.4114	0.12	1.93			

	4	0.4485	0.12	1.92			
	5	0.4746	0.11	1.92			
24	1	0.6641	0.12	2.26	59	0	17
48	2	0.6694	0.14	2.27	43	4	19
72	3	0.5613	0.12	2.25	36	2	16
96	4	0.5863	0.13	2.32	31	9	21
168	5	0.7012	0.13	2.20	48	18	15

Polymer 1C

Time (hrs)	Number	mass (g)	height (cm)	diameter (cm)	change in mass (%)	change in height (%)	change in diameter (%)
0 (dry)	1	0.3852	0.13	1.89			
	2	0.424	0.12	1.87			
	3	0.2898	0.07	1.88			
	4	0.4077	0.14	1.90			
	5	0.4189	0.14	1.87			
24	1	0.6042	0.14	2.22	57	8	18
48	2	0.7493	0.14	2.36	77	18	26
72	3	0.4916	0.09	2.19	70	18	16
96	4	0.7898	0.16	2.64	94	16	39
168	5	1.0515	0.16	2.68	151	14	43

5.3.2.2 Swelling in PBS buffer

The previous experiment was repeated using the PBS buffer at pH 6.7 in order to more closely represent biological fluid, the results of this experiment are shown below, Table 5-2. From this PBS swelling data it can be concluded that the polymers resulting from monomer **1** appear swell in buffer to a similar extent to that which was previously observed. Although only monomer **1** polymers were tested in this manner from the data collected it could be easily deduced that water, or buffer, was being taken up over time. The other polymers, although not visibly increasing in size may also be effected by the water leaching into them over time, using the results of these experiments as a guide the properties of the polymers in the library were examined more closely using texture profile analysis and finally polymer compression.

Table 5- 2 Initial swelling experiment to determine gain in mass and change in dimensions over time submerged in PBS (pH 6.7) at 37°C.

Polymer 1B							
Time (hrs)	**Number**	**mass (g)**	**height (cm)**	**diameter (cm)**	**change in mass (%)**	**change in height (%)**	**change in diameter (%)**
0 (dry)	1	0.4865	0.15	1.90			
	2	0.4596	0.13	1.89			
	3	0.4422	0.13	1.92			
	4	0.5044	0.14	1.96			
	5	0.4158	0.11	1.92			
24	1	0.8703	0.16	2.38	79	5	25
48	2	0.6982	0.14	2.29	52	15	21
72	3	0.7681	0.13	2.30	74	5	20
96	4	0.8429	0.15	2.40	67	6	22
168	5	0.8485	0.11	2.44	104	3	27
Polymer 1C							
Time (hrs)	**Number**	**mass (g)**	**height (cm)**	**diameter (cm)**	**change in mass (%)**	**change in height (%)**	**change in diameter (%)**
0 (dry)	1	0.4253	0.13	1.88			
	2	0.407	0.11	1.89			
	3	0.4357	0.12	1.88			
	4	0.4103	0.11	1.88			
	5	0.3861	0.10	1.86			
24	1	0.6919	0.14	2.26	63	13	20
48	2	0.7376	0.11	2.42	81	5	28
72	3	0.8483	0.14	2.43	95	14	29
96	4	0.8373	0.12	2.53	104	8	35
168	5	0.8458	0.12	2.51	119	16	35

5.3.3 Texture Profile Analysis

Texture profile analysis was carried out using the methodology stated previously, 2.6.2. In accordance with the work carried out by (Szczesniak, 1963), (Szczesni.As, 1966) and (Bourne, 1978) parameters from the texture profile were identified and their means of calculation. These are listed in Table 5- 3.

Texture profiles were taken for 4 replicates of each polymer disc before and after 24hrs in ultrapure water at 37°C. The same discs cannot be used twice as the initial compression may alter their behaviour during swelling or the eventual second compression cycle so different polymer samples must be used for the pre and post swelling analysis. This may lead to some variation however; this should be diminished by the use of a number of replicates for each experiment. The data collected is graphed and a number of parameters can be determined from this plot or further simple calculations, see Table 5- 3 and Figure 5- 4 for information which can be gleaned from this experiment.

Table 5- 3 Texture profile analysis parameters for identification and means of calculation (Jones et al., 1996).

Parameter	Calculation
Hardness	Peak force after 1st compression (F_1)
Fracturability	Force at first fracture
Adhesiveness	Area under 1st compression peak (A_1)
Cohesiveness	Area under 2nd compression divided by area under 1st compression(A_2)/(A_1)
Gumminess	Hardness (F_1) x cohesiveness (A_2)/(A_1)

5.3.3.1 TPA – Dry Polymer

Polymers tested at 0.1mms^{-1}, 1mms^{-1} and 3mms^{-1} to determine any differences between results. Results from these experiments are shown in Table 5- 4.

At 1mms^{-1} and 3mms^{-1} no fracturing of polymer samples was observed, however around a third of polymers did break upon 0.1mms^{-1} compression. Samples **1BN** and **1BC** were very similar, as expected and were harder than the majority of polymer samples. In general polymers synthesised using thiol **B** were harder, gummier and less easy to fracture than those synthesised from thiols **A** and **C**. From this experiment it was concluded that for wet polymer testing only 0.1mms^{-1} and 1mms^{-1} compression rates were used, this was due to

the similarity of the results from 1mms^{-1} and 3mms^{-1} tests in the dry polymers. Slower rates of compression appeared to show the fracturability of the polymers more efficiently.

5.3.3.2 TPA – Wet Polymer

After testing using dry polymer discs, new polymer discs were submerged in 50ml ultrapure water in petri dishes water for 24hr at 37°C before being tested in the same manner. This was chosen as a vessel to attempt to reduce any curling of the polymer discs upon water uptake as has been observed in the relatively cramped conditions of the biological well plates and 50ml centrifuge tubes. These samples were tested in quadruplicate using the same methodology as previously in order to ensure reproducibility, but in this instance only at 0.1mms^{-1} and 1mms^{-1} compression rates. Results from these tests can be seen in Table 5- 5. It was noted that a much larger proportion of samples were fracturing at both speeds and some samples had undergone significant changes upon swelling. Polymer **1BN** had swollen to a much larger extent than **1BC**, **1C** became gel like with little resistance to cutting and unable to adhere to plate using fixative due to large volume of imbibed water (samples must be held in place or movements on the lower plantain can alter results, for **1C** samples this must be carried out manually). Samples **5C** and **6C** became opaque and white after swelling suggesting some degree of crystallinity. Due to the polymers resulting from monomer **1** continuing to have unusual behaviours upon swelling these were further investigated using compression techniques more commonly suited to the investigation of cartilage compression in human patients.

Table 5- 4 Averaged results from TPA testing showing the hardness, fracturability, adhesiveness, cohesiveness and gumminess of all thiol-ene polymers before swelling at 0.1mms-1, 1mms-1 and 3mms-1 compression rates.

	0.1 mms^{-1}					1mms^{-1}					3mms^{-1}				
Sample	**Hardness**	**Fracturability**	**Adhesiveness**	**Cohesiveness**	**Gumminess**	**Hardness**	**Fracturability**	**Adhesiveness**	**Cohesiveness**	**Gumminess**	**Hardness**	**Fracturability**	**Adhesiveness**	**Cohesiveness**	**Gumminess**
1BC	14.36	-	0.42	0.98	14.04	12.47	-	0.001	0.97	12.15	16.09	-	0.004	0.99	15.96
1BN	14.46	-	0.05	0.97	14.06	10.60	-	0.000	1.00	10.58	11.88	-	0.003	0.99	11.74
1C	4.51	-	0.09	0.86	3.89	5.99	-	-0.002	0.90	5.39	7.91	-	0.018	0.93	7.38
2A	5.15	-	0.53	0.98	5.05	3.32	-	0.002	1.00	3.31	8.52	-	0.002	1.02	8.65
2B	11.27	-	0.38	0.94	10.62	11.93	-	0.001	1.01	12.04	8.81	-	0.006	0.99	8.69
2C	5.34	2.39	0.61	1.15	6.14	5.59	-	0.002	0.96	5.36	11.68	-	0.001	0.96	11.17
3A	7.43	-	0.27	0.96	7.16	8.92	-	0.000	0.98	8.77	10.08	-	0.002	1.01	10.19
3B	16.60	7.72	0.29	0.96	15.99	8.86	-	0.000	0.99	8.78	10.05	-	0.002	0.92	9.23
3C	6.92	5.79	0.30	0.82	5.67	6.81	-	0.001	0.99	6.75	7.58	-	0.002	0.99	7.54
4A	5.44	0.39	0.52	0.93	5.05	8.85	-	0.001	1.02	8.99	8.42	-	0.000	1.02	8.60
4B	13.06	-	0.25	0.96	12.56	14.89	-	0.001	0.99	14.76	14.45	-	0.005	0.99	14.28
4C	7.57	1.56	0.35	0.85	6.47	6.82	-	0.001	0.99	6.76	9.66	-	0.002	1.00	9.63

5A	6.85	-	0.24	0.92	6.28	2.83	-	0.003	0.99	2.79	5.16	-	0.001	0.98	5.07
5B	9.48	-	0.20	0.99	9.35	6.84	-	0.000	0.99	6.78	11.85	-	0.001	0.99	11.77
5C	10.52	-	0.37	0.90	9.44	8.70	-	0.001	1.02	8.88	3.71	-	0.000	0.99	3.65
6A	15.12	-	0.31	0.65	9.76	8.79	-	0.002	1.00	8.81	12.20	-	0.002	0.98	11.98
6B	3.47	-	0.53	0.96	3.33	3.15	-	0.001	0.96	3.02	2.91	-	0.000	0.99	2.87
6C	5.85	-	0.62	0.98	5.76	5.10	-	0.000	0.89	4.54	8.00	-	0.001	1.03	8.21
7A	4.67	-	0.25	0.94	4.41	4.15	-	0.000	1.00	4.16	5.42	-	0.002	1.03	5.57
7B	7.40	-	0.30	0.97	7.17	6.67	-	0.002	1.00	6.66	11.63	-	0.003	0.98	11.38
7C	5.52	1.62	0.42	0.76	4.20	6.74	-	0.001	0.98	6.60	7.67	-	0.002	1.00	7.69

Table 5- 5 Averaged results from TPA testing showing the hardness, fracturability, adhesiveness, cohesiveness and gumminess of all thiol-ene polymers after swelling for 24hrs in ultrapure water at 37°C. Compression rates 0.1mms-1 and 1mms-1.

	$0.1mms^{-1}$					$1mms^{-1}$				
Sample	**Hardness**	**Fracturability**	**Adhesiveness**	**Cohesiveness**	**Gumminess**	**Hardness**	**Fracturability**	**Adhesiveness**	**Cohesiveness**	**Gumminess**
1BC	8.86	7.36	0.005	0.00	0.00	6.95	3.80	0.001	0.08	0.57
1BN	1.22	3.20	0.021	0.41	0.50	2.05	3.77	0.000	0.02	0.05
1C	0.85	0.70	0.001	0.02	0.00	0.77	0.69	0.000	0.01	0.00
2A	7.10	5.86	0.393	0.52	3.68	8.73		0.004	0.73	6.41
2B	8.06	13.82	0.098	0.29	2.30	18.66	12.23	0.006	0.80	14.94
2C	3.33	2.69	0.188	0.48	1.61	11.15	9.66	0.003	0.72	8.07
3A	5.70	4.45	0.140	0.48	2.71	7.58	7.35	0.002	0.70	5.33
3B	13.23	13.97	0.912	0.59	7.86	13.68		0.008	0.94	12.82
3C	4.81	5.77	0.044	0.27	1.28	7.03	6.54	0.001	0.40	2.84
4A	5.06	4.12	0.350	0.57	2.89	6.57		0.004	0.66	4.33
4B	7.36		1.029	0.81	5.94	8.61		0.006	0.96	8.28
4C	4.21	4.06	0.052	0.29	1.22	4.61	5.35	0.002	0.42	1.93
5A	3.98	3.66	0.638	0.66	2.62	6.95		0.002	0.90	6.25

5B	10.31		0.651	0.58	6.01	11.77		0.008	0.96	11.35
5C	1.77		0.726	0.86	1.53	6.23		0.001	0.69	4.31
6A	4.94	4.32	0.617	0.61	3.01	6.29		0.005	0.87	5.46
6B	4.00		0.488	0.80	3.22	3.48		0.006	0.94	3.27
6C	4.47	3.40	0.313	0.72	3.19	3.87		0.003	0.79	3.06
7A	5.38	4.79	0.140	0.41	2.19	7.40	7.29	0.005	0.70	5.18
7B	8.97		0.977	0.83	7.42	10.15		0.005	0.96	9.73
7C	6.17	8.96	0.013	0.14	0.89	13.23		0.006	0.42	5.61

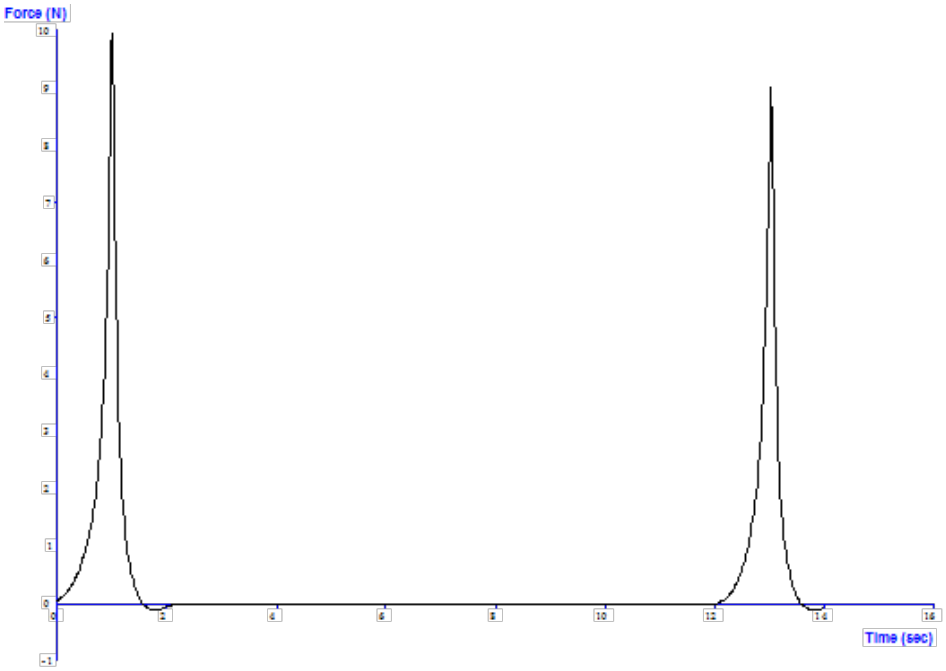

Figure 5- 2 TPA results from polymer 1C pre-swelling. Peak force around 10N during both depressions and no fracturing observed. Graph from 1st and 2nd compressions are almost identical showing litte change.

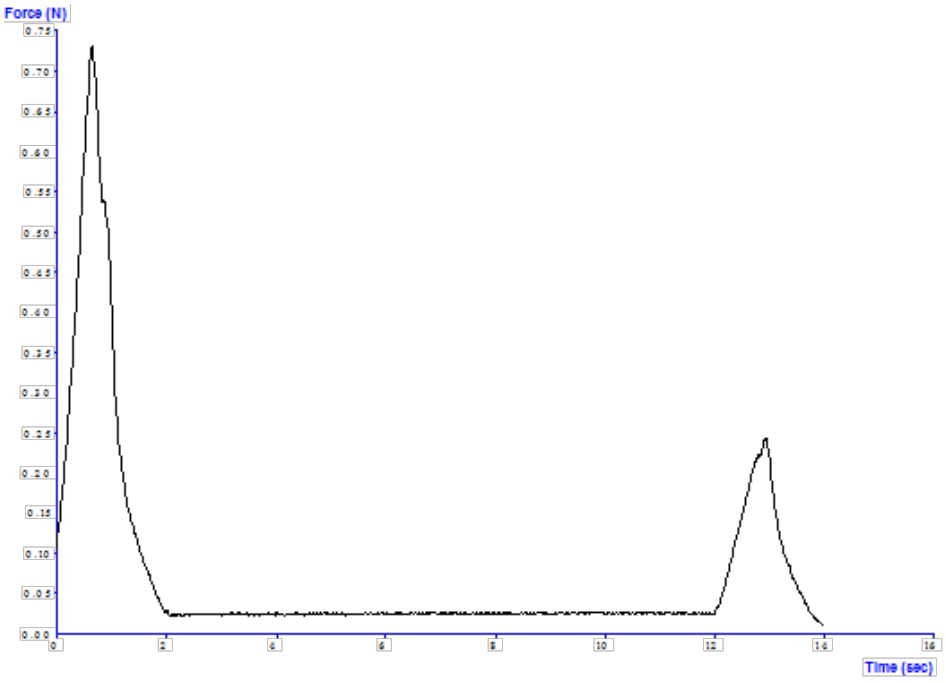

Figure 5- 3 TPA results from polymer 1C post-swelling. Peak force 0.75N during first depression and 0.25 during second depression. Fracturing observed during first penetration and obvious in second due to drastically lowered forces. Differences observed between depressions indicitive of change in disc structure, for example fracturing.

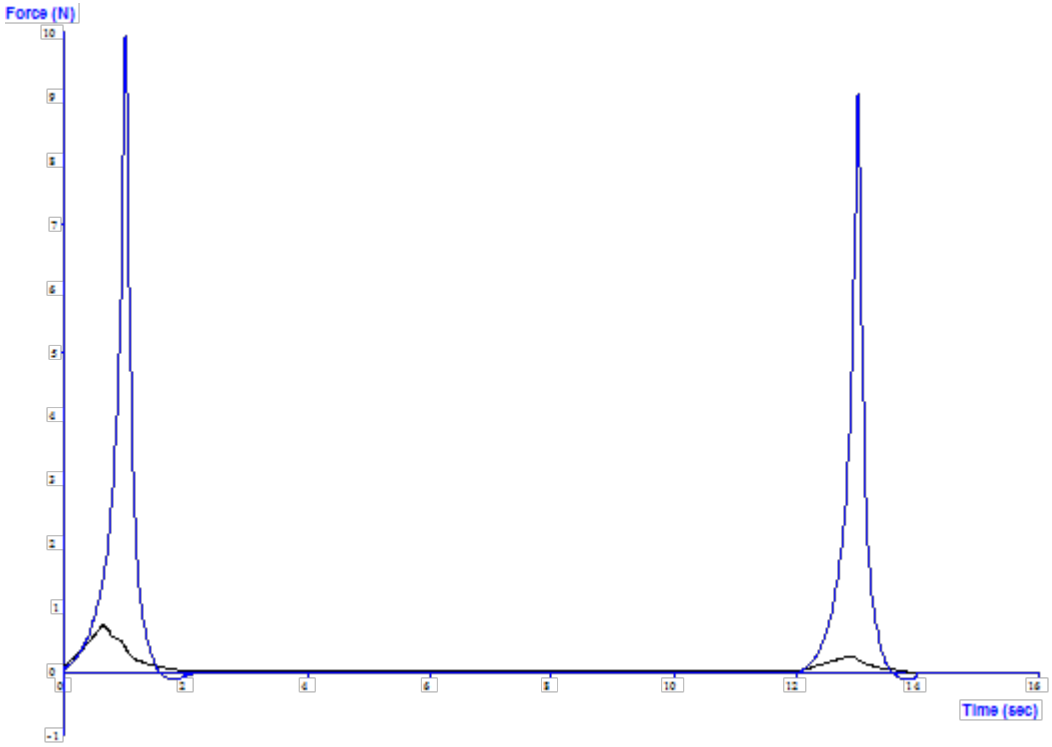

Figure 5- 4 TPA of polymer 1C pre and post swelling. Blue line denotes dry polymer test and black line shows results post submersion in water at 37°C for 24hrs.

Figure 5-3 and Figure 5- 4 show the results from one of the polymers tested using TPA. Polymer **1C** undergoes swelling upon submersion in water and thus its properties are altered. The significant differences pre and post swelling are more easily observed however if viewed in a singular chart, Figure 5- 5. It can be easily seen from this plot that the properties of this polymer have been significantly altered by swelling. This polymer had one of the most extreme changes in morphology upon swelling, hence its use as a descriptor, however there were changes observed in most polymers, not only the ones that increased in size. The numerical results from this work are shown in Table 5- 4 and Table 5- 5 for more information on each polymer generated by this technique.

5.3.4 Polymer Compression

Confined and unconfined compression studies were successfully carried out using a Bose Electroforce 3200 material characterisation system on wet and dry monomer **1** polymer samples respectively.

5.3.4.1 Confined Compression

Confined compression experiments were carried out using 5mm diameter polymer discs cut from original thiol-ene discs which had been held in 50ml of ultrapure water for 24h at 37°C.

Using the time recorded for a compression in seconds the platen displacement in microns and the stress in kPa (force/area) the H_a modulus, stiffness, could be calculated via data modelling. The data was fitted to the linear biphasic model (Mow et al., 1980) using a custom code written in MATLAB (Riches, 2012). An exponential permeability-strain relationship was included in these calculations [3] (Lai and Mow, 1980). Results of this data analysis can be seen in Table 5- 6.

Table 5- 6 Confined compression results after data analysis. H_a = modulus (stiffness) in confined compression, k_0 = zero-strain hydraulic permeability, M = coefficient describing loss of permeability with compression, R^2 = measure of data fitting. * Polymer still swelling after 24h submersion, calculations could not be undertaken. ** Polymers have no inherent stiffness and thus are completely relaxed after compression thus calculations could not fit the data.

Sample Name	H_a (kPa)	k_0 (m^4/Ns)	K_0 (m^2)	M	R^2
1BC	232.7	0.57×10^{-15}	5.7×10^{-13}	56.4	0.53
	*Stress continually increases in hold phase. Polymer still swelling.**				
	*Stress continually increases in hold phase. Polymer still swelling.**				
1BN	181.9	1.56×10^{-15}	1.56×10^{-12}	69.8	0.43
	183.2	1.24×10^{-15}	1.24×10^{-12}	60.9	0.82
	362.8	0.76×10^{-15}	7.6×10^{-13}	63.3	0.70
1C	*Final stress is positive, stress completely relaxed, no inherent stiffness.***				
	*Final stress is positive, stress completely relaxed, no inherent stiffness.***				
	*Final stress is positive, stress completely relaxed, no inherent stiffness.***				

The values generated from this experiment, when they could be calculated, are relatively close especially when compared to tissue compression data. They describe the polymer stiffness, zero-strain permeability, and permeability-strain relationship.

5.3.4.2 Unconfined Compression

Young's modulus, a measure of the stiffness of the dry polymer material, was calculated using the data collected from the unconfined compression measurements. These were carried out in triplicate to ensure reproducibility. Average and standard deviations were calculated and are shown in Table 5- 7. It can be seen that the stiffness of the **1B** cured polymer was higher than the non-cured counterpart and **1C** polymer. This is not surprising as it mimics the results from the unconfined

compression studies. The **1BC** results are also much more reproducible than the **1BC** and **1C** values, for further clarification Figure 5- 5.

Table 5- 7 Calculated Young's modulus (Pa) results from confined compression experiments on dry polymer samples with standard deviations.

Sample Name	Young's Modulus (Pa)	Average (Pa)	Standard Deviation (Pa)	Standard Deviation (%)
1BC	0.65	0.67	0.06	9
	0.62			
	0.76			
1BN	0.26	0.42	0.12	28
	0.45			
	0.54			
1C	0.08	0.1	0.02	16
	0.1			
	0.12			

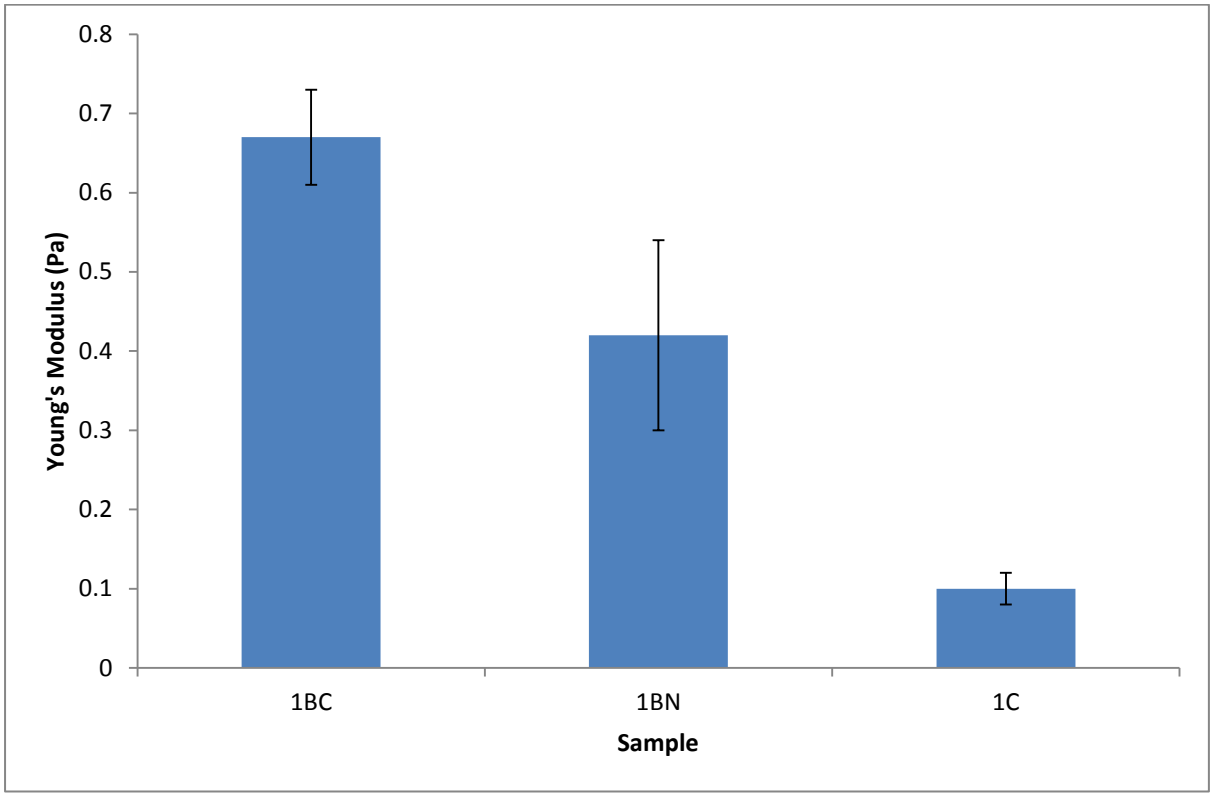

Figure 5- 5 Mean calculated Young's modulus (Pa) results from confined compression experiments on dry polymer samples 1BC, 1BN and 1C with standard deviations.

5.4 Discussion

5.4.1 Polymer Synthesis

Polymer synthesis was successful in all instances; all polymers were generated via the methodology stated in chapter 2. As previously the majority of polymers prepared were facile to generate, however, polymer **1B** again spontaneously solidified post addition of the thiol reagent. All polymers generated via this uv methodology were flexible solid discs as in all other synthesis and they were in all instances translucent and coloured from colourless to light brown. Again all polymers possessed an odour related to the thiol they were prepared with however, the potency of this was seriously reduced from that of the monomer alone and this was further reduced upon submersion in water. A number of batches of these polymers have been synthesised with consistent results. This has ensured that the methodology for preparation is repeatable and reliable. In order to make the testing of these species as facile as possible an active effort was made to ensure that polymers remained flat, before and after submersion in water. The discs produced were, in general, flat with some concave nature and to retain this, polymers were stored in petri dishes prior to testing. The slight concave nature of the polymers is thought to be due to the meniscus present upon addition of the reagent mixture to the wells which is retained in the very quick and static synthesis process.

5.4.2 Swelling Behaviour

Polymer swelling behaviour was qualitatively and quantitatively measured by these initial experiments. Polymers synthesised using monomer 1 had previously shown an ability to absorb water and swell in a fairly unidirectional manner. Using these experiments this ability was further investigated. Polymers were placed in 50ml of ultrapure water, or PBS buffer, in a 50ml centrifuge tube at 37°C for noted periods of time. At each time point the polymers were weighed and measured to determine the amount of liquid which has been taken up the results of which are noted previously.

5.4.2.1 Water Swelling

The polymers tested; **1BC** and **1C**, showed water uptake over the period of 1week. However, the uptake was not consistent in both cases. Polymer **1BC** took up an additional 50% of its mass in water over the course of the week however; this uptake was rapid and quickly achieved a steady state, 24h. There are differences between the mass of water taken up for each replicate however these are similar suggesting that the water taken up in the first 24h does not allow for further uptake over the course of the experiment. The diameter of the polymers increased between 15 and 21% over

the week but, like the mass increase, this was rapid and remained unchanged post the first 24h. This is contrary to the results of the **1C** polymer testing. In this case water was steadily taken up over the course of the experiment resulting in an increase in mass of 150%. This is higher than that of the **1BC** polymer and is reflected in the diameter increase which is double that of the **1BN** polymer at 43%. Polymer **1BC** retains much of its structural integrity throughout the testing with the only notable changes (other than the increase in diameter) being a slight increase in the concave nature of the polymer disc with some occasion splitting. In contrast the **1C** polymers become progressively more fragile and softer with the final measurements being greatly hampered by the slippery and friable nature of the discs. This would suggest that there are a number of additional bonds in the **1BC** polymer and that they are stronger thus, less water can infiltrate the surface and push these apart allowing the polymer to retain its shape and rigidity to a greater extent. This is not surprising as thiol **B** has number –SH entities which can bond multiple times to the acrylate monomer and brancher within the reagent mixture. To confirm whether this phenomenon only occurs within ultrapure water the experiment was repeated in PBS giving a more complete view of the polymer behaviour under biological conditions with pH and salt content altered.

5.4.2.2 PBS Swelling

PBS swelling was carried out in the same manner as the water swelling experiment. Polymer **1BC** more than doubled in mass over the course of the experiment which is 50% higher than the mass gained in the water experiment. The diameter change is also increased in this experiment with the maximum value reached being 27% and the change in height measured in this experiment remains minimal with an apparently anomalous 15% increase after 48hrs which is not observed at any other time point. Polymer C was also tested in the same manner, the increase in mass with this polymer is again higher than that observed for polymer **1BC** but is lower than that observed in the previous water experiments at 120%. Again the diameter and the height of the polymer discs increase over time but to a lesser extent than in the water experiment. These results are different to those seen in the water based experiments as polymer **1BC** has gained a larger proportion of mass than in the previous experiment with only a minimal change in the height of the polymer disc. The pattern of mass increase however is the same with the majority of the increase occurring over the first 24hrs and then gaining a steady state. To account for this larger increase in mass there must be a higher volume of water imbibed into the polymer matrix, this may in part be due to the addition of salts which can crystallise within the polymer and force chains apart allowing in a larger volume of water in the same time frame. The opposite however is true for the **1C** polymer discs; they gained significantly less mass over the time period than previously. This would suggest that the salts present in the PBS buffer are having the opposite effect on the polymer in that they are crystallising

within the polymer and blocking the ingression of water into the disc and slowing the increase in mass and dimensions. Both these phenomenon could be acting in this experiment and altering the results in unexpected ways and as such all further experiments were carried out in ultrapure water to lessen any influence occurring due to the changes in both pH and salt content.

5.4.3 Texture Profile Analysis

Texture profile analysis was carried out on all polymers synthesised both pre and post swelling. As changes in the polymer structure are likely to be made by the texture analysis method it was deemed more accurate to carry these compressions out on different polymers and not repeat the experiments on the same material.

5.4.3.1. Dry Polymers

The dry experiments were carried out at three velocities, 0.1mm/s, 1mm/s and 3mm/s. All experiments were carried out in quadruplicate and the level of reproducibility in the dry polymers was increased as the speed of the compression is increased, see Figure 5- 6, Figure 5- 7 and Figure 5- 8. It can be seen that the difference between the highest and lowest peak forces in the 0.1mm/s experiment is approximately 6N, in the 1mm/s experiment this is reduced to 3N and finally for the 3mm/s experiment this is falls further to only 1.5N. The peak forces measured, which represent the hardness of the polymer, were averaged and noted in Table 5- 4. Due to the similarity of the results from the 1mm/s and 3mm/s tests in the dry experiments only 0.1mm/s and 1mm/s experiments were repeated on the wet polymers.

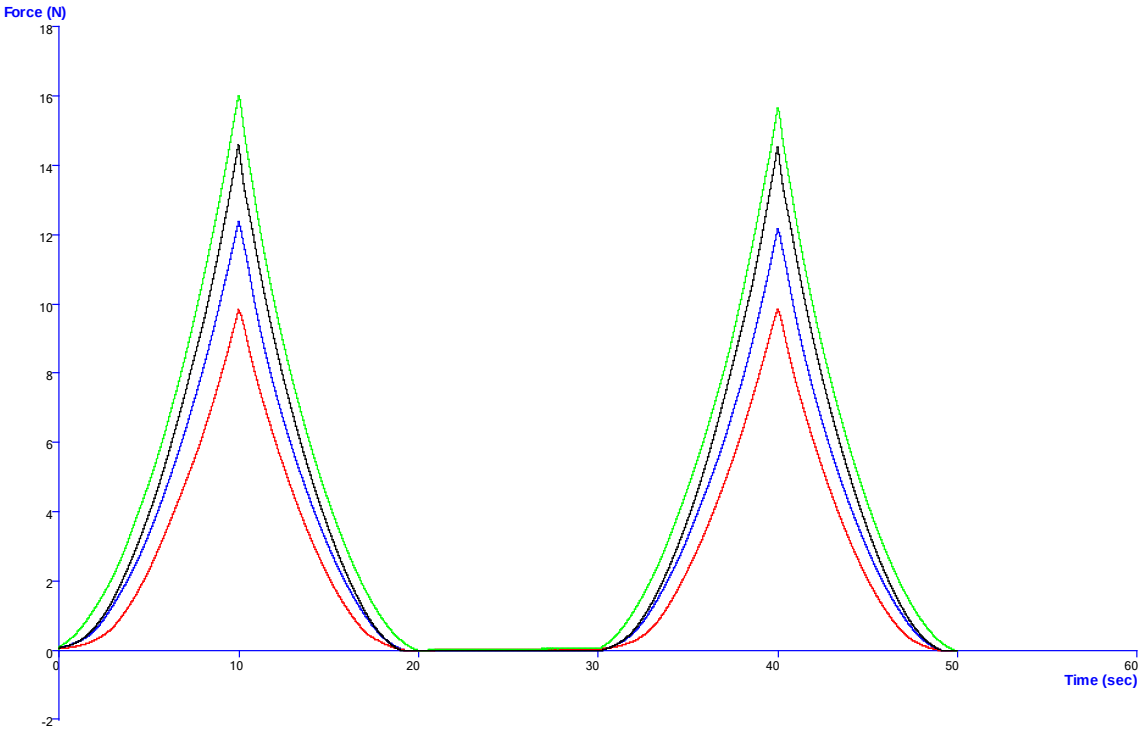

Figure 5- 6 Polymer 1BC results from dry TPA measurements at 0.1mm/s showing reproducibility.

The dry polymers did not fracture in any instance at the higher test velocities, 1 and 3mm/s, however six polymers did break when tested at 0.1mm/s, for an example see Figure 5- 9. The majority of these were polymers synthesised using thiol **C**; **2A**, **3C**, **4C** and **7C**. This would suggest that these polymers were weaker and more friable than those synthesised using thiols A or B which could be due to this thiol only possessing one –SH entity to react with the acrylate species present in comparison to the other thiols which have 2 and 4 respectively.

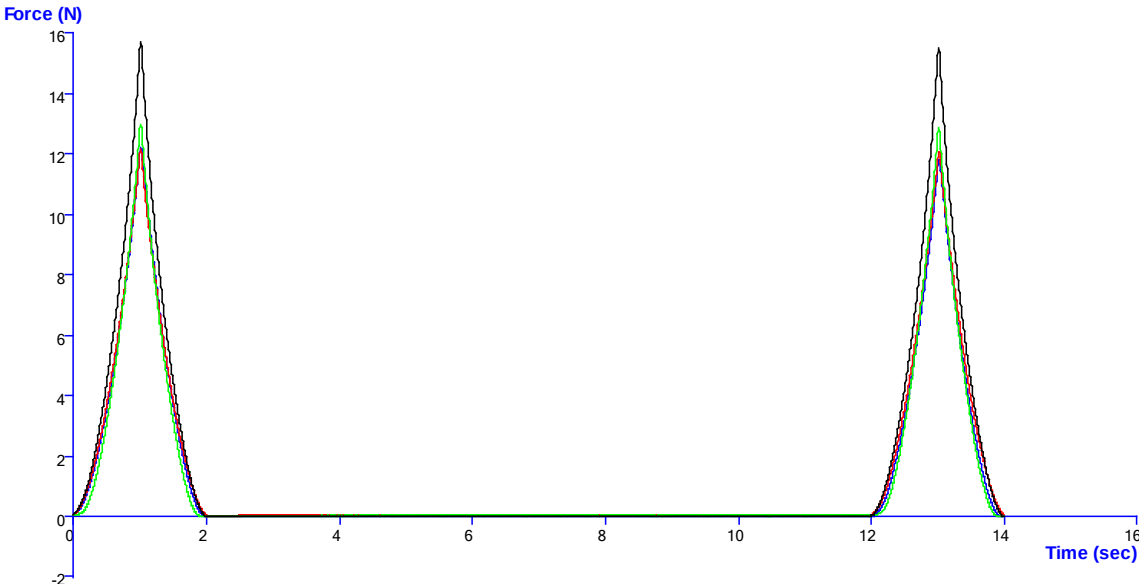

Figure 5- 7 Polymer 1BC results from dry TPA measurements at 1mm/s showing increased reproducibility from 0.1mm/s experiment.

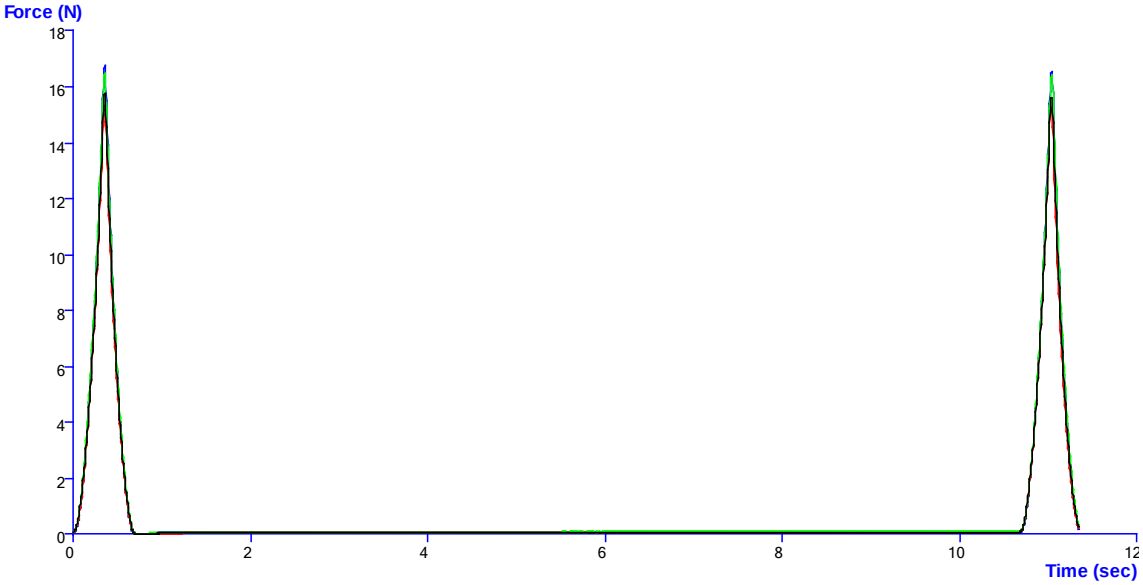

Figure 5- 8 Polymer 1BC results from dry TPA measurements at 3mm/s showing increased reproducibility from 1mm/s and 0.1mm/s experiments.

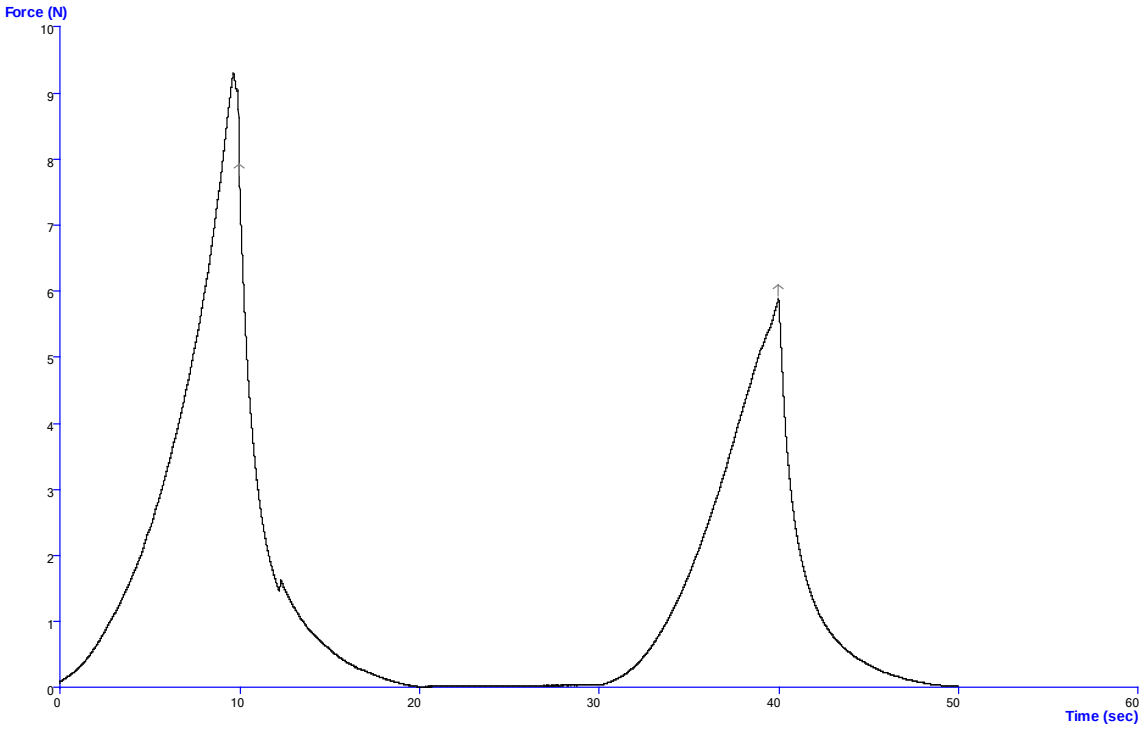

Figure 5- 9 Polymer 7C 0.1mm/s dry experiment showing a fracture occurring within the polymer at 13sec which then lowers peak force measured in second compression. The asymmetry observed is due to a weakening of the polymer disc due to this small fracture which, whilst not being visible in the product, has made a significant difference to the innate hardness.

As polymers synthesised using monomer **1** were of heightened interest due to previous observations, unidirectional swelling and hydrogel like behaviour, it was surprising that did not show any vastly different results from the other polymers tested. Polymer **1BC** is harder than polymer **1BN** at 1 and 3mm/s which is expected as the curing process should increase the number of bonds between the polymer chains and thus the hardness of the resultant material and although the 0.1mm/s experiment would suggest otherwise the difference between these results is within the standard deviation in the experiment. None of the monomer **1** polymers fractured during the testing and although polymer **1C** has much lower hardness and gumminess than the others this is still similar to other polymers within the set. In order to learn more about the swelling behaviours of all polymers synthesised the wet polymers were tested after 24hrs submerged in ultrapure water at 37°C. All analysed data collected from these experiments is recorded in Table 5- 4.

5.4.3.2. Wet Polymers

The testing of these polymers was significantly more complex than the dry experimentation. This was due to the polymers becoming more friable, slippery and difficult to handle after water immersion. In particular polymer **1C** could not be adhered to the base metal plantain using adhesive

as previously and thus had to be manually held in place in order to allow for testing. The results of these experiments also had much greater variation which can be seen in Figure 5- 10 and Figure 5-11. The peak asymmetry shown in Figure 5- 9 is observed with great frequency throughout this testing as the initial compression changes the polymer significantly in every case; the second peak force measured is dependent on the polymer itself and any changes which occur within the matrix during the first compression.

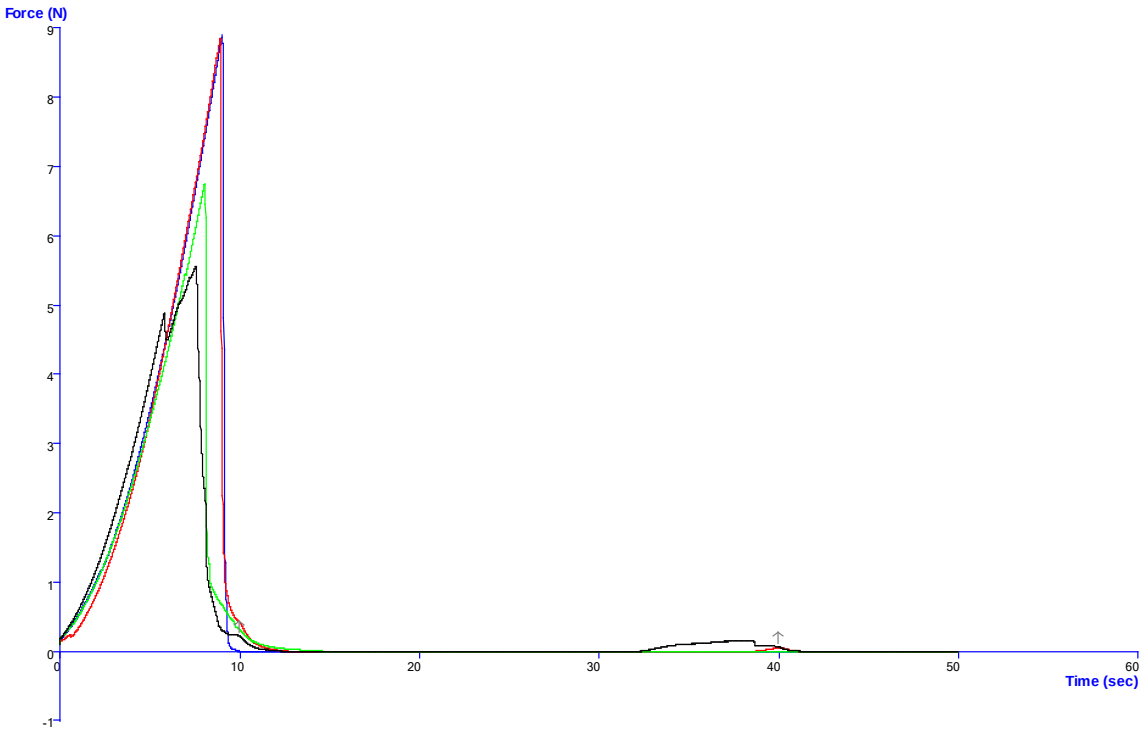

Figure 5- 10 Polymer 1BC results from wet TPA measurements at 0.1mm/s showing the differences between the repeats, the lowered peak force and the fracture of the polymer in every instance.

These plots are from the same polymer as shown in the previous section to aid comparisons between the dry polymer material and that which is imbibed with water. In these tests the vast majority of the polymers tested fractured during testing at 0.1mm/s with a number also fracturing at the higher velocity. This appears to be due to the water entering the polymer matrix and forcing the chains apart and weakening the internal structure allowing it to be forced apart by the compression. Polymers synthesised using monomer **1** had again visibly increased in diameter and thus were of great interest. In comparison to the previously collected data polymer **1BC** again had a higher peak force, hardness, than that of **1BN** at both test speeds and polymer **1C** had a very low measured hardness post swelling. Polymer **1C** fractured in every case and exceptionally low peak forces were measured at all test velocities. This coupled with the difficulties in testing resulting from their very slippery nature indicted that these polymers were vastly different to all others tested, see Figure 5-

12 and Figure 5- 13. All polymers synthesised using monomer **1** were different to the others within the library and due to the exceptionally weak structure further, more sensitive, analysis was carried out to determine the properties of these materials more accurately. The results of this compression analysis are detailed in the following chapters.

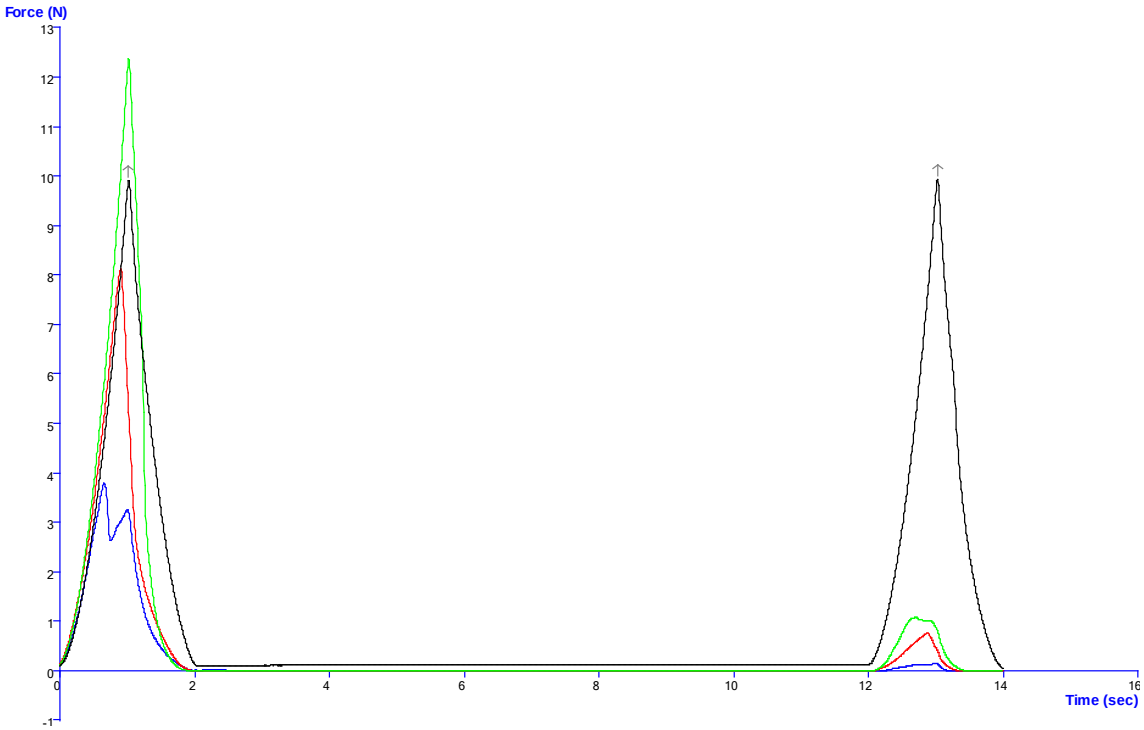

Figure 5- 11 Polymer 1BC results from wet TPA measurements at 1mm/s again showing the differences between the repeats, the lowered peak force and the fracture of the polymer in most cases.

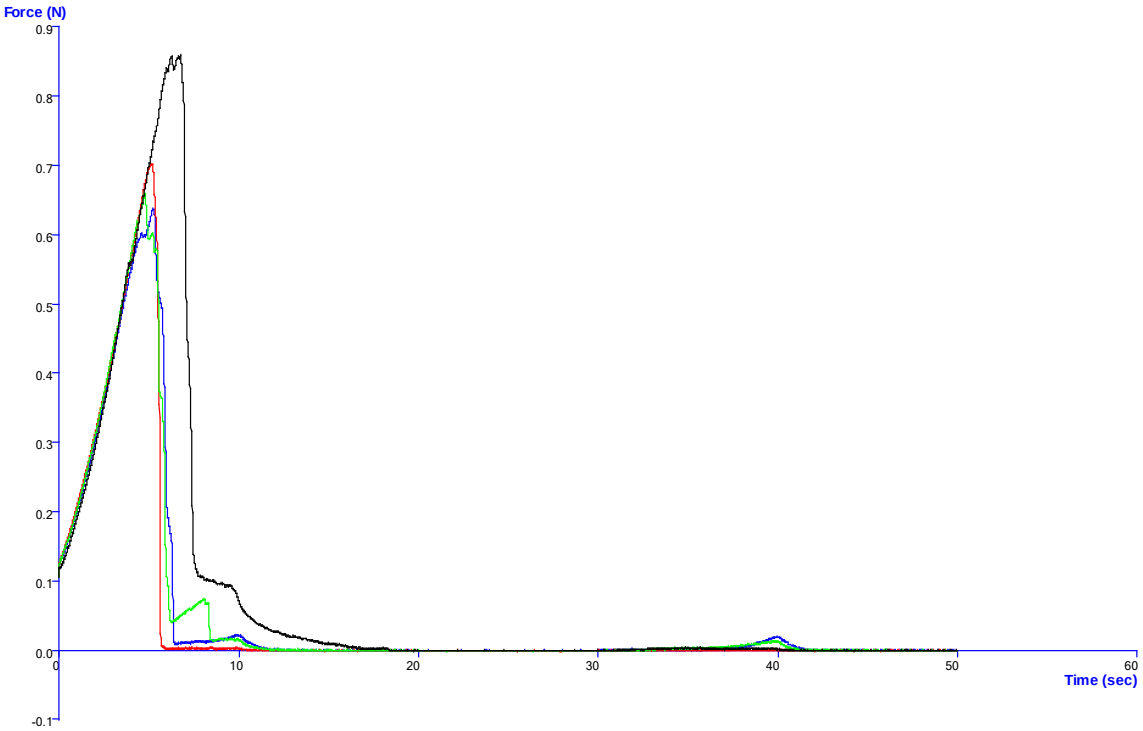

Figure 5- 12 Polymer 1C results from wet TPA measurements at 0.1mm/s showing the lowest peak forces measured and the fracture of the polymer in all instances.

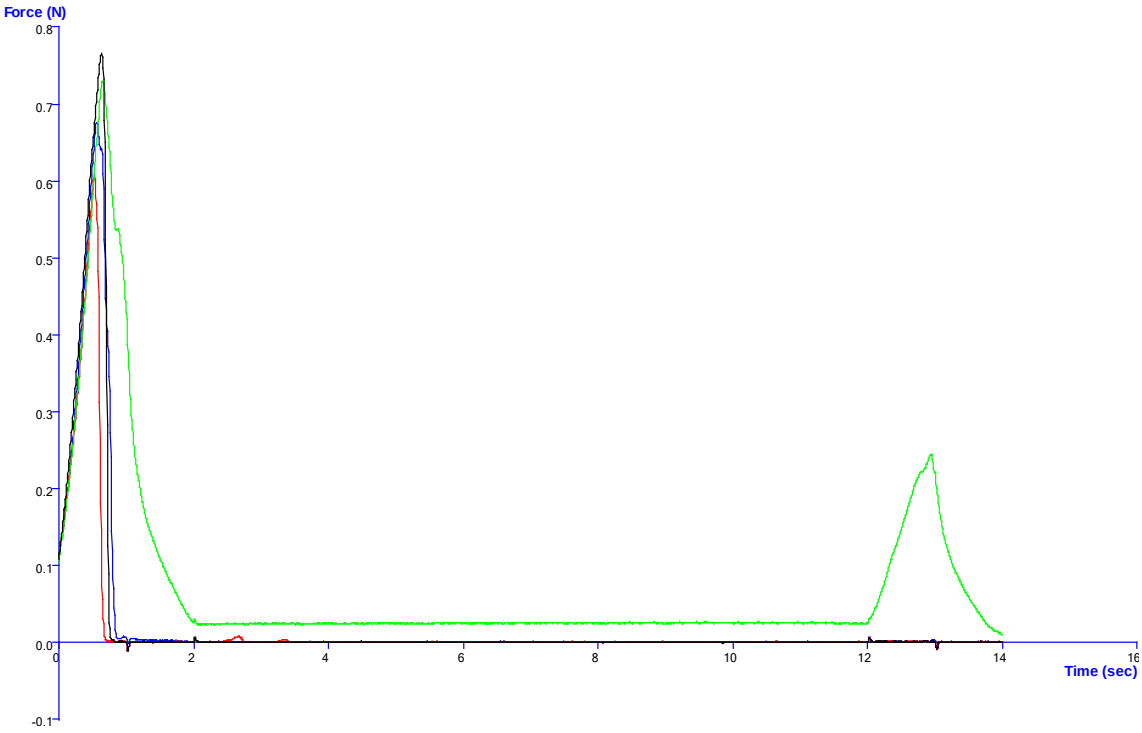

Figure 5- 13 Polymer 1C results from wet TPA measurements at 1mm/s showing the lowest peak forces measured and the fracture of the polymer in all instances.

5.4.4 Polymer Compression

Confined and unconfined compression studies carried out using a Bose Electroforce 3200 material characterisation system on wet and dry polymers **1BC**, **1BN** and **1C**. Only these polymers were tested as they show visible swelling upon submersion in water and significant changes in there texture analysis thereafter. Confined and unconfined compressions were measured in order to define important characteristics of the polymers.

5.3.4.1 Confined Compression

The results from the confined compressions carried out on the water swollen polymers show that the three polymers tested are different to one another albeit that polymers **1BC** and **1BN** were formed using the same reagents. Polymer **1BN**, the naturally cured polymer using daylight, upon testing is deemed to have stopped swelling and have a stiffness which is most likely around 180 kPa. The third replicate in this experiment appears to be greatly different to that of the other samples, although when compared to the data regularly generated using this technique, on biological samples; these results are all in good agreement. Polymer **1BC**, the UV cured polymer synthesised from monomer **1** and thiol **B**, differs from the non-cured version in that at after 24hrs submersion in water these polymers are, in general, still increasing in size and thus swelling. This is unexpected as it was initially theorised that polymers **1BC** and **1BN** would behave similarly due to their near identical chemical analyses. Finally polymer **1C** was tested, it was known from the texture analysis study that this polymer imbibes a large volume of water which renders it friable, soft and slippery and these observations are reinforced by this compression work. All three replicates for this polymer result in a final stress which is increased from the initial measurement, this suggests that the polymer is completely relaxed with no inherent stiffness and the polymer has no structural integrity. As the polymers have no inherent stiffness they cannot be fitted using the MATLAB data analysis and thus no further information regarding their properties could be gathered.

5.3.4.2 Unconfined Compression

Unconfined compressions were carried out on dry polymer material in order to calculate the Young's modulus of each polymer sample. This is a measure of the stiffness of the polymer and is determined using polymer discs in an unconfined compression set up. Again all samples were tested in triplicate to determine repeatability. The non-cured polymer **1BN** had a lower calculated young's modulus than that of the cured **1BC** sample however it did also have the largest deviation between the results. This may be due to the curing of these polymers being less well defined as it is not being

forced by the inclusion of the powerful UV lamp allowing each of the polymer discs to cure separately and to differing levels of completion. The cured polymer **1BC** has a higher measured young's modulus, 0.67Pa, than any other tested which is what was expected as thiol B has a large number of –SH entities which can bond numerous times to the acrylate monomer and brancher. The curing process also appears to generate the largest number of bonds as this polymer has a higher stiffness than its non-cured counterpart. Finally polymer **1C** was tested and again this had a much lower stiffness than all other polymers tested. This lower value is expected as polymer **1C** has a more pliable and deformable nature than the others generated. This low stiffness is also carried forward to the confined compression study where there is no stiffness which can be calculated after submersion in water for 24hrs.

5.5 Conclusions

From the initial water uptake experiments it can be concluded that polymers **1BC** and **1C** both take on water over the course of 1 week however, this is uptake was not consistent. Polymer **1BC** rapidly (over 24h) increased in mass by 50% whilst polymer **1C** steadily took up mass over the course of the experiment eventually gaining 150% of its original weight. Upon repetition in PBS buffer it was noted that the polymer behaviour was different in buffered media. In fact polymer **1BC** more than doubled in mass over the course of the experiment whilst **1C** polymer discs gained less mass over the time period than previously

From the TPA experiments it was seen that no dry polymers did not fractured at the higher test velocities, 1 and 3mm/s, however a number did break when tested at 0.1mm/s. The majority of these were polymers synthesised using thiol **C** suggesting that these polymers were weaker and more friable than those synthesised using the dithiol or quarternary thiol. After water submersion the results of TPA experiments had much greater variation. In these tests the majority of the polymers fractured during testing at 0.1mm/s with a number also fracturing at the higher velocity, which appears to be due to the water entering the polymer matrix and forcing the chains apart and weakening the internal structure allowing it to be fractured apart by the compression.

From the experiments carried out using the compression setup the differences between polymer **1BN**, the naturally cured polymer using daylight, and **1BC**, the polymer cured in the UV oven, could be determined. Polymer 1BN had stopped swelling after 24hrs and could be measured accurately whilst polymer **1BC** replicated were increasing in size and thus swelling after the same time lapse. This is unexpected as it was initially theorised that polymers **1BC** and **1BN** would behave similarly due to their near identical chemical analyses. Polymer **1C** was different, as expected, from these other two as it was previously known that it imbibed a large volume of water which renders it friable, soft and slippery. These observations are reinforced by this compression work.

The mechanical properties of the polymers synthesised using monomer **1** and thiols **B** and **C** are very interesting. Not only do they take on large volumes of water, with respect to their size, but they swell in a unidirectional manner causing their properties to change greatly before and after submersion. The most interesting results in this section show that polymers **1BC** and **1BN**, synthesised from the same reaction mixture and thus being chemically identical, have differing properties before and after swelling. This would suggest that the irradiation of the polymers using the UV light source causes them to change their mechanical properties due to, most likely, their degree of crosslinking.

6. SUMMARY AND FURTHER WORK

6.1. Summary

In this work, the properties of branched thiol-ene and acrylate polymers for biomaterial purposes have been explored. In the initial stages, the development and characterisation of the parallel synthesis of branched acrylate polymers was carried out. This method was then utilised to synthesise a number of branched polymer species at differing brancher proportions. The library of acrylate compounds generated was then characterised using a number of analytical techniques. These ensured that the material prepared was fully polymerised and determined any differences between each polymer dependant on their reagent material. A number of surface analytical techniques, AFM and CAG in particular, were then employed to determine the surface properties of the polymer which is the area in the greatest contact with biological fluid. Finally all polymers were tested using a number of bacterial strains to determine their effect, if any, on the proliferation of bacterial biofilms. It was discovered that upon addition of further brancher into the reaction mixture the bacterial colonisation of the polymer surface was lessened in a stepwise manner.

Another method investigated in this thesis was the use of UV polymerisation to generate branched thiol-ene polymer material. In the initial development of this methodology the use of metal plates for synthesis had to be adopted to negate the challenges which arose from the high temperatures and deformation effects observed even over short irradiation periods. However synthesis of thiol-ene polymers was successful and a collection of materials was generated in order to be tested in a similar manner to the acrylates. Characterisation using analytical techniques clarified that level of polymerisation within these polymers was in general, high, however a number did appear to retain some unreacted acrylate material. The surface properties of each of the materials present were also probed prior to biological testing to allow some indication of biofouling to be determined. In this instance it was discovered that the thiol-ene polymers synthesised lessened biological proliferation in comparison to a control however, there was no obvious pattern within data suggesting the most beneficial thiol/monomer combination.

During the biological testing of the thiol-ene polymers it was noted that the polymers synthesised using monomer **1** underwent swelling in biological media over 24hrs at 37°C. In order to further investigate this, synthesis of these polymers was repeated and the swelling capabilities of the polymers were tested further using a number of methodologies. Using basic mass uptake experiments it was shown that the polymers can not only imbibe biological media but also ultrapure water and PBS buffer which is more akin to that of the fluid it would be in contact with in a medical application. Testing using TPA and compression analysis suggest that polymer **1B** retained the

majority of its structure over the period of swelling however, polymer **1C** synthesised with a simpler thiol molecule, was rendered structurally unsound after 24hrs submersion in water. This final area of work suggested that all thiol-ene polymers undergo some structural change after water submersion which may hinder their use as biomaterials alone but they could still prove beneficial as wound coverings or as a bioresitive coating for structural biomaterials already in use.

The work presented in this thesis holds significant value in adding to the understanding of branched polymers as bioresistive biomaterials. Understanding the impact of the reagents chosen and the level of branching present within the polymer on the bacterial colonisation at the surface allows for future biomaterials to be better screened. This knowledge could influence the choice of polymers investigated for a number of biological applications as the prevention of biofilm formation upon the surface of these implants is currently costly, invasive and highly detrimental to patient health.

6.2 Further Work

Following the investigations carried out in this thesis, several potential areas of research have been identified, which could be pursued in the future.

In the first instance it would be beneficial to expand the bacterial work carried out on the polymers using other known strains of bacterial which are prolific biofilm former. Further to this work it would be interesting to test the polymers synthesised using cell lines. This would give an indication of whether these polymers are beneficial or detrimental to cell growth upon their surface and further narrow the options available for their eventual use. Further to using simple cell lines; stem cells could also be grown on these materials in order to assess their effect on cell differentiation and development.

In addition to this work, a second area of interest could be pursued an attempt to investigate the branching capabilities of the thiol-ene polymers in a similar manner to the acrylate work carried out in the first chapter. This could confirm the ideal levels of each reagent which produce the most bioresistive surface properties along with the ideal topography for cell growth and differentiation.

Finally, in the initial planning stages it was anticipated that the use of GPC-MALLS (Gel permeation chromatography multi angle laser light scattering) to determine the molecular weight of the polymers synthesised as this techniques does not require the accurate dissolution of known masses of polymer which is near impossible due to their lack of solubility. However, due to a number of instrument failures and time constraints this work could not be carried out. It would be beneficial to know the molecular weight of the polymer chains synthesised using both the UV and thermal methodologies employed throughout this thesis. (Laboratory, 2010)

Finally it would be interesting to further investigate the use of the self curing thiol-ene polymer (**1BN**) as a wound dressing. This would include the investigation of porosity of the polymer, to guarantee there are no tracks to allow bacteria to gain access to the wound, the flexibility of the polymer, for use in areas which are required to move, and finally to determine whether this polymer shield is safe for use in contact with patients bodily fluids.

REFERENCES

ADAMSON, A. W. & GAST, A. P. 1997. *In: Physical Chemistry of Surfaces,* New York, John Wiley & Sons.

ADLER, J., JAYAN, A. & MELIA, C. D. 1999. A method for quantifying differential expansion within hydrating hydrophilic matrixes by tracking embedded fluorescent microspheres. *Journal of Pharmaceutical Sciences,* 88**,** 371-377.

AIMETTI, A. A., MACHEN, A. J. & ANSETH, K. S. 2009. Poly(ethylene glycol) hydrogels formed by thiol-ene photopolymerization for enzyme-responsive protein delivery. *Biomaterials,* 30**,** 6048-6054.

ALPERT, N. L., KEISER, W. E. & SZYMANSKI, H. A. 1970. *IR Theory and Practice of Infrared Spectroscopy,* New York, Plenum Press.

AMBADE, A. V. & KUMAR, A. 2000. Controlling the degree of branching in vinyl polymerization. *Prog. Polym. Sci.,* 25.

AMIGO, J. M. 2010. Practical issues of hyperspectral imaging analysis of solid dosage forms. *Analytical and Bioanalytical Chemistry,* 398**,** 93-109.

AMIRFAZLI, A. & NEUMANN, A. W. 2004. Status of the three-phase line tension. *Advances in Colloid and Interface Science,* 110**,** 121-141.

ANDERSON, D. G., BURDICK, J. A. & LANGER, R. 2004. Smart Biomaterials. *Science,* 305.

ASTHANA, R., KUMAR, A. & DAHOTRE, N. B. 2006. *Materials Processing and Manufacturing Science*, Butterworth-Heinemann.

BABENSEE, J. E., ANDERSON, J. M., MCINTIRE, L. V. & MIKOS, A. G. 1998. Host response to tissue engineered devices. *Advanced Drug Delivery Reviews,* 33.

BAEKELAND, L. H. 1909. The synthesis, constitution, and uses of bakelite. *Journal of Industrial and Engineering Chemistry-Us,* 1**,** 149-161.

BAJPAI, A. K., SHUKLA, S. K., BHANU, S. & KANKANE, S. 2008. Responsive polymers in controlled drug delivery. *Progress in Polymer Science,* 33**,** 1088-1118.

BAUDRY, R. & SHERRINGTON, D. C. 2006a. Synthesis of highly branched poly(methyl methacrylate)s using the "strathclyde methodology" in aqueous emulsion. *Macromolecules,* 39**,** 1455-1460.

BAUDRY, R. & SHERRINGTON, D. C. 2006b. Synthesis of Highly Branched Poly(methyl methacrylate)s Using the “Strathclyde Methodology” in Aqueous Emulsion. *Macromolecules,* 39.

BEECH, I. B., SMITH, J. R., STEELE, A. A., PENEGAR, I. & CAMPBELL, S. A. 2002. The use of atomic force microscopy for studying interactions of bacterial biofilms with surfaces. *Colloids and Surfaces B-Biointerfaces,* 23**,** 231-247.

BILLMEYER, F. W. 1984. *Textbook of Polymer Science*, Wiley.

BLANCHARD, C. R. 1996. Atomic Force Microscopy. *THE C H EMICAL EDUCATOR,* 1**,** 1-8.

BLASCHKE, U., PASCHKE, A., RENSCH, I. & SCHUURMANN, G. 2010. Acute and Chronic Toxicity toward the Bacteria Vibrio fischeri of Organic Narcotics and Epoxides Structural Alerts for Epoxide Excess Toxicity. *Chemical Research in Toxicology,* 23**,** 1936-1946.

BOURNE, M. C. 1978. TEXTURE PROFILE ANALYSIS. *Food Technology,* 32**,** 62-&.

BOWEN, W. R., DONEVA, T., HILAL, N. & WRIGHT, C. J. 2001. Atomic Force Microscopy: Images and Interactions. *MICROSCOPY AND ANALYSIS*.

BOYLE, A. 1994. POLYMER-CHAIN PACKING ANALYSIS USING MOLECULAR MODELING. *Journal of Molecular Graphics,* 12.

BROCHARD, F. & DEGENNES, P. G. 1983. KINETICS OF POLYMER DISSOLUTION. *Physicochemical Hydrodynamics,* 4**,** 313-322.

BURGER, J. E. 2006. *Hyperspectral NIR Image Analysis.* PhD, Swedish University of Agricultural Sciences.

BUTANY, J., CARMICHAEL, K., LEONG, S. W. & COLLINS, M. J. 2005. Coronary artery stents: identification and evaluation. *Journal of Clinical Pathology,* 58**,** 795-804.

CALLAGHAN, J. J., ROSENBERG, A. G. & RUBASH, H. E. 2007. *The Adult Hip*, Lippincott Williams & Wilkins.

CAMPBELL, J. D., TEYMOUR, F. & MORBIDELLI, M. 2005. Production of hyperbranched polystyrene by high-temperature polymerization. *Macromolecules,* 38**,** 752-760.

CAMPOCCIA, D., MONTANARO, L., SPEZIALE, P. & ARCIOLA, C. R. 2010. Antibiotic-loaded biomaterials and the risks for the spread of antibiotic resistance following their prophylactic and therapeutic clinical use. *Biomaterials,* 31.

CASTNER, D. G. & RATNER, B. D. 2002. Biomedical surface science: Foundations to frontiers. *Surface Science,* 500.

CHALFIE, M., TU, Y., EUSKIRCHEN, G., WARD, W. W. & PRASHER, D. C. 1994. GREEN FLUORESCENT PROTEIN AS A MARKER FOR GENE-EXPRESSION. *Science,* 263**,** 802-805.

CHEUNG, A., HUI, S., LIN, T. & WANG, C. 2004. Observation of a Peak in T4 Phage Development in Escherichia coli Biofilm Grown on Millipore Filters for Four Days. *Journal of Experimental Microbiology and Immunology (JEMI),* 12, 79-83.

CHISHOLM, M., HUDSON, N., KIRTLEY, N., VILELA, F. & SHERRINGTON, D. C. 2009. Application of the "Strathclyde Route" to Branched Vinyl Polymers in Suspension Polymerization: Architectural, Thermal, and Rheological Characterization of the Derived Branched Products. *Macromolecules,* 42**,** 7745-7752.

CLAYDEN, J., GREEVES, N. & WARREN, S. 2012. Polymerisation. *Organic Chemistry.* 2, illustrated ed. Oxford: Oxford University Press.

COLOMBO, P. 1993. SWELLING-CONTROLLED RELEASE IN HYDROGEL MATRICES FOR ORAL ROUTE. *Advanced Drug Delivery Reviews,* 11**,** 37-57.

COSTERTON, J. W., STEWART, P. S. & GREENBERG, E. P. 1999. Bacterial biofilms: A common cause of persistent infections. *Science,* 284**,** 1318-1322.

CRAMER, N. B., DAVIES, T., O'BRIEN, A. K. & BOWMAN, C. N. 2003. Mechanism and modeling of a thiol-ene photopolymerization. *Macromolecules,* 36**,** 4631-4636.

DOUGHERTY, S. H. 1988. Infections in the bionic man. *Pharmacotherapy,* 8**,** 7S-10S.

FAN, S., BOEY, F. Y. C. & ABADIE, M. J. M. 2008. The application of thiol-ene reaction on preparing UV curable bismaleimide-containing liquid formulations. *European Polymer Journal,* 44**,** 2123-2129.

FERRARO, J. R., NAKAMOTO, K. & BROWN, C. W. 2003. *Introductory Raman Spectroscopy*, Academic Press.

FRECHET, J. M. J., HENMI, M., GITSOV, I., AOSHIMA, S., LEDUC, M. R. & GRUBBS, R. B. 1995. Self-Condensing Vinyl Polymerization: An Approach to Dendritic Materials. *SCIENCE,* 269.

FU, Q., LIU, J. H. & SHI, W. F. 2008. Preparation and photopolymerization behavior of multifunctional thiol-ene systems based on hyperbranched aliphatic polyesters. *Progress in Organic Coatings,* 63**,** 100-109.

FURTH, M. E., ATALA, A. & VAN DYKE, M. E. 2007. Smart biomaterials design for tissue engineering and regenerative medicine. *Biomaterials,* 28**,** 5068-5073.

GAJEWSKI, A. 2005. A method for contact angle measurements under flow conditions. *International Journal of Heat and Mass Transfer,* 48**,** 4829-4834.

GAO, P. & MEURY, R. H. 1996. Swelling of hydroxypropyl methylcellulose matrix tablets .1. Characterization of swelling using a novel optical imaging method. *Journal of Pharmaceutical Sciences,* 85**,** 725-731.

GARDINER, D. J., GRAVES, P. R. & BOWLEY, H. J. 1989. *Practical Raman Spectroscopy,* University of Michigan, Springer.

GAYNOR, S. G., EDELMAN, S. & MATYJASZEWSKI, K. 1996. Synthesis of Branched and Hyperbranched Polystyrenes. *Macromolecules,* 29.

GENDRIN, C., ROGGO, Y. & COLLET, C. 2008. Pharmaceutical applications of vibrational chemical imaging and chemometrics: A review. *Journal of Pharmaceutical and Biomedical Analysis,* 48**,** 533-553.

GHOSH, P. 2001. *Polymer Science and Technology: Plastics, Rubbers, Blends and Composites*, Tata McGraw-Hill Education.

GOOD, R. J. & KOO, M. N. 1979. EFFECT OF DROP SIZE ON CONTACT-ANGLE. *Journal of Colloid and Interface Science,* 71**,** 283-292.

GOODRUM, J. W. 2002. Volatility and boiling points of biodiesel from vegetable oils and tallow. *Biomass & Bioenergy,* 22**,** 205-211.

GORDON, C. A., HODGES, N. A. & MARRIOTT, C. 1988. ANTIBIOTIC INTERACTION AND DIFFUSION THROUGH ALGINATE AND EXOPOLYSACCHARIDE OF CYSTIC FIBROSIS-DERIVED PSEUDOMONAS-AERUGINOSA. *Journal of Antimicrobial Chemotherapy,* 22**,** 667-674.

GOWEN, A. A., O'DONNELL, C. P., CULLEN, P. J. & BELL, S. E. J. 2008. Recent applications of Chemical Imaging to pharmaceutical process monitoring and quality control. *European Journal of Pharmaceutics and Biopharmaceutics,* 69**,** 10-22.

GRISTINA, A. G. & COSTERTON, J. W. 1985. BACTERIAL ADHERENCE TO BIOMATERIALS AND TISSUE - THE SIGNIFICANCE OF ITS ROLE IN CLINICAL SEPSIS. *Journal of Bone and Joint Surgery-American Volume,* 67A**,** 264-273.

GULEC, H. A., SARIOGLU, K. & MUTLU, M. 2006. Modification of food contacting surfaces by plasma polymerisation technique. Part I: Determination of hydrophilicity, hydrophobicity and surface free energy by contact angle method. *Journal of Food Engineering,* 75**,** 187-195.

HARLAND, R. S., GAZZANIGA, A., SANGALLI, M. E., COLOMBO, P. & PEPPAS, N. A. 1988. DRUG POLYMER MATRIX SWELLING AND DISSOLUTION. *Pharmaceutical Research,* 5**,** 488-494.

HARRIS, D. C. & BERTOLUCCI, M. D. 1989. *Symmetry and Spectroscopy: An Introduction to Vibrational and Electronic Spectroscopy*, Courier Dover Publications.

HASEGAWA, M. & AZUMA, T. 1979. MECHANICAL-PROPERTIES OF SYNTHETIC ARTERIAL GRAFTS. *Journal of Biomechanics,* 12.

HEATON 1994. *The Chemical Industry*, Springer.

HOARE, T. R. & KOHANE, D. S. 2008. Hydrogels in drug delivery: Progress and challenges. *Polymer,* 49.

HOLLY, F. J. 1975. WETTABILITY OF HYDROGELS .1. POLY(2-HYDROXYETHYL METHACRYLATE). *Journal of Biomedical Materials Research,* 9**,** 315-326.

HOYLE, B. D., ALCANTARA, J. & COSTERTON, J. W. 1992. PSEUDOMONAS-AERUGINOSA BIOFILM AS A DIFFUSION BARRIER TO PIPERACILLIN. *Antimicrobial Agents and Chemotherapy,* 36**,** 2054-2056.

HOYLE, C. E. & BOWMAN, C. N. 2010. Thiol-Ene Click Chemistry. *Angewandte Chemie-International Edition,* 49**,** 1540-1573.

HOYLE, C. E., LEE, T. Y. & ROPER, T. 2004. Thiol-enes: Chemistry of the past with promise for the future. *Journal of Polymer Science Part a-Polymer Chemistry,* 42**,** 5301-5338.

HUBBELL, J. A. 1995. BIOMATERIALS IN TISSUE ENGINEERING. *Bio-Technology,* 13**,** 565-576.

HUGEL, T. & SEITZ, M. 2001. The study of molecular interactions by AFM force spectroscopy. *Macromolecular Rapid Communications,* 22**,** 989-1016.

HULT, A., JOHANSSON, M. & MALMSTRÖM, E. 1999. Hyperbranched Polymers. *Advances in Polymer Science,* 143.

HÖHNE, G., HEMMINGER, W. F. & FLAMMERSHEIM, H.-J. 2003. *Differential Scanning Calorimetry*, Springer.

IHA, R. K., WOOLEY, K. L., NYSTROM, A. M., BURKE, D. J., KADE, M. J. & HAWKER, C. J. 2009. Applications of Orthogonal "Click" Chemistries in the Synthesis of Functional Soft Materials. *Chemical Reviews,* 109**,** 5620-5686.

IKADA, Y. 2002. Biological Materials. *In:* BARBUCCI, R. (ed.) *Integrated Biomaterials Science.* illustrated ed.: Springer.

ISAURE, F., CORMACK, P. A. G. & SHERRINGTON, D. C. 2003a. Facile synthesis of branched poly(methyl methacrylate)s. *J. Mater. Chem.,* 13.

ISAURE, F., CORMACK, P. A. G. & SHERRINGTON, D. C. 2003b. Facile synthesis of branched poly(methyl methacrylate)s. *Journal of Materials Chemistry,* 13**,** 2701-2710.

JACOBINE, A. F., GLASER, D. M., GRABEK, P. J., MANCINI, D., MASTERSON, M., NAKOS, S. T., RAKAS, M. A. & WOODS, J. G. 1992. PHOTOCROSSLINKED NORBORNENE THIOL COPOLYMERS - SYNTHESIS, MECHANICAL-PROPERTIES, AND CURE STUDIES. *Journal of Applied Polymer Science,* 45**,** 471-485.

JALILI, N. & LAXMINARAYANA, K. 2004. A review of atomic force microscopy imaging systems: application to molecular metrology and biological sciences. *Mechatronics,* 14**,** 907.

JANCZUK, B., BIALOPIOTROWICZ, T. & ZDZIENNICKA, A. 1999. Some remarks on the components of the liquid surface free energy. *Journal of Colloid and Interface Science,* 211**,** 96-103.

JANG, J. G. & BAE, Y. C. 1999. Phase behaviors of hyperbranched polymer solutions. *Polymer,* 40**,** 6761-6768.

JASCHKE, M., BUTT, H. J., MANNE, S., GAUB, H. E., HASEMANN, O., KRIMPHOVE, F. & WOLFF, E. K. 1996. The atomic force microscope as a tool to study and manipulate local surface properties. *Biosensors & Bioelectronics,* 11**,** 601-612.

JONES, D. S., WOOLFSON, A. D. & BROWN, A. F. 1997. Textural analysis and flow rheometry of novel, bioadhesive antimicrobial oral gels. *Pharmaceutical Research,* 14**,** 450-457.

JONES, D. S., WOOLFSON, A. D., DJOKIC, J. & COULTER, W. A. 1996. Development and mechanical characterization of bioadhesive semi-solid, polymeric systems containing tetracycline for the treatment of periodontal diseases. *Pharmaceutical Research,* 13**,** 1734-1738.

KADE, M. J., BURKE, D. J. & HAWKER, C. J. 2010. The Power of Thiol-ene Chemistry. *Journal of Polymer Science Part a-Polymer Chemistry,* 48**,** 743-750.

KAYE, G. W. C. & LABY, T. H. 1995. *Tables of Physical and Chemical Constants,* The University of Michigan, Longman.

KIM, S. W., BAE, Y. H. & OKANO, T. 1992. HYDROGELS - SWELLING, DRUG LOADING, AND RELEASE. *Pharmaceutical Research,* 9**,** 283-290.

KOENIG, J., L 1999. *Spectroscopy of Polymers*, Elsevier.

KOHN, J. 2004. New approaches to biomaterials design. *Nature Materials,* 3**,** 745-747.

KOLB, H. C., FINN, M. G. & SHARPLESS, K. B. 2001. Click chemistry: Diverse chemical function from a few good reactions. *Angewandte Chemie-International Edition,* 40**,** 2004-+.

KOLMAN, J., MENG, P. & SCOTT, G. 1998. *Good Clinical Practice: Standard Operating Procedures for Clinical Researchers*, John Wiley & Sons.

KOPECEK, J. 2009. Hydrogels: From Soft Contact Lenses and Implants to Self-Assembled Nanomaterials. *Journal of Polymer Science Part a-Polymer Chemistry,* 47**,** 5929-5946.

KROSCHWITZ, J. I. 1989. *Polymers: biomaterials and medical applications*, Wiley.

LABORATORY, N. P. 2010. *Differential Scanning Calorimetry* [Online]. Hampton Road
Teddington
Middlesex
TW11 0LW: National Physical Laboratory. [Accessed 18 March 2013 2013].

LAI, W. M. & MOW, V. C. 1980. DRAG-INDUCED COMPRESSION OF ARTICULAR-CARTILAGE DURING A PERMEATION EXPERIMENT. *Biorheology,* 17**,** 111-123.

LAMPROU, D. A. 2009. *Towards the determination of surface energy at the nanoscale.* PhD, University of Portsmouth.

LEE, K. Y. & MOONEY, D. J. 2001. Hydrogels for tissue engineering. *Chemical Reviews,* 101.

LEE, T. Y., ROPER, T. M., JONSSON, E. S., GUYMON, C. A. & HOYLE, C. E. 2004. Thiol-ene photopolymerization kinetics of vinyl acrylate/multifunctional thiol mixtures. *Macromolecules,* 37**,** 3606-3613.

LI, H. T. & GU, X. C. 2007. Correlation between drug dissolution and polymer hydration: A study using texture analysis. *International Journal of Pharmaceutics,* 342**,** 18-25.

LONG, J., HYDER, M. N., HUANG, R. Y. M. & CHEN, P. 2005. Thermodynamic modeling of contact angles on rough, heterogeneous surfaces. *Advances in Colloid and Interface Science,* 118**,** 173-190.

LOWE, A. B. 2010. Thiol-ene "click" reactions and recent applications in polymer and materials synthesis. *Polymer Chemistry,* 1**,** 17-36.

LUB, J., BROER, D. J. & ALLAN, J. E. 1999. The synthesis and polymerisation of a liquid crystalline crosslinkable thiol-ene molecule. *Molecular Crystals and Liquid Crystals Science and Technology Section a-Molecular Crystals and Liquid Crystals,* 332**,** 2769-2776.

LUNDBERG, P. 2010. *DESIGNING POLYMERS FOR BIOLOGICAL INTERFACES - FROM ANTIFOULING TO DRUG DELIVERY.* PhD, KTH School of Chemical Science and Engineering.

MADIGAN, M. T., MARTINKO, J. M., CLARK, D. P. & STAHL, D. A. 2010. *Brock Biology of Microorganisms*, Benjamin Cummings.

MAJOROS, I. J., MYC, A., THOMAS, T., MEHTA, C. B. & BAKER, J. R. 2006. PAMAM dendrimer-based multifunctional conjugate for cancer therapy: Synthesis, characterization, and functionality. *Biomacromolecules,* 7**,** 572-579.

MALAFAYA, P. B., SILVA, G. A. & REIS, R. L. 2007. Natural-origin polymers as carriers and scaffolds for biomolecules and cell delivery in tissue engineering applications. *Advanced Drug Delivery Reviews,* 59.

MANSOUR, J. M. 2008. Biomechanics of Cartilage. *In:* OATIS, C. A. (ed.) *Kinesiology: the mechanics and pathomechanics of human movement.* 2 ed. Philadelphia: Lippincott Williams and Wilkins.

MAO, R., TANG, J. & SWANSON, B. G. 2000. Texture properties of high and low acyl mixed gellan gels. *Carbohydrate Polymers,* 41**,** 331-338.

MARTIN, D. P. & WILLIAMS, S. F. 2003. Medical applications of poly-4-hydroxybutyrate: a strong flexible absorbable biomaterial. *Biochemical Engineering Journal,* 16.

MATYJASZEWSKI, K. & DAVIS, T. P. 2003. *Handbook of Radical Polymerization*, John Wiley & Sons.

MERGY, J., FOURNIER, A., HACHET, E. & AUZELY-VELTY, R. 2012. Modification of polysaccharides via thiol-ene chemistry: A versatile route to functional biomaterials. *Journal of Polymer Science Part a-Polymer Chemistry,* 50**,** 4019-4028.

MERRITT, K. & CHANG, C. C. 1991. Factors influencing bacterial adherence to biomaterials. *Journal of biomaterials applications,* 5**,** 185-203.

MERRITT, W. & SETTLE, D. 1981. *Instrumental Methods of Analysis*, Litton Educational Publication.

MEYER, E., HUG, H. J. & BENNEWITZ, R. 2004. *Scanning Probe Microscopy: The Lab on a Tip,* Berlin, Springer-Verlag.

MIESZAWSKA, A. J. & KAPLAN, D. L. 2010. Smart biomaterials - regulating cell behavior through signaling molecules. *Bmc Biology,* 8.

MITIK-DINEVA, N., WANG, J., MOCANASU, R. C., STODDART, P. R., CRAWFORD, R. J. & IVANOVA, E. P. 2008. Impact of nano-topography on bacterial attachment. *Biotechnology Journal,* 3**,** 536-544.

MIYAGI, A., TSUNAKA, Y., UCHIHASHI, T., MAYANAGI, K., HIROSE, S., MORIKAWA, K. & ANDO, T. 2008. Visualization of intrinsically disordered regions of proteins by high-speed atomic force microscopy. *Chemphyschem,* 9**,** 1859-1866.

MORRIS, V. J., KIRBY, A. R. & GUNNING, A. P. 1999. Using atomic force microscopy to probe food biopolymer functionality. *Scanning,* 21**,** 287-292.

MOW, V. C., KUEI, S. C., LAI, W. M. & ARMSTRONG, C. G. 1980. BIPHASIC CREEP AND STRESS-RELAXATION OF ARTICULAR-CARTILAGE IN COMPRESSION - THEORY AND EXPERIMENTS. *Journal of Biomechanical Engineering-Transactions of the Asme,* 102**,** 73-84.

NAIR, L. S. & LAURENCIN, C. T. 2006. Polymers as biomaterials for tissue engineering and controlled drug delivery. *In:* LEE, K. & KAPLAN, D. (eds.) *Tissue Engineering I: Scaffold Systems for Tissue Engineering.* Berlin: Springer-Verlag Berlin.

NAIR, L. S. & LAURENCIN, C. T. 2007. Biodegradable polymers as biomaterials. *Progress in Polymer Science,* 32**,** 762-798.

NALLY, J. D. 2006. *Good Manufacturing Practices for Pharmaceuticals, Sixth Edition*, CRC Press.

NANJWADE, B. K., BECHRA, H. M., DERKAR, G. K., MANVI, F. V. & NANJWADE, V. K. 2009. Dendrimers: Emerging polymers for drug-delivery systems. *European Journal of Pharmaceutical Sciences,* 38.

NEUMANN, A. W. & GOOD, R. J. 1979. Techniques of measuring contact angles. *Surface and Colloid Science,* 11**,** 31-91.

ODIAN, G. G. 2004. *Principles of polymerization*, John Wiley and Sons.

OSTROVIDOVA, G. U., MAKEEV, A. V. & SHAMTSIAN, M. M. 2003. Polyfunctional film coatings for medical use. *Materials Science & Engineering C-Biomimetic and Supramolecular Systems,* 23**,** 545-550.

PADERA, R. F. 2006. Infection in ventricular assist devices: the role of biofilm. *Cardiovascular Pathology,* 15.

PAINTER, P. C. & COLEMAN, M. M. 2008. *Essentials of Polymer Science and Engineering*, DEStech Publications, Inc.

PAPADIMITRIOU, E., BUCKTON, G. & EFENTAKIS, M. 1993. PROBING THE MECHANISMS OF SWELLING OF HYDROXYPROPYLMETHYLCELLULOSE MATRICES. *International Journal of Pharmaceutics,* 98**,** 57-62.

PEPPAS, N. A. 1986. Hydrogels in medicine and pharmacy. Boca Raton, Florida: CRC Press.

PEPPAS, N. A., HUANG, Y., TORRES-LUGO, M., WARD, J. H. & ZHANG, J. 2000. Physicochemical, foundations and structural design of hydrogels in medicine and biology. *Annual Review of Biomedical Engineering,* 2.

PEPPAS, N. A., MOYNIHAN, H. J. & LUCHT, L. M. 1985. THE STRUCTURE OF HIGHLY CROSSLINKED POLY(2-HYDROXYETHYL METHACRYLATE) HYDROGELS. *Journal of Biomedical Materials Research,* 19**,** 397-411.

PITTS, B., HAMILTON, M. A., ZELVER, N. & STEWART, P. S. 2003. A microtiter-plate screening method for biofilm disinfection and removal. *Journal of Microbiological Methods,* 54**,** 269-276.

POLERECKY, L., BISSETT, A., AL-NAJJAR, M., FAERBER, P., OSMERS, H., SUCI, P. A., STOODLEY, P. & DE BEER, D. 2009. Modular Spectral Imaging System for Discrimination of Pigments in Cells and Microbial Communities. *Applied and Environmental Microbiology,* 75**,** 758-771.

PORTER, B. D., OLDHAM, J. B., HE, S. L., ZOBITZ, M. E., PAYNE, R. G., AN, K. N., CURRIER, B. L., MIKOS, A. G. & YASZEMSKI, M. J. 2000. Mechanical properties of a biodegradable bone regeneration scaffold. *Journal of Biomechanical Engineering-Transactions of the Asme,* 122**,** 286-288.

POSNER, T. 1905. Unsaturated Compounds. II. Mercaptan Addition to Unsaturated Hydrocarbons. *Berichte der Deutschen Chemischen Gesellschaft,* 38**,** 646-657.

PRENDERGAST, F. G. & MANN, K. G. 1978. CHEMICAL AND PHYSICAL-PROPERTIES OF AEQUORIN AND GREEN FLUORESCENT PROTEIN ISOLATED FROM AEQUOREA-FORSKALEA. *Biochemistry,* 17**,** 3448-3453.

RAJABISIAHBOOMI, A. R., BOWTELL, R. W., MANSFIELD, P., HENDERSON, A., DAVIES, M. C. & MELIA, C. D. 1994. STRUCTURE AND BEHAVIOR IN HYDROPHILIC MATRIX SUSTAINED-RELEASE DOSAGE FORMS .2. NMR-IMAGING STUDIES OF DIMENSIONAL CHANGES IN THE GEL LAYER AND CORE OF HPMC TABLETS UNDERGOING HYDRATION. *Journal of Controlled Release,* 31**,** 121-128.

RASAL, R. M., JANORKAR, A. V. & HIRT, D. E. 2010. Poly(lactic acid) modifications. *Progress in Polymer Science,* 35**,** 338-356.

RAVN, C. 2009. *Near-infrared Chemical Imaging in Formulation*

Development of Solid Dosage Forms. PhD, University of Copenhagen.

RAZZAK, M. T., DARWIS, D., ZAINUDDIN & SUKIRNO 2001. Irradiation of polyvinyl alcohol and polyvinyl pyrrolidone blended hydrogel for wound dressing. *Radiation Physics and Chemistry,* 62**,** 107-113.

REPKA, M. A., GUTTA, K., PRODDUTURI, S., MUNJAL, M. & STODGHILL, S. P. 2005. Characterization of cellulosic hot-melt extruded films containing lidocaine. *European Journal of Pharmaceutics and Biopharmaceutics,* 59**,** 189-196.

RICCI, D. & BRAGA, P. C. 2004. Recognizing and avoiding artifacts in AFM imaging. *Methods in molecular biology (Clifton, N.J.),* 242**,** 25-37.

RICHES, P. E. 2012. Sensitivity analysis of permeability parameters of bovine nucleus pulposus obtained through inverse fitting of the nonlinear biphasic equation: effect of sampling strategy. *Computer Methods in Biomechanics and Biomedical Engineering,* 15**,** 29-36.

RIEGEL, E. R. & KENT, J. A. 2003. *Riegel's Handbook of Industrial Chemistry*, Springer.

RINCON LASPRILLA, A. J., RUEDA MARTINEZ, G. A., LUNELLI, B. H., JAIMES FIGUEROA, J. E., JARDINI, A. L. & MACIEL FILHO, R. 2011. Synthesis and Characterization of Poly (Lactic Acid) for Use in Biomedical Field. *Icheap-10: 10th International Conference on Chemical and Process Engineering, Pts 1-3,* 24**,** 985-990.

ROBINSON, J. A., PULS, C. P., STALEY, N. E., STITT, J. P., FANTON, M. A., EMTSEV, K. V., SEYLLER, T. & LIU, Y. 2009. Raman Topography and Strain Uniformity of Large-Area Epitaxial Graphene. *Nano Letters,* 9**,** 964-968.

ROGERO, S. O., MALMONGE, S. M., LUGAO, A. B., IKEDA, T. I., MIYAMARU, L. & CRUZ, A. S. 2003. Biocompatibility study of polymeric biomaterials. *Artificial Organs,* 27.

ROOVERS, J. 1999. *Advances in Polymer Science, Branched Polymers II*, Springer.

ROPER, T. M., KWEE, T., LEE, T. Y., GUYMON, C. A. & HOYLE, C. E. 2004. Photopolymerization of pigmented thiol-ene systems. *Polymer,* 45**,** 2921-2929.

ROSENTHAL, A. J. 2010. TEXTURE PROFILE ANALYSIS - HOW IMPORTANT ARE THE PARAMETERS? *Journal of Texture Studies,* 41**,** 672-684.

RYAN, K. J., RAY, C. G., AHMAD, N., DREW, W. L. & PLORDE, J. J. 2010. *Sherris Medical Microbiology*, McGraw-Hill Prof Med/Tech.

RYDHOLM, A. E., ANSETH, K. S. & BOWMAN, C. N. 2007. Effects of neighboring sulfides and pH on ester hydrolysis in thiol-acrylate photopolymers. *Acta Biomaterialia,* 3**,** 449-455.

RYDHOLM, A. E., BOWMAN, C. N. & ANSETH, K. S. 2005. Degradable thiol-acrylate photopolymers: polymerization and degradation behavior of an in situ forming biomaterial. *Biomaterials,* 26**,** 4495-4506.

SALINAS, C. N. & ANSETH, K. S. 2008. The enhancement of chondrogenic differentiation of human mesenchymal stem cells by enzymatically regulated RGD functionalities. *Biomaterials,* 29**,** 2370-2377.

SALINAS, C. N., COLE, B. B., KASKO, A. M. & ANSETH, K. S. 2007. Chondrogenic differentiation potential of human mesenchymal stem cells photoencapsulated within poly(ethylene glycol)-arginine-glycine-aspartic acid-serine thiol-methacrylate mixed-mode networks. *Tissue Engineering,* 13**,** 1025-1034.

SAMBROOK, J. & RUSSELL, D. W. 2001. *Molecular Cloning: A Laboratory Manual*, CSHL Press.

SEAL, B. L., OTERO, T. C. & PANITCH, A. 2001. Polymeric biomaterials for tissue and organ regeneration. *Materials Science & Engineering R-Reports,* 34.

SEILER, J. P. 2012. *Good Laboratory Practice: The Why and the How*, Springer.

SENCADAS, V., GREGORIO FILHO, R. & LANCEROS-MENDEZ, S. 2006. Processing and characterization of a novel nonporous poly(vinilidene fluoride) films in the beta phase. *Journal of Non-Crystalline Solids,* 352.

SEVEGNEY, M. S., KANNAN, R. M., SIEDLE, A. R., NAIK, R. & NAIK, V. M. 2006. Vibrational spectroscopic investigation of stereoregularity effects on syndiotactic polypropylene structure and morphology. *Vibrational Spectroscopy,* 40**,** 246-256.

SHI, D. 2004. *Biomaterials and Tissue Engineering*, Springer.

SHIN, J., NAZARENKO, S. & HOYLE, C. E. 2008. Enthalpy relaxation of photopolymerized thiol-ene networks: Structural effects. *Macromolecules,* 41**,** 6741-6746.

SHOICHET, M. S. 2010. Polymer Scaffolds for Biomaterials Applications. *Macromolecules,* 43**,** 581-591.
SKLODOWSKA, A., WOZNIAK, M. & MATLAKOWSKA, R. 1999. The method of contact angle measurements and estimation of work of adhesion in bioleaching of metals. *Biological Procedures Online,* 1.
SLAUGHTER, B. V., KHURSHID, S. S., FISHER, O. Z., KHADEMHOSSEINI, A. & PEPPAS, N. A. 2009. Hydrogels in Regenerative Medicine. *Advanced Materials,* 21.
SMITH, A. 1999. Atomic force microscopy. *MICROBIOLOGY TODAY,* 26**,** 54-55.
SOCRATES, G. 2004. *Infrared and Raman Characteristic Group Frequencies: Tables and Charts*, John Wiley & Sons.
SPERLING, L. H. 2005. *Introduction to Physical Polymer Science*, John Wiley & Sons.
STEWART, P. S. 1998. A review of experimental measurements of effective diffusive permeabilities and effective diffusion coefficients in biofilms. *Biotechnology and Bioengineering,* 59**,** 261-272.
STEWART, P. S. & COSTERTON, J. W. 2001. Antibiotic resistance of bacteria in biofilms. *Lancet,* 358**,** 135-138.
SUCI, P. A., MITTELMAN, M. W., YU, F. P. & GEESEY, G. G. 1994. INVESTIGATION OF CIPROFLOXACIN PENETRATION INTO PSEUDOMONAS-AERUGINOSA BIOFILMS. *Antimicrobial Agents and Chemotherapy,* 38**,** 2125-2133.
SUNDARARAJAN, S. & BHUSHAN, B. 2002. Development of AFM-based techniques to measure mechanical properties of nanoscale structures. *Sensors and Actuators a-Physical,* 101**,** 338-351.
SZCZESNI.AS 1966. TEXTURE MEASUREMENTS. *Food Technology,* 20**,** 1292-&.
SZCZESNIAK, A. S. 1963. CLASSIFICATION OF TEXTURAL CHARACTERISTICS. *Journal of Food Science,* 28**,** 385-&.
TAYLOR, M., URQUHART, A. J., ANDERSON, D. G., WILLIAMS, P. M., LANGER, R., ALEXANDER, M. R. & DAVIES, M. C. 2008. A Methodology for Investigating Protein Adhesion and Adsorption to Microarrayed Combinatorial Polymers. *Macromol. Rapid Commun.,* 29.
TECHNOLOGIES, R. D. 2013. *Radleys Discovery Technologies* [Online]. Available: http://www.radleys.com/index.shtml [Accessed 15 May 2013 2013].
TECHNOLOGIES, T. 1998-2011. *Probes and Fixtures* [Online]. 18 Fairview Road
Scarsdale [Accessed 15 May 2013 2013].
NY 10583: Texture Technologies Corp and Stable Micro Systems. [Accessed 18 March 2013 2013].
TSIEN, R. Y. 1998. The green fluorescent protein. *Annual Review of Biochemistry,* 67**,** 509-544.
VAN TOMME, S. R., STORM, G. & HENNINK, W. E. 2008. In situ gelling hydrogels for pharmaceutical and biomedical applications. *International Journal of Pharmaceutics,* 355**,** 1-18.
VINOGRADOV, S. V., BRONICH, T. K. & KABANOV, A. V. 2002. Nanosized cationic hydrogels for drug delivery: preparation, properties and interactions with cells. *Advanced Drug Delivery Reviews,* 54**,** 135-147.
WILLIAMS, D. F. 1999. *The Williams Dictionary of Biomaterials,* Liverpool, Liverpool University Press.
WILLIAMS, I., VENABLES, W. A., LLOYD, D., PAUL, F. & CRITCHLEY, I. 1997. The effects of adherence to silicone surfaces on antibiotic susceptibility in Staphylococcus aureus. *Microbiology-Uk,* 143**,** 2407-2413.
WOODWARD, R. P. Contact Angle Measurements Using the Drop Shape Method.
YIMSIRI, P. & MACKLEY, M. R. 2006. Spin and dip coating of light-emitting polymer solutions: Matching experiment with modelling. *Chemical Engineering Science,* 61**,** 3496-3505.
YOUNG, R. J. & LOVELL, P. A. 1991. *Introduction to Polymers*, CRC Press.
ZISMAN, W. A. 1964a. *Advances in Chemistry*.
ZISMAN, W. A. 1964b. Relation of the Equilibrium Contact Angle to Liquid and Solid Constitution. *In:* GOULD, R. F. (ed.) *Contact Angle, Wettability and Adhesion.* Washington, DC: American Chemical Society.

APPENDIX 1

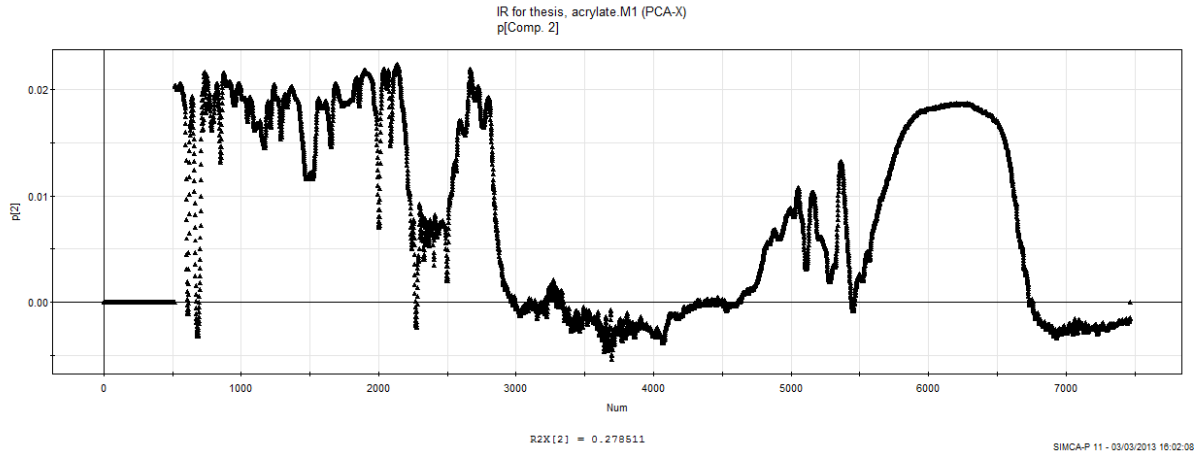

Figure appendix 1- 1 Loadings plot for principal component 2, IR analysis.

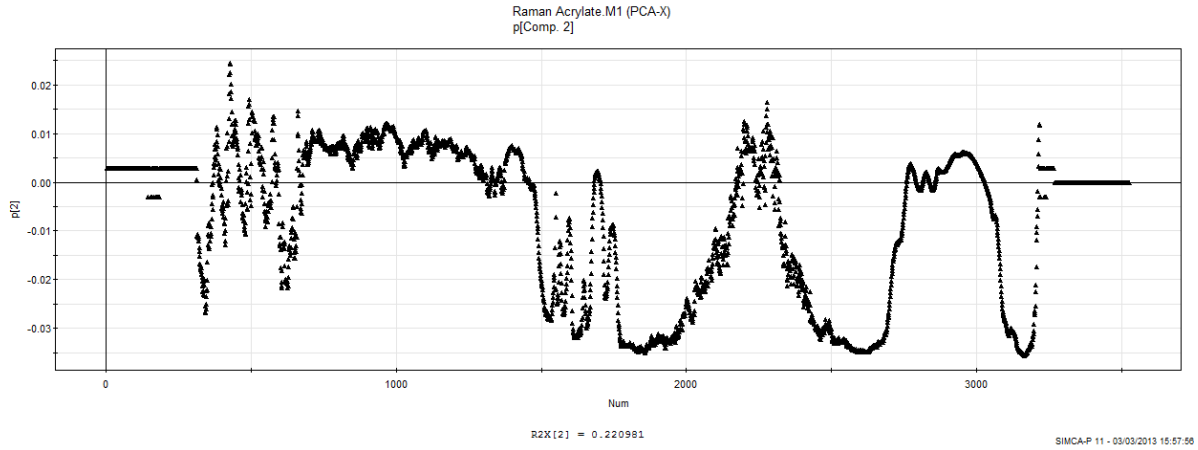

Figure appendix 1- 2 Loadings plot for principal component 2, Raman analysis.

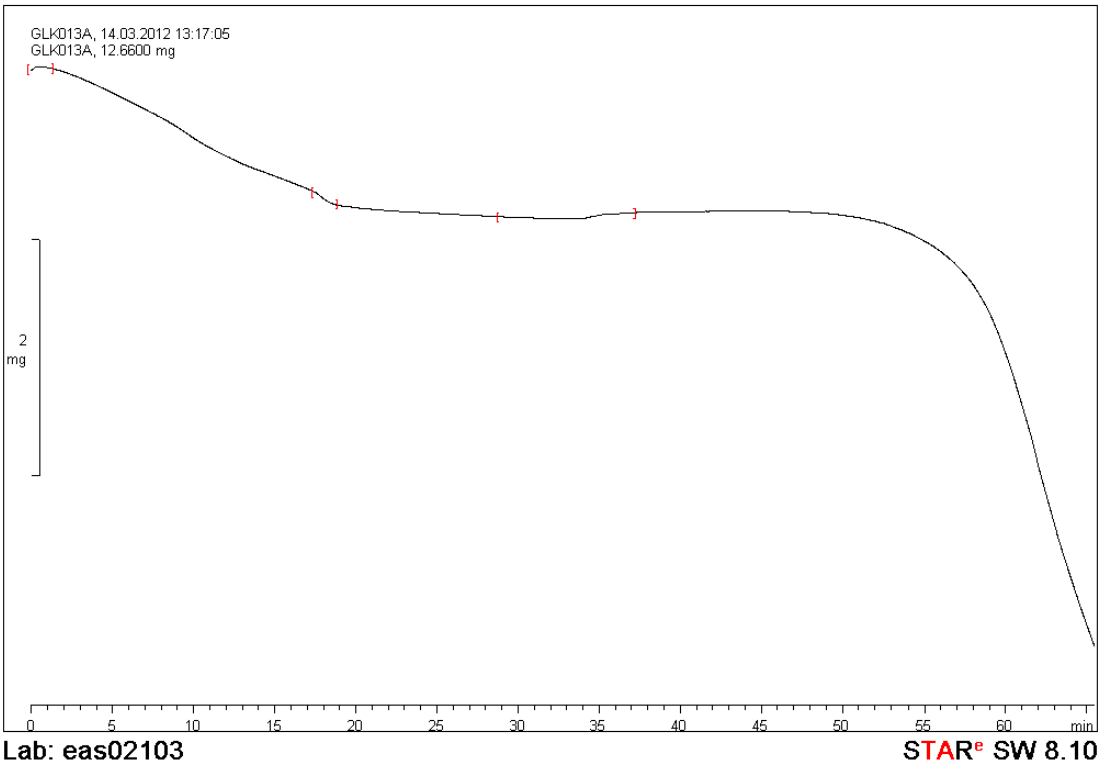

Figure appendix 1- 3 TGA trace polymer 1+x20%

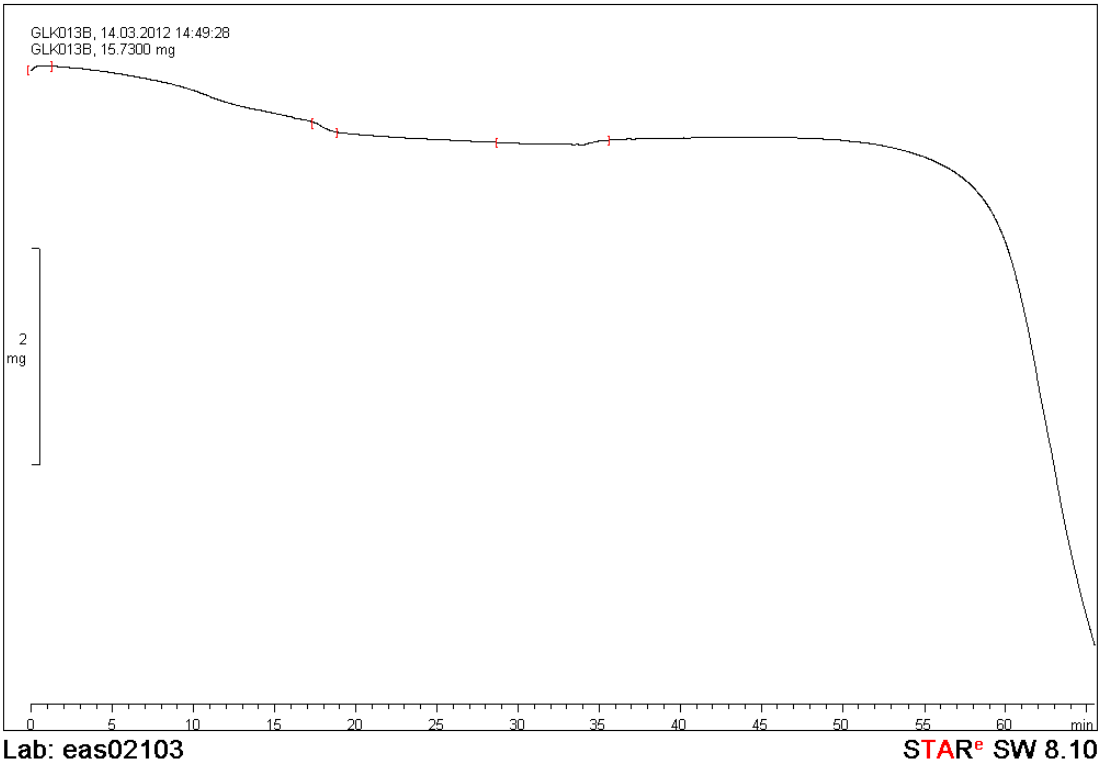

Figure appendix 1- 4 TGA trace polymer 1+x30%

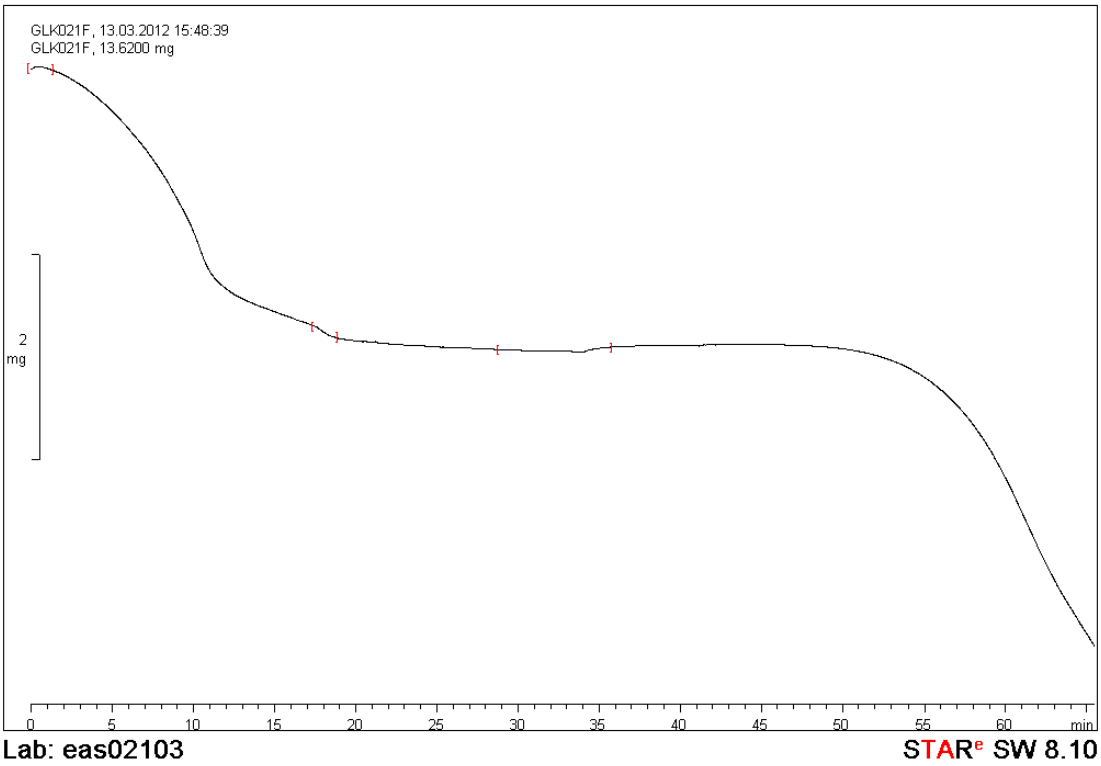

Figure appendix 1- 5v TGA trace polymer 1+x50%

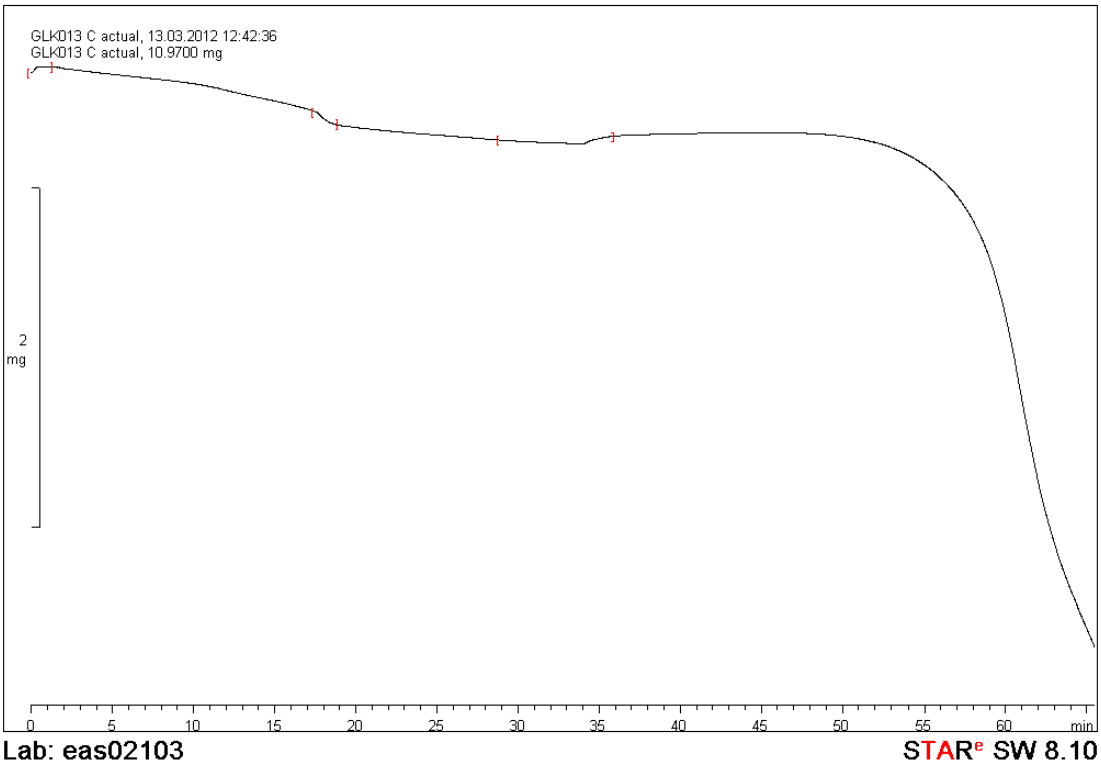

Figure appendix 1- 6 TGA trace polymer 1+y20%

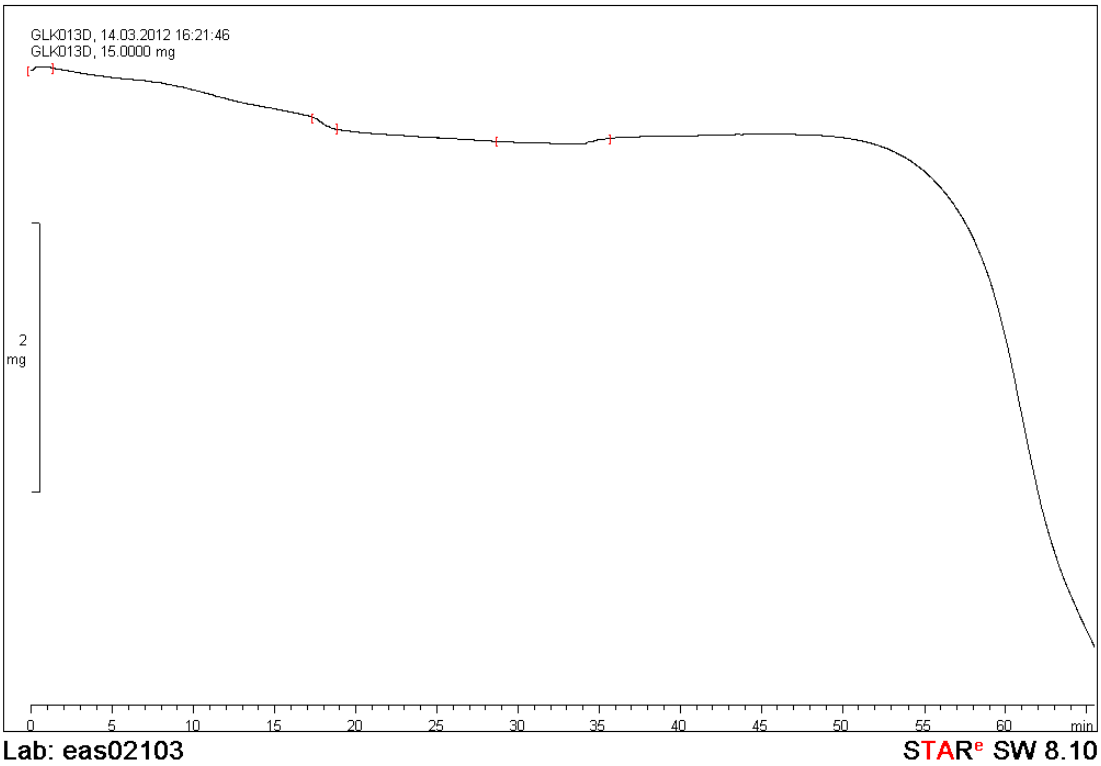

Figure appendix 1- 7 TGA trace polymer 1+y30%

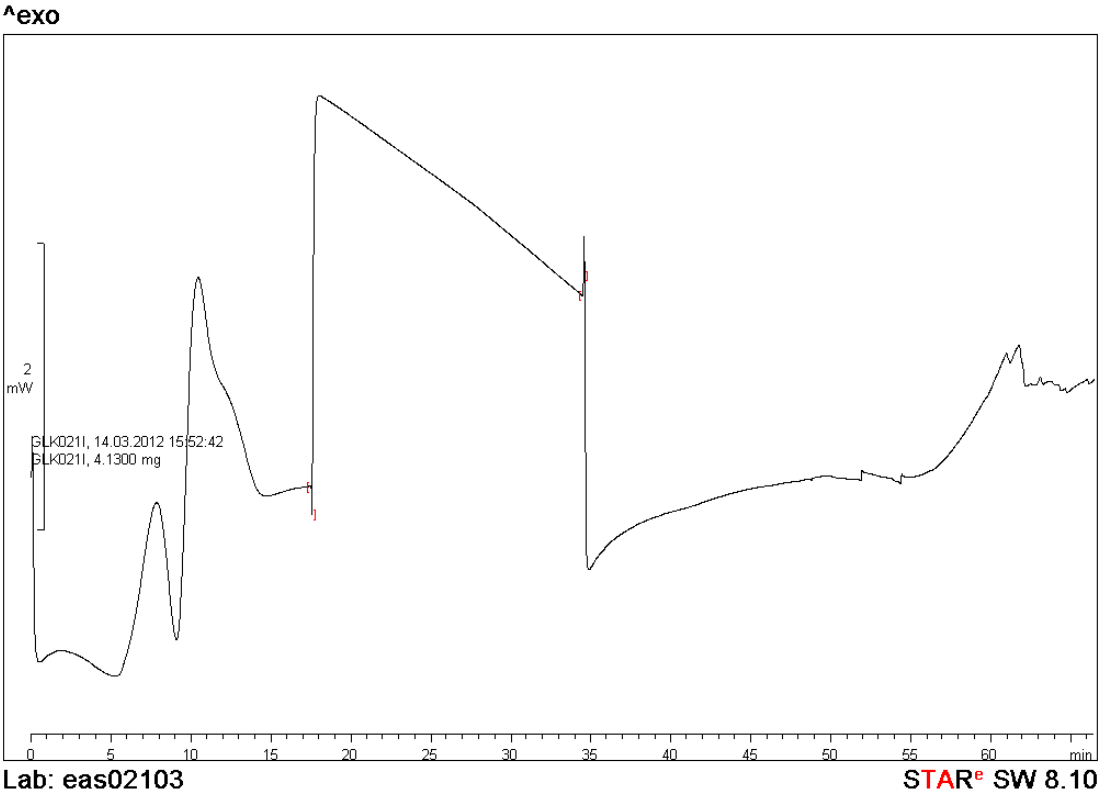

Figure appendix 1- 8 DSC trace polymer 1+y50%

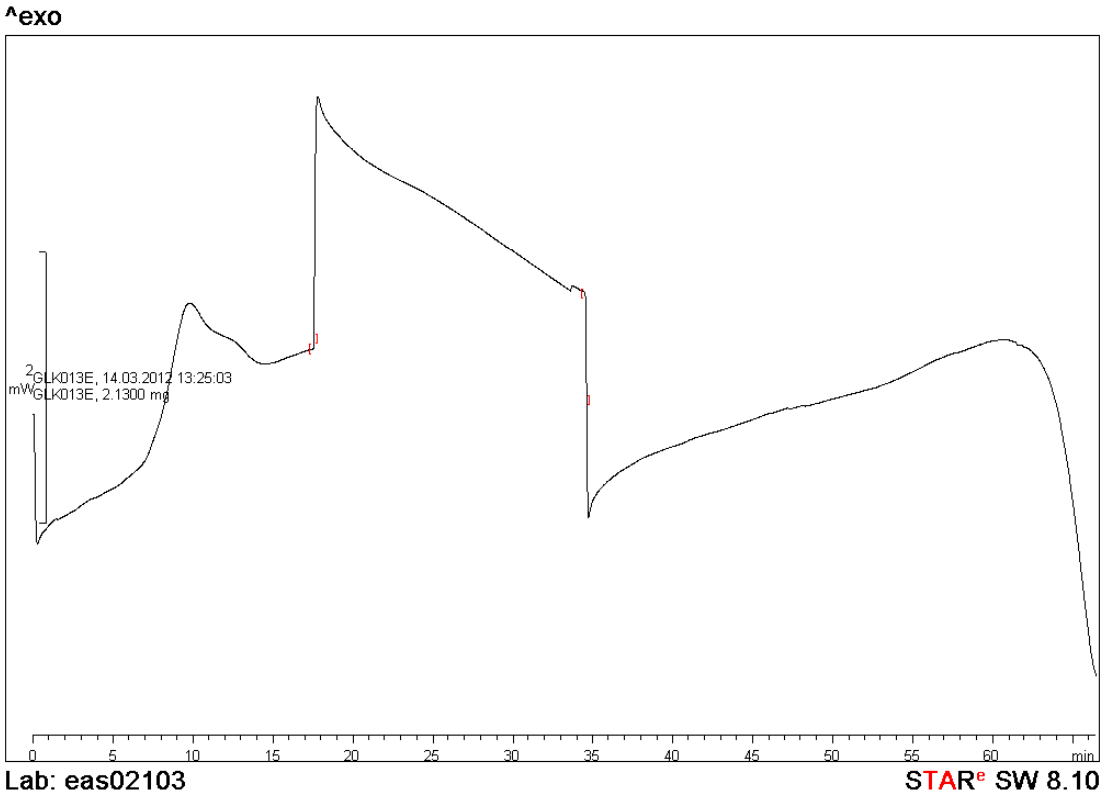

Figure appendix 1- 9 DSC trace polymer 2+x20%

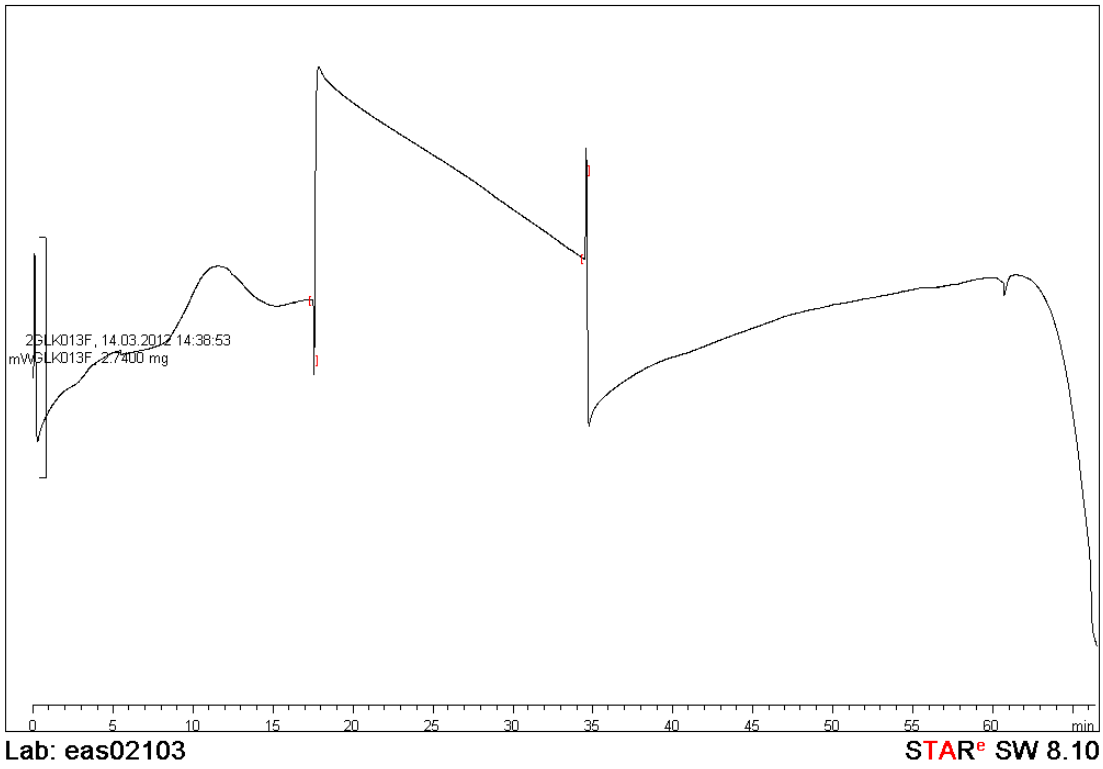

Figure appendix 1- 10 DSC trace polymer 2+x30%

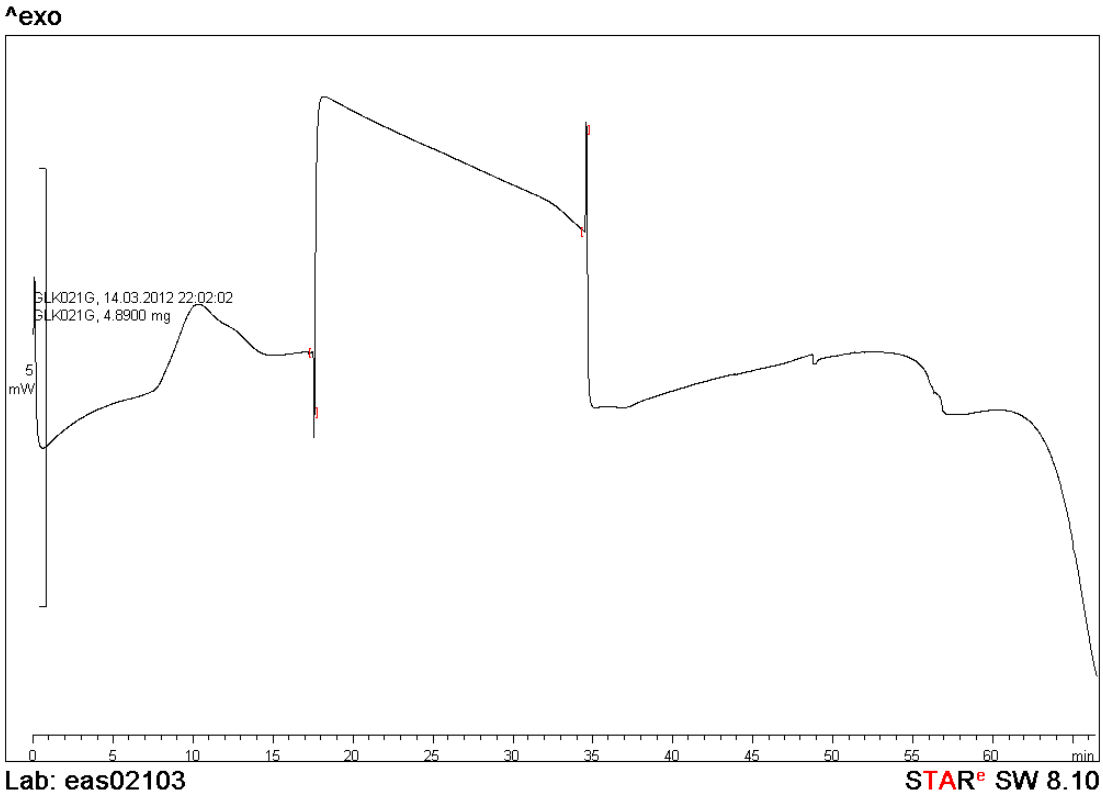

Figure appendix 1- 11 DSC trace polymer 2+x50%

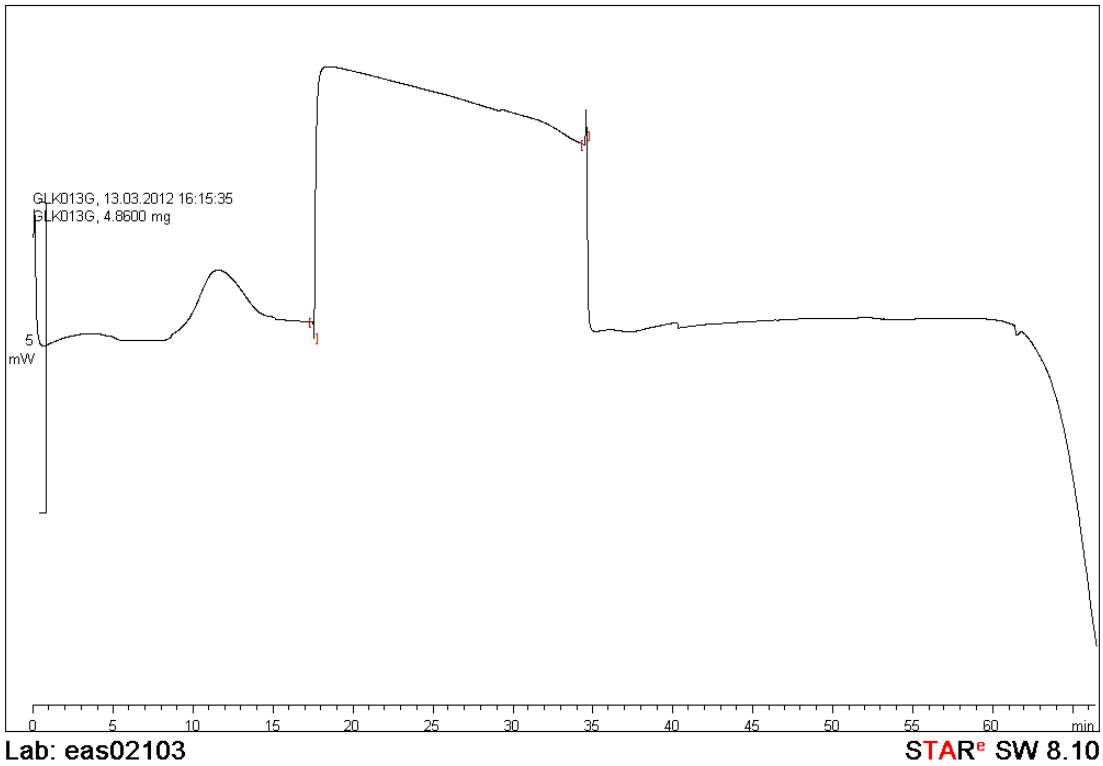

Figure appendix 1- 12 DSC trace polymer 2+y20%

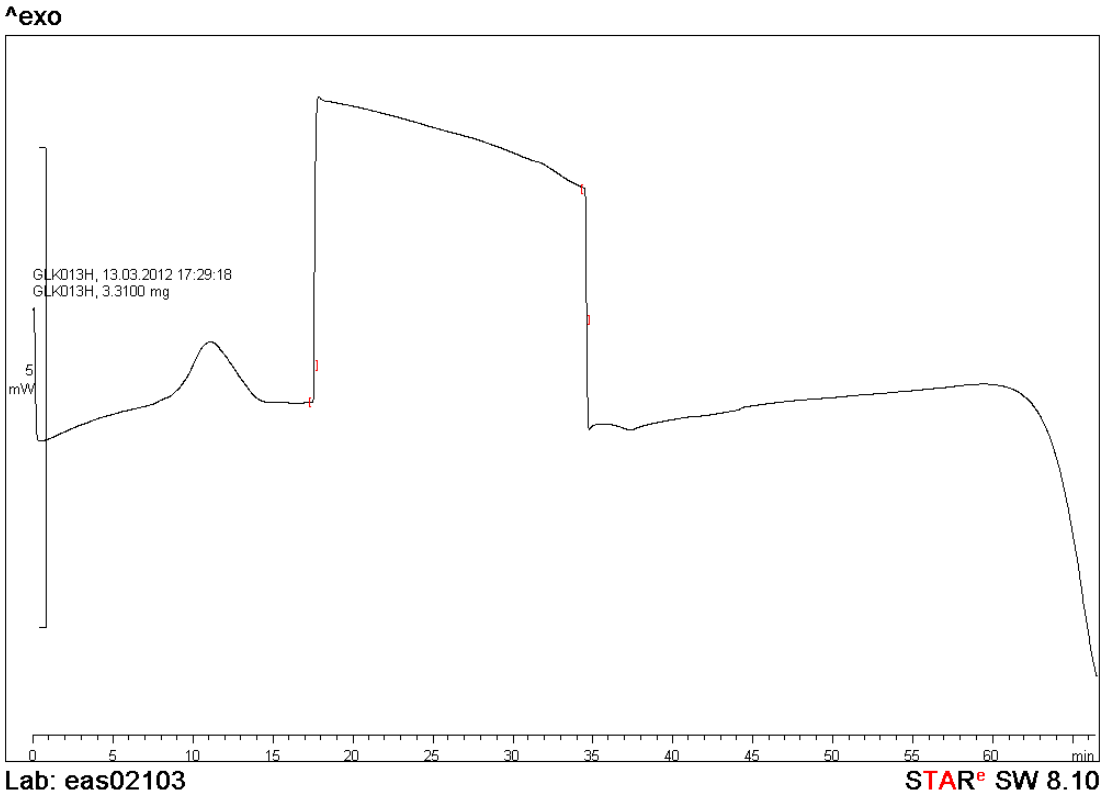

Figure appendix 1- 13 DSC trace polymer 2+y30%

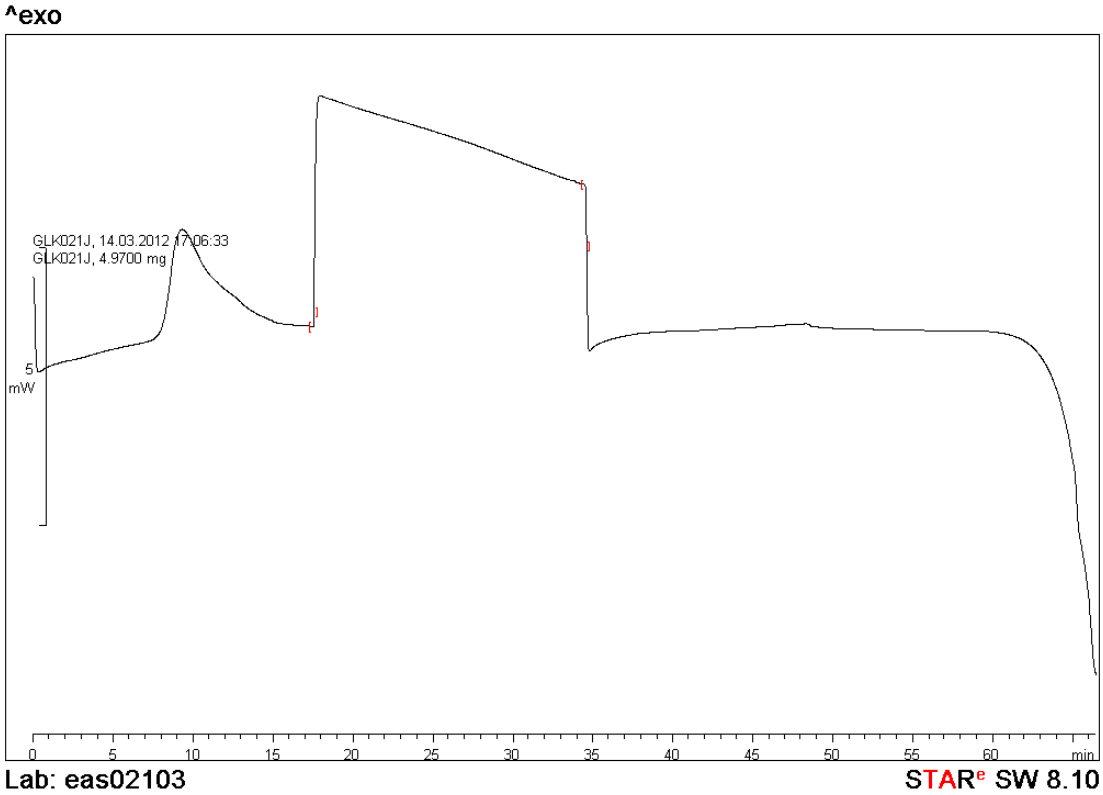

Figure appendix 1- 14 DSC trace polymer 2+y50%

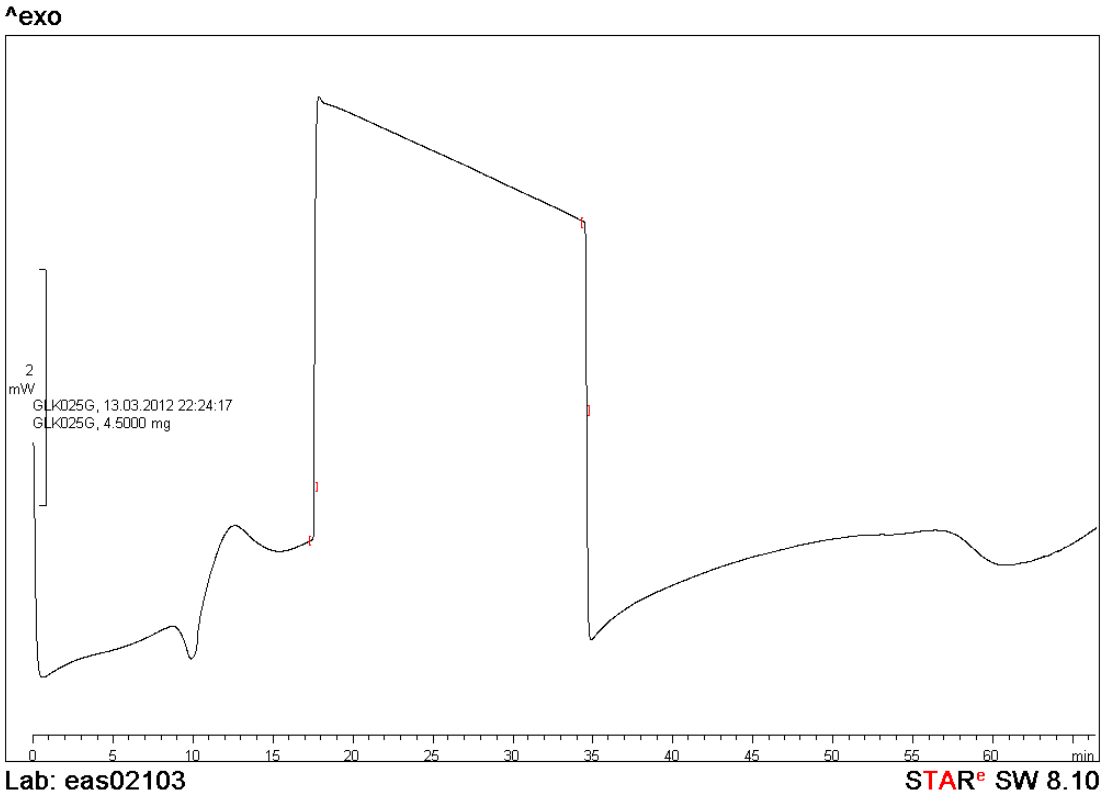

Figure appendix 1- 15 DSC trace polymer linear3

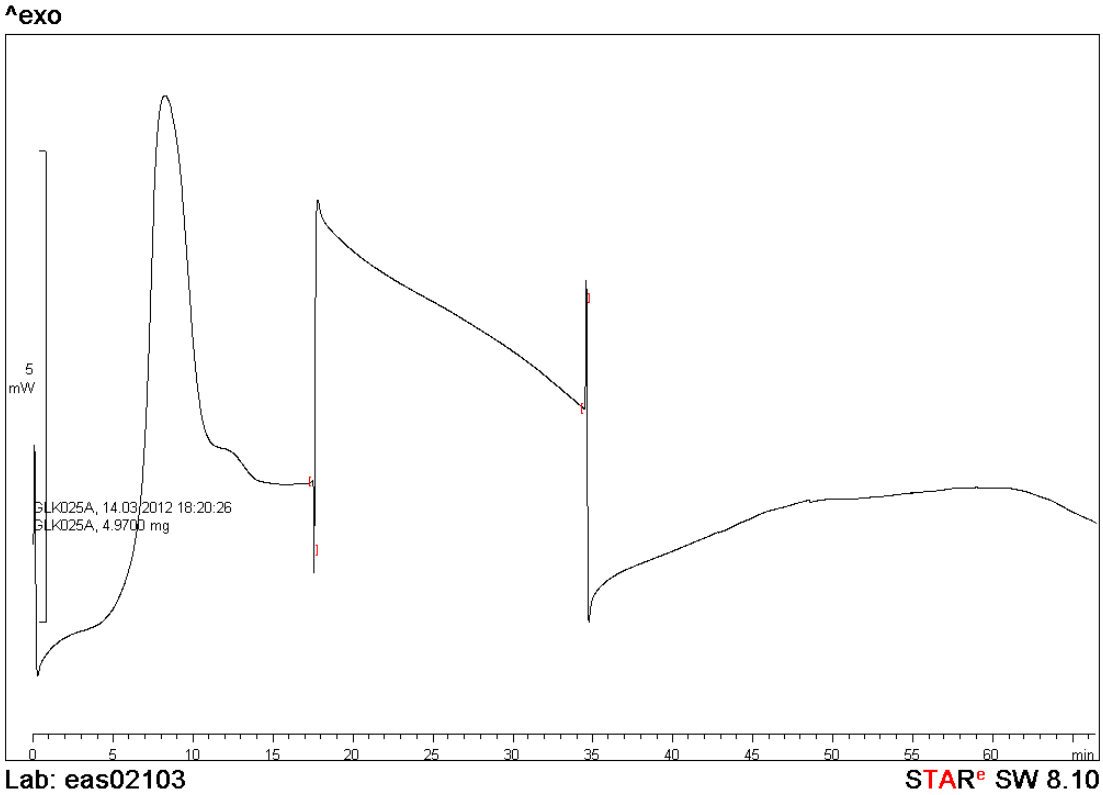

Figure appendix 1- 16 DSC trace polymer 3+x20%

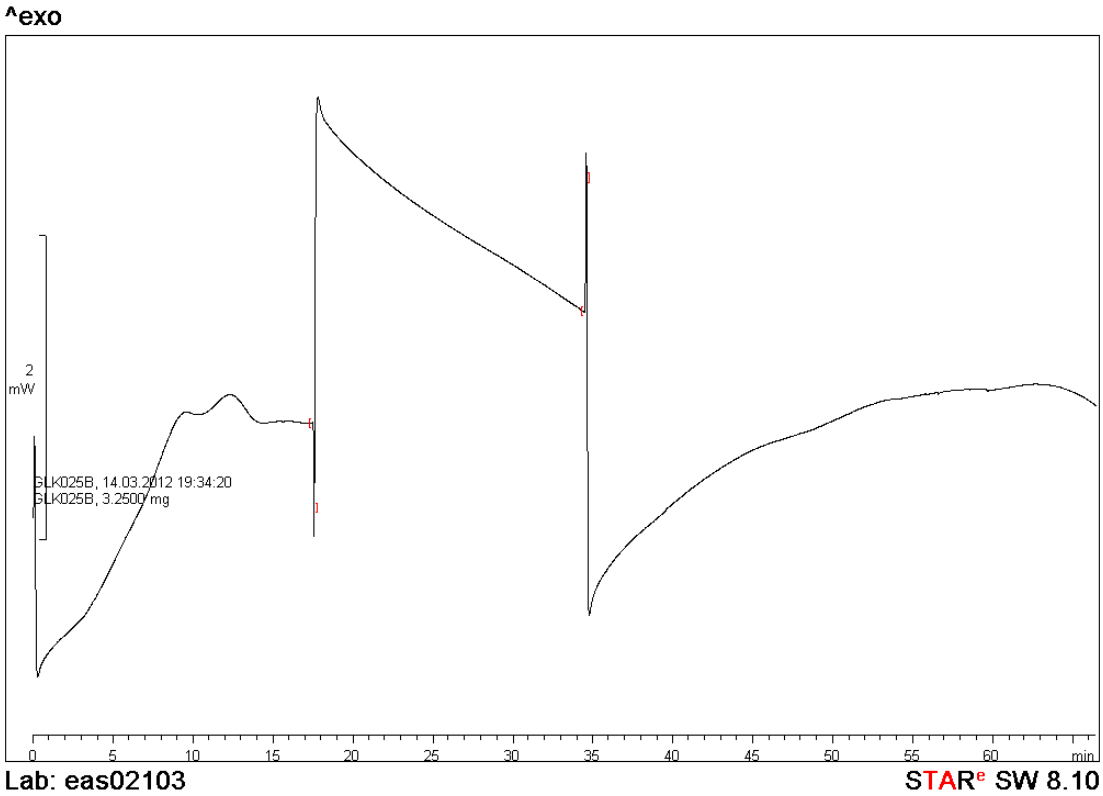

Figure appendix 1- 17 DSC trace polymer 3+x30%

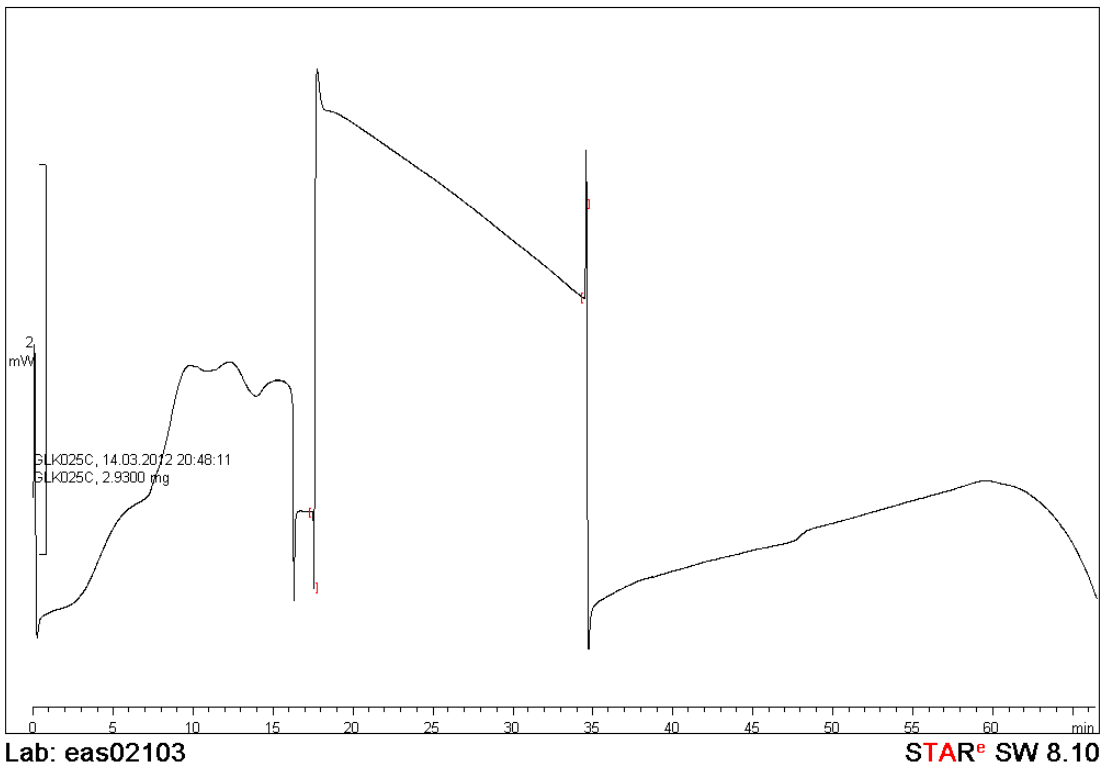

Figure appendix 1- 18 DSC trace polymer 3+x50%

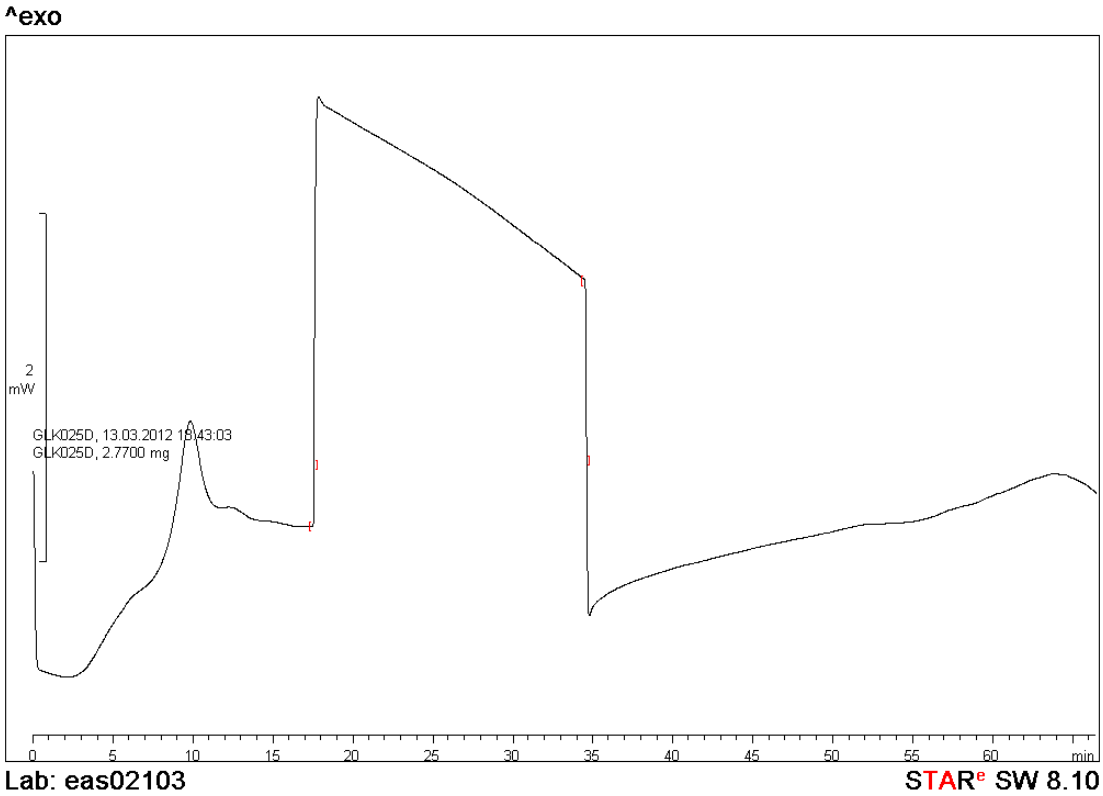

Figure appendix 1- 19 DSC trace polymer 3+y20%

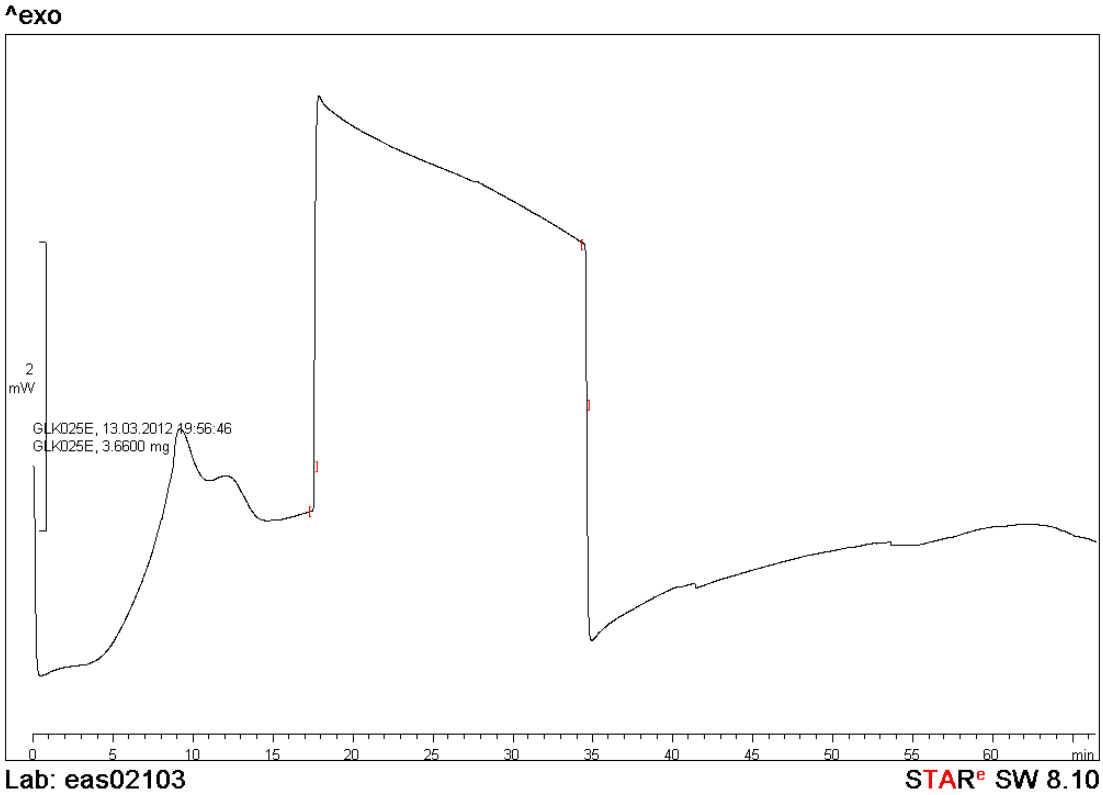

Figure appendix 1- 20 DSC trace polymer 3+y30%

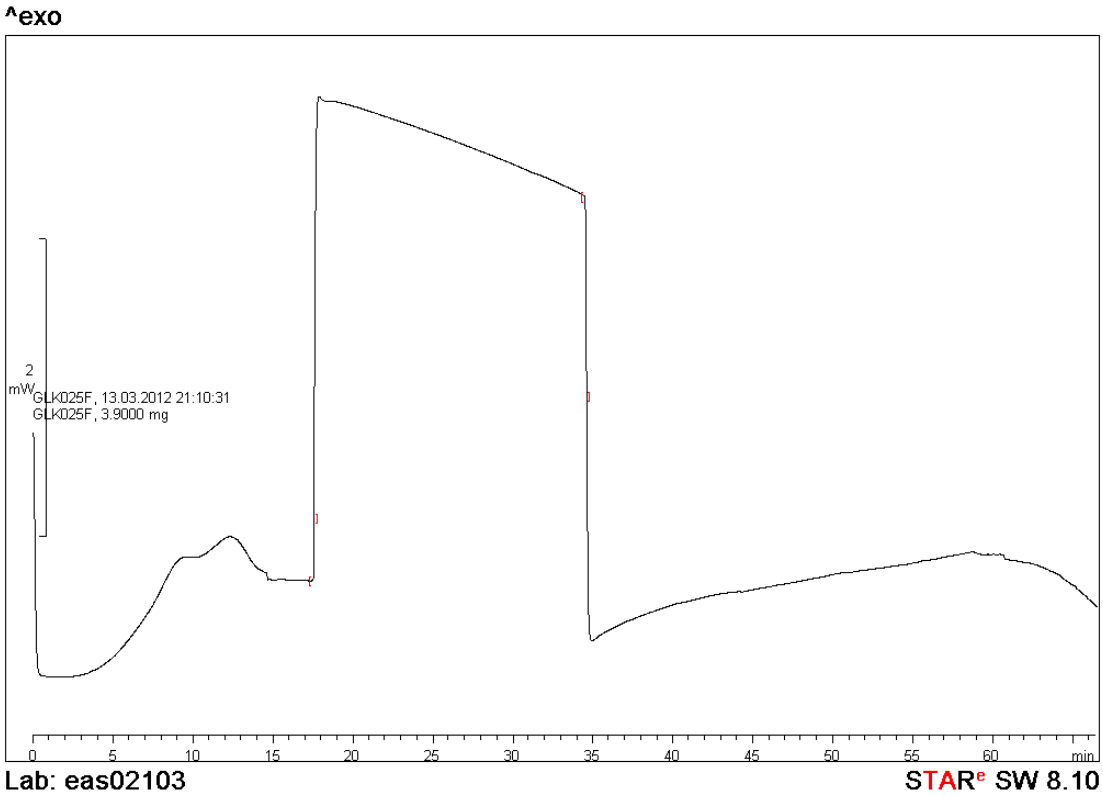

Figure appendix 1- 21 DSC trace polymer 3+y50%

APPENDIX 3

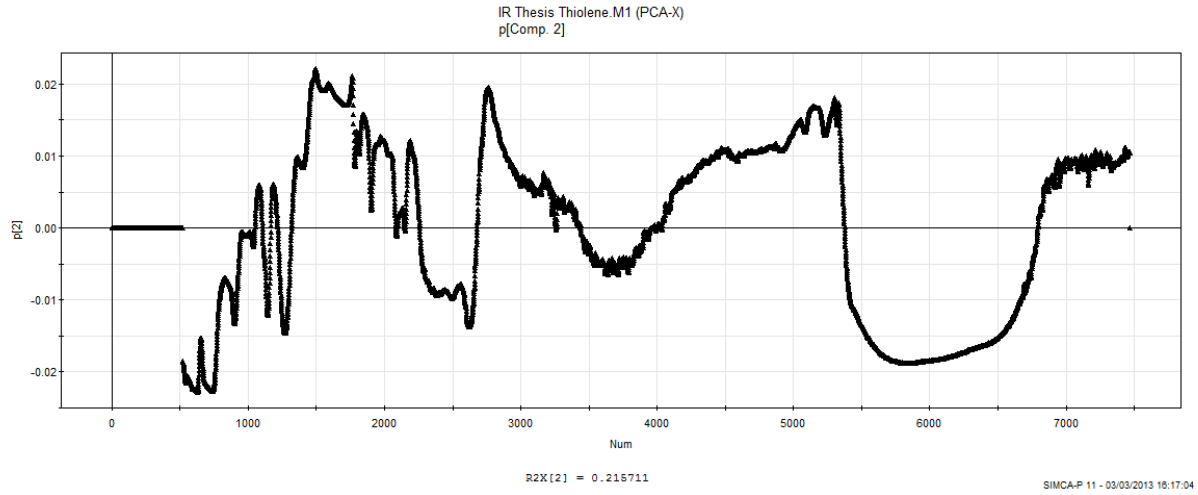

Figure appendix 2- 1 Loadings plot for principal component 2, IR analysis thiol-ene.

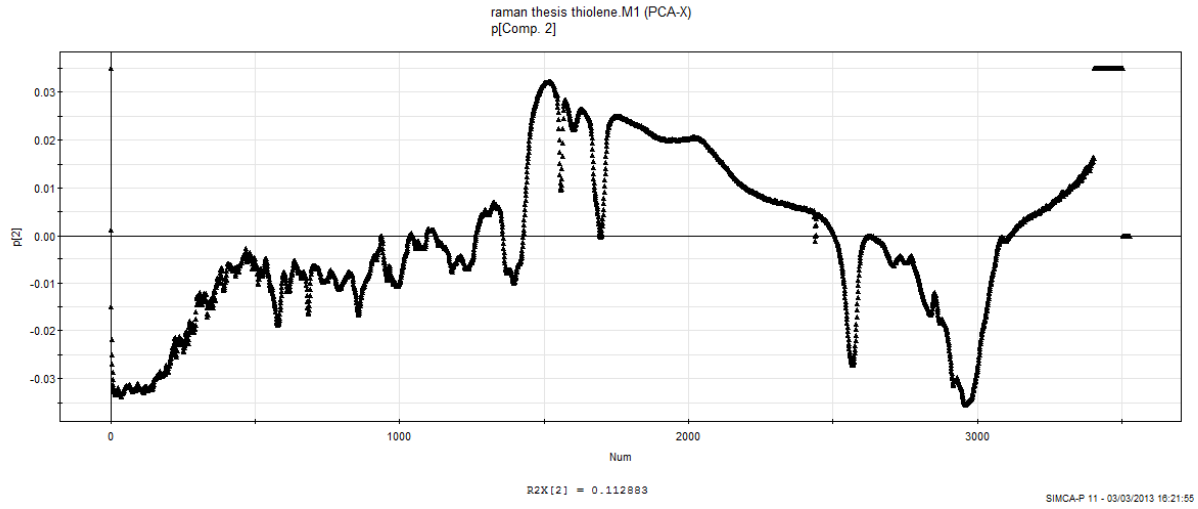

Figure appendix 2- 2 Loadings plot for principal component 2, raman analysis thiol-ene.

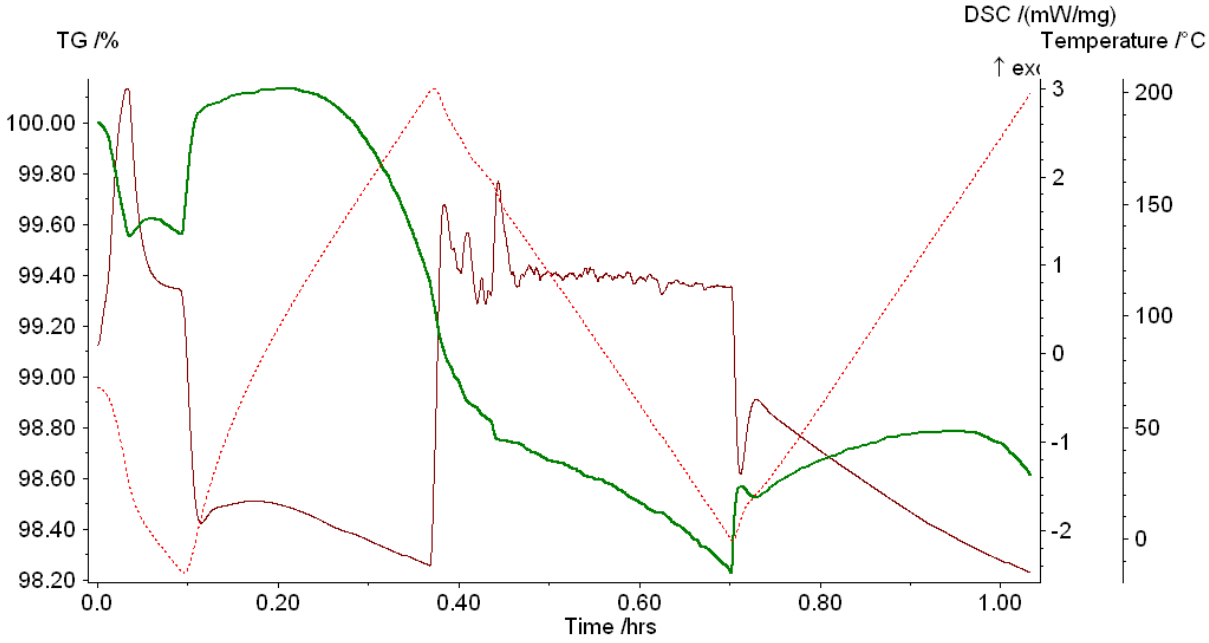

Figure appendix 2- 3 DSC trace polymer 1BC

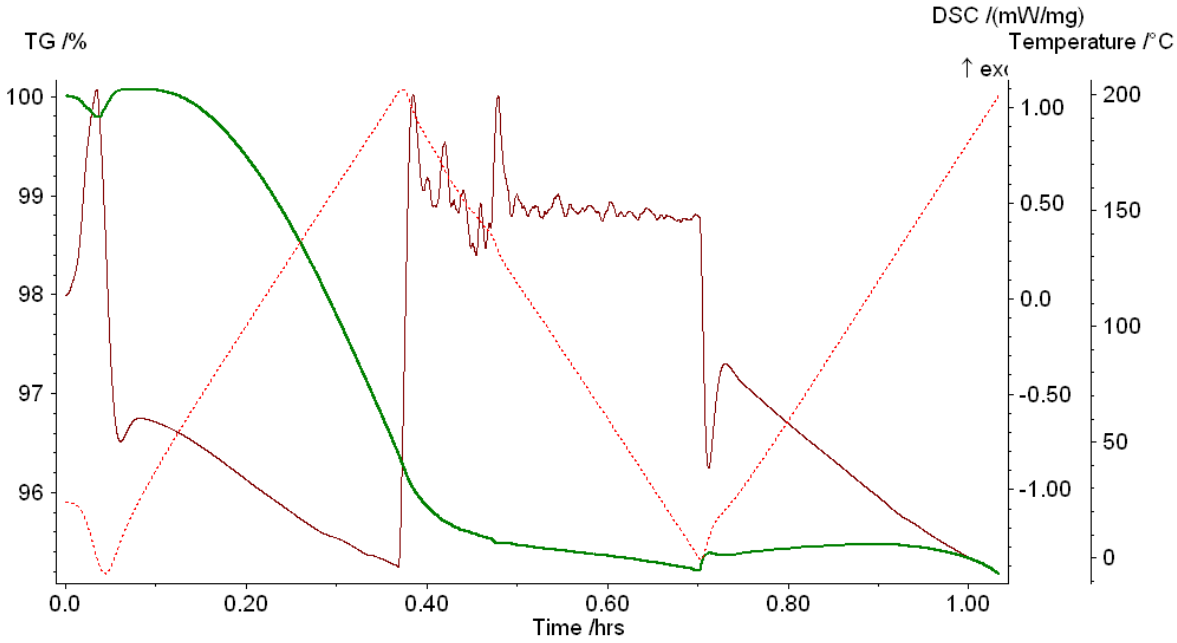

Figure appendix 2- 4 DSC trace polymer 1BN

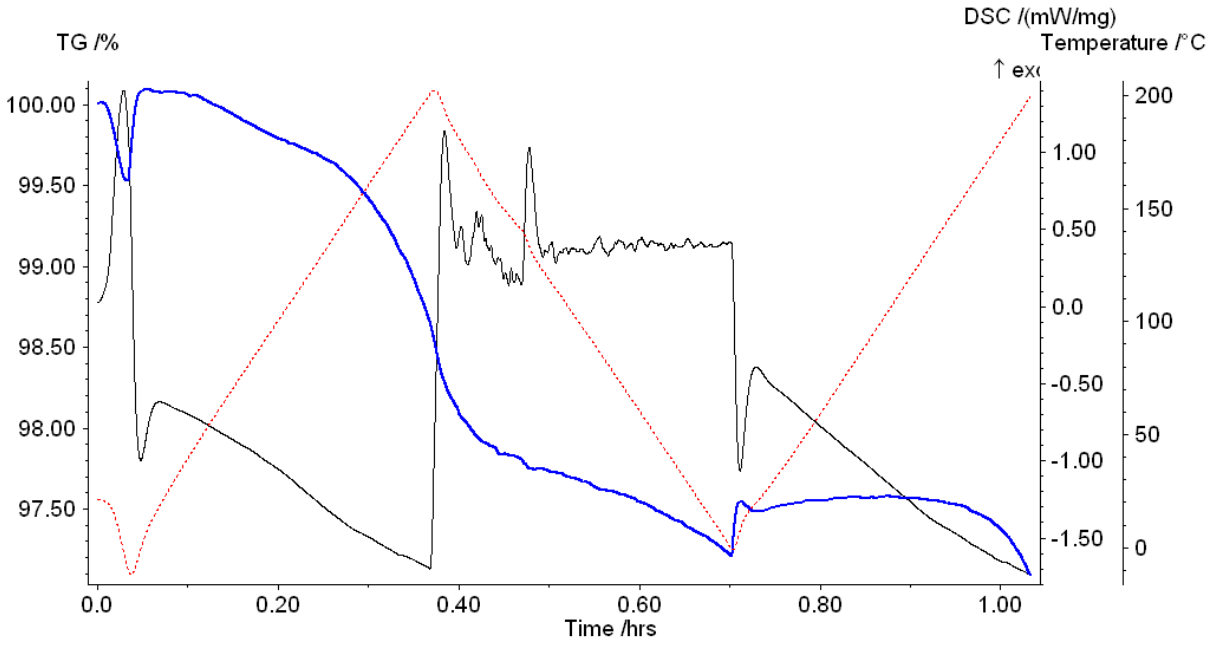

Figure appendix 2- 5 DSC trace polymer 1C

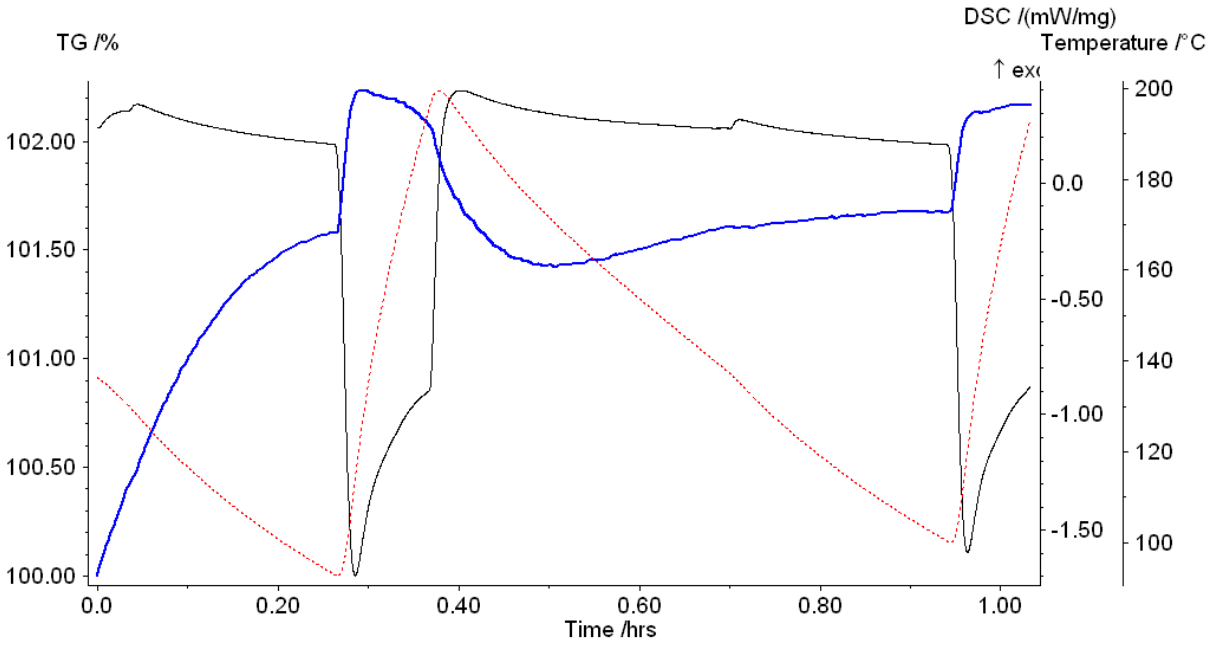

Figure appendix 2- 6 DSC trace polymer 2A

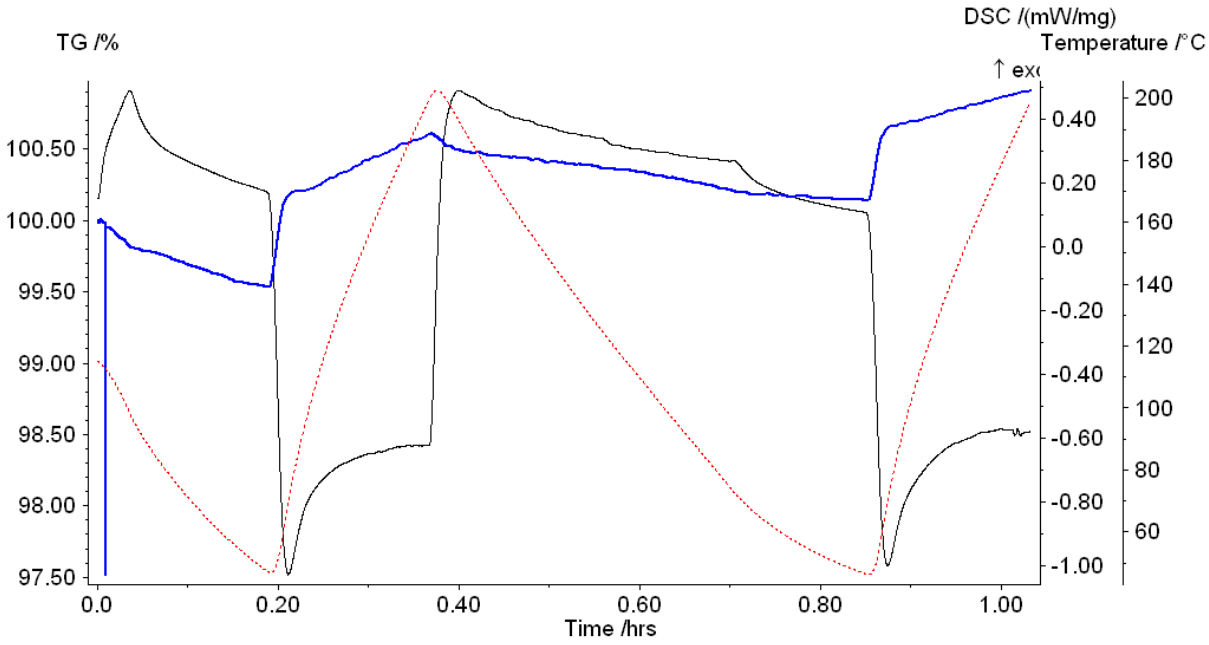

Figure appendix 2- 7 DSC trace polymer 2B

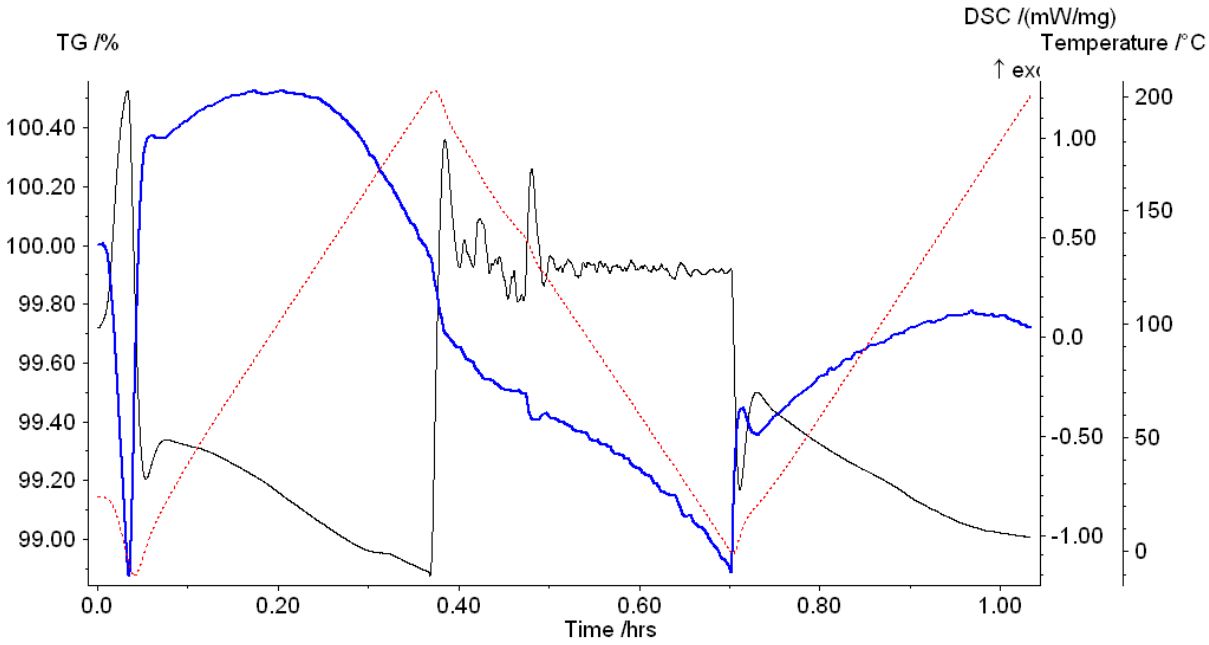

Figure appendix 2- 8 DSC trace polymer 2C

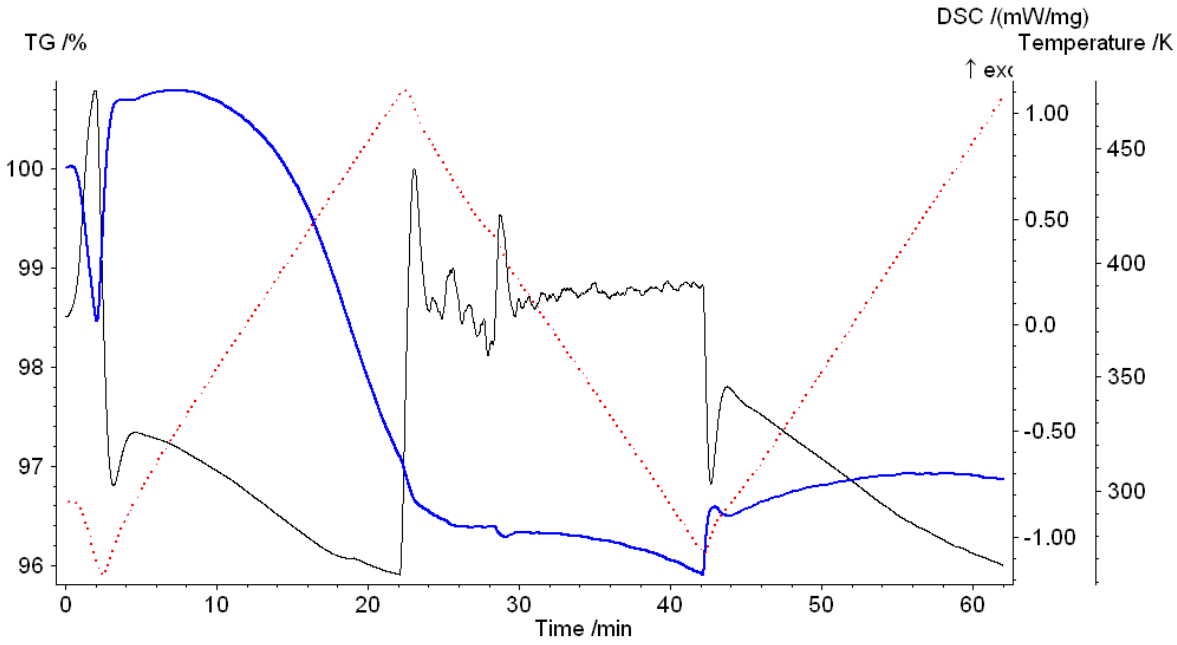

Figure appendix 2- 9 DSC trace polymer 3A

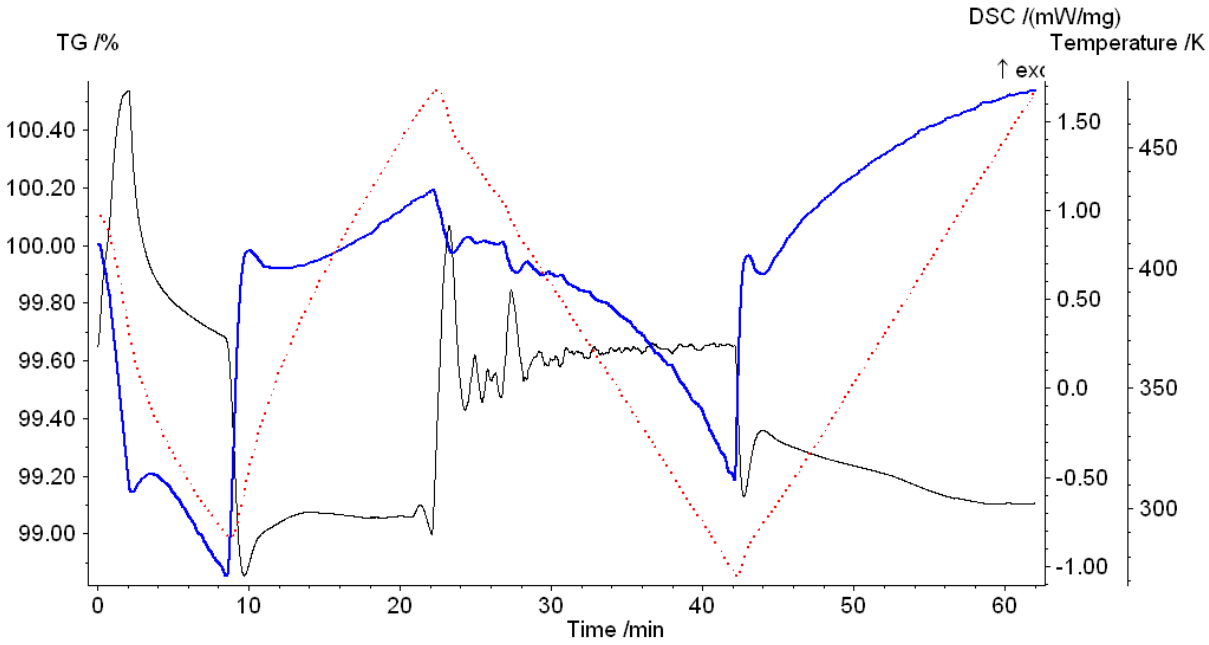

Figure appendix 2- 10 DSC trace polymer 3B

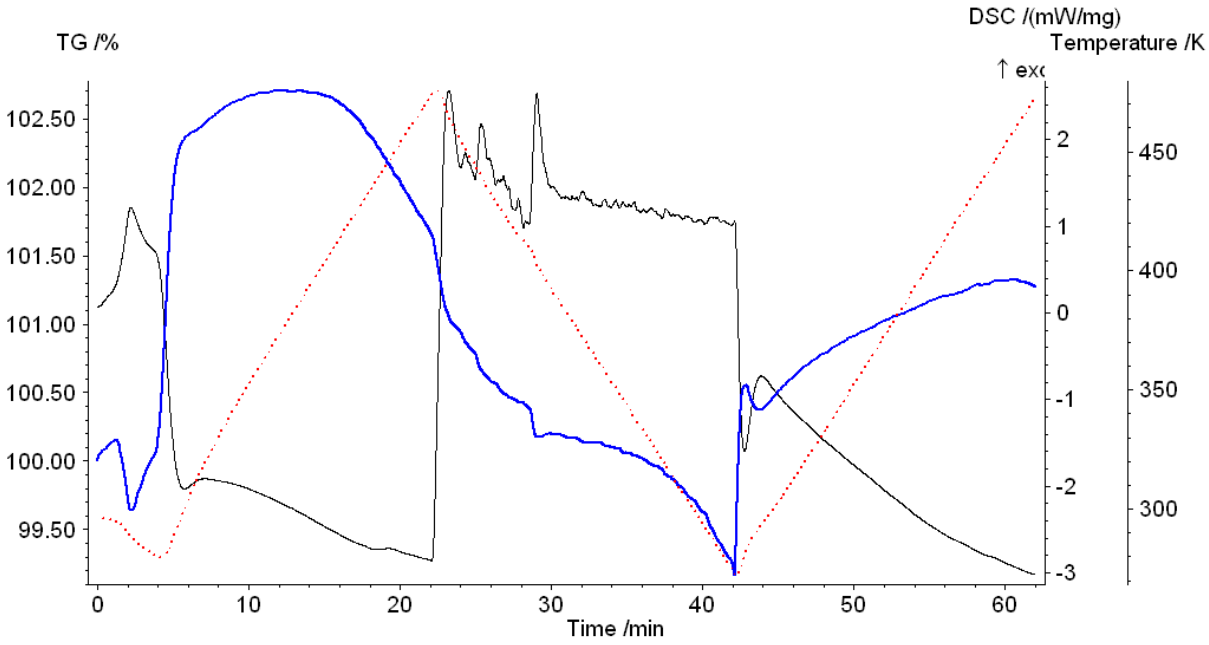

Figure appendix 2- 11 DSC trace polymer 3C

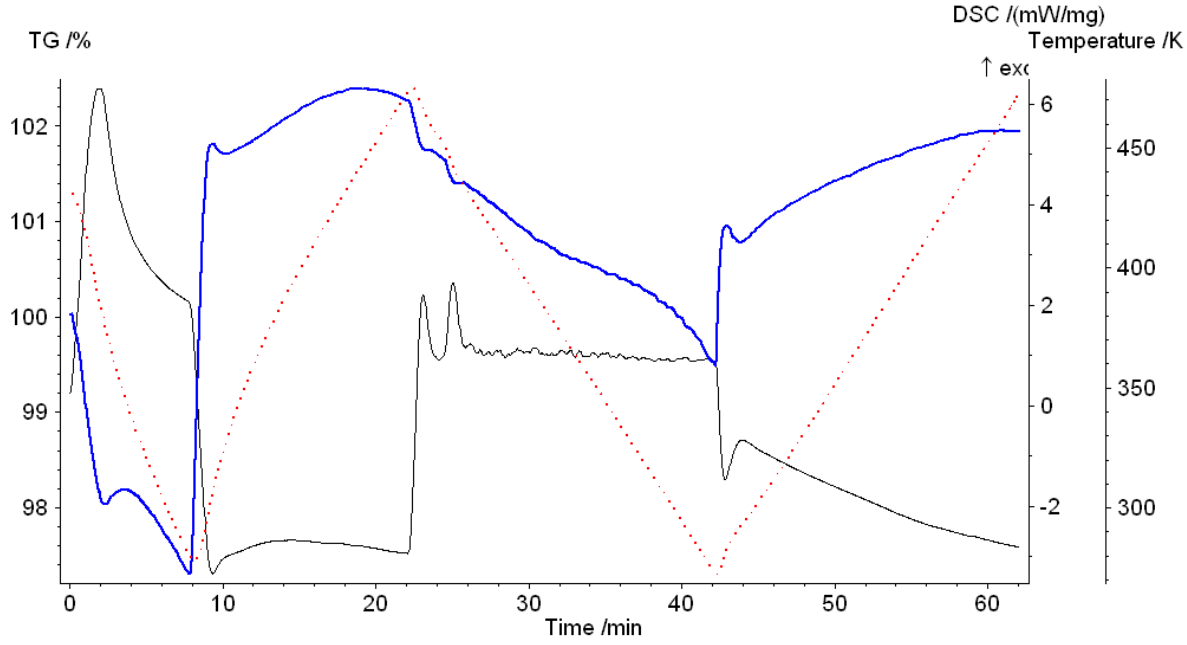

Figure appendix 2- 12 DSC trace polymer 4A

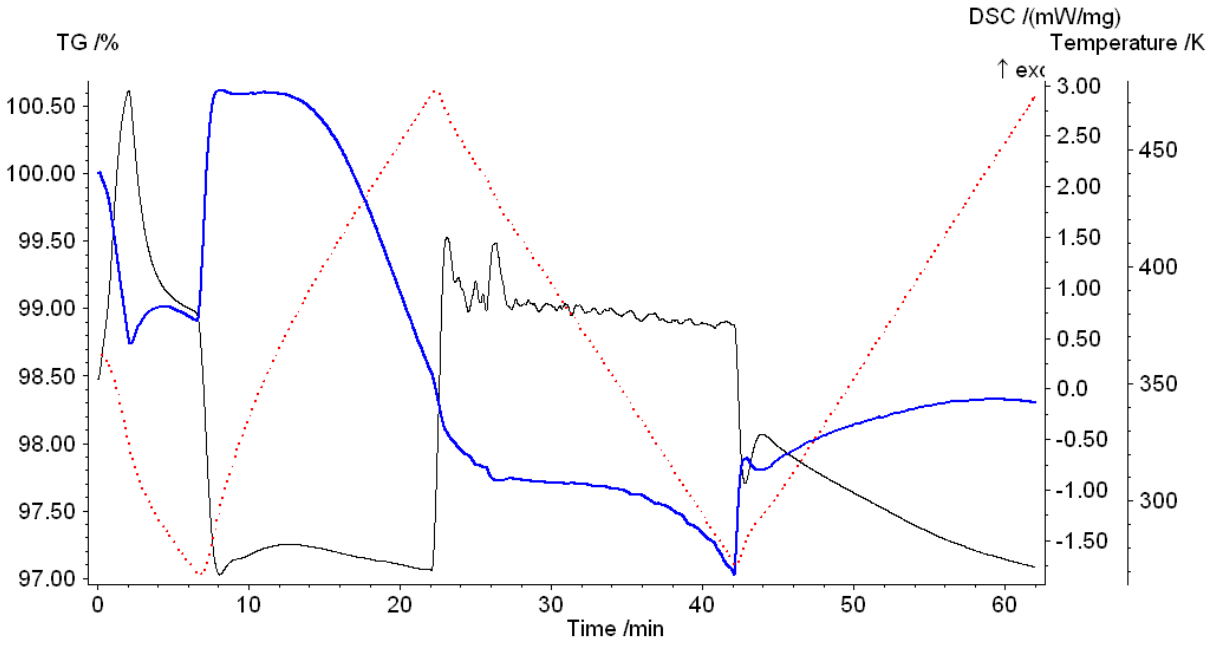

Figure appendix 2- 13 DSC trace polymer 4B

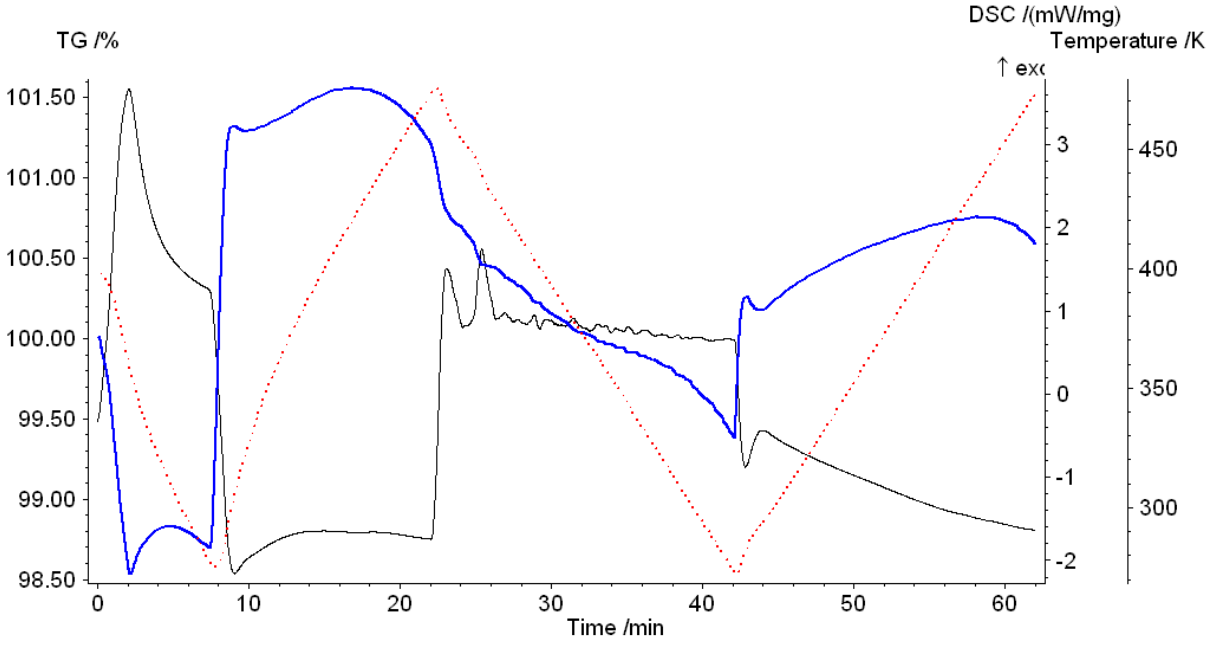

Figure appendix 2- 14 DSC trace polymer 4C

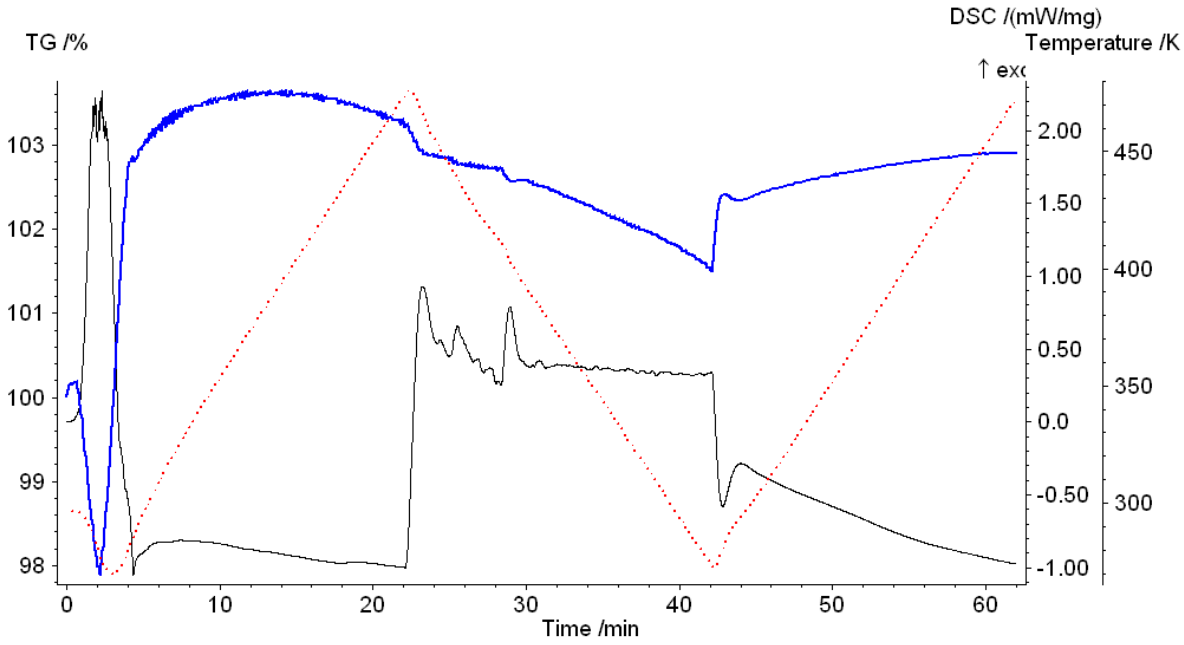

Figure appendix 2- 15 DSC trace polymer 5A

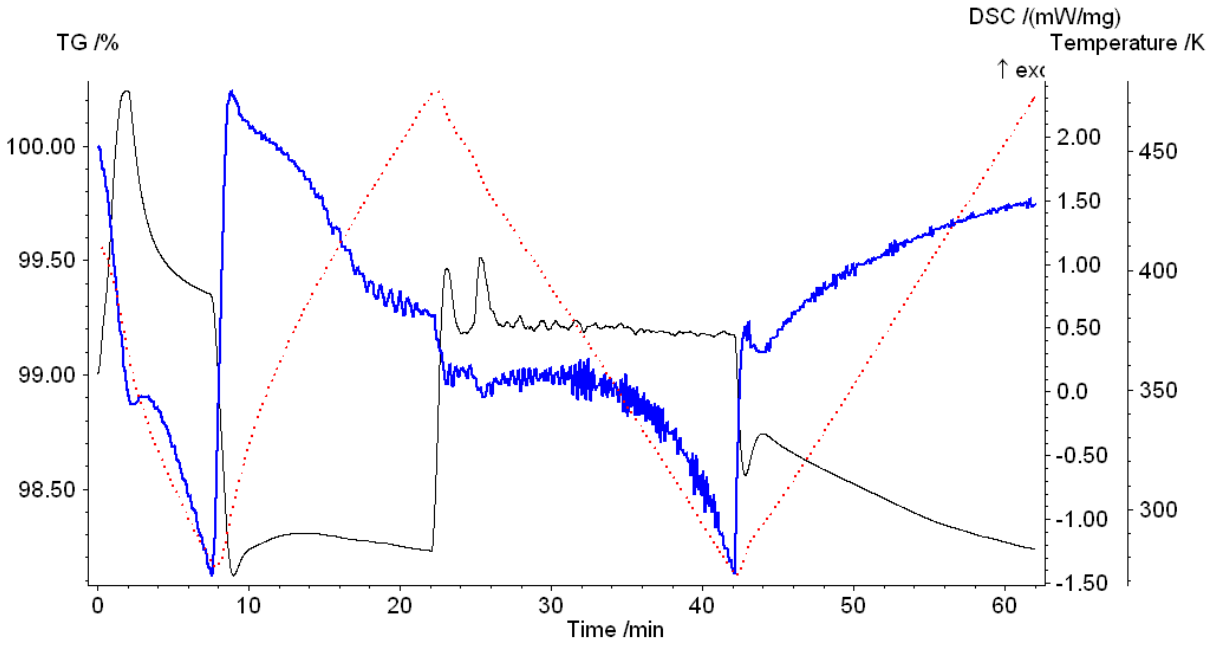

Figure appendix 2- 16 DSC trace polymer 5B

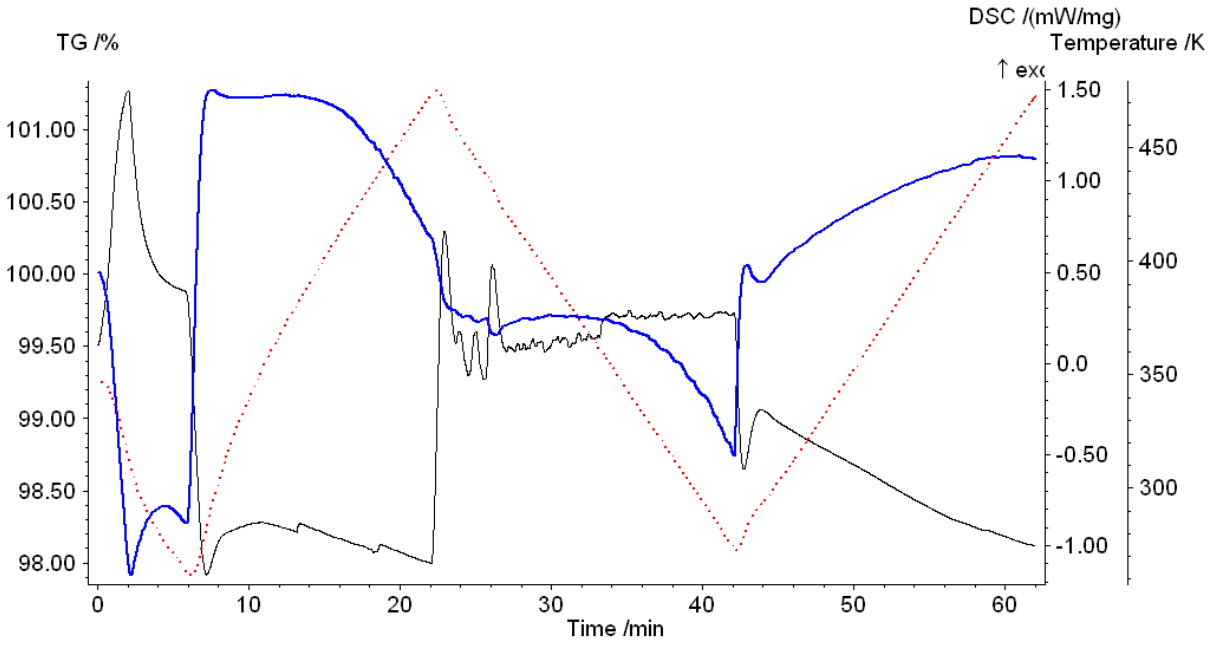

Figure appendix 2- 17 DSC trace polymer 5C

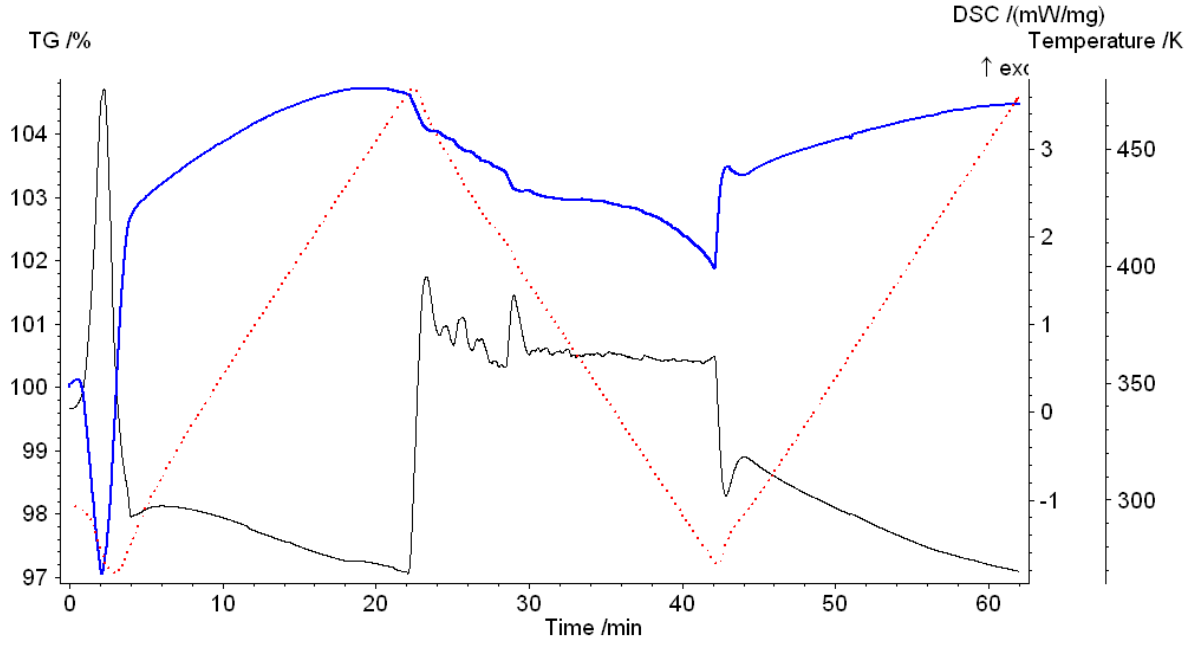

Figure appendix 2- 18 DSC trace polymer 6A

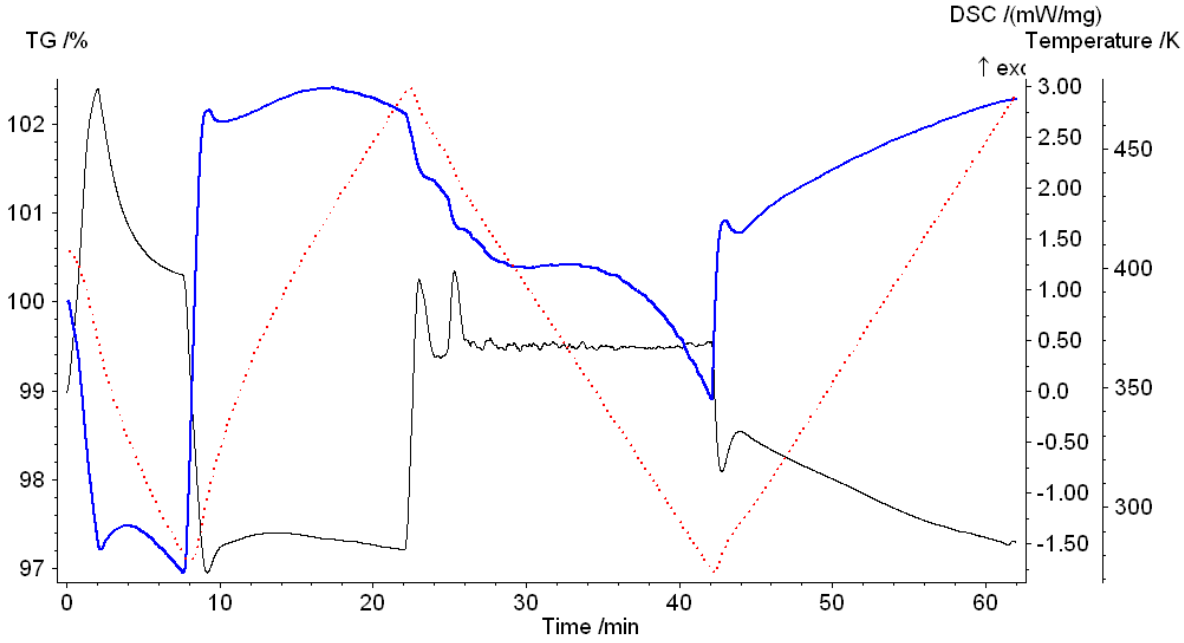

Figure appendix 2- 19 DSC trace polymer 6B

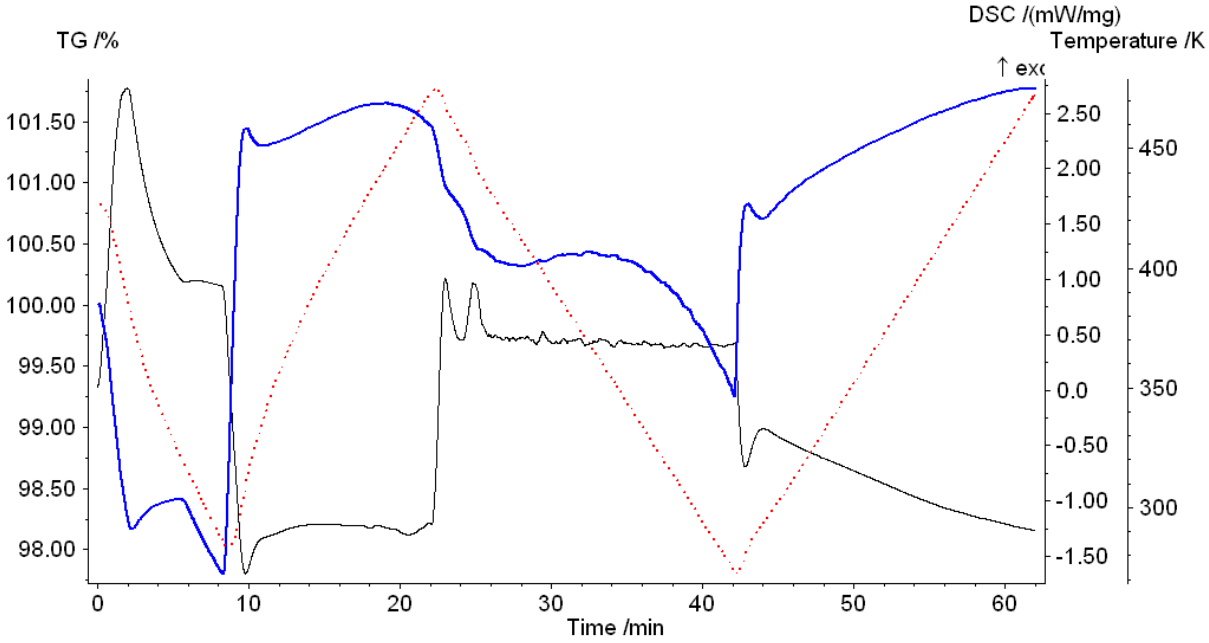

Figure appendix 2- 20 DSC trace polymer 6C

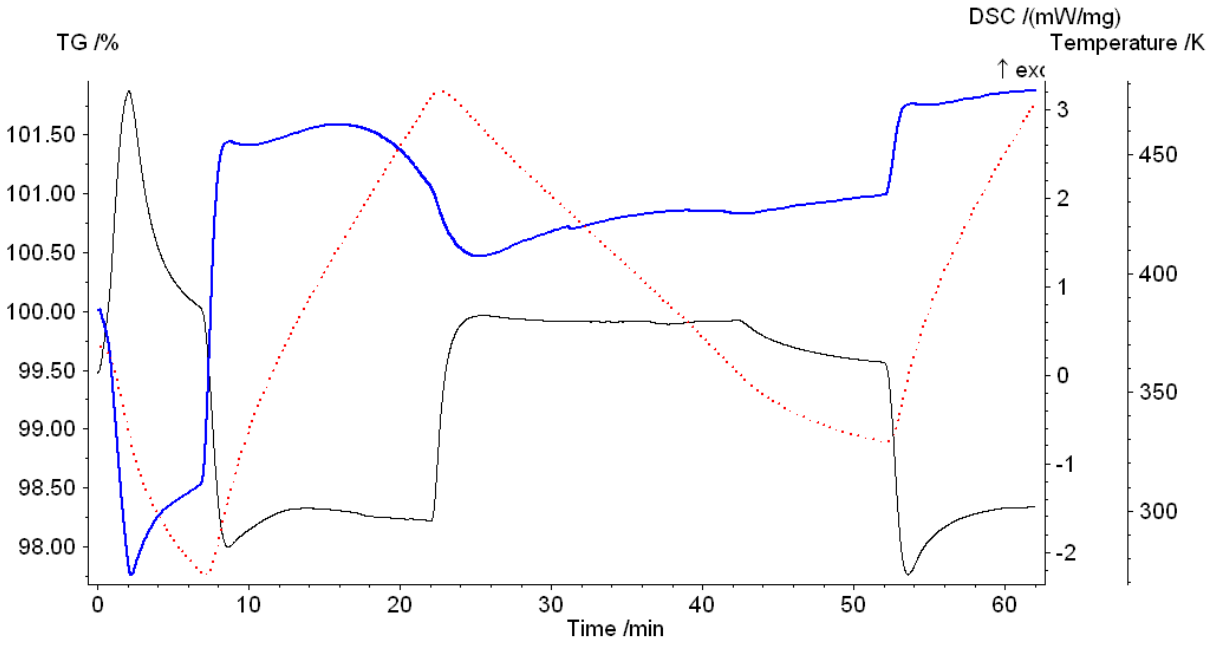

Figure appendix 2- 21 DSC trace polymer 7A

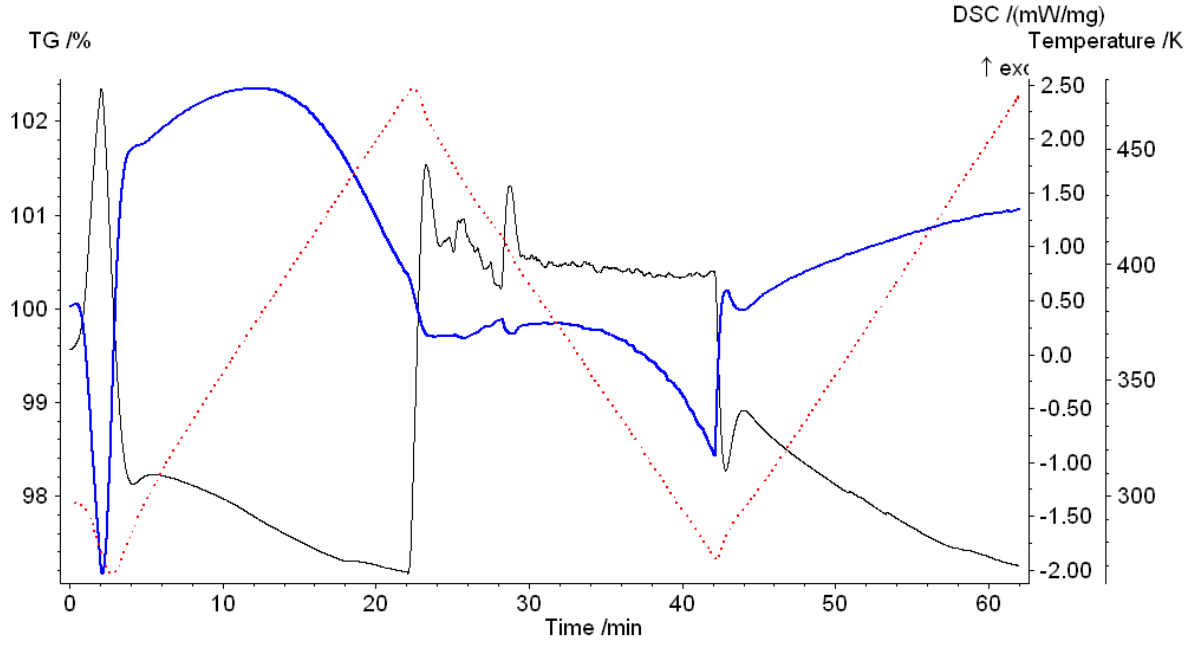

Figure appendix 2- 22 DSC trace polymer 7B

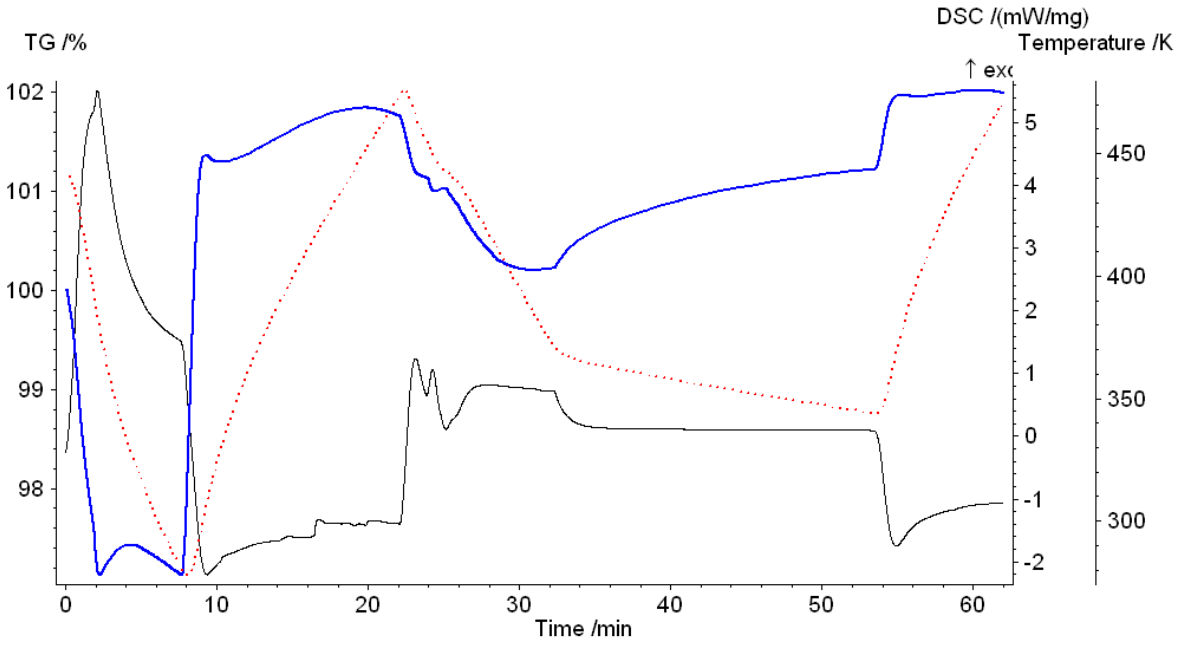

Figure appendix 2- 23 DSC trace polymer 7C

PCA SCORES FROM RAW IMAGE FIGURE 4- 24

Figure appendix 2- 1 PCA scores 1.

Figure appendix 2- 2 PCA scores 2.

Figure appendix 2- 3 PCA scores 3.

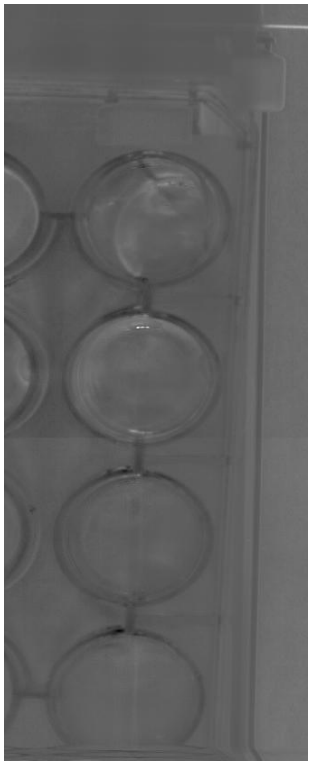

Figure appendix 2- 4 PCA scores 4.

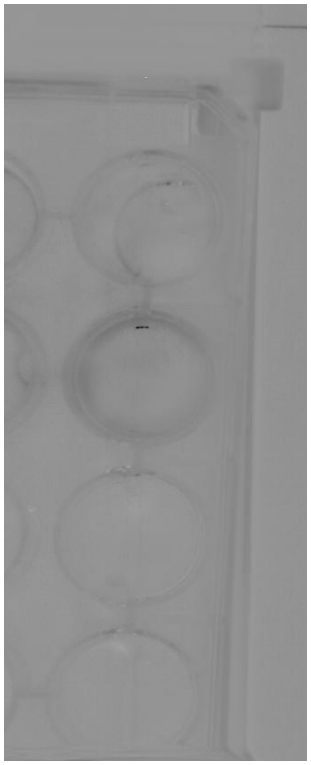

Figure appendix 2- 5 PCA scores 5.

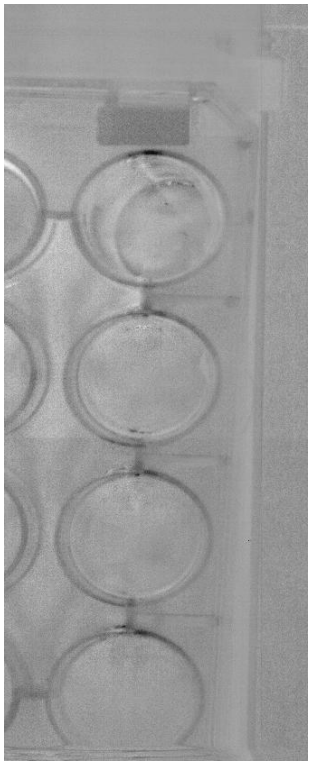

Figure appendix 2- 6 PCA scores 6.

PCA SCORES FROM RAW IMAGE FIGURE 4- 27

Figure appendix 2- 7 PCA scores 1.

Figure appendix 2- 8 PCA scores 2.

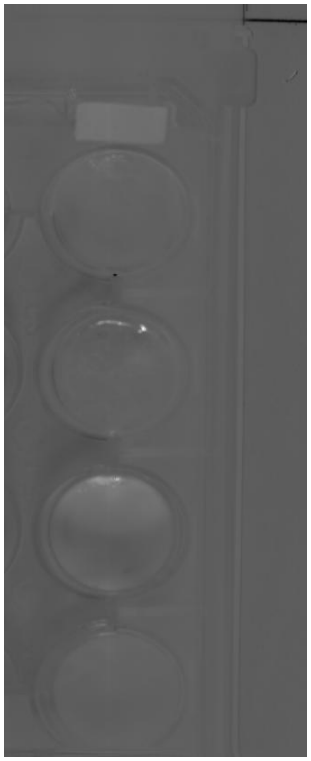

Figure appendix 2- 9 PCA scores 3.

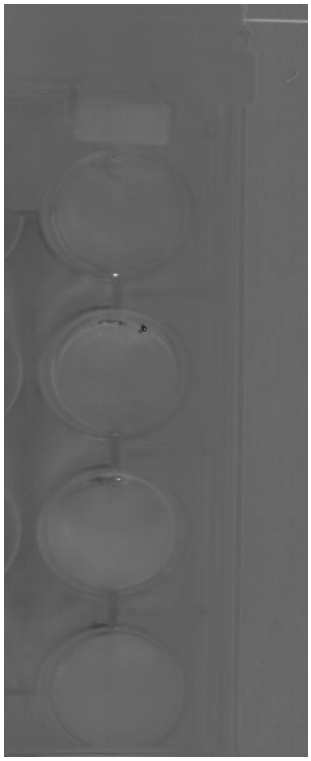

Figure appendix 2- 10 PCA scores 4.

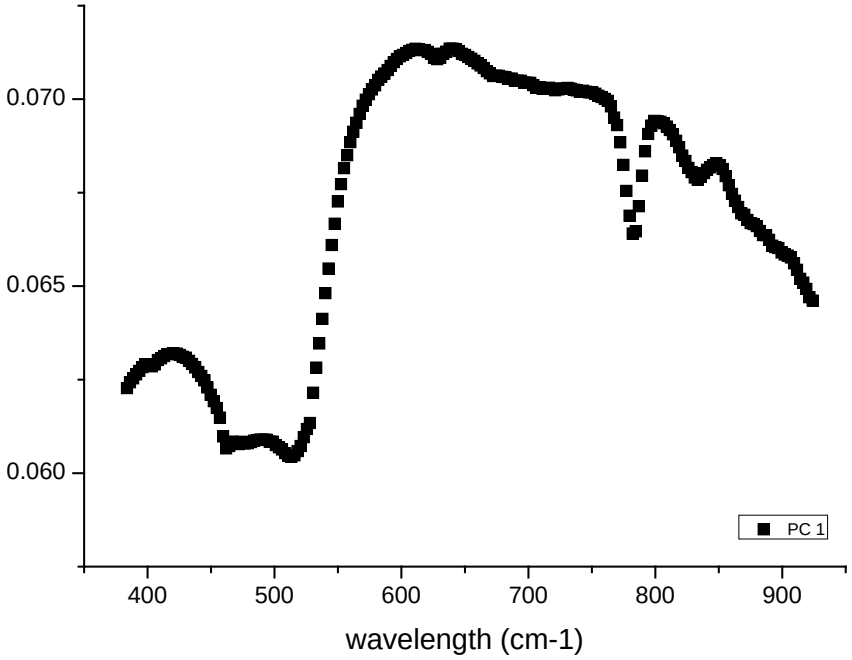

Figure appendix 2- 11 PC1 loadings plot, HSI.

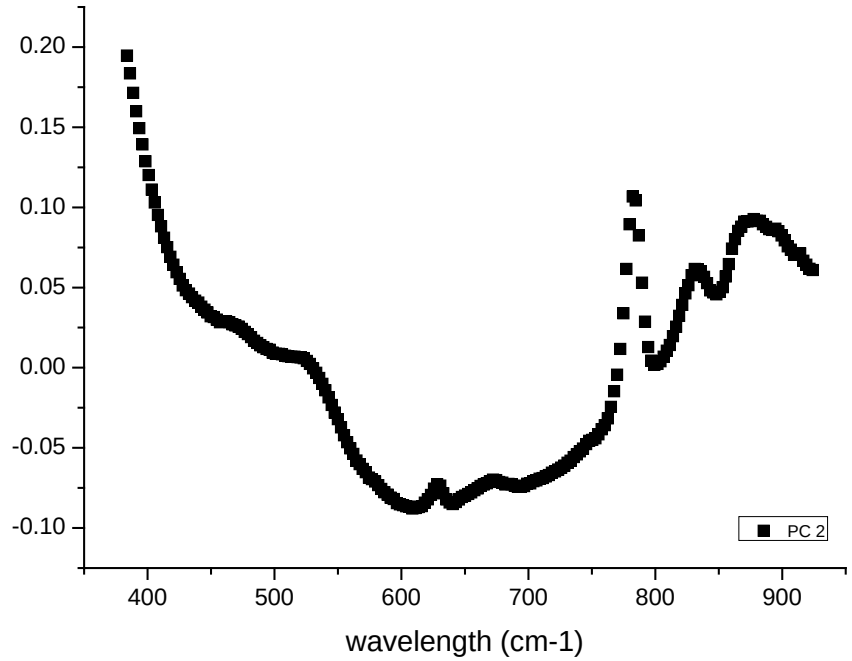

Figure appendix 2- 12 PC2 loadings plot, HSI.

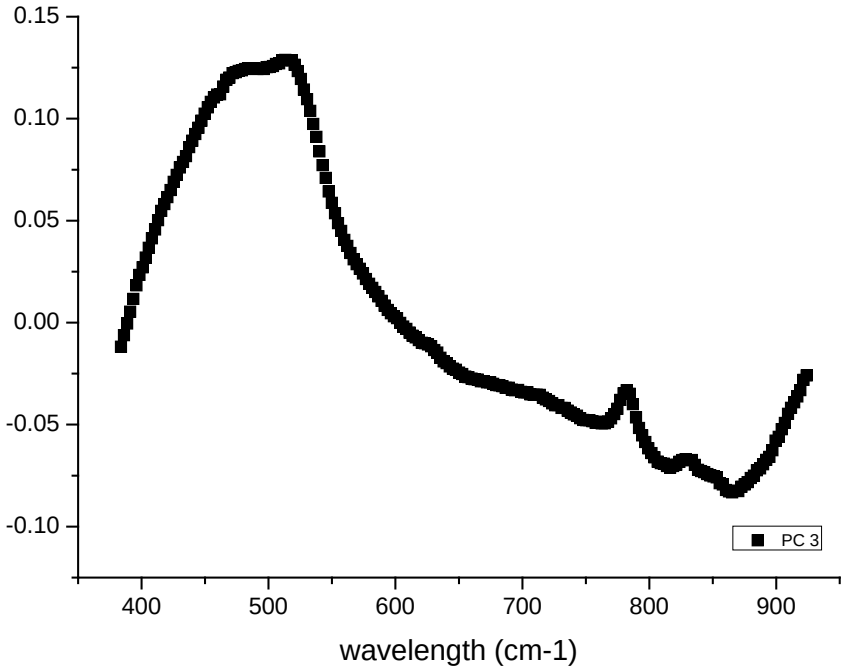

Figure appendix 2- 13 PC3 loadings plot, HSI.

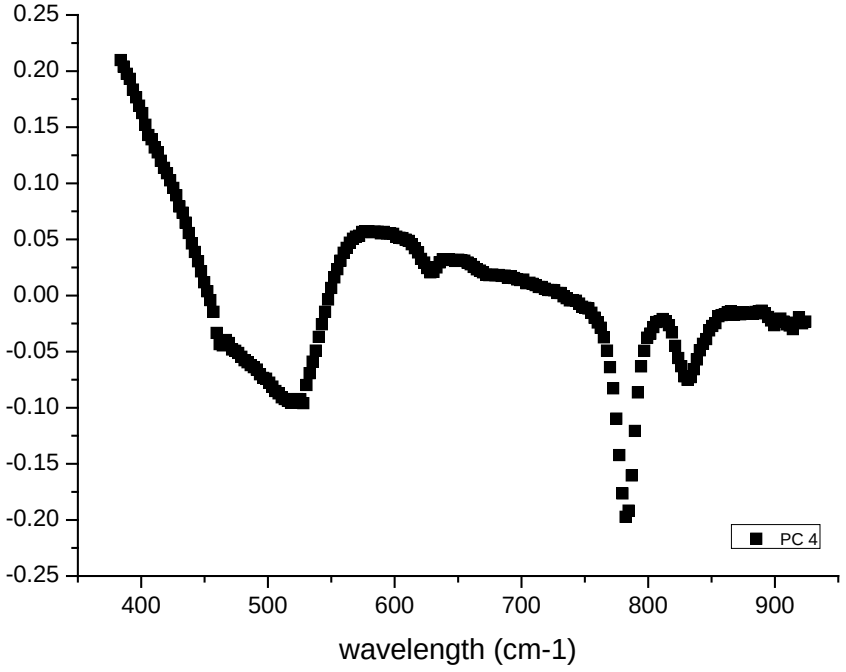

Figure appendix 2- 14 PC4 loadings plot, HSI.

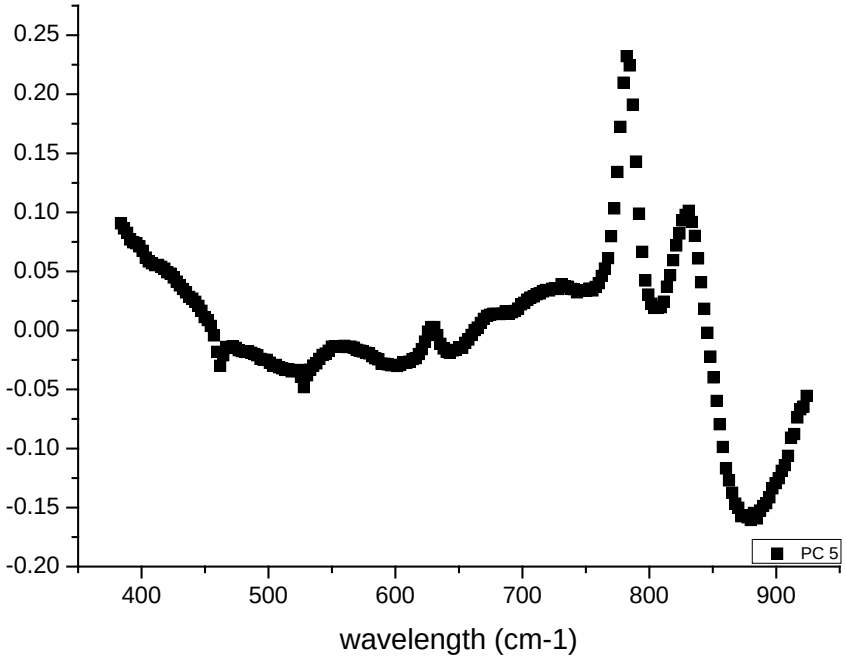

Figure appendix 2- 15 PC5 loadings plot, HSI.

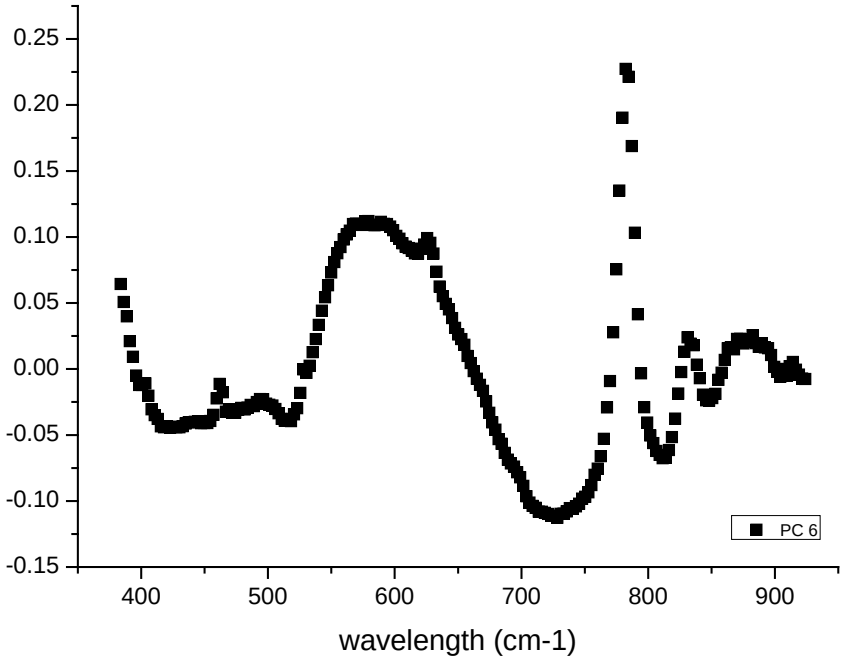

Figure appendix 2- 16 PC6 loadings plot, HSI.

PCA LOADINGS FROM IMAGE FIGURE 4- 27

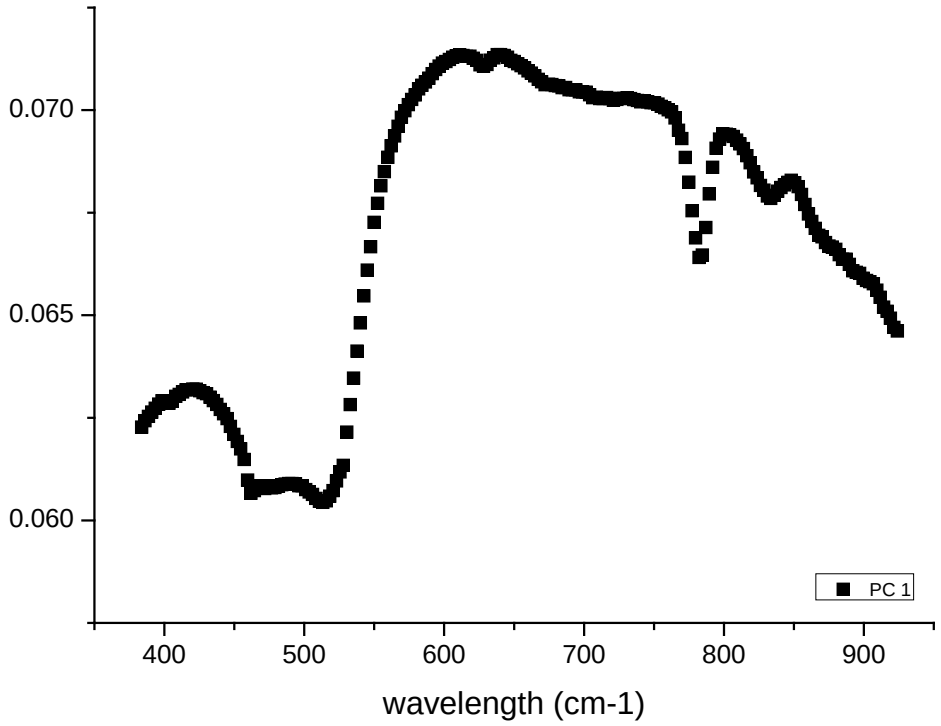

Figure appendix 2- 17 PC1 loadings plot, HSI.

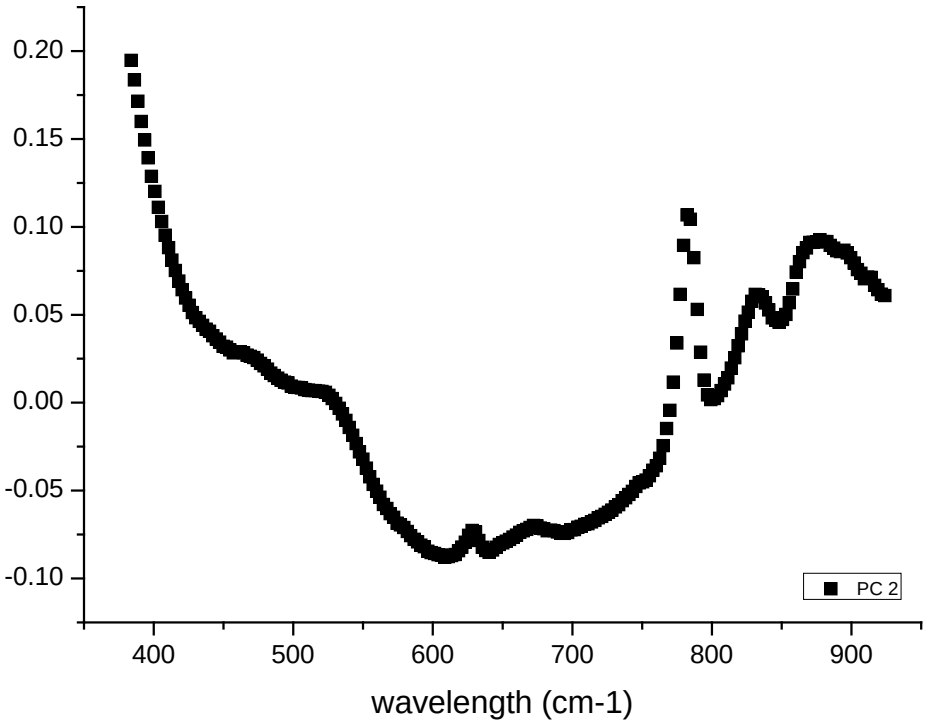

Figure appendix 2- 18 PC2 loadings plot, HSI.

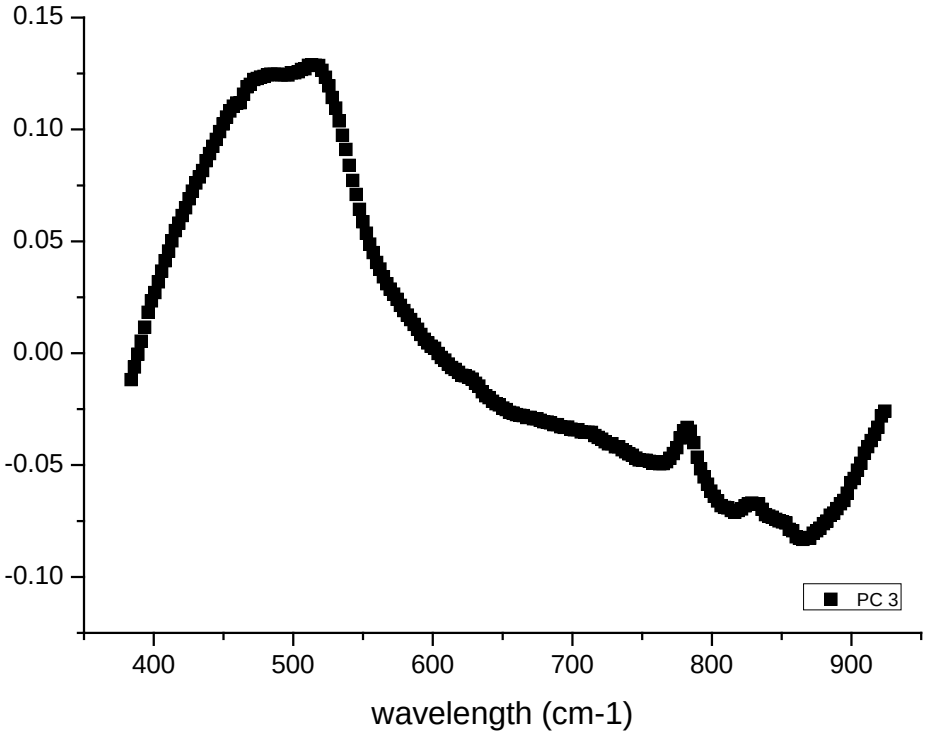

Figure appendix 2- 19 PC3 loadings plot, HSI.

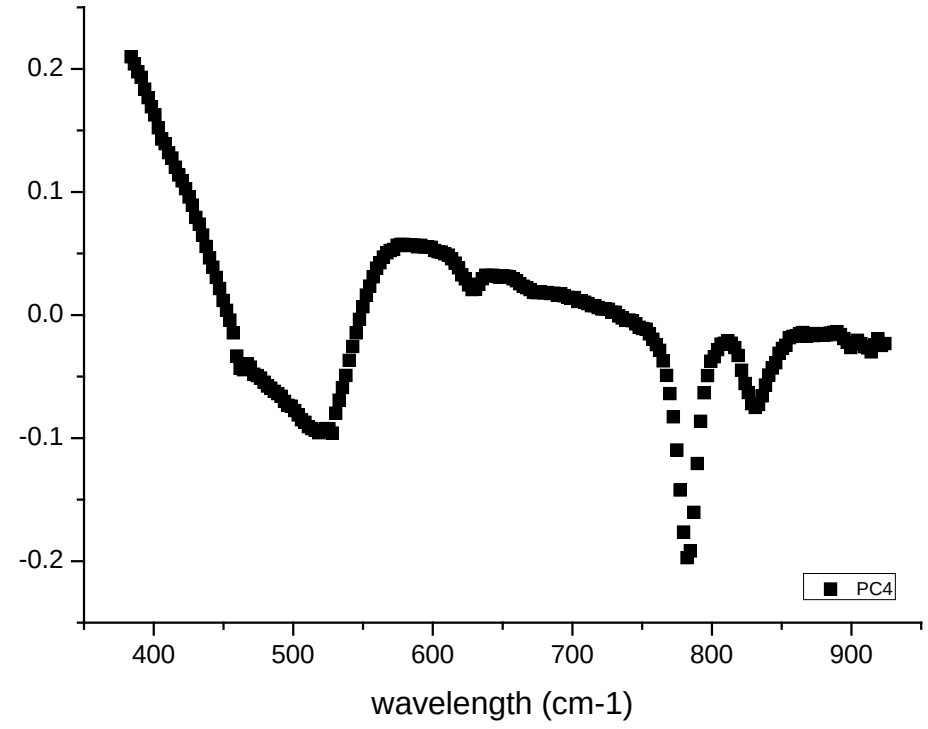

Figure appendix 2- 20 PC4 loadings plot, HSI.

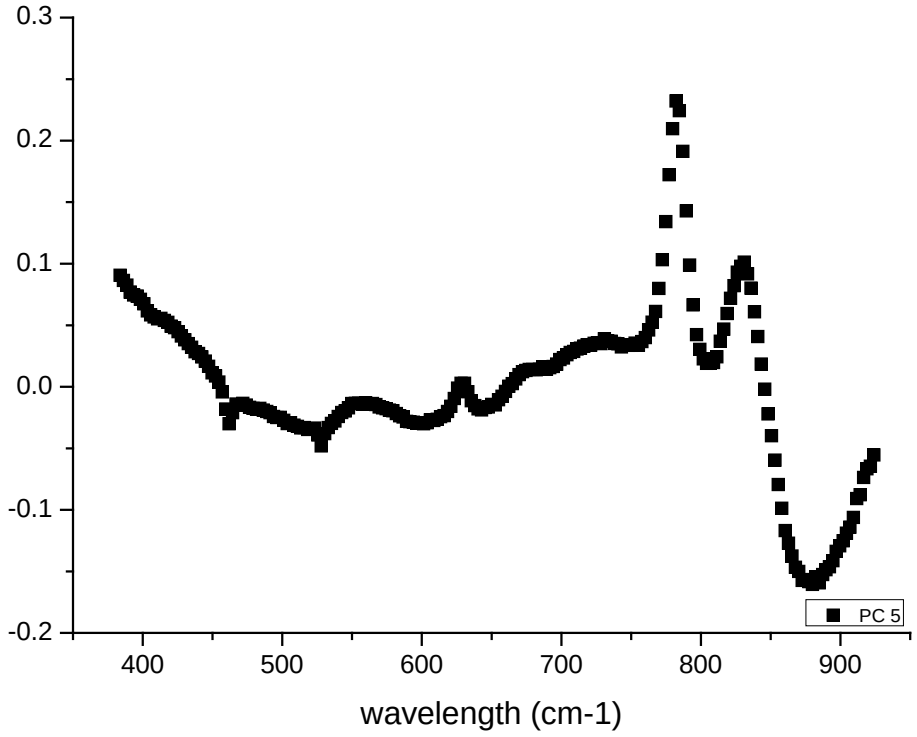

Figure appendix 2- 21 PC5 loadings plot, HSI.

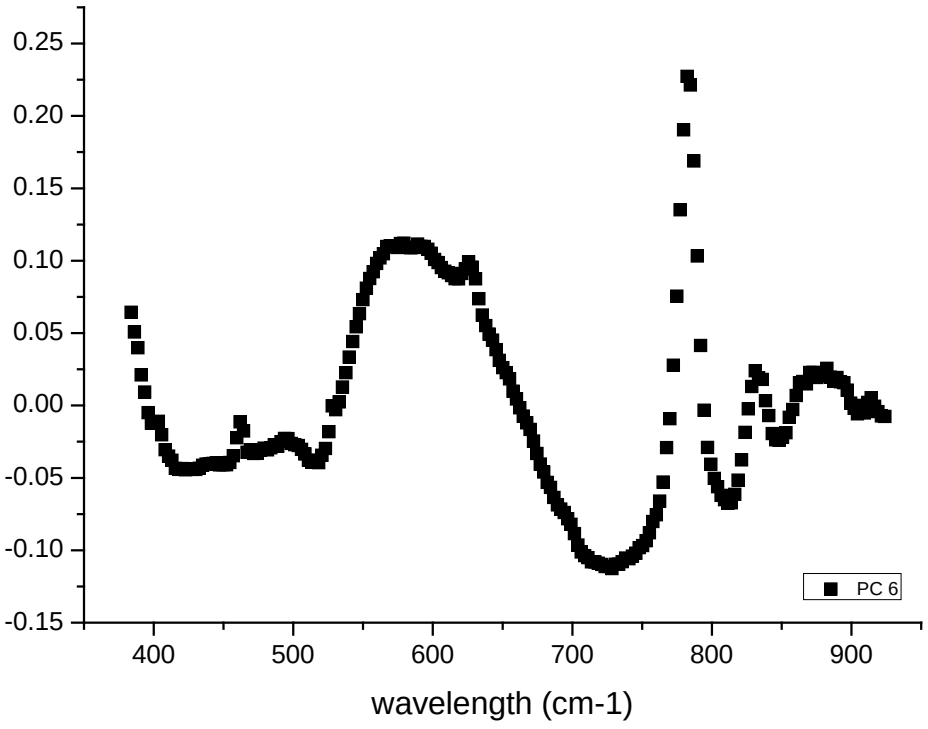

Figure appendix 2- 22 PC6 loadings plot, HSI.

APPENDIX 3: TPA PLOTS

Dry Polymer Testing

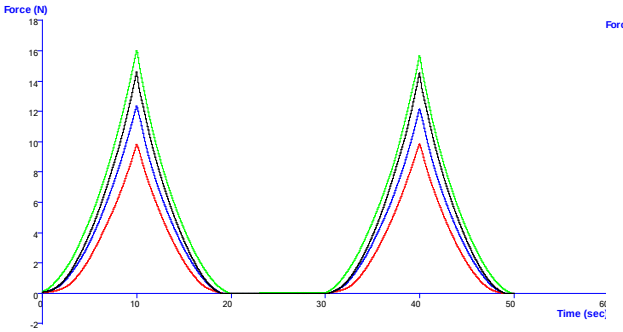

Figure appendix 3- 1 TPA 1BC 0.1mm/s

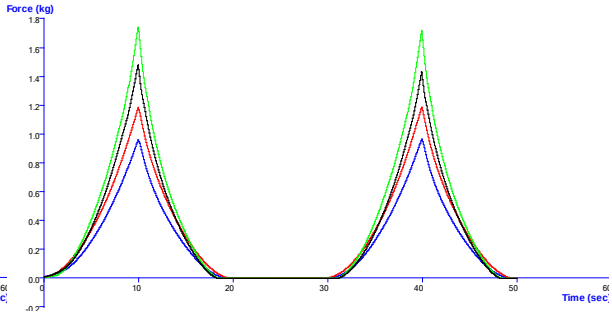

Figure appendix 3- 23 TPA 1BN 0.1mm/s

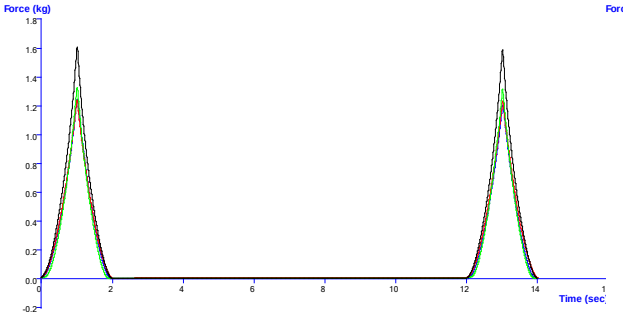

Figure appendix 3- 3 TPA 1BC 1mm/s

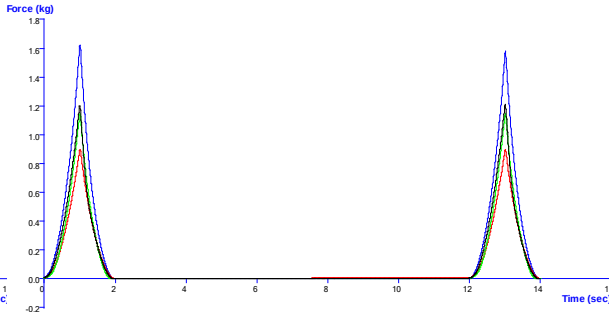

Figure appendix 3- 4 TPA 1BN 1mm/s

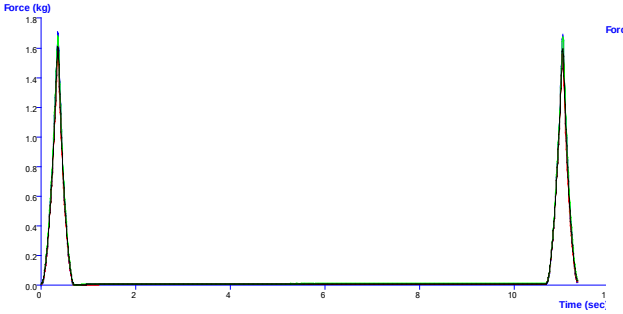

Figure appendix 3- 524 TPA 1BC 3mm/s

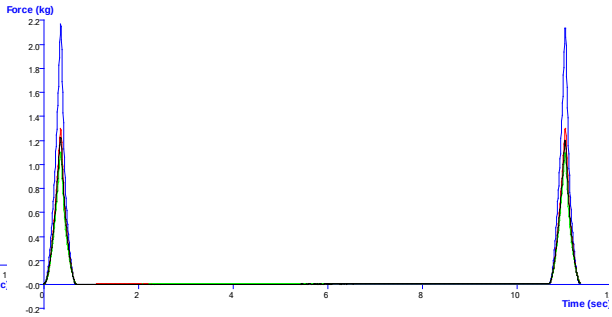

Figure appendix 3- 6 TPA 1BN 3mm/s

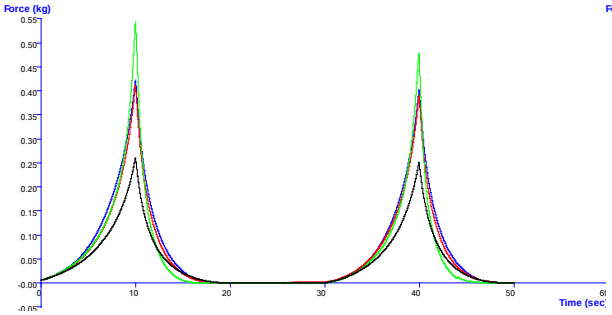

Figure appendix 3- 725 TPA 1C 0.1 mm/s

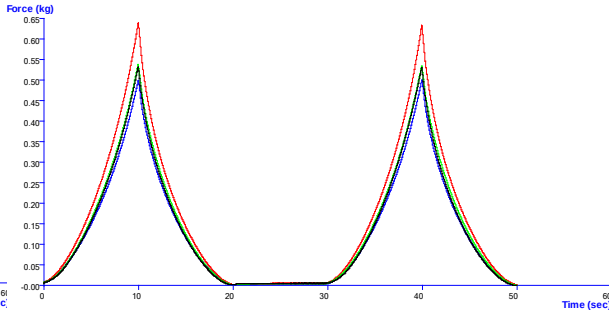

Figure appendix 3- 826 TPA 2A 0.1mm/s

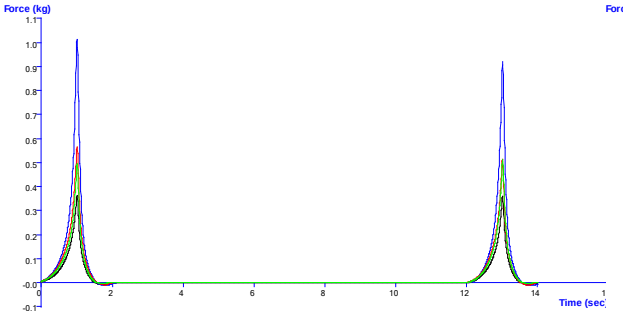

Figure appendix 3- 927 TPA 1C 1mm/s

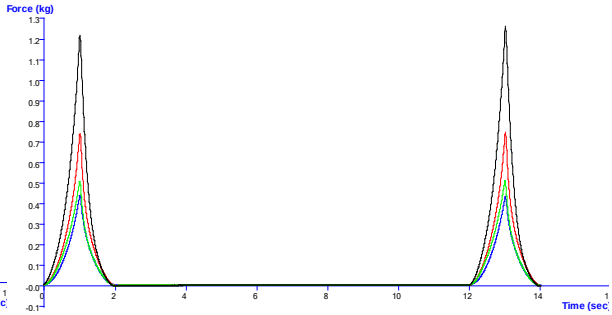

Figure appendix 3- 1028 TPA 2A 1mm/s

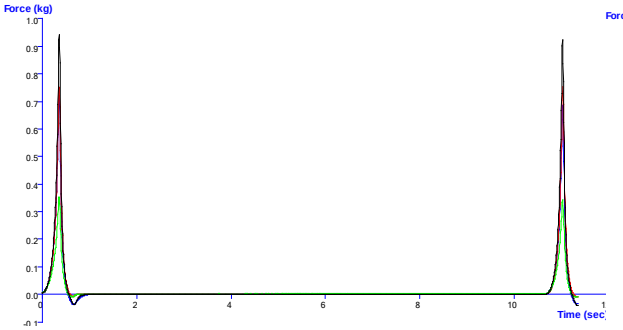

Figure appendix 3- 1129 TPA 1C 3mm/s

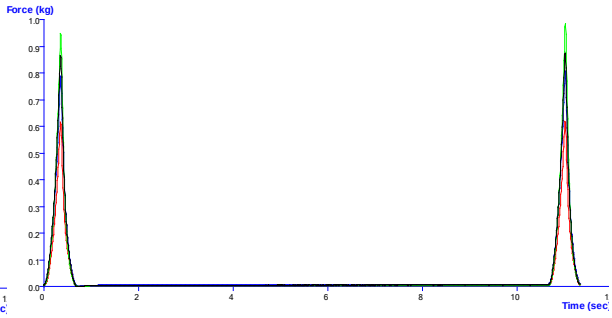

Figure appendix 3- 1230 TPA 2A 3mm/s

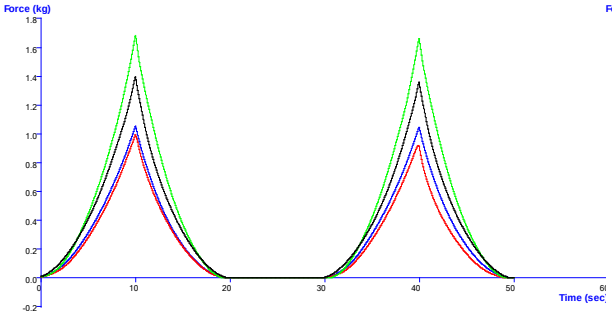

Figure appendix 3- 1331 TPA 2B 0.1mm/s

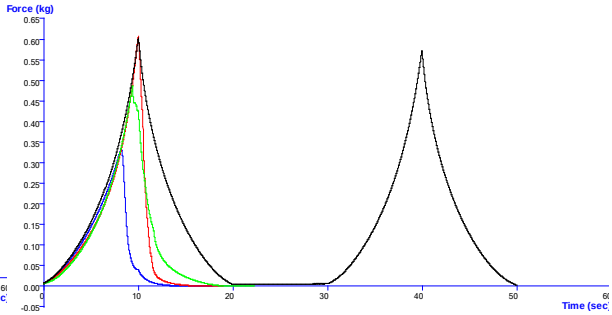

Figure appendix 3- 1432 TPA 2C 0.1mm/s

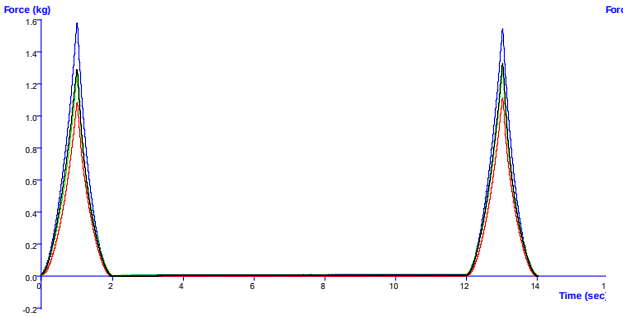

Figure appendix 3- 1533 TPA 2B 1mm/s

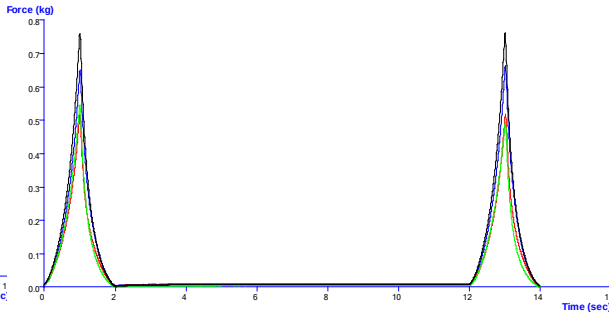

Figure appendix 3- 16 TPA 2C 1mm/s

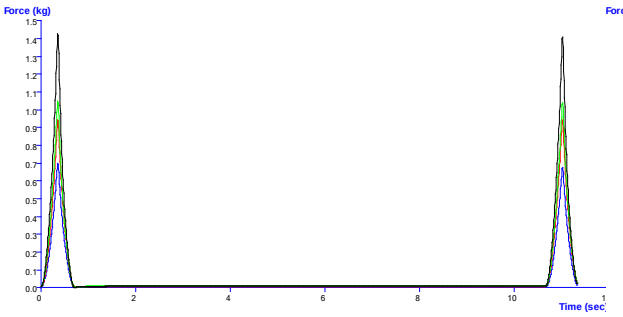

Figure appendix 3- 17 TPA 2B 3mm/s

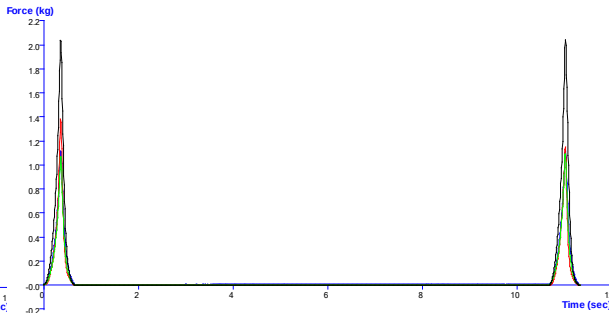

Figure appendix 3- 1834 TPA 2C 3mm/s

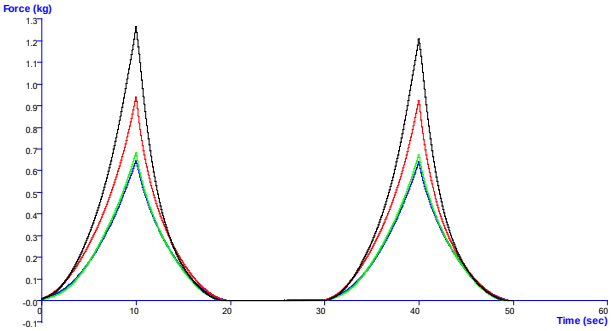

Figure appendix 3- 1935 TPA 3A 0.1mm/s

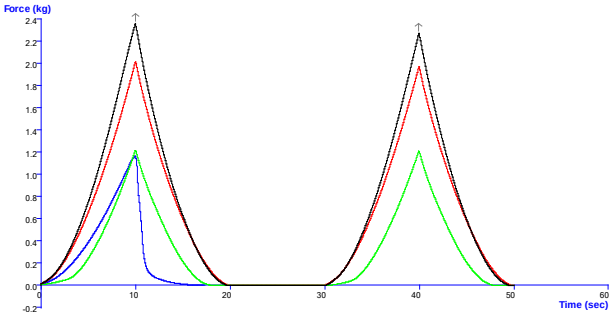

Figure appendix 3- 2036 TPA 3B 0.1mm/s

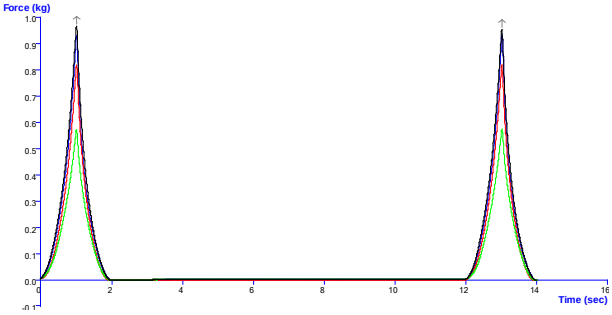

Figure appendix 3- 2137 TPA 3A 1mm/s

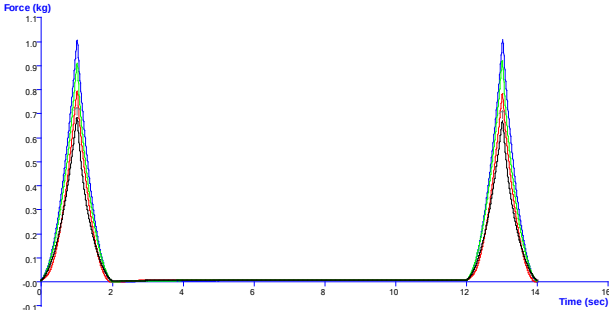

Figure appendix 3- 2238 TPA 3B 1mm/s

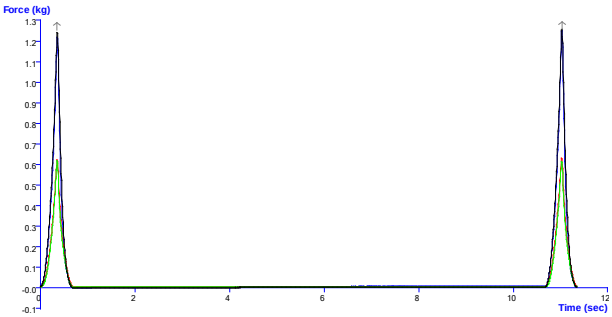

Figure appendix 3- 2339 TPA 3A 3mm/s

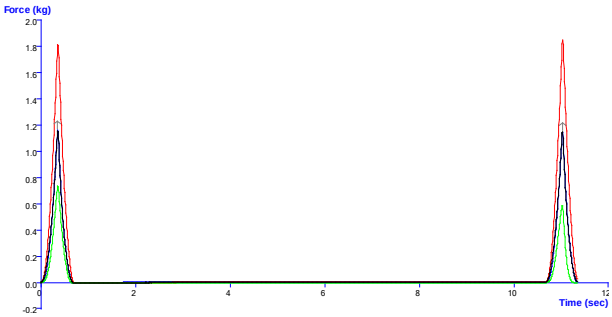

Figure appendix 3- 2440 TPA 3B 3mm/s

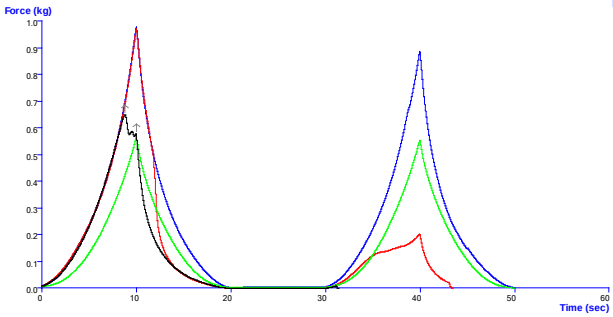

Figure appendix 3- 2541 TPA 3C 0.1mm/s

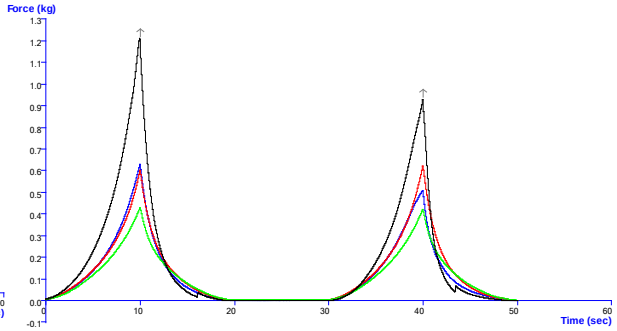

Figure appendix 3- 2642 TPA 4A 0.1mm/s

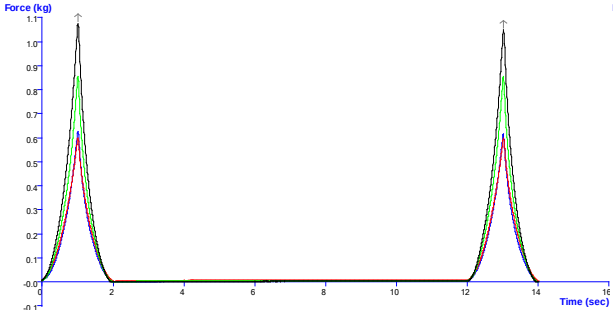

Figure appendix 3- 2743 TPA 3C 1mm/s

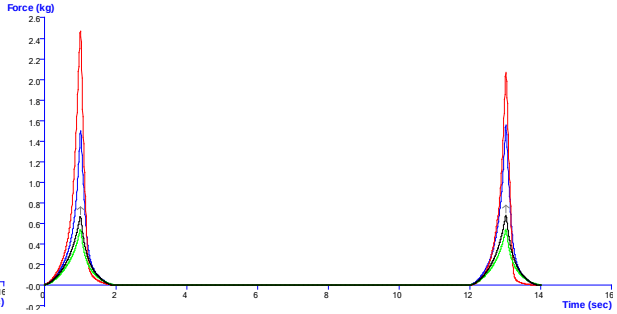

Figure appendix 3- 2844 TPA 4A 1mm/s

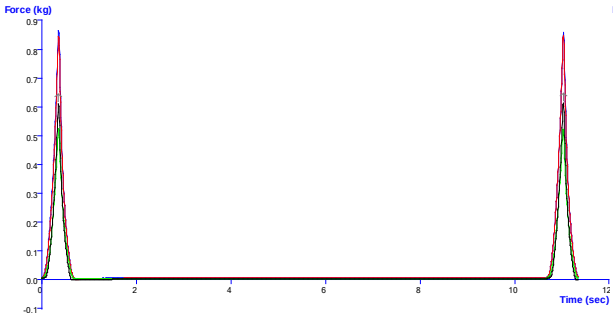

Figure appendix 3- 2945 TPA 3C 3mm/s

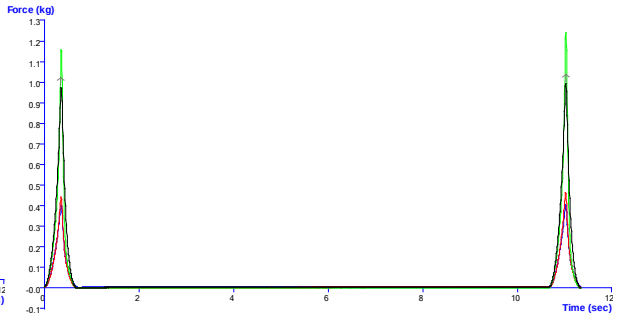

Figure appendix 3- 3046 TPA 4A 3mm/s

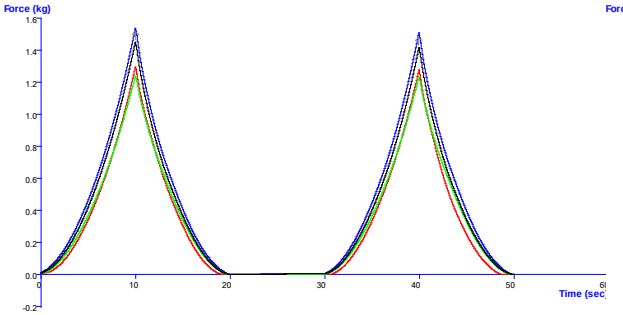

Figure appendix 3- 31 TPA 4B 0.1mm/s

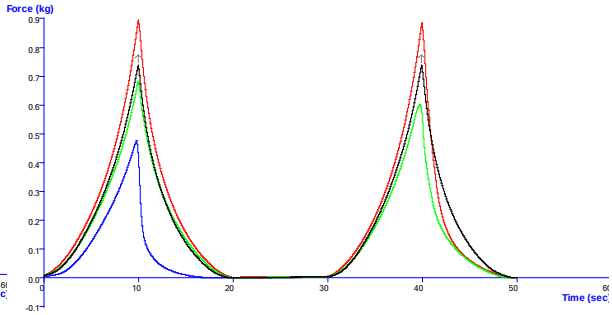

Figure appendix 3- 3247 TPA 4C 0.1mm/s

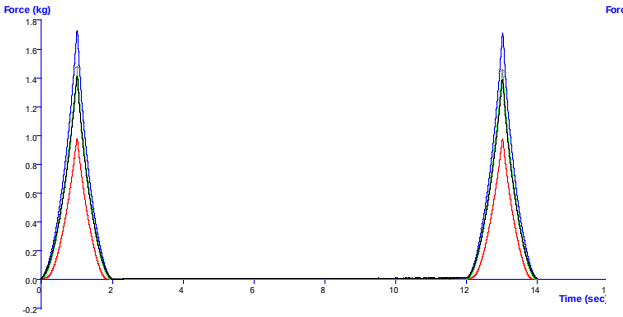

Figure appendix 3- 3348 TPA 4B 1mm/s

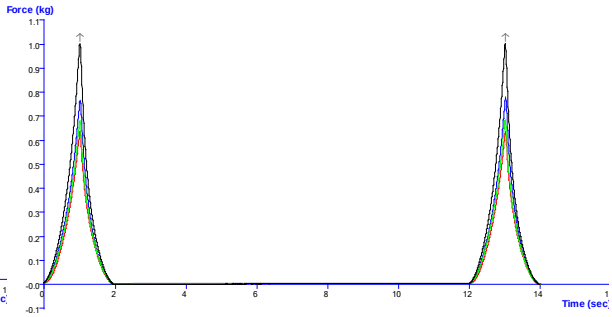

Figure appendix 3- 3449 TPA 4C 1mm/s

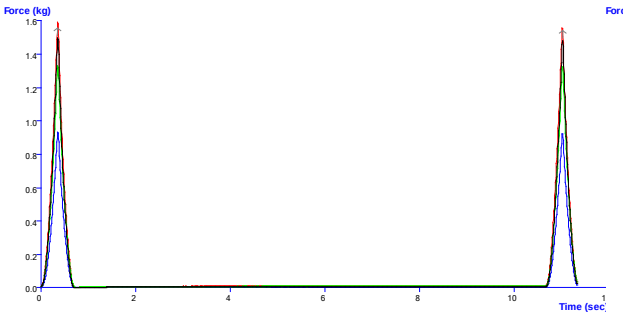

Figure appendix 3- 3550 TPA 4B 3mm/s

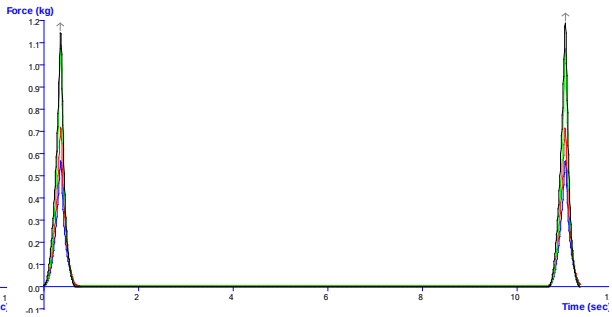

Figure appendix 3-3651 TPA 4C 3mm/s

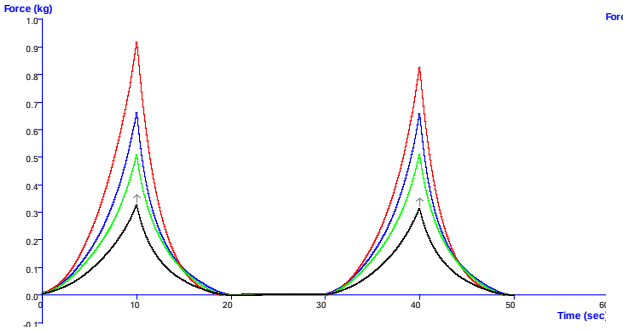

Figure appendix 3- 3752 TPA 5A 0.1mm/s

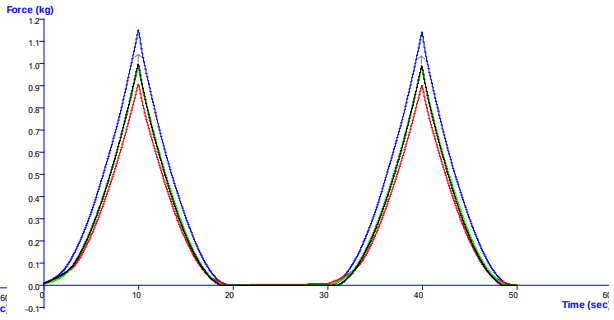

Figure appendix 3- 3853 TPA 5B 0.1mm/s

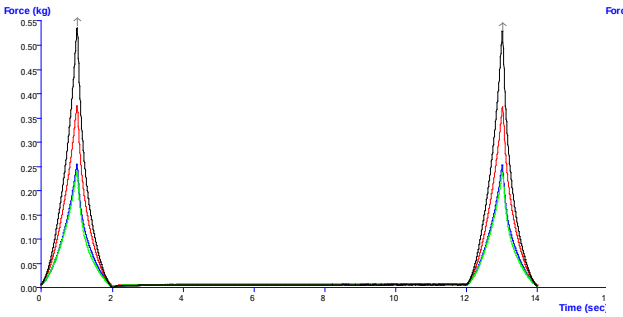

Figure appendix 3- 3954 TPA 5A 1mm/s

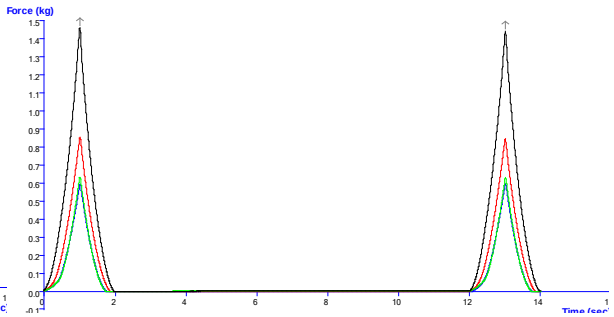

Figure appendix 3- 4055 TPA 5B 1mm/s

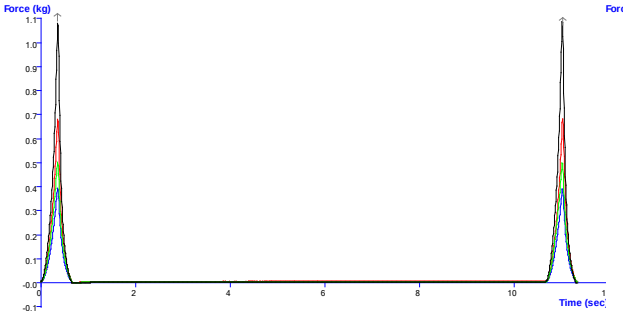

Figure appendix 3- 4156 TPA 5A 3mm/s

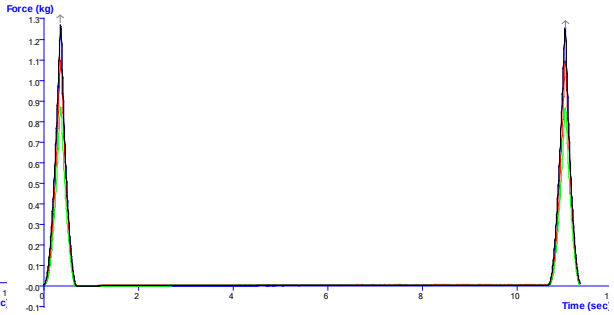

Figure appendix 3- 4257 TPA 5B 3mm/s

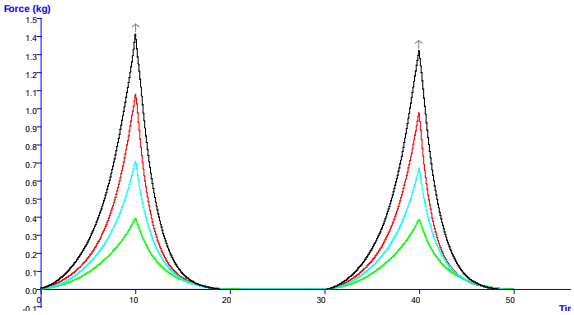

Figure appendix 3- 4358 TPA 5C 0.1mm/s

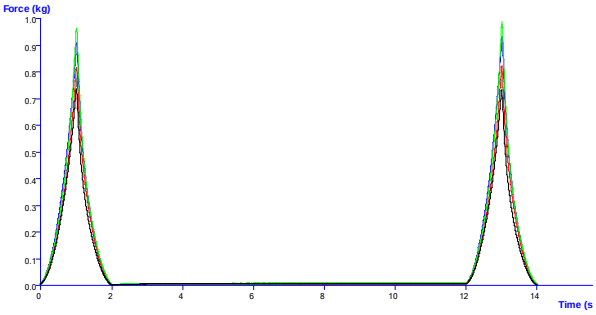

Figure appendix 3- 4459 TPA 6A 0.1mm/s

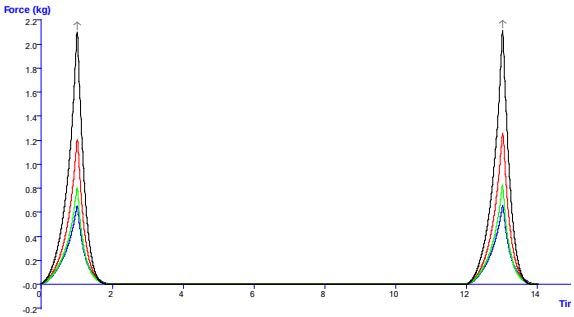

Figure appendix 3- 4560 TPA 5C 1mm/s

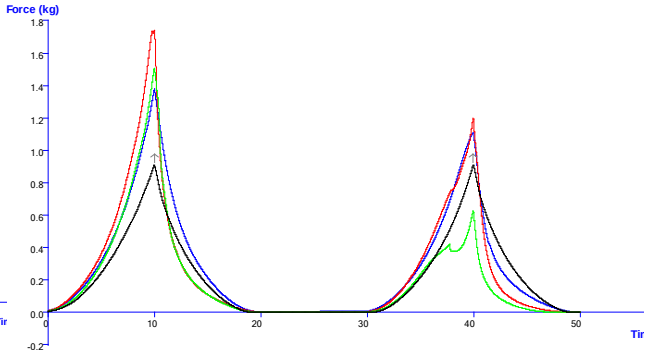

Figure appendix 3- 4661 TPA 6A 1mm/s

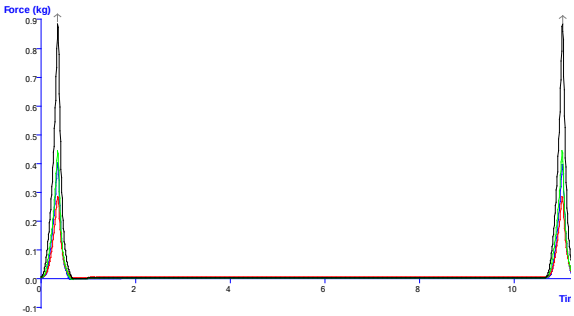

Figure appendix 3- 4762 TPA 5C 3mm/s

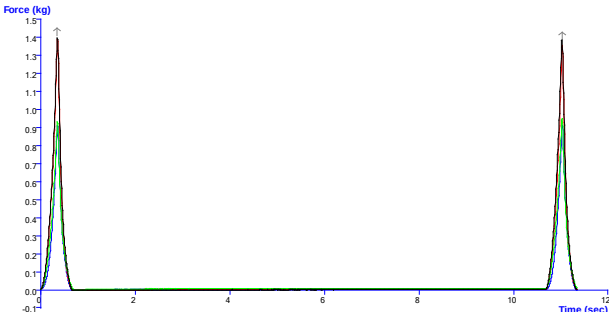

Figure appendix 3- 4863 TPA 6A 3mm/s

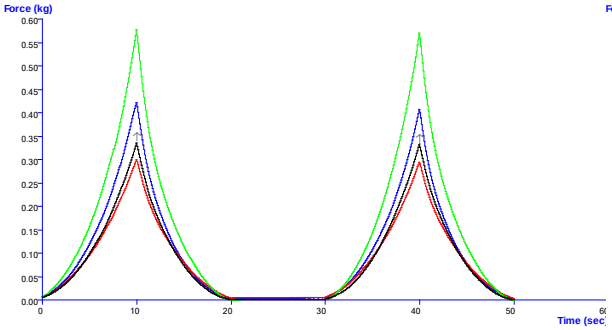

Figure appendix 3- 4964 TPA 6B 0.1mm/s

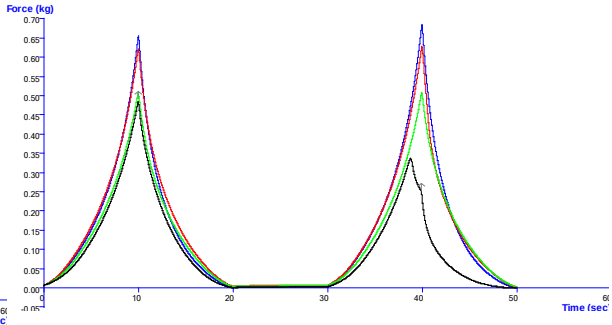

Figure appendix 3- 5065 TPA 6C 0.1mm/s

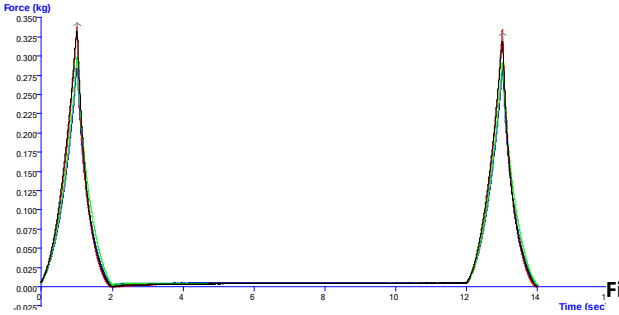

Figure appendix 3- 5166 TPA 6B 1mm/s

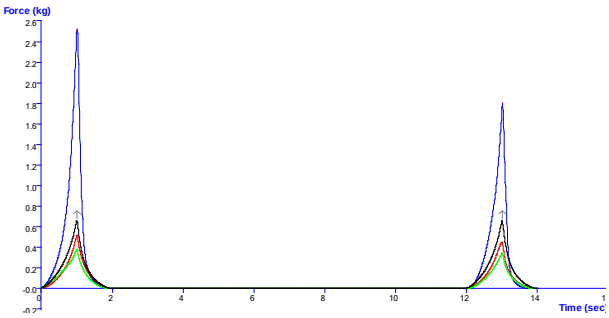

Figure appendix 3- 5267 TPA 6C 1mm/s (thin polymer disc, probe hit lower plantain)

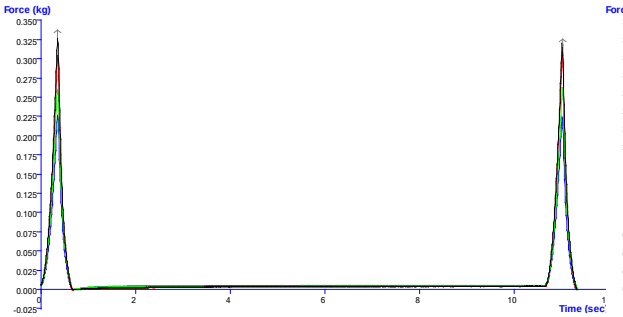

Figure appendix 3- 5368 TPA 6B 3mm/s

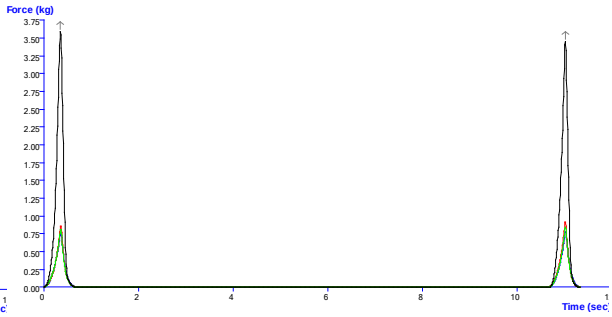

Figure appendix 3- 5469 TPA 6C 3mm/s

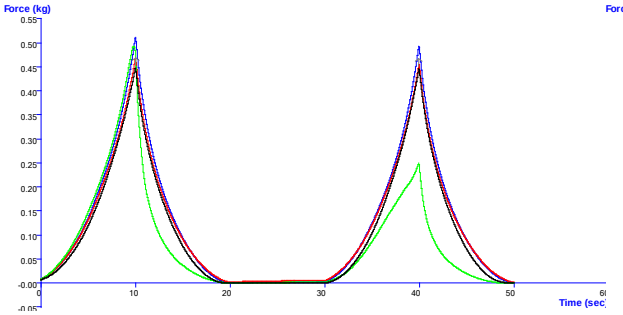

Figure appendix 3- 5570 TPA 7A 0.1mm/s

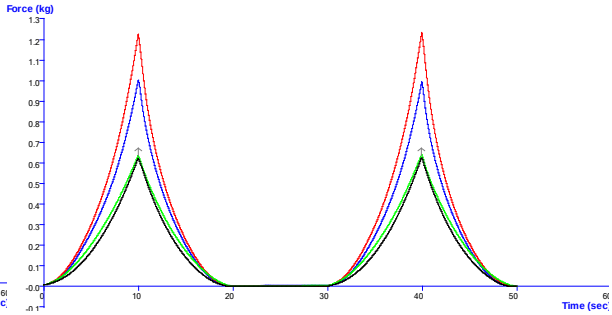

Figure appendix 3- 5671 TPA 7B 0.1mm/s

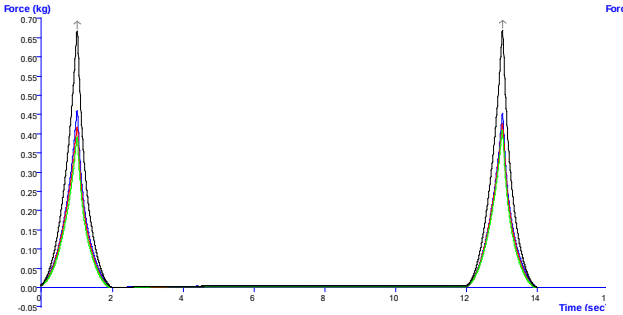

Figure appendix 3- 5772 TPA 7A 1mm/s

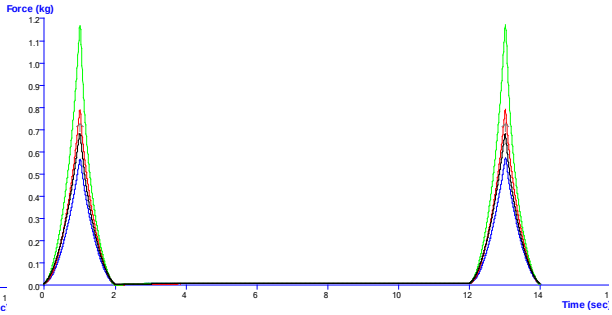

Figure appendix 3- 5873 TPA 7B 1mm/s

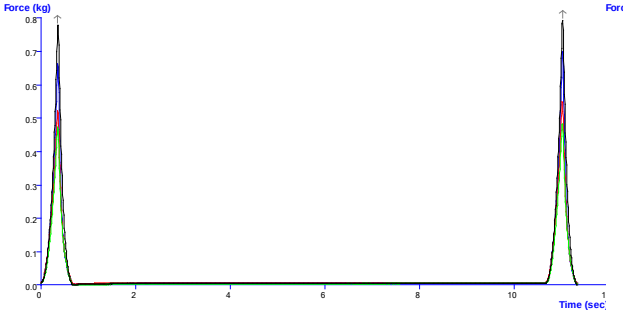

Figure appendix 3- 5974 TPA 7A 3mm/s

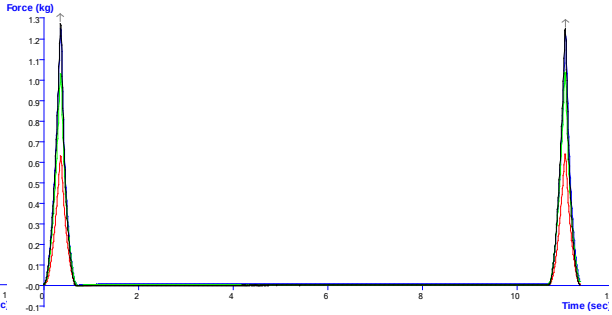

Figure appendix 3- 6075 TPA 7B 3mm/s

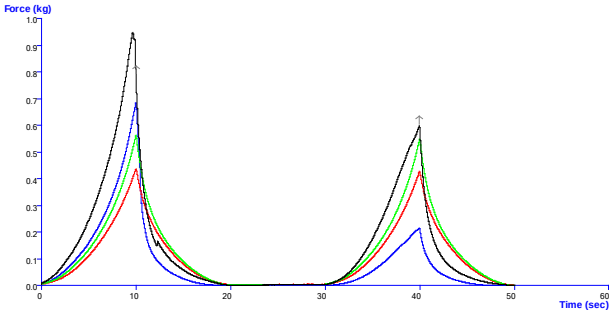

Figure appendix 3- 61 TPA 7C 0.1mm/s

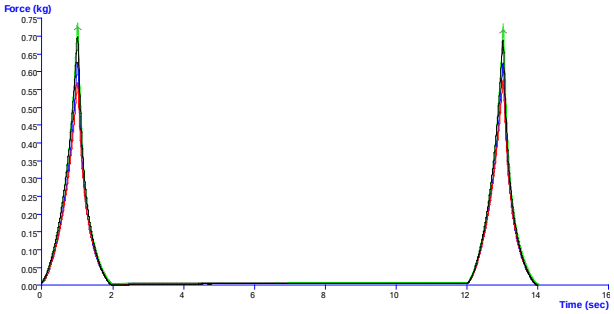

Figure appendix 3- 6276 TPA 7C 1mm/s

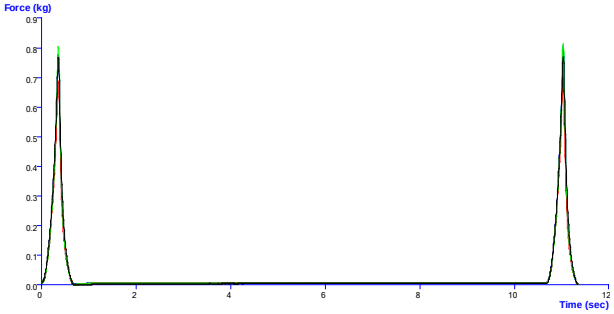

Figure appendix 3- 6377 TPA 3mm/s

Wet Polymer Testing

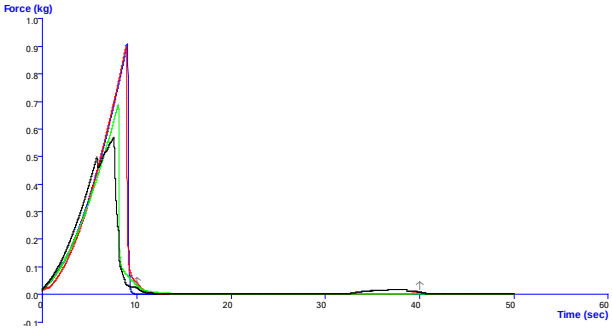

Figure appendix 3- 64 TPA 1BC 0.1mm/s

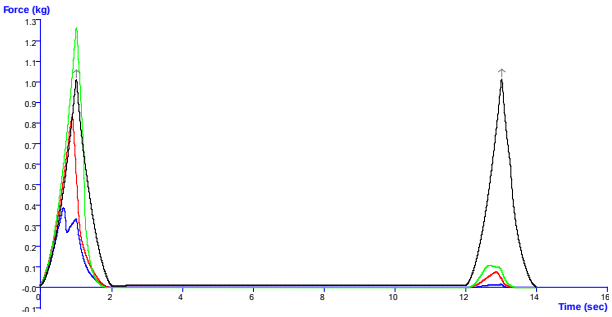

Figure appendix 3- 65 TPA 1BC 1mm/s

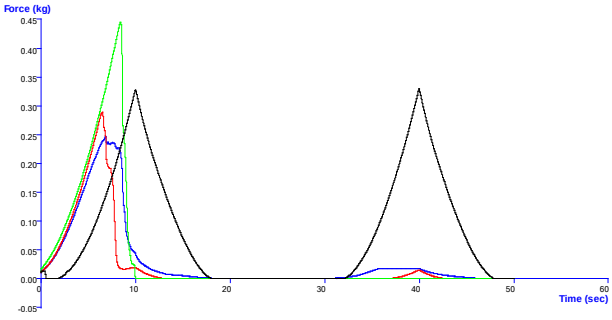

Figure appendix 3- 66 TPA 1BN 0.1mm/s

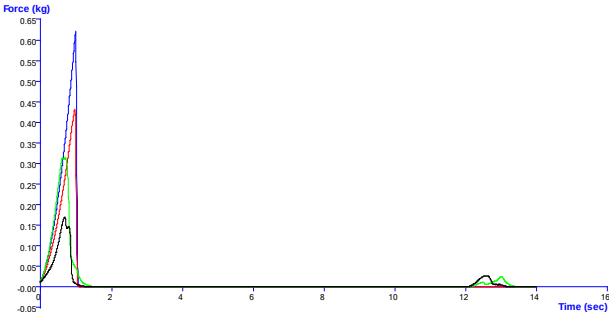

Figure appendix 3- 67 TPA 1BN 1mm/s

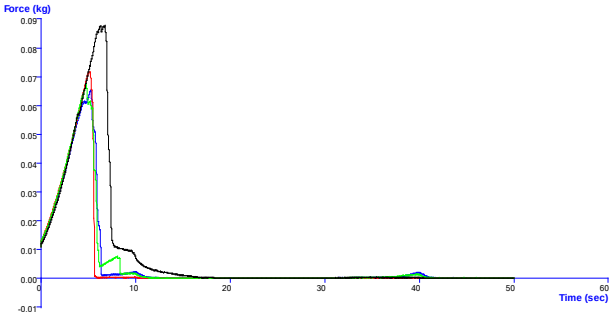

Figure appendix 3- 68 TPA 1C 0.1mm/s

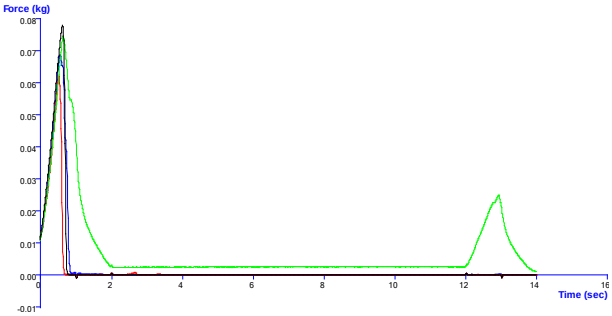

Figure appendix 3- 69 TPA 1C 1mm/s

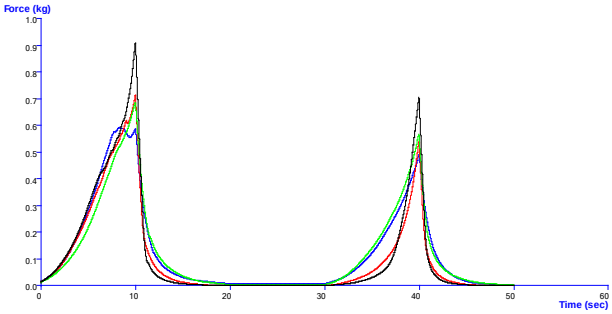

Figure appendix 3- 70 TPA 2A 0.1mm/s

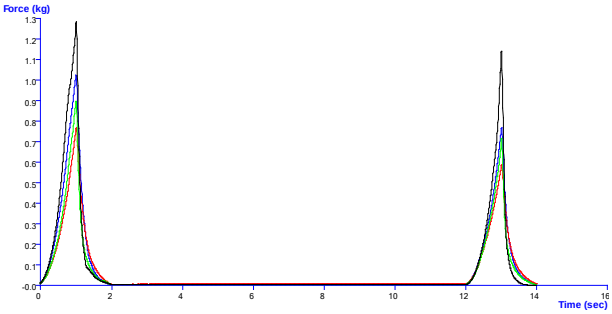

Figure appendix 3- 71 TPA 2A 1mm/s

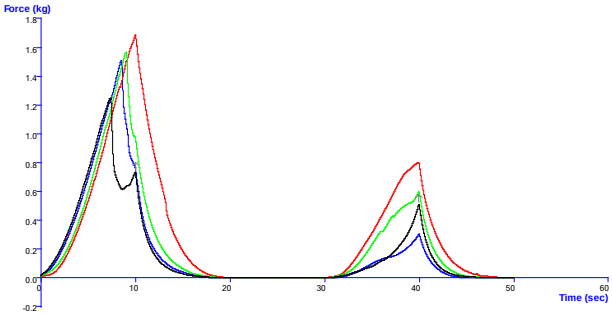

Figure appendix 3- 72 TPA 2B 0.1mm/s

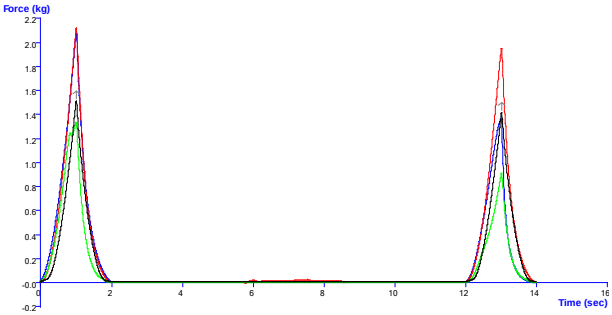

Figure appendix 3- 73 TPA 2B 1mm/s

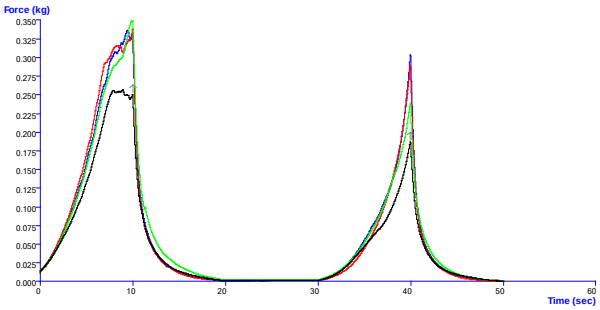

Figure appendix 3- 74 TPA 2C 0.1mm/s

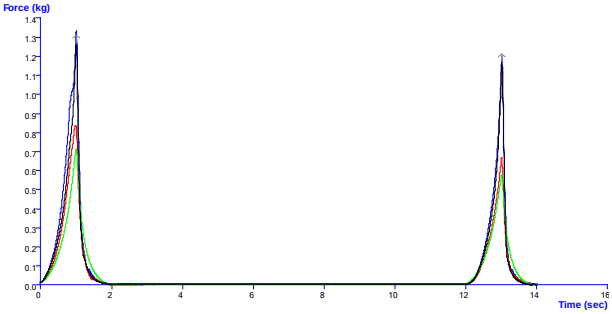

Figure appendix 3- 75 TPA 2C 1mm/s

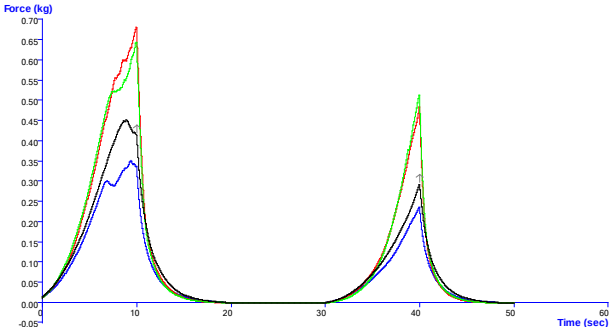

Figure appendix 3- 76 TPA 3A 0.1mm/s

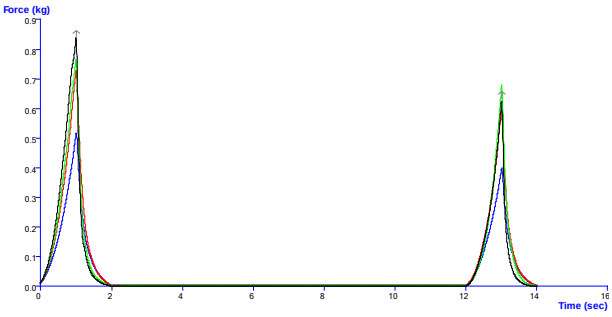

Figure appendix 3- 77 TPA 3A 1mm/s

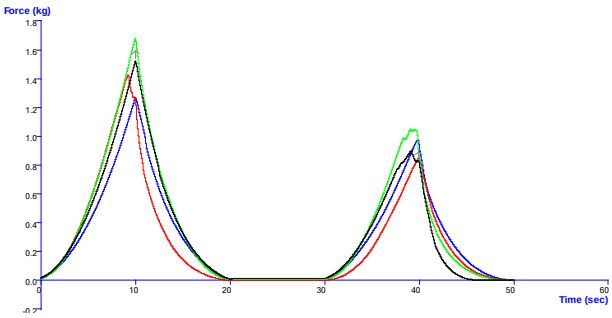

Figure appendix 3- 78 TPA 3B 0.1mm/s

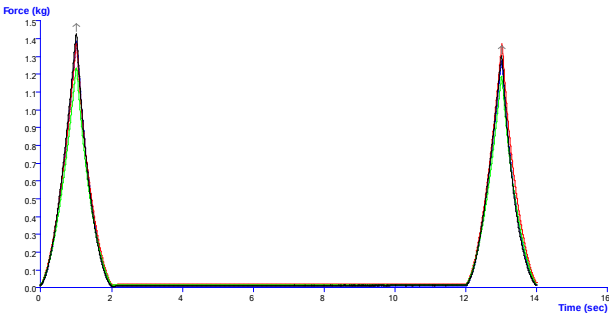

Figure appendix 3- 79 TPA 3B 1mm/s

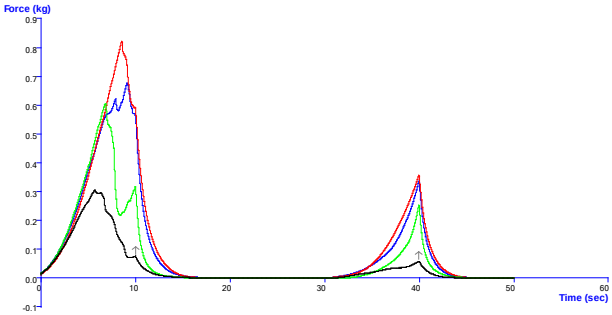

Figure appendix 3- 80 TPA 3C 0.1mm/s

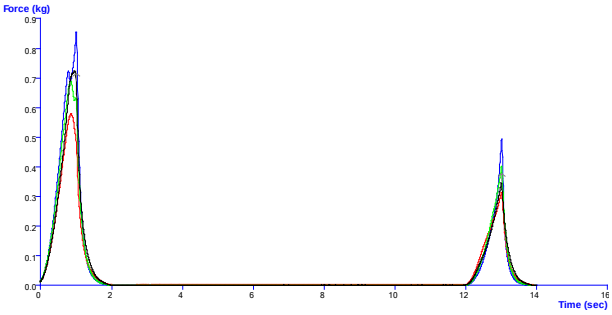

Figure appendix 3- 81 TPA 3C 1mm/s

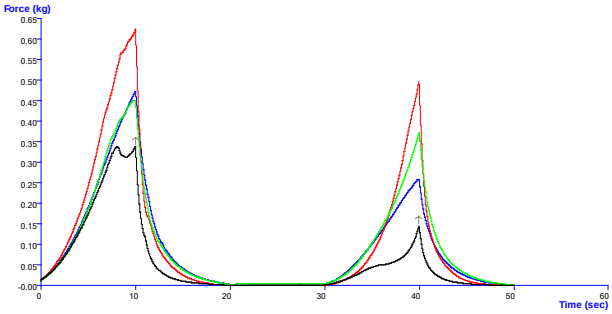

Figure appendix 3- 82 TPA 4A 0.1mm/s

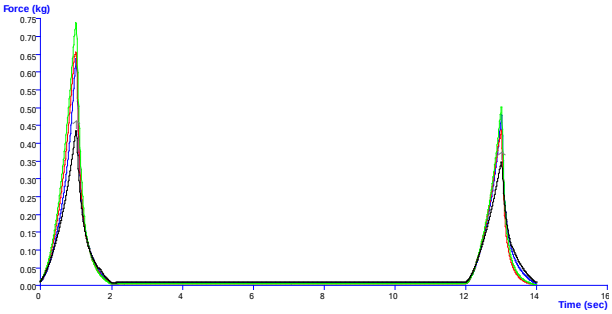

Figure appendix 3- 83 TPA 4A 1mm/s

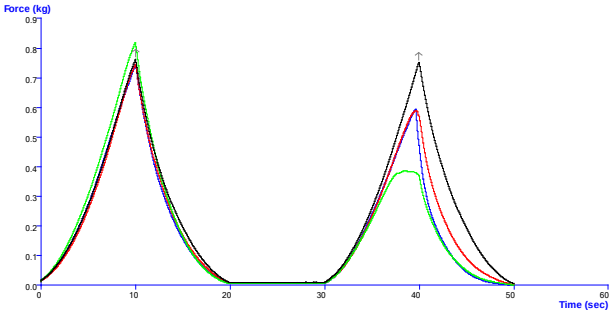

Figure appendix 3- 84 TPA 4B 0.1mm/s

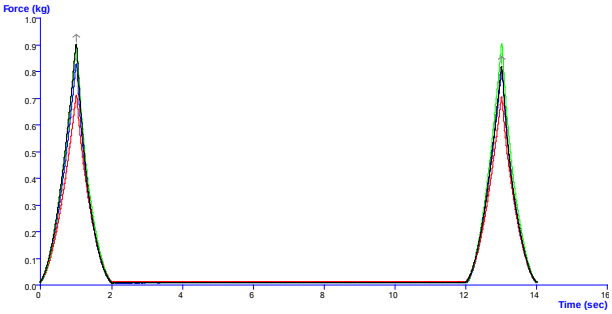

Figure appendix 3- 85 TPA 4B 1mm/s

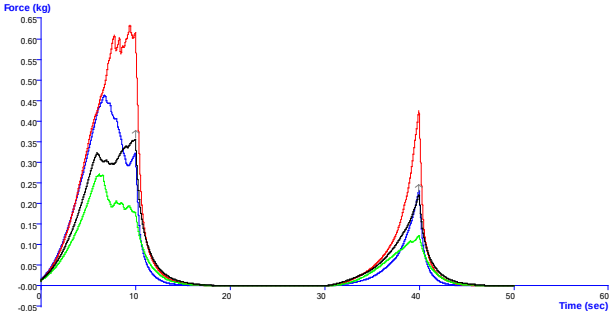

Figure appendix 3- 86 TPA 4C 0.1mm/s

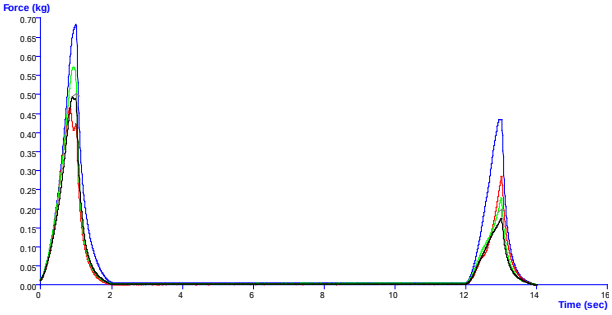

Figure appendix 3- 87 TPA 4C 1mm/s

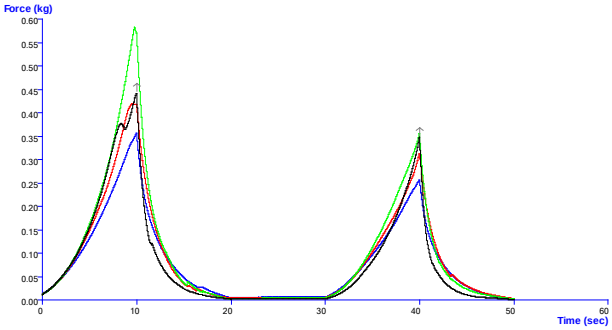

Figure appendix 3- 88 TPA 5A 0,1mm/s

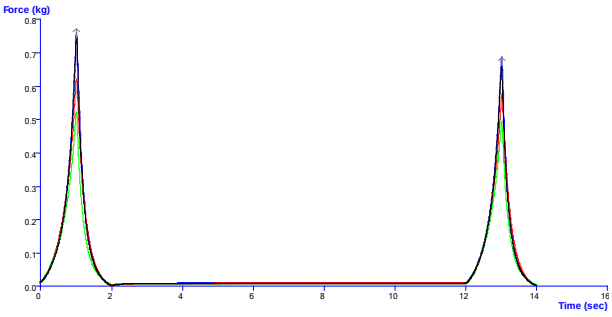

Figure appendix 3- 89 TPA 5A 1mm/s

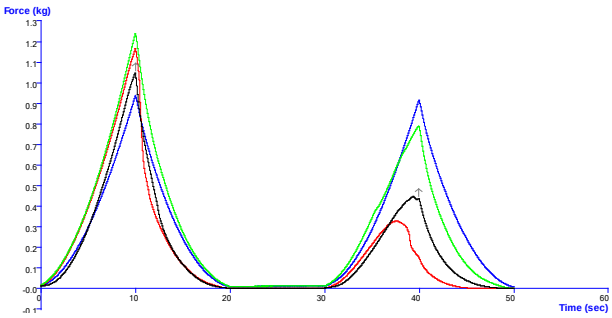

Figure appendix 3- 90 TPA 5B 0.1mm/s

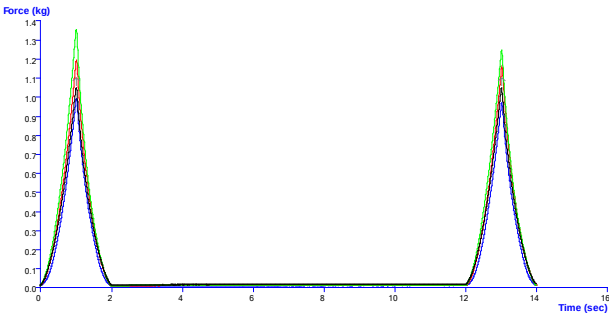

Figure appendix 3- 91 TPA 5B 1mm/s

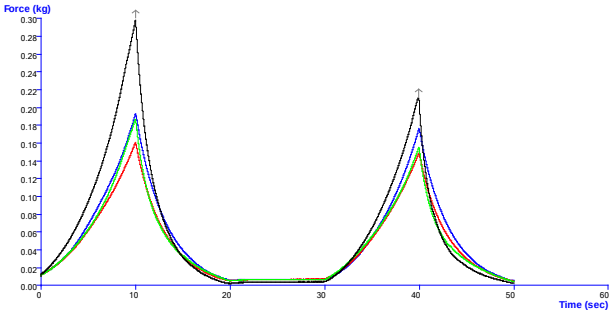

Figure appendix 3- 92 TPA 5C 0.1mm/s

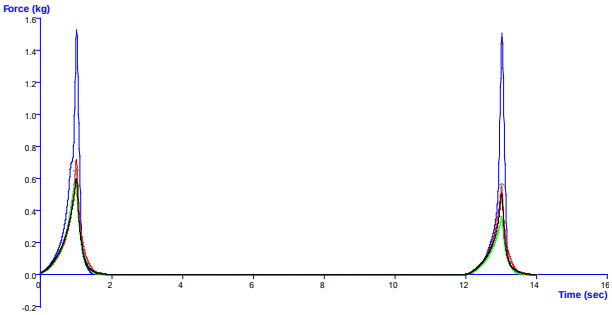

Figure appendix 3- 93 TPA 5C 1mm/s

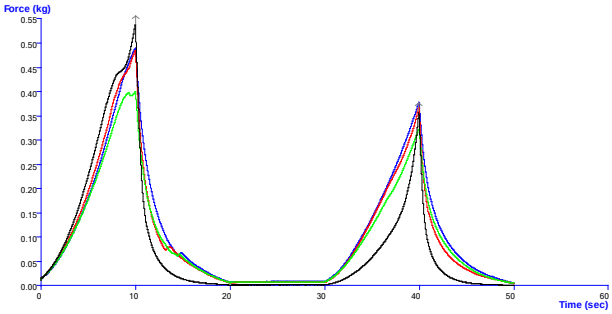

Figure appendix 3- 94 TPA 6A 0.1mm/s

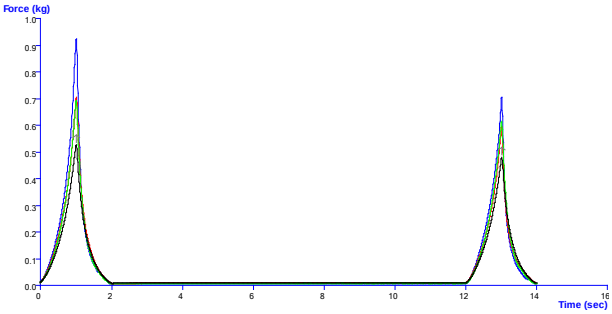

Figure appendix 3- 95 TPA 6A 1mm/s

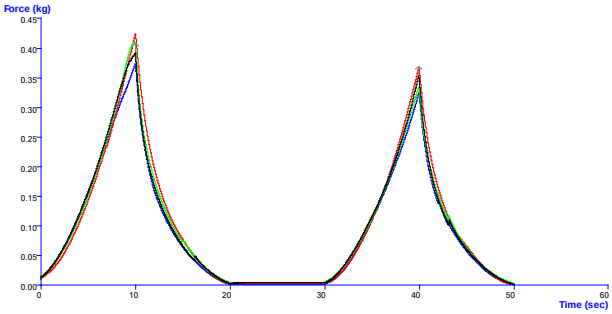

Figure appendix 3- 96 TPA 6B 0.1mm/s

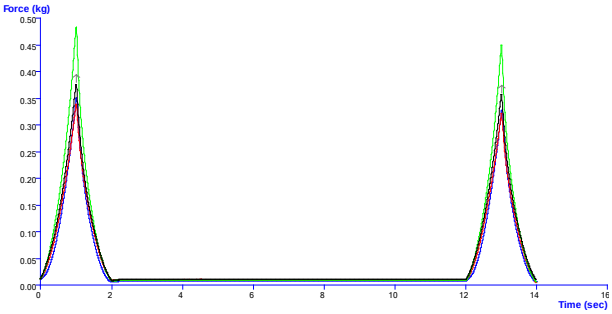

Figure appendix 3- 97 TPA 6B 1mm/s

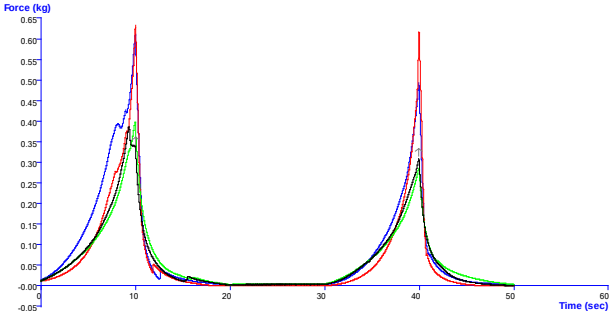

Figure appendix 3- 98 TPA 6C 0.1mm/s

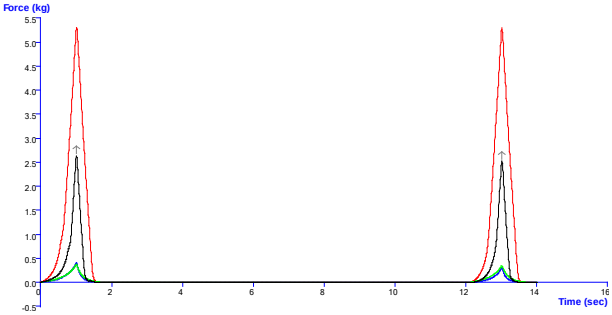

Figure appendix 3- 99 TPA 6C 1mm/s

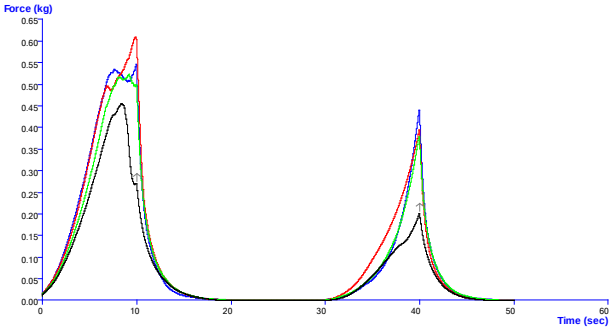

Figure appendix 3- 100 TPA 7A 0.1mm/s

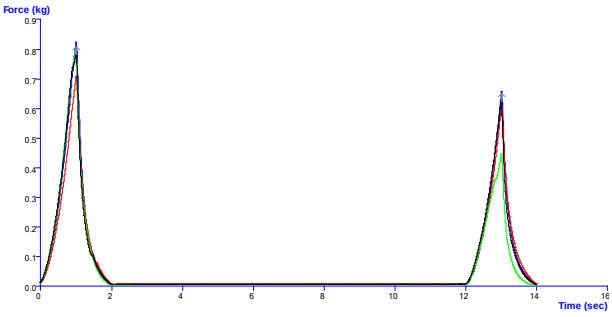

Figure appendix 3- 101 TPA 7A 1mm/s

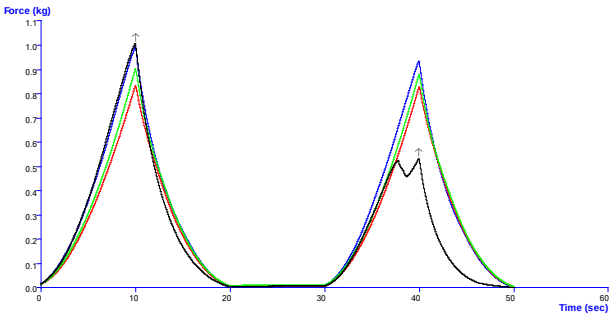

Figure appendix 3- 102 TPA 7B 0.1mm/s

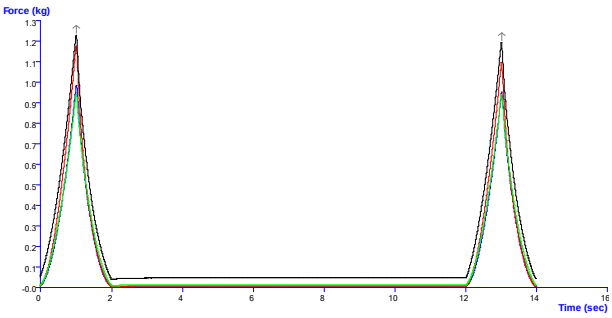

Figure appendix 3- 103 TPA 7B 1mm/s

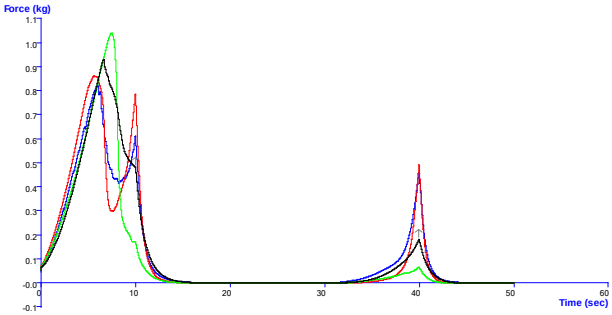

Figure appendix 3- 104 TPA 7C 0.1mm/s

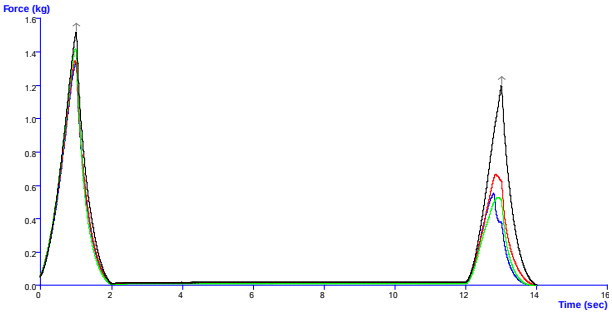

Figure appendix 3- 105 TPA 7C 1mm/s

TABLES AND FIGURES INDEX